Ronald Keith Mitchell FGA
1912 -2006

A tribute by Christopher Cavey FGA
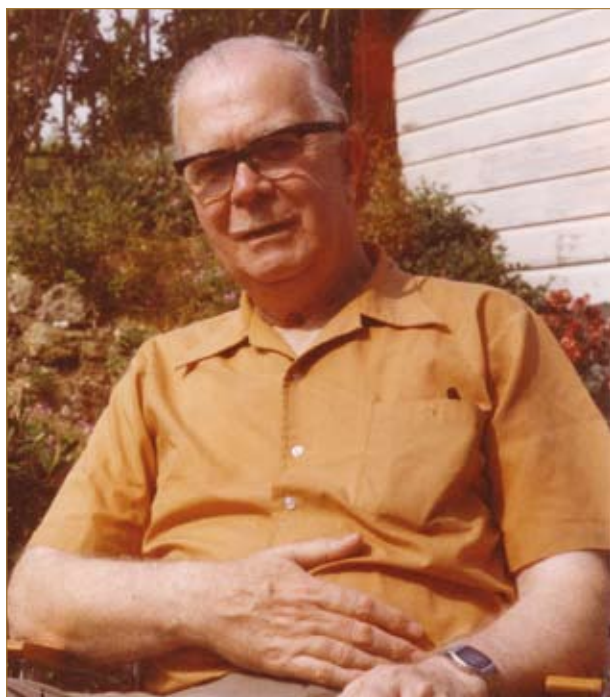
I was extremely sad to receive the news that Keith had passed away, as this was not only a personal loss for me, but a great loss for the entire gemmological world. Keith was a remarkable man as well as being a truly exceptional gemmologist, and after he retired from dealing in gems on a daily basis, he never lost interest and continued to read and write about gems whenever he could.

Keith started his career in the silver buying department of Mappin & Webb Ltd in 1928 at the age of 16. He was already interested in gemstones and was waiting for an opportunity to open up for him in the jewellery department, which he joined in 1933. Whilst he was in this employ he started his gemmological studies enrolling at Chelsea Polytechnic. He studied very hard and spent his lunch hours carefully perusing the gem collections in the Geological Museum which was then located in Jermyn Street, just off Piccadilly in London's West End. In 1934 he sat the Diploma in Gemmology Examination; this was to prove a tough year in the gem exams as there was

considerable competition but, despite coming up against Robert Webster, it was Keith who won the day and gained the most prestigious prize in gemmology - the B.J. Tully Memorial Medal.

As the winner of the Tully Medal Keith was immediately elected to the Gemmological Association's council, which he served faithfully until his calling up into the Royal Corps of Signals during the early years of World War II. He was posted to Singapore and it was not long afterwards that the Japanese invaded and he found himself a Prisoner of War. A number of his fellow POWs were taken to Thailand to build the infamous Burmese railroad, but Keith was taken to mainland Japan, where he and his fellow inmates were forced to labour making steel for the Japanese war effort, surviving on the poorest of diets for some three and a half years. It has to be said that anyone who can survive such conditions for such a period has indeed to be quite exceptional, and Keith was that in many ways.

After the war he returned to London and took up work with jewellers A & E Davis, situated in Piccadilly in the West End of London. In 1947 he became a tutor at Chelsea polytechnic assisting Thorold Jones who ran the classes in those days, and in 1948 was re-elected to the Council of the Gemmological Association.

In 1950 he took on the task of running the first year correspondence courses for the GA as an Instructor. Only one year later he took over the second year as well, and he ran them single-handed for some years until eventually Vera Hinton took over some of the first-year students.

Keith was a very decent and proper man and expected very high standards from those who worked with him, and of those he was teaching, He expected his students to work hard and continued to give private tuition right up until his retirement. He used

to send out material to his students and ask for their observations. When he received these he would then give them a copy of his own observations on the same materials, so they could see just what they had missed!

He was the sole author of the correspondence courses used by the GA from the 1950s to 1983.

In the early 1960s,, Keith needed a change and more independence, so struck out on his own dealing in gems, mineral specimens and jewellery. He took over an office in Halton House just round the corner from Hatton Garden in Holborn. During that time he handled many gems from A C D Pain in Burma and formed close relationships with a number of dealers in Sri Lanka. He acquired the Taaffe collection along with the first ever specimen of taaffeite, which was the 'type specimen' for this species. He left this on loan to the Natural History Museum in London. He was a regular contributor to gemmological journals, not only in England but also in Australia, and made many original observations on a number of gem species.

He invented the 'Mitchell' spectroscope stand and was a major contributor to items coming into the London Gem Testing Laboratory. He was a close friend of Basil Anderson, Robert Webster and Alec Farn, and enjoyed an affable relationship with Alan Jobbins and Pat Statham at the Geological Museum in London. He worked with Charles Mathews, the famous lapidaries in Hatton Garden, and was instrumental in the cutting of some very rare gem species for the first time. He handled a large part of the E H Rutland collection upon his untimely death in 1976, and was one of the very few gemmologists in London who regularly handled very rare gem species.

He continued to run the correspondence courses for the GA until 1969 when he was diagnosed with a heart condition. This made him re-consider his overall workload but he continued to trade in gems on a daily basis until his retirement in 1979.

Despite his retirement Keith continued to work on gems and carried on publishing

gemmological papers and he finally went on to publish over 40 papers in all. He also performed a great service to thousands of gemmologists with his masterly use of the English language in abstracting papers from other publications; his vast experience of a wide range of gems supported many an enlightening and penetrating supplement to an abstract.

For some time, he had also been working on the memoirs of his wartime experiences. After some searching he managed to find a publisher, although much to his disappointment the size of his book was cut in half before going to press. He did at least have some satisfaction in knowing that a part of his story had at last been told.

Keith revised Basil Anderson's and James Payne's work *The Spectroscope and Gemmology*, adding extra chapters and diagrams.

He privately published sets of slides (each one an original photograph shot by his own hand) showing crystal habits and symmetry together with an explanatory booklet which was retailed by the GA. These were available for a number of years, to assist students of gemmology with their understanding of crystals. Keith was also a good photographer and pioneered a number of techniques for photographing gem materials in daylight and down the microscope.

He was made Vice President of the GA in 1984 and remained in this office until his death on 7 April 2006 at the age of 94.

Keith had lost his loving wife of many years some time ago, but thankfully is survived by his two sons, two grandchildren and a great granddaughter.

For those of us that knew him well he was a great friend with an extraordinary sense of humanity and humour. I believe him to have been a truly great gemmologist and the pertinence and wisdom expressed in his publications should ensure that he is remembered as one of the founding fathers of British gemmology in the twentieth Century.

The role of Be, Mg, Fe and Ti in causing colour in corundum

Dr Visut Pisutha-Arnond [1,2], Dr Tobias Häger [3],
Wilawan Atichat [1] and Dr Pornsawat Wathanakul [1,4]

1. Gem and Jewelry Institute of Thailand, Faculty of Science,
   Chulalongkorn University, Bangkok 10330, Thailand
2. Department of Geology, Faculty of Science, Chulalongkorn University,
   Bangkok 10330, Thailand. E-mail: pvisut@gmail.com
3. Institute of Gemstone Research, University of Mainz, Germany
4. Earth Science, Department of General Science, Faculty of Science, Kasetsart
   University, Bangkok 10900, Thailand

Abstract: New beryllium-diffusion experiments on pure synthetic and iron-doped synthetic sapphire samples and on natural blue sapphires were undertaken to fully understand how colour is affected by Fe, Ti, Mg and Be in corundum. LA-ICP-MS analyses were carried out on sections through and on the treated surfaces of the sapphires. The results have confirmed that the divalent Be acts essentially in the same way as that of Mg, i.e. as a stabilizer of colour centres.

Keywords: beryllium diffusion, blue sapphire, colour centres, heat treatment, LA-ICP-MS analysis, yellow sapphire

Introduction

Although corundum diffusion-treated with beryllium (Be) has been discussed recently by a number of authors including McClure *et al.* (2002), Peretti and Günther (2002), Peretti *et al.* (2003), Hänni (2002), Hänni and Pettke (2002), Emmett *et al.* (2003), Fritsch *et al.* (2003), Themelis (2003), Pisutha-Arnond *et al.* (2003 and 2004) and Schmetzer and Schwarz (2004, 2005), the role of Be in corundum has not yet been fully understood. Pisutha-Arnond *et al.* (2004) presented studies on UV-Vis-spectroscopy and trace-element chemistry of irradiated and Be-treated synthetic and natural colourless sapphires, yellow and orangey yellow Be-treated natural sapphires and some Be-treated natural blue sapphires, and established that the majority of Be-treated sapphires showed indications of Be diffusion into the corundum lattice from an external source. The chemical analyses obtained by laser ablation inductively coupled plasma mass spectrometry (LA-ICP-MS) consistently showed that there were excess contents of (Be+Mg) over Ti in all of the yellow sapphires which were coloured by stable defect centres. The oxidation and reduction heating experiments also showed that oxidizing conditions were an important factor in the formation of stable colour centres. So, currently it is believed that after combining Mg and Be with any Ti present to form colourless $MgTiO_3$ and/or

BeTiO$_3$ clusters, any excess of (Be+Mg), in combination with iron and the heat treatment in an oxidizing atmosphere can produce stable yellow colour centres in yellow Be-treated natural sapphires.

In the previous study, Pisutha-Arnond *et al.* (2004) assumed the divalent Be could have the same effect in the corundum structure as Mg. However, Mg and many other trace elements are usually present in natural corundum and this makes it difficult to understand the direct relationship of Be and Fe in any natural sapphire treated with Be. Hence in order to prove such an assumption it was necessary

Materials and methods

In order to test whether Be has a comparable effect to Mg in producing brown coloration in an otherwise pure synthetic sapphire (i.e. Be in the Al$_2$O$_3$ system), a comparison experiment was performed on a piece of synthetic colourless 'watch glass' sapphire with high purity (THSCS01). The piece was cut in half, and one half was heat-treated with ground chrysoberyl in a crucible while the other half was heated in another crucible without chrysoberyl in an electric furnace. Each crucible was held at 1750°C (measured by a thermocouple in which a certain degree of temperature gradient was unavoidable) for 30 hours in an oxidizing atmosphere. After the treatment, both halves of the 'watch glass' were lightly polished, cleaned and their trace element contents determined using LA-ICP-MS at the GEMOC Key Centre, Department of Earth and Planetary Sciences, Maquarie University, Sydney, Australia. The UV-Vis spectrum of the chrysoberyl-treated half was also recorded.

To further confirm that Fe needs to be present to form yellow (rather than brown) defect centres an Fe-doped sapphire was synthesized by a flame-fusion technique, irradiated with X-rays for 30 minutes using a Rh-tube at 60 kV and 53 mA, and then shortly after, subjected to a fading test. The fading was carried out for one hour at a distance of 3 cm from a 100W light bulb. The sample was subsequently heated in a crucible with ground chrysoberyl at 1780°C for 50 hours in an oxidizing atmosphere. This Be-treated sample was then subjected to the fading test again. The sample was photographed and at each step of the experiments, UV-Vis spectra were recorded with E perpendicular to the *c*-axis (o-ray), except where noted otherwise. The sample was then cut in half, lightly polished, cleaned and analysed for trace element contents across the cut surface using LA-ICP-MS.

Additionally, two simply heat-treated natural blue sapphires and one natural blue sapphire Be-treated under unknown conditions were obtained from Thai stone heaters. The samples were cut in half and the cut surface was lightly polished and cleaned. Their trace element contents were obtained using LA-ICP-MS at five positions namely: Rim1, Mid-Point1, Core, Mid-Point2 and Rim2 to yield a profile of analyses.

Detailed descriptions of LA-ICP-MS instrumentation, analytical and calibration procedures are similar to those given by Norman *et al.* (1996). The UV laser ablation microprobe (a New Wave Research 266 nm Nd:YAG) is coupled to an Agilent 7500 ICP-MS. All analyses were done with a pulse rate of 5 Hz and a beam energy of approximately 0.5 mJ per pulse, producing a spatial resolution of 30-50 micrometres in diameter on the samples. Quantitative results for 9 trace elements (Be, Na, Mg, Ti, V, Cr, Mn, Fe and Ga) were obtained through calibration of relative element sensitivities using the internal standards NIST-610 multi-element glass and pure Al$_2$O$_3$, and the external standard BCR2G basaltic glass. The detection limits vary from analysis to analysis and are typically less than 1 ppm for Be, V, Ga; less than 4 ppm for Mg, Ti, Mn; less than 13 ppm for Cr; less than 40 ppm for Na and less than 80 ppm for Fe. The results significant in this study are presented in diagrams and detailed numerical results can be obtained from the senior author.

to carry out more Be-diffusion experiments with pure synthetic and Fe-doped synthetic sapphires without the influence of Mg and other trace elements. In addition, more LA-ICP-MS analyses needed to be carried out on natural blue sapphires both untreated and treated with Be to test the assumption of similarity of Be and Mg.

In order to understand the Be-diffusion process and its mechanism, the role of trace elements and the cause of stable yellow colour centres are reviewed briefly. The role or interaction of Mg, Ti and Fe in creating stable yellow colour centres or blue colours is well understood (Häger, 1992, 1993, 1996, 2001; Emmett and Douthit, 1993). The divalent Mg and tetravalent Ti form colourless $MgTiO_3$ (geikielite) clusters, and after formation of these clusters, any excess Mg could combine with Fe in an oxidizing atmosphere to produce colour-active defect centres or stable yellow colour centres. However, in corundums with rather low Fe

excess of Ti after the calculation of $MgTiO_3$, the excess Ti in combination with Fe could form colour-active $FeTiO_3$ clusters under both reducing and oxidizing conditions. These clusters create Fe^{2+}/Ti^{4+} inter-valence charge transfer absorption bands near 578 and 735 nm which are responsible for the blue coloration of sapphire (Townsend, 1968; Ferguson and Fielding, 1972; Häger, 1992, 1996, 2001; Emmett and Douthit, 1993).

Results

Simple heat-treatment and beryllium-diffusion treatment of a pure synthetic colourless sapphire

After simple heat treatment (i.e. heat treatment that is not accompanied by other minerals or chemicals), the pure synthetic sapphire (THSCS01) remained colourless but it turned brown after Be diffusion treatment (*Figure 1*). Trace element analyses

Figure 1: A colourless sapphire disc (THSCS01) was cut in half, one half was heat-treated with ground chrysoberyl in a crucible (a, brown) while the other half was heat-treated in another crucible without chrysoberyl (b, colourless). After the treatment, five-points on a traverse were analysed on the polished surface of each half. Photo by C. Somboon.

content such as Mg-doped synthetic stones, stable brown or brownish violet colour centres, rather than yellow, are produced (Wang *et al.*, 1983; Häger, 1996, 2001). The Mg seems to act as a stabilizer of the defect centre. On the other hand, if there is an

of the colourless half show that the original material is relatively pure with only traces of Ti (< 4ppm) and Na (< 200 ppm). The brown half contains about 10 ppm by weight of Be, that is, about 20 atom mole ppm of Be has diffused into the corundum lattice,
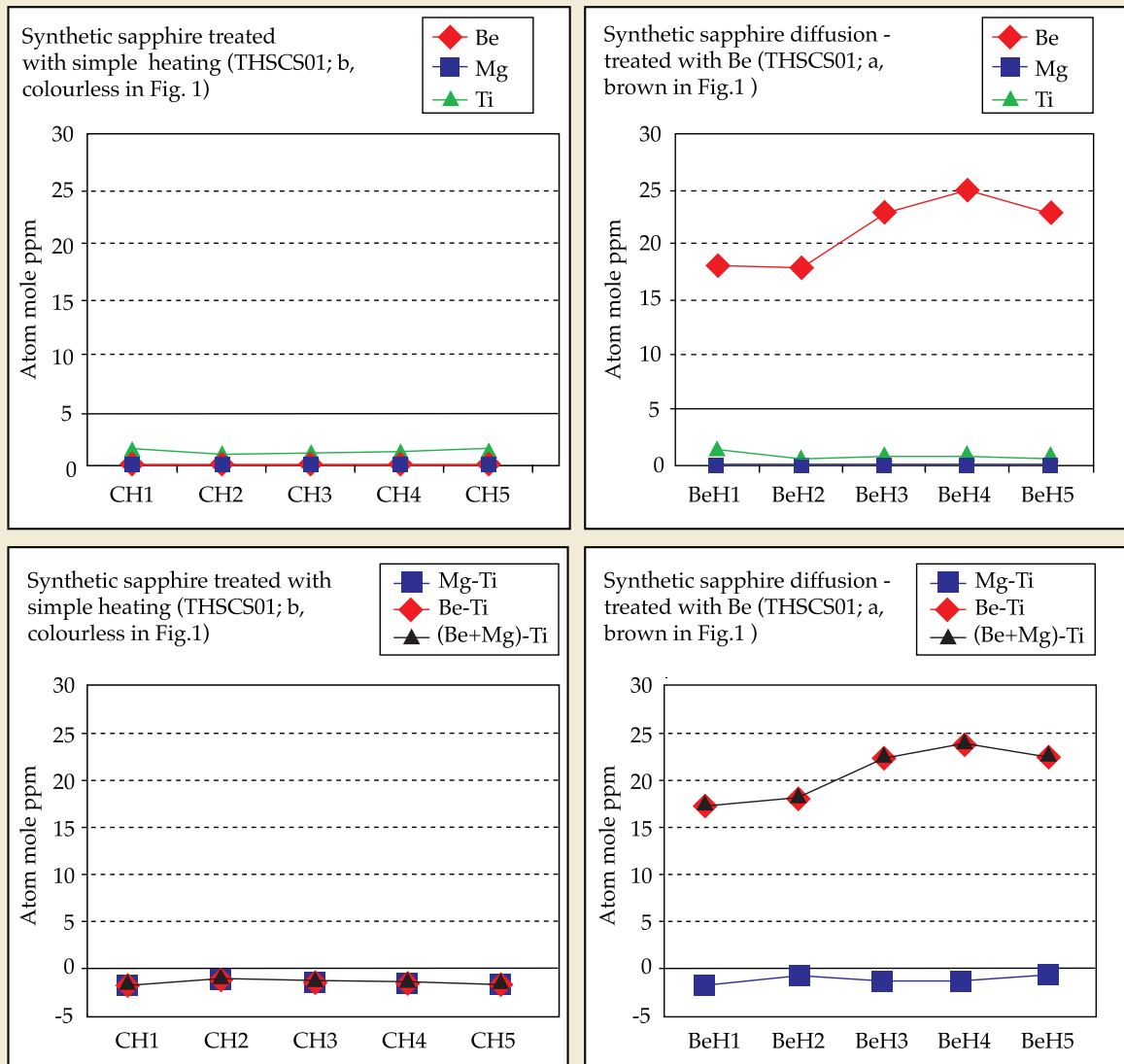
Figure 2: Be, Mg and Ti contents at the surfaces of the simply heat treated (CH numbers) and chrysoberyl-treated (BeH numbers) sections of the sapphire disc (THSCS01) shown in Figure 1. The right-hand diagrams illustrate the positive values of (Be – Ti) in the Be-treated half and Mg points are included in view of discussion later in the paper.

while the presence of any of the other eight trace elements is negligible (*Figure 2*). The UV-Vis spectrum of the Be-treated brown half shows exactly the same pattern as that of the flame-fusion grown sapphire (PKSCS01) treated under unknown conditions by a Thai heat-treater (*Figure 3*) with a broad absorption band centred at around 420 nm.

Treatments of an iron-doped synthetic sapphire

An Fe-doped synthetic sapphire was colourless before treatment (*Figure 4a*) and contained abundant gas bubbles typical of flame-fusion grown material (*Figures 4* and *5*).

The sample became yellow after irradiation treatment (*Figure 4b*) and its UV-Vis spectrum shows a continuous increase in absorption towards shorter wavelengths with a shoulder at about 450 nm (*Figure 6*). After a fading test, this sample became colourless (*Figure 4c*) but it turned yellow again after treatment with Be and this colour was stable after a fading test (*Figure 4d*).

The UV-Vis spectrum of the sample treated with Be shows exactly the same pattern as that of the sample irradiated with X-rays (*Figure 6*), and these spectra are also similar to that of a Sri Lankan yellow sapphire coloured by stable defect centres and to
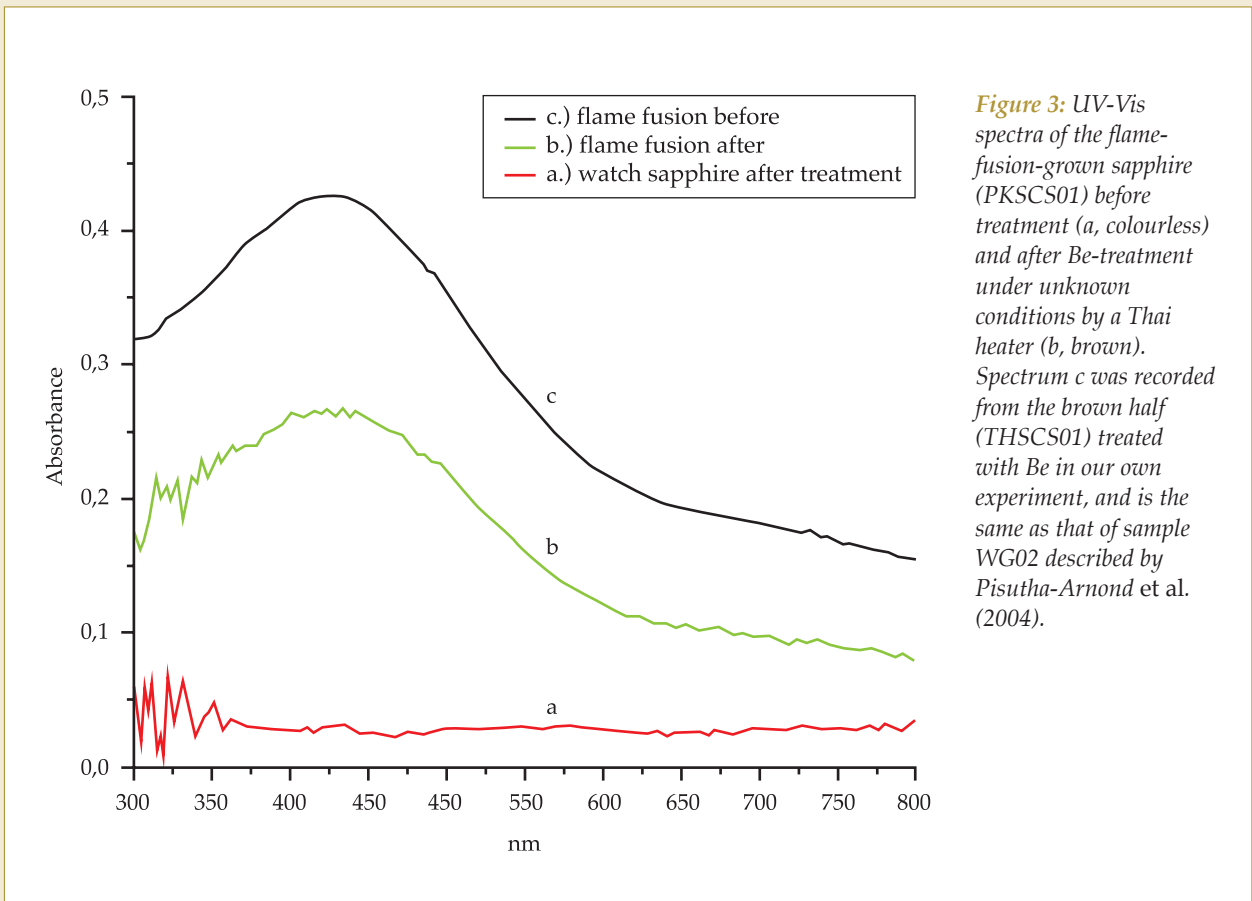
Figure 3: *UV-Vis spectra of the flame-fusion-grown sapphire (PKSCS01) before treatment (a, colourless) and after Be-treatment under unknown conditions by a Thai heater (b, brown). Spectrum c was recorded from the brown half (THSCS01) treated with Be in our own experiment, and is the same as that of sample WG02 described by Pisutha-Arnond et al. (2004).*
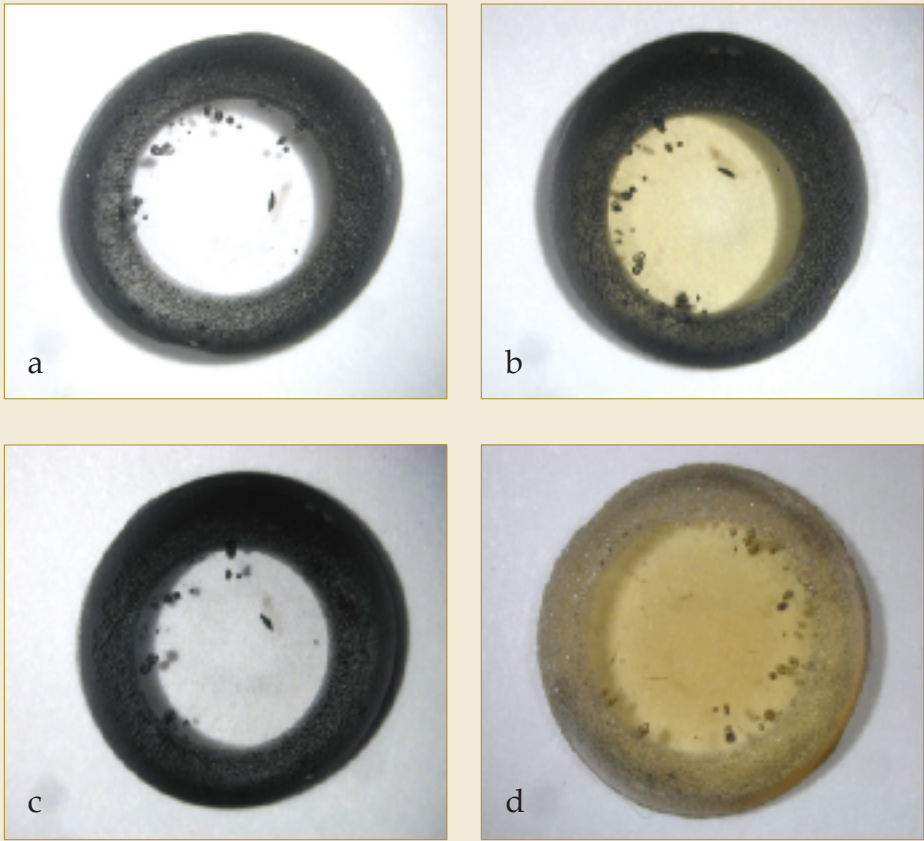
Figure 4: *Photographs of an Fe-doped colourless flame-fusion sapphire before treatment (a), yellow after X-ray irradiation treatment (b), colourless after a fading test (c), and yellow again after Be-treatment (d). The final colour was stable under the fading test. Photos by T. Häger.*

The role of Be, Mg, Fe and Ti in causing colour in corundum
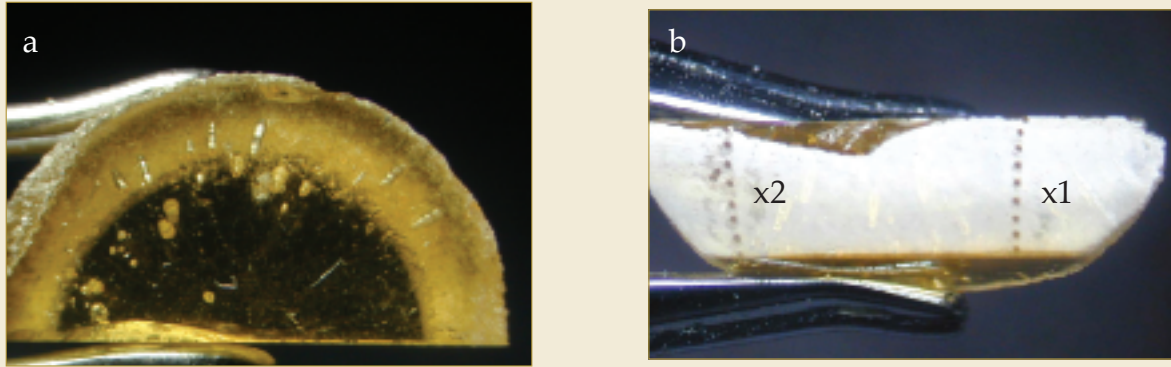
Figure 5: The Fe-doped sapphire described in Figure 4, treated with Be and cut in half (a), with details of abundant gas bubbles. In (b) are shown the positions of two traverses (X1 and X2) on the cut surface where analyses were obtained using LA-ICP-MS. Photos by C. Somboon.
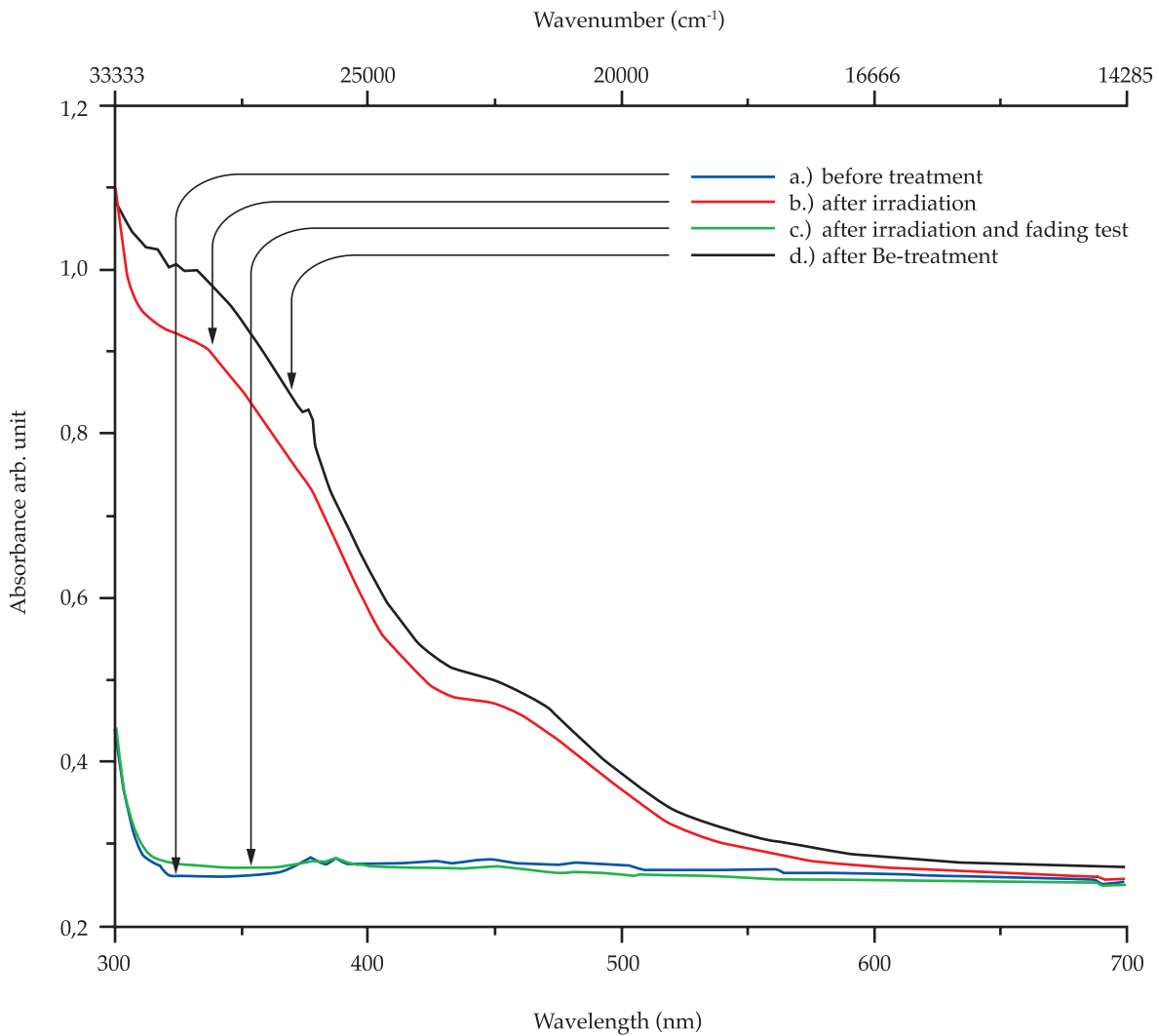
Figure 6: UV-Vis spectra of the Fe-doped flame-fusion-grown sapphire before treatment (a), after X-ray irradiation treatment (b), after a fading test (c), and after Be-treatment (d). All spectra were measured with E perpendicular to the c-axis (o-ray).

that of a synthetic sapphire doubly-doped with Mg and Fe (*Figure 7*). The trace element analyses confirm that significant contents of Be and Fe (about 25-30 atom mole ppm of Be and 50-60 atom mole ppm of Fe) are present in this sample after Be treatment while the other trace element contents are negligible (*Figure 8*). Hence it is clear that colour in the sample can be attributed solely to Be+Fe with no influence from other trace elements.

Heat-treated natural blue sapphires

As expected the two simply heat-treated natural blue sapphires, one from Australia (AUS1) and the other from an unknown source, are homogeneous in colour throughout (*Figures 9* and *11*). The five point profile analyses across the cut surfaces reveal no detectable Be (below 1 ppm detection limit) (*Figures 10* and *12*), but show significant Fe and Ti with trace amounts of Mg. At all the analysed points Ti exceeds Mg+Be.

Be-treated natural blue sapphire

A 2.28 ct rectangular cut blue-green sapphire (BG1) reportedly from Bang Kacha (Chanthaburi, Thailand) was heat-treated with Be under unknown conditions by a Thai stone heater. After treatment the sample clearly showed a thin surface-related yellow rim surrounding a blue core with complex zoning (*Figure 13a*). The sapphire was cut
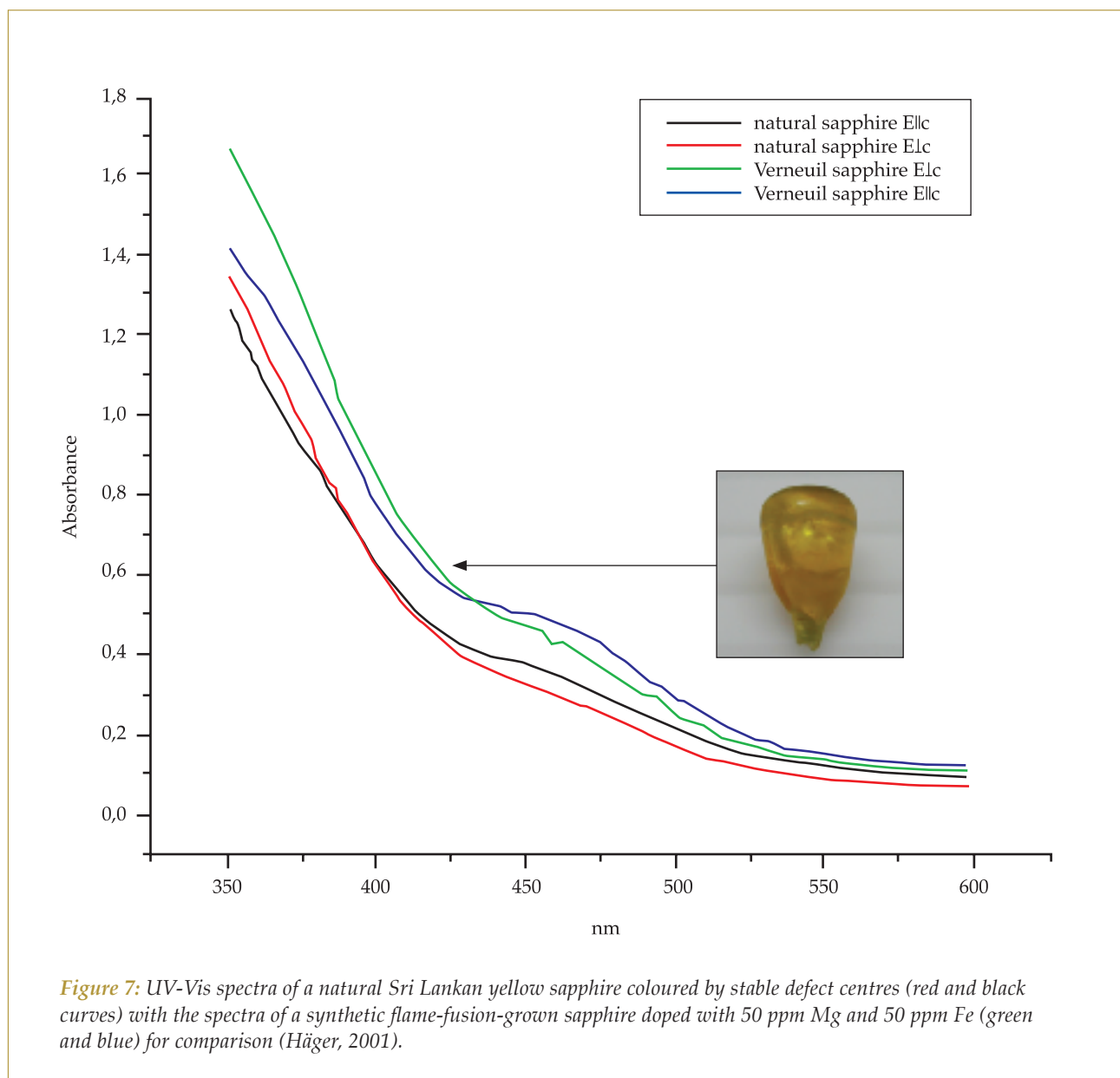
Figure 7: *UV-Vis spectra of a natural Sri Lankan yellow sapphire coloured by stable defect centres (red and black curves) with the spectra of a synthetic flame-fusion-grown sapphire doped with 50 ppm Mg and 50 ppm Fe (green and blue) for comparison (Häger, 2001).*

into two and the blue core of one piece can be seen in *Figures 13b* and *c*. The LA-ICP-MS profile analysis shows negligible Be (< 1 ppm) in the core and elevated Be content towards the yellow rims (*Figure 14*). All the analysed points in the blue core show an excess of Ti over total Mg+Be content. At the points near each rim, at the blue-yellow boundary, the analyses do show elevated Be contents but the Ti contents still exceed the sum of Be+Mg (*Figure 14*). However, at all the points analysed on the outer surface of the stone, which are definitely on the yellow rim (*Figure 15*), there is an excess of Be+Mg over

Ti (*Figure 16*). Additionally, all analyses indicate a rather high Fe content which is typical of sapphire from a basaltic source.

Discussion

The experiments described above on pure synthetic sapphire with and without Be diffusion indicate that the brown coloration is due to the presence of Be. The Be-diffusion treatment in an oxidizing atmosphere did produce stable brown colour centres similar to those found earlier in the synthetic sapphire doped with Mg. However they
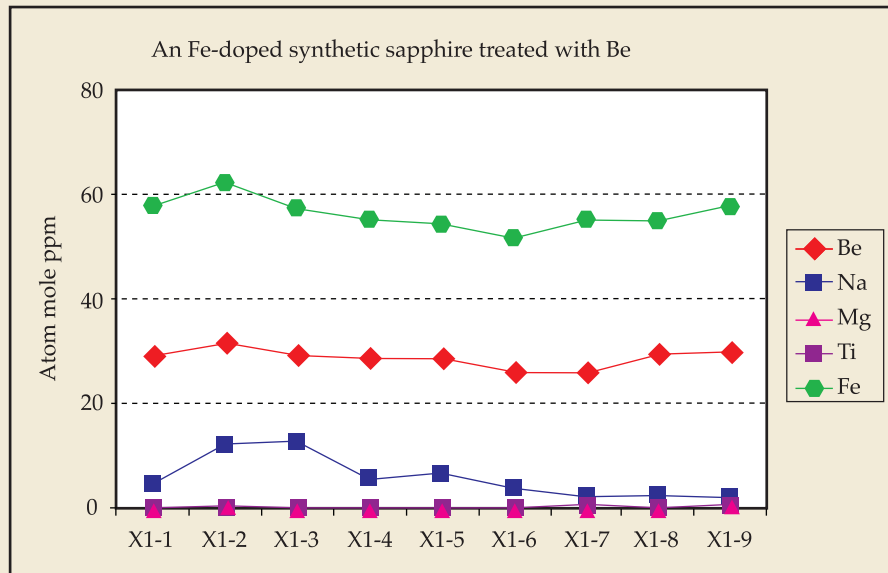
Figure 8: Trace element content along the traverse X1 of the Fe-doped synthetic sapphire treated with Be. The Fe and Be contents are constantly high across the cut surface; Mg and Ti contents are at or below the limits of detection.
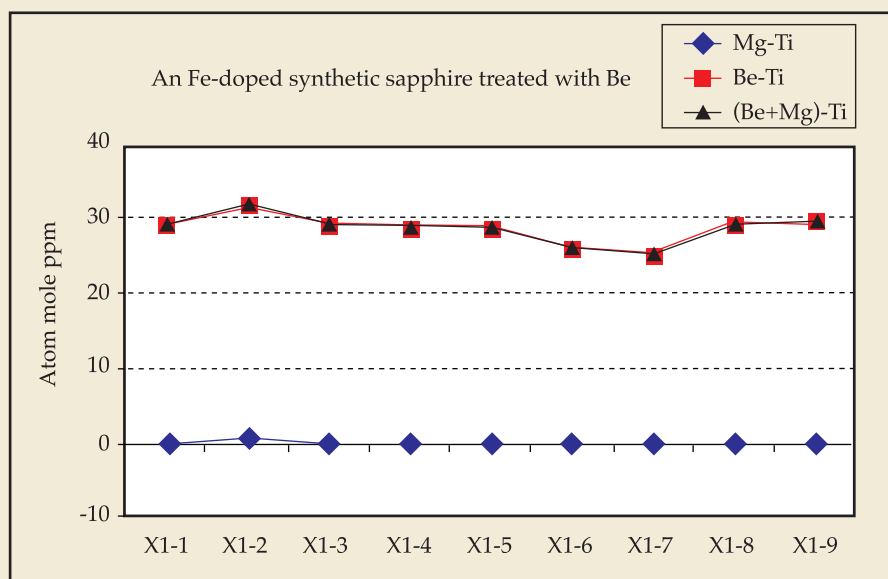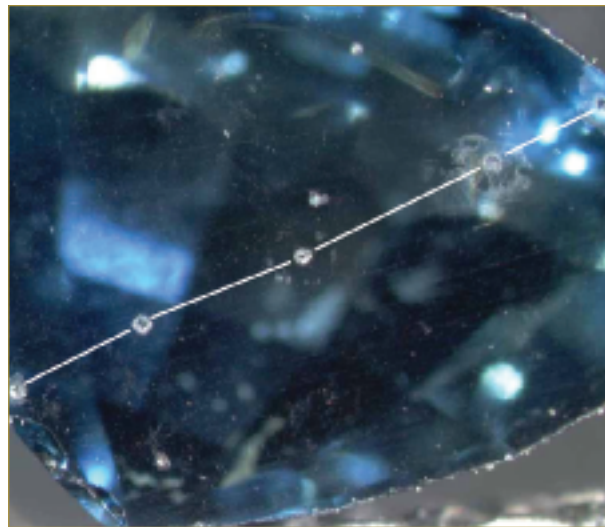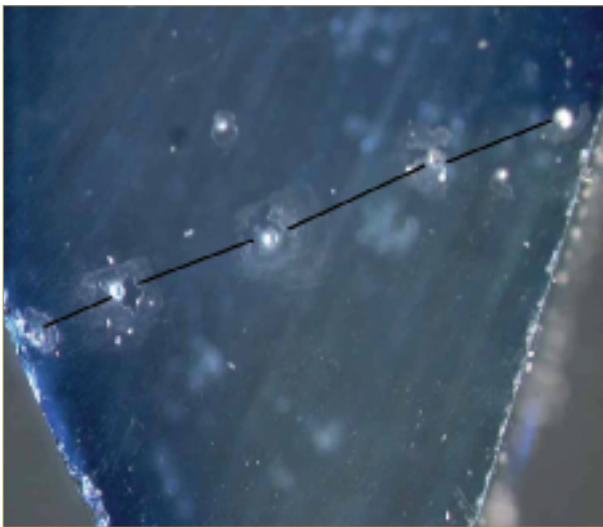
Figure 9: A natural blue sapphire (DIF1), reportedly simply heat-treated, was cut in half and the five points shown where LA-ICP-MS analyses were made (see Figure 10). Photo by P. Lomthong

Figure 11: Cut section of an Australian blue sapphire (AUS1) reportedly simply heat-treated. LA-ICP-MS analyses were carried out at the five points marked and data for Be, Mg and Ti shown in Figure 12. Photo by P. Lomthong.
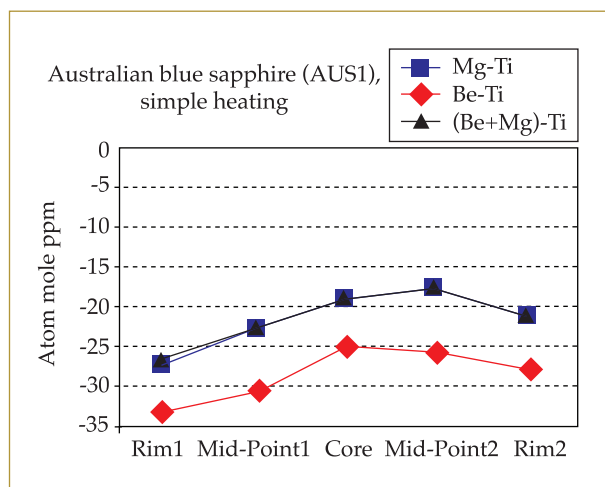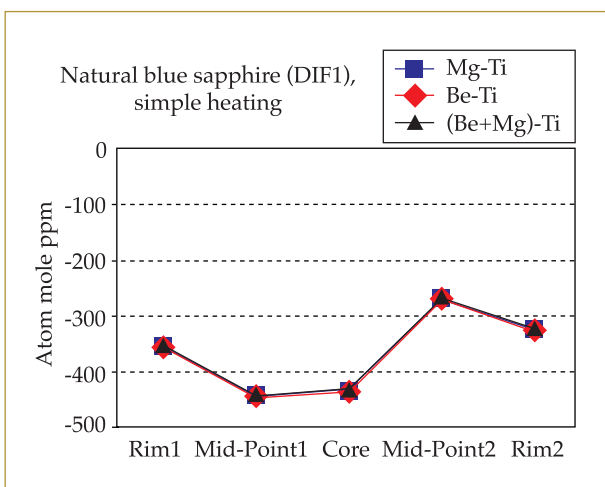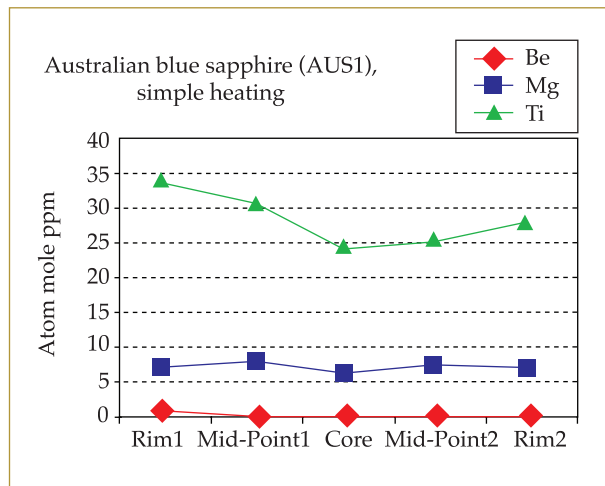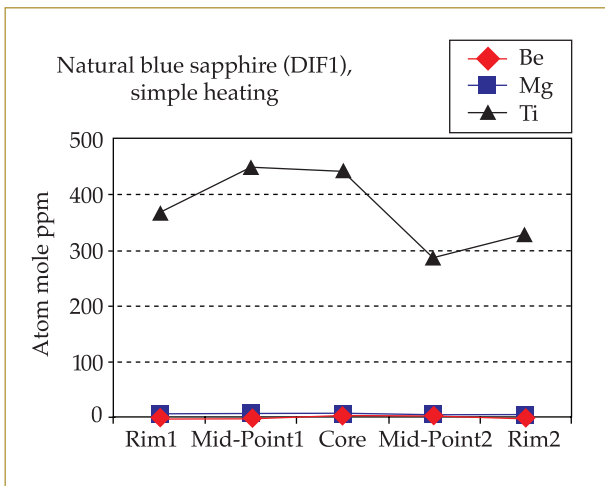
Figure 10: Plots of trace element content variation across the cut surface of the heat-treated blue sapphire (DIFI) shown in Figure 9. The anlyses show negligible contents of Be, Mg and Ti > Mg at all points analysed.

Figure 12: Contents of Be, Mg and Ti across the cut surface of the Australian blue sapphire (AUS1) shown in Figure 11. The analyses show negligible contents of Be, and Ti > Mg at all five points analysed.
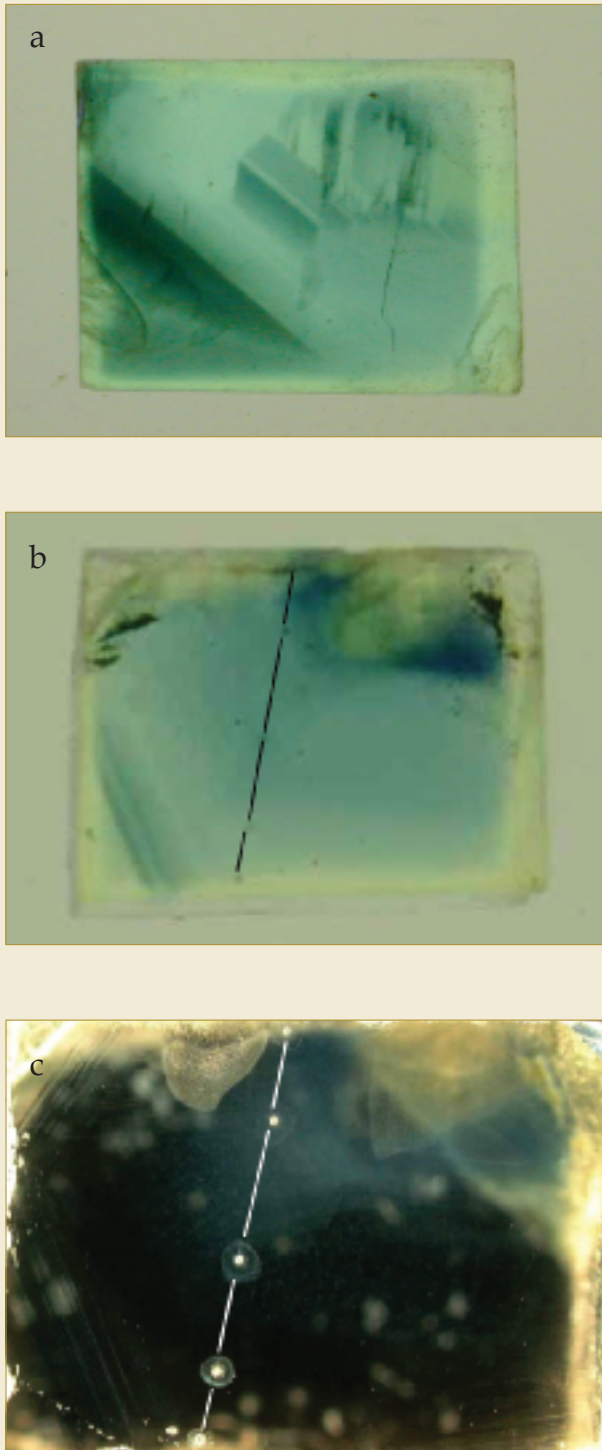
produce different absorption spectra with the main peak centred at around 420 nm for the Be-diffusion-treated sample and at around 450 nm for the Mg-doped sample (see Pisutha-Arnond *et al.*, 2004, Figure 28).

The experiments on the synthetic sapphire doped with Fe and afterwards diffusion-treated with Be indicate that the combination of Be+Fe in the Al_2O_3 system behaves in the same way as Mg+Fe. That is, when divalent Be in combination with Fe in the Al_2O_3 structure is heat-treated in an oxidizing atmosphere stable yellow colour centres are produced that are similar to those in synthetic sapphire double-doped with Fe and Mg. The spectrum produced by sapphire doped with Be+Fe or Mg+Fe might therefore be attributed to 'metal[2+]+Fe-related stable colour centres' while that produced solely by irradiation of Fe-doped sapphire could be referred to 'Fe-related unstable colour centres'.

In the natural blue sapphire subjected to normal heat-treatment described above (*Figures 9* to *12*), all the analysed points show Ti > Mg+Be. After calculation of $MgTiO_3$ and $BeTiO_3$ clusters, the excess Ti could form colour-active $FeTiO_3$ clusters or Fe-Ti intervalence charge transfer, which caused blue coloration of the stones.

In the Be-treated natural blue sapphire, all the analysed points in the blue core show an excess of Ti over Mg+Be content (i.e. after the calculation of $MgTiO_3$ and $BeTiO_3$ clusters). At the boundary of the blue core and the yellow rim there are elevated Be contents but the Ti contents still exceed the sum of Be+Mg (*Figure 14*). The excess Ti could therefore form colour-active $FeTiO_3$ clusters which cause blue coloration in the core area.

In contrast, at all the points analysed on the outer surface or rim of the stone (*Figure 15*) there is an excess of Be+Mg over Ti (*Figure 16*) and the colour is yellow. All the analysed points also indicate the presence of Fe which suggests that the excess of Be+Mg in combination with Fe in an oxidizing atmosphere have led to the formation of stable yellow colour centres. The blue sapphire (BG1) shown in *Figures 13* to *16*
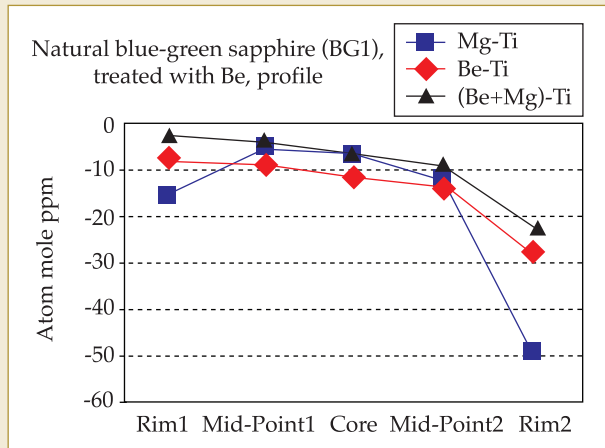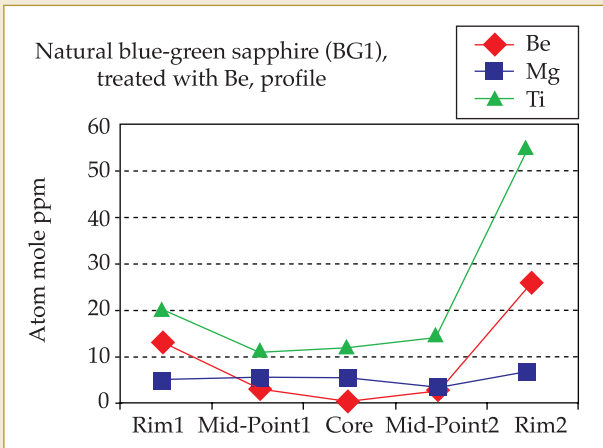
Figure 14: *Contents of Be, Mg and Ti at five points across the cut surface of the Be-treated blue-green sapphire (BG1)shown in Figure 13 (b* and *c). The Be contents are high at the rims and decrease toward the core. The analyses show Ti> (Be+Mg) in all the analysed points which are within the blue area.*
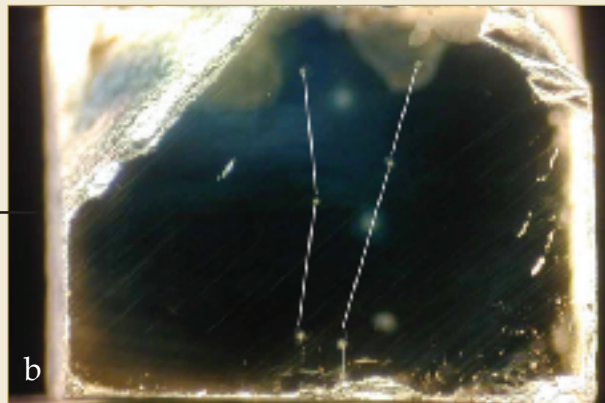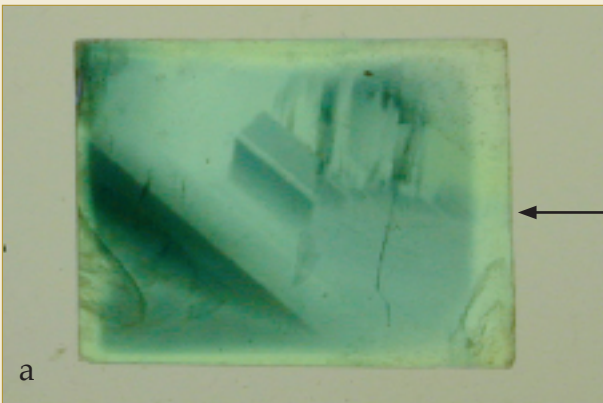
Figure 15: *(a) Rectangular block of Be-treated natural blue-green sapphire (BG1) shown in Figure 13(a). (b) is a view of the right face of (a), looking in the direction of the arrow and shows the locations of the seven analyses by LA-ICP-MS, all at the yellow surface of the Be-treated sapphire. Photos by C. Somboon.*
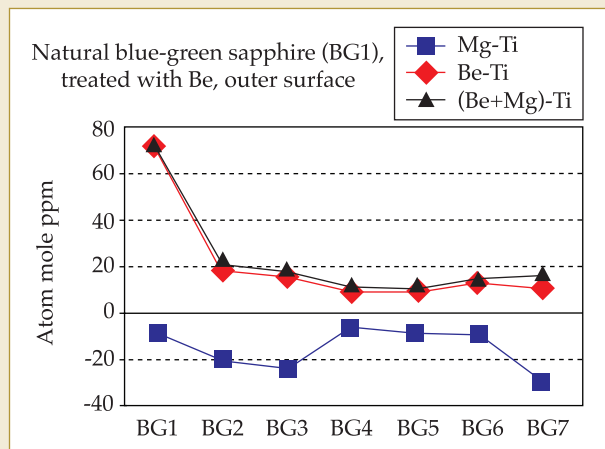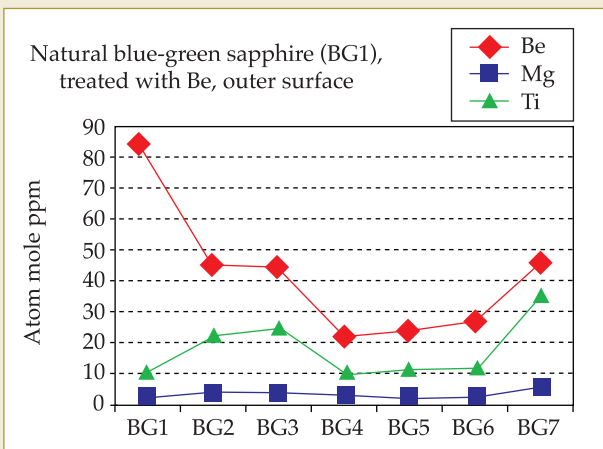
Figure 16: *Be, Mg and Ti contents at seven points on the outer surface of the Be-treated blue-green sapphire (BG1) shown in Figure 15. The analyses show variable contents of Be and Ti but Be content is generally high. So (Be+Mg) exceeds Ti at all points in the yellow rim and when plotted, the profile is clearly distinct from the profile of (Mg-Ti) points below the zero line.*

Figure 17: Approximate compositions of some treated sapphires discussed in this paper plotted on the triangular diagram proposed by Häger (1996). This model relates the colours in sapphires to their trace element content in an oxidizing atmosphere. Fe_{tot} Means $Fe^{2+}+Fe^{3+}$ and the field relates to the proportions of trace elements in a corundum host.
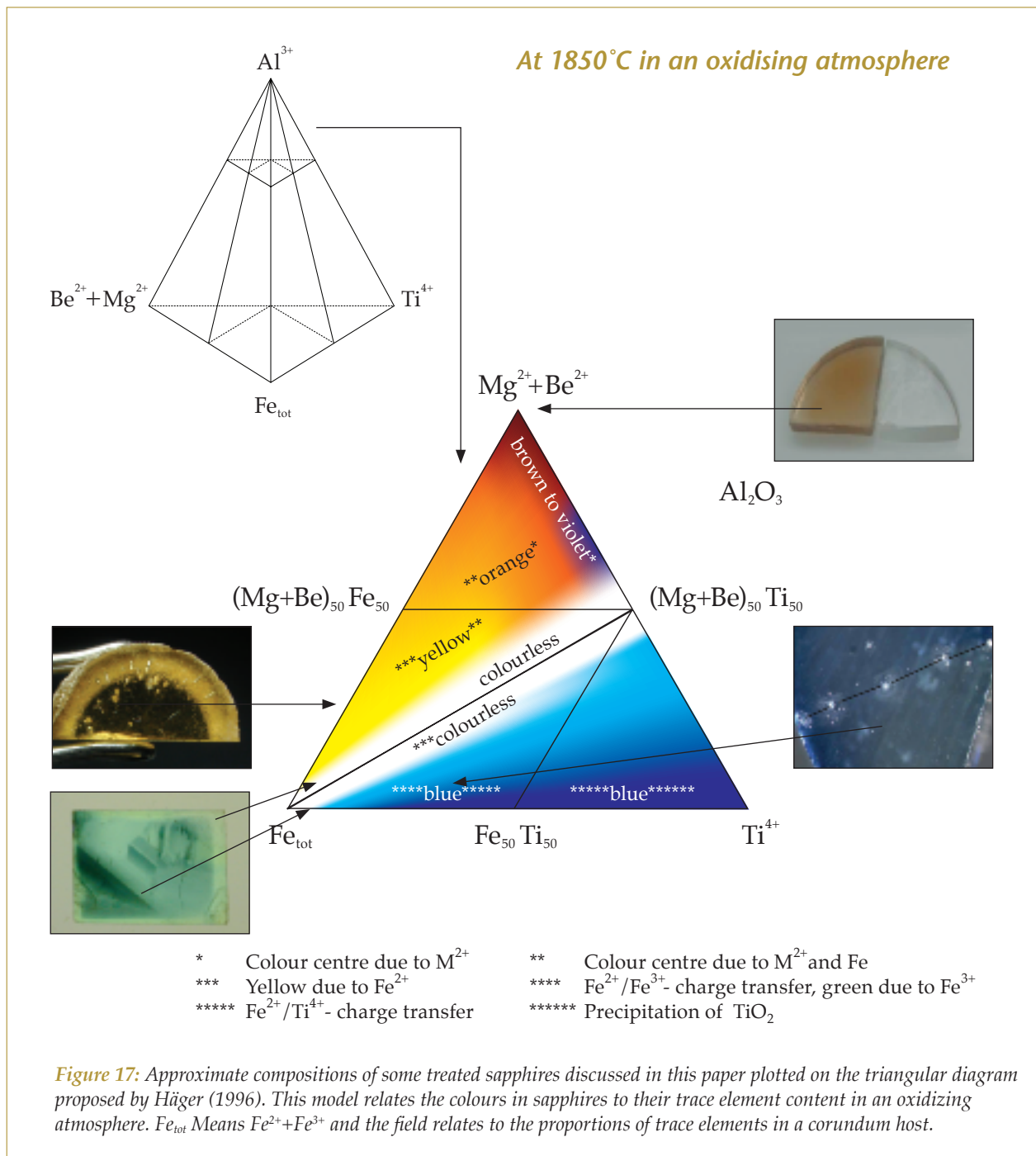
is another stone in which Ti exceeds the Mg content at all the analysed points. These data confirm that simple heat-treatment is unlikely to change a blue sapphire to yellow. But if the blue sapphire is subjected to diffusion of Be it is possible to increase the (Be+Mg) /Ti ratio and turn the rim yellow when the ratio exceeds 1.

Conclusion

If the results presented above are combined with those of Pisutha-Arnond *et al.* (2004),

it can be concluded that Be and Mg act in a very similar way in the 'pure' Al_2O_3 system although in the UV-Vis spectrum they produce absorption peaks at different wavelengths. In the Al_2O_3 system doped with Fe, addition of Be and Mg produces essentially similar results, as they do when the system also contains Ti. Thus, it is now valid to add Be into the Mg corner in the triangular diagram model proposed by Häger (1996 and 2001; see also Schmetzer and Schwarz, 2004). In so doing we can plot the approximate compositions of some treated

stones in the diagram as shown in *Figure 17*. The colours of these treated stones fit the model reasonably well.

Acknowledgements

References

Emmett, J.L., and Douthit, T.R., 1993. Heat treating the sapphires of Rock Creek, Montana. *Gems & Gemology*, **29**(4), 250-72

Emmett, J.L., Scarratt, K., McClure, S.F., Moses, T., Douthit, T.R., Hughes, R.W., Novak, S., Shigley, J.E., Wang, W., Bordelon, O., and Kane, R.E., 2003. Beryllium diffusion of ruby and sapphire. *Gems & Gemology*, **39**(2), 84-135

Ferguson, J., and Fielding, P.E., 1972. The origins of the colours of natural yellow, green, and blue sapphires. *Aust. J. Chem*, **25**, 1372-85

Fritsch, E., Chalain, J.-P., Hänni, H.A., Devouard, B., Chazot, G., Giuliani, G., Schwarz, D., Rollion-Bard, C., Garnier, V., Barda, S., Ohnenstetter, D., Notari, F., and Maitrallet, P., 2003. Le nouveau traitement produisant des couleurs orange à jaune dans les saphirs. *Revue de Gemmologie A.F.G.*, **147**, 11-23

Häger, T., 1992. Fargebende und ″farbhemmende″ Spurenelemente in blauen Saphiren. *Ber. Dt. Mineral. Ges. Beih. Europ. J. Mineral.* **4**, 109

Häger, T., 1993. Stabilisierung der Farbzentren von gelben natürlichen Saphiren. *Ber. Dt. Mineral. Ges. Beih. Europ. J. Mineral.* **5**, 188

Häger, T., 1996. *Farbrelevante Wechselwirkungen von Spurenelementen in Korund*: Ph.D. Thesis, University of Mainz, 170 pp

Häger, T., 2001. High temperature treatment of natural corundum. In: Hofmeister, E., Dao, N.Q., and Quang, V.X. (eds), *Proceedings of the International Workshop on Material Characterization by Solid State Spectroscopy: The Minerals of Vietnam*. Hanoi, Vietnam. April 4-10, 2001, 24-37

Hänni, H.A., 2002. Orange treated sapphire – towards finding a name for a new product. *Journal of the Gemmological Association of Hong Kong.* **23**, 23-9

Hänni, H.A., and Pettke, T., 2002. Eine neue Diffusions behandlung liefert orangefarbene und gelbe Saphire. *Gemmologie. Zeitschrift der Deutschen Gemmologischen Gesellschaft*, **51**(4), 137-52

McClure, S.F., Moses, T., Wang, W., Hall, M., and Koivula, J.I., 2002. A new corundum treatment from Thailand. *Gems & Gemology*, **38**(1), 86-90

Norman, M.D., Pearson, N.J., Sharma, A., and Griffin, W.L., 1996. Quantitative analysis of trace elements in geological materials by laser ablation ICPMS: instrumental operating conditions and calibration values of NIST glasses. *Geostandards newsletter*, **20**, 247-61

Peretti, A., and Günther, D., 2002. The color enhancement (E) of fancy sapphires with a new heat-treatment technique. (Part A): Introducing color zoning by internal (I) migration (M) and formation of color centers. *Contributions to Gemology*, **1**, 1-48

Peretti, A., Günther, D., and Graber, A.L., 2003. The beryllium treatment of fancy sapphires with a new heat-treatment technique (part B). *Contributions to Gemology*, **2**, 21-33

Pisutha-Arnond, V., Häger, T., Wathanakul, P., and Atichat, W., 2004. Yellow and brown colouration in beryllium treated sapphires. *Journal of Gemmology*, **29**(2), 77-103

Pisutha-Arnond, V., Wathanakul, P., Atichat, W., Häger, T., Win, T.T., Leelawatanasuk, T., and Somboon, C., 2003. Beryllium-treated Vietnamese and Mong Hsu rubies. In: Hofmeister W., Quang V.X., Doa N.Q., and Nghi T. (eds). *Proceedings of the 2nd International Workshop on Geo- and Material-Science on Gem-Minerals of Vietnam*. Hanoi, October 1-8, 2003, 171-5

Schmetzer, K. and Schwarz, D., 2004. The causes of colour in untreated, heat treated and diffusion treated orange and pinkish-orange sapphires - a review. *Journal of Gemmology*, **29**(3), 149-82

Schmetzer, K., and Schwarz, D., 2005. A microscopy-based screening system to identify natural and treated sapphires in the yellow to reddish-orange colour range. *Journal of Gemmology*, 29(7/8), 407-49

Themelis, T., 2003. *Beryllium-treated rubies and sapphires*. Bangkok, 48 pp

Townsend, M.G., 1968. Visible charge transfer band in blue sapphire. *Solid State Commun.*, **6**, 81-3

Wang, H.A., Lee, C.H., Kroger, F.A., and Cox, R.T., 1983. Point defects in Alpha- Al_2O_3: Mg studied by electrical conductivity, optical absorption and ESR. *Physical Review B*, **27**, 6, 3821-41

A new find of sapphire placer deposits on Nosy-Bé, Madagascar

Dr Reinhard Ramdohr[1] and Dr Claudio C. Milisenda[2]

1. *Consulting Geologist, P.O.Box 101124, D-69451 Weinheim, Germany.*
   Email: reinramdohr@yahoo.com
2. *Deutsche Stiftung Edelsteinforschung (DSEF), Prof.-Schlossmacher-Str.1,*
   D-55743 Idar-Oberstein, Germany. Email: info@gemcertificate.com

Abstract: *The north of Madagascar is rich in corundum occurrences. Late Mesozoic basaltic extrusions have brought with them many corundum xenocrysts, which can be found now in various types of placer deposits. A new deposit on Nosy-Bé is described and compared with the occurrences on the Ambato peninsula and at Ambilobe, NE Madagascar. Sapphires are found mainly in the alluvium of small creeks. Searching and exploration is largely done by local villagers, who mine selectively in creek beds. Although up to 20 ct/m³ are found, the size of the deposit does not appear to suffice for a large scale mining operation. The bulk of the corundum recovered is opaque. A minority of stones can be enhanced by heat treatment. Their gemmological characteristics correspond to those found in sapphires from basaltic-type deposits.*

Keywords: *corundum, gemmological characteristics, geology, Madagascar, placer deposits*

Introduction

Madagascar is well known for its many gemstone deposits. There are countless occurrences of virtually all types of gemstone, with the exception of diamonds. In the past ten years much sapphire has been found in the NE of Madagascar (*Figure 1*). The recent discoveries of sapphires in the region between Ambilobe and Antsiranana, the former Diego Suarez have been described by Superchi *et al*. (1997) and Schwarz *et al*. (2000). There, sapphires are found in karsts of the Ankarana limestones. At the centre of the mining activity, which sprung up in the last six years, are the villages Andranonakoho and Ambondromifehy, some 38 and 43 km, respectively, NE of Ambilobe.

The source of the sapphires has been identified as the basalts of the Massif d' Ambre. They are of Pliocene or Quaternary age. These basalts brought with them corundum, some of which is of gem-quality. With erosion of the basalts, the sapphires were transported by streams and eventually accumulated in fractures in the underlying limestone (*Figure 2*). Extraction and recovery of the gemstones in this environment is rather strenuous and quite dangerous for the miners (*Figures 3* and *4*).
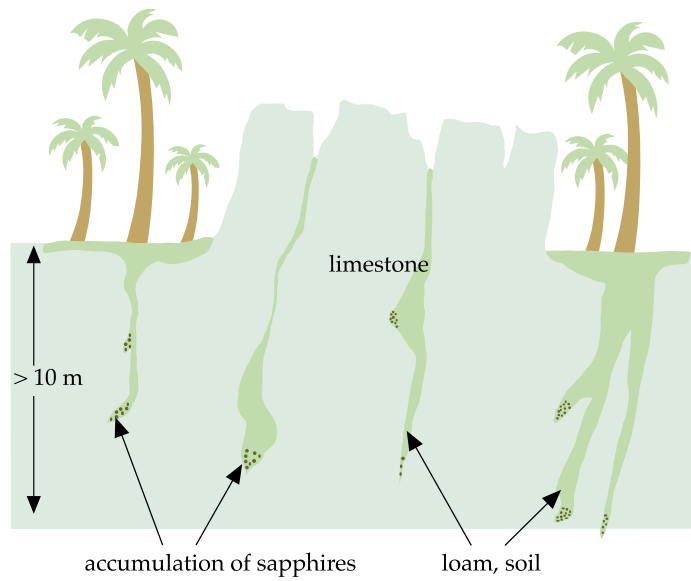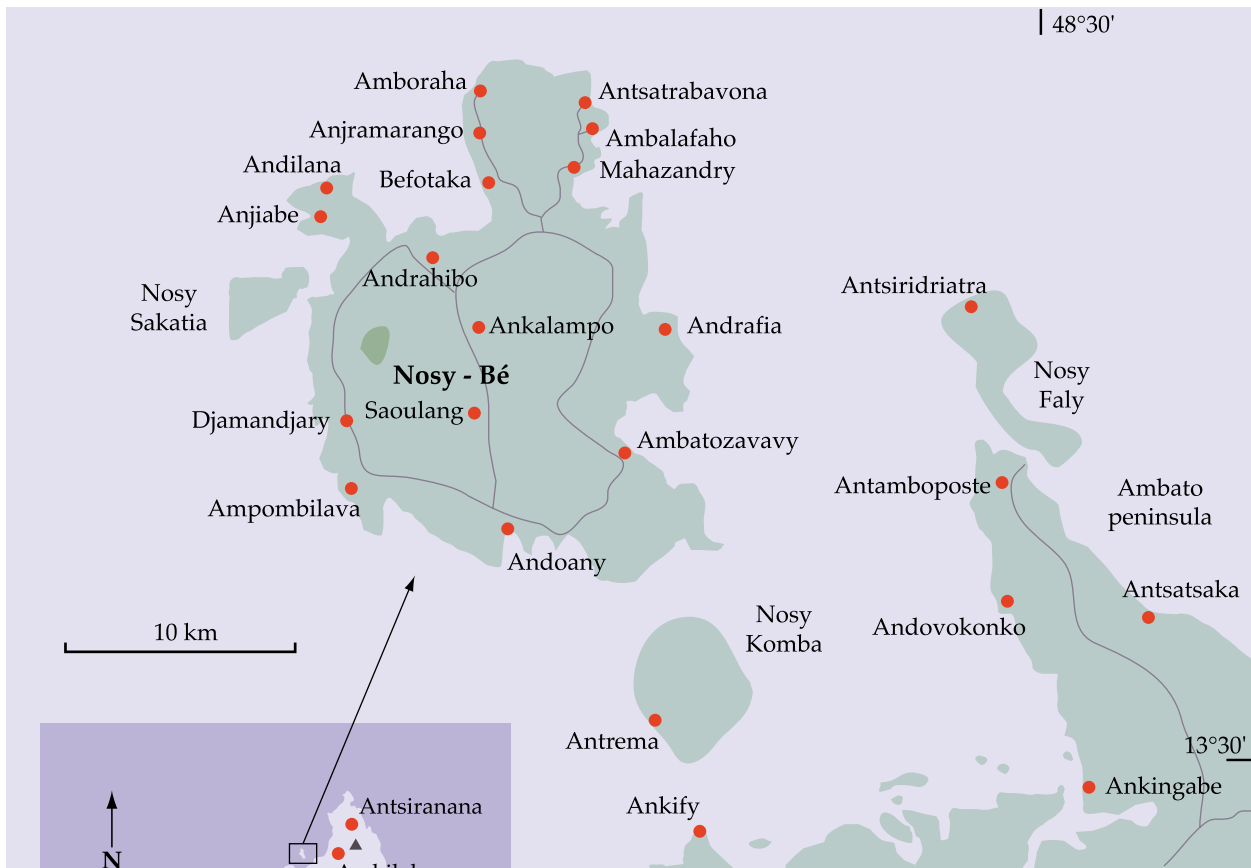
Figure 1: Simplified geographical map of northern Madagascar showing the sample localities at Befotaka on Nosy-Bé island and Andovokonko on Ambato peninsula. The inset shows the well-known sapphire occurrences in the North between Ambilobe and Antsiranana (Ambondromifehy) and in the South at Ilakaka and Andranondambo.

Figure 2: Simplified cross-section, showing the accumulation of sapphires in limestone karst, NE of Ambilobe, northern Madagascar. Weathering and rain water dissolve limestone along joints and cracks; this enlarges them and they are then filled with detrital minerals and soils.

Recent discoveries of sapphires and zircons on the Ambato peninsula and on Nosy-Bé demonstrate the widespread occurrence of these precious stones in traps and placers and have enabled a fuller understanding of their formation. The following description deals largely with the deposit on northern Nosy-Bé with some comments on the occurrences at Andovokonko, Ambato peninsula.

Figure 3: A miner showing loam containing sapphire, recovered from karst cavities.

Figure 5: Crater lakes, northern Nosy-Bé.

Figure 4: Women and children wash the sapphires from the loam.

Figure 6: Sedimentary layers of basaltic tuff and lapilli.

Regional geology

Basement rocks, probably ranging from Archaean to Proterozoic in age, are quite common in Madagascar, but have not been encountered on the northern part of Nosy-Bé. There the rock succession begins with Lias sediments, largely sandstones, intercalated with argillites and marls. These sediments have been intruded by syenites and microgranites. During this process, the sediments have been folded and deformed and now dip 35° to 55° to the N or to the S, and generally strike 70° to 90°.

On top of the sediments, a sequence of mafic lavas and tuffs of basanitic and phono-tephritic composition yield K – Ar ages of 7.32 Ma and 10.15 Ma, respectively (Melluso and Morra, 2000). These ages, however, do not match with geological field observations. The sequence of lavas and tuffs (with many lapilli) found on Nosy-Bé is generally loose, uncompacted and very vulnerable to erosion, as can be seen in the landforms around the crater lakes shown in *Figure 5*. Such loosely packed material erodes rapidly in a tropical climate with heavy rainfall (*Figure 6*). It is possible that these volcanic rocks are not older that 0.1 Ma.

Mineral assemblages

The commonest heavy minerals are iron oxides and minor ilmenite, with zircon and sapphire, and these are concentrated in parts of the river beds. The iron oxides consist of very fine grains and form 'black sands'; they are noticeable in the washing pan as 'tails' only, while the precious minerals are usually of millimetre size and larger. Much of the corundum is up to 5 mm across but some specimens can reach 30 mm in diameter. Zircons and sapphires are generally angular to subangular with little evidence of rounding, indicating short transport distances. Sapphire comprises >40% of the recovered stones and should be described as 'coloured corundum' since it is usually fractured, more or less opaque and not of gem-quality.

Some olivine has also been found, and could readily be mistaken for green sapphire, if not examined carefully. Zircons are described as opaque hyacinth (*Figure 7*) and are not of commercial interest.

Characteristics of the sapphires

The sapphires may be blue, blue-violet, greenish-blue, greenish-yellow or yellow and, as such, represent a characteristic basaltic-type sapphire suite, comparable to those from Australia, Nigeria, Thailand, Laos and Cambodia. Sutherland *et al.* (1998) referred to them as 'BGY (blue-green-yellow) sapphire'. Although most rough material is corroded, some long-prismatic, six-sided, barrel-shaped crystals have also been found. Most of the stones showed a distinct colour-zoning, some with bicoloured (blue-yellow) and others with tricoloured (blue, green-yellow, yellow) patterns.

Refractive indices and specific gravities fall within the known ranges for the mineral species corundum. n_o varies between 1.760 and 1.765 and n_e between 1.768 and 1.773 with a maximum birefringence of 0.008. The SGs, determined with a hydrostatic balance, range from 3.98 to 4.03. The sapphires were inert under both long and short wave UV.

Figure 7: Group of zircon hyacinth crystals between two groups of differently coloured sapphires.
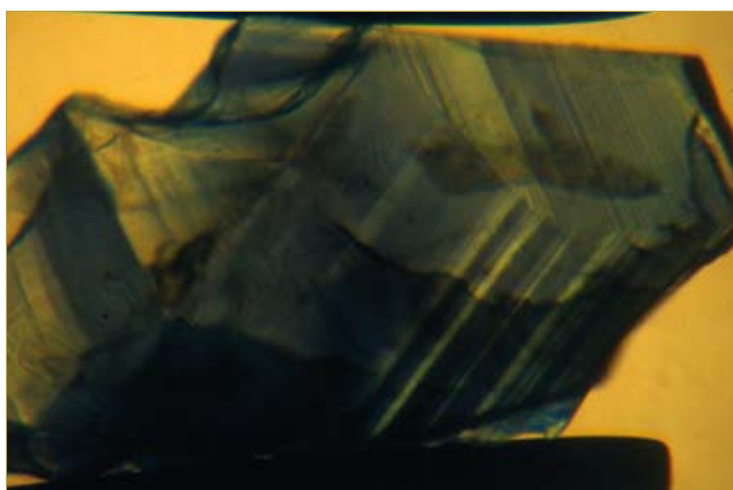
Figure 8: Intense colour zoning and growth structure form a typical inclusion pattern in the sapphires from northern Madagascar. Immersion, transmitted light, field of view 3 mm.
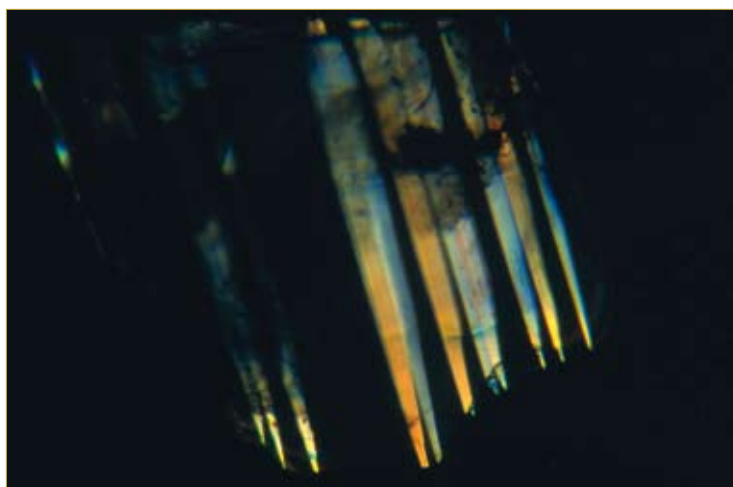
Figure 9: Distinct twinning lamellae in a sapphire from northern Madagascar. Immersion, transmitted light, crossed polars, field of view 2 mm.
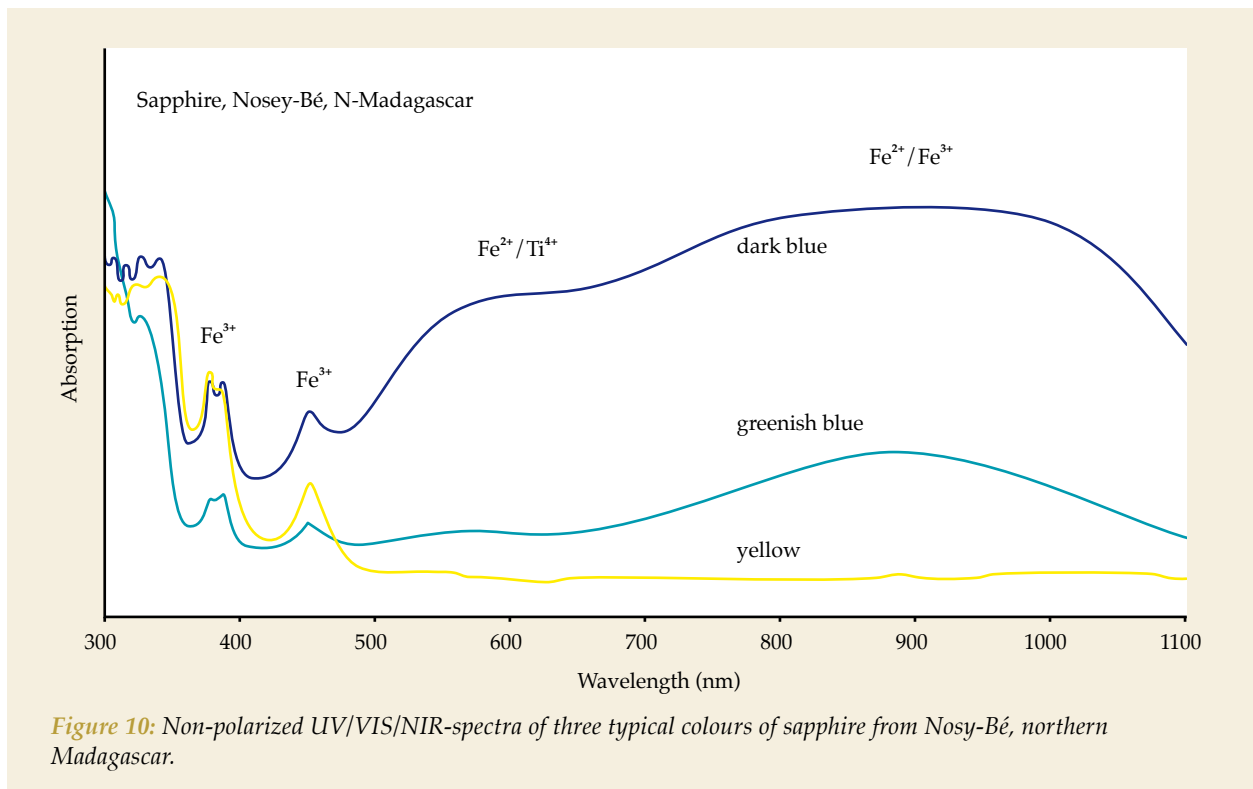
Figure 10: *Non-polarized UV/VIS/NIR-spectra of three typical colours of sapphire from Nosy-Bé, northern Madagascar.*

The most characteristic inclusion pattern is a distinct growth- and colour-zoning (*Figure 8*), which in most stones is visible with the naked eye. Twinning lamellae are also commonly present (*Figure 9*). In addition, healing planes and minute birefringent mineral inclusions have also been found. The absorption spectra of the samples investigated are typical of basaltic-type corundum (*Figure 10*). Irrespective of the colour, all spectra show distinct absorption bands due to trivalent iron at 376, 388 and 450 nm. The blue and greenish-blue specimens show an additional Fe^{2+}/Ti^{4+} charge-transfer band at 580 nm and a Fe^{2+}/Fe^{3+} charge-transfer band with a maximum near 850 nm, which is characteristic for basaltic-type sapphires. These spectra are comparable to those found in sapphires from other occurrences in northern Madagascar and distinct from the metamorphic-type sapphires from the southern part of the island (cf. Milisenda *et al.*, 2001).

Genesis of the placer deposits

At Nosy-Bé, the classical process of the formation of placer deposits can be observed:

erosion, alluvial transport and early deposition of heavy minerals. The primary occurrence of corundum in a host rock has not yet been found, but there is no doubt that it was brought to the surface with alkaline basalts, which themselves originate from the Earth's mantle. According to Sutherland and Schwarz (2001) corundums associated with basalts crystallized in a syenitic melt within metasomatised mantle at formation temperatures estimated to be around 1000°C. Melluso and Morra (2000) calculated a depth of the sapphire source of 60 to 80 km.

The basalt at Nosy-Bé has been largely eroded, similar to the basalt associated with the sapphire deposits near Ambilobe, in the Antsiranana Province of northern Madagascar. In late Tertiary (?) or Quaternary times, the fractured and porous basalt flows and tuffs on Nosy-Bé had been eroded rapidly during severe rains and subsequent floods. The heavy mineral fraction of the washed-out material was transported towards the sea but deposited at the foot of the hills and on the alluvial plains as soon as the speed of the rivers slowed down. The heavy mineral assemblages are found in thin layers, irregularly distributed within coarse-grained sand and pebble horizons as well

as directly above the basement rocks. There are indications that some of the placers have been reworked.

The deposit at Befotaka started quite recently and is still in the formation process; the small river near the village is transporting debris towards the sea, forming a mini-delta which is gradually expanding. During severe floods, heavy minerals are transported further than normal and deposited near the expanding shore line. We thus have the situation that placers are found at the foot of the hills, under several metres of loamy overburden and in the deeply carved river bed, while at the shore line traces of heavy minerals are noticed at the surface, because the lighter fraction is washed out to the sea.

On Ambato Peninsula sapphires have accumulated on uneven basalt surfaces (*Figures 11* and *12*).

Prospecting procedure

Like so many discoveries of ore deposits and mineral occurrences the sapphire strikes at Befotaka and Ambato Peninsula are not the result of systematic prospecting but rather of diggings by local inhabitants, presumably stimulated by other finds on the main island of Madagascar (*Figures 12* and *13*).

On Nosy-Bé, people working in rice paddies at the little river at Befotaka noticed some glittery stones, which they gave to experienced dealers for assessment. Quickly the potential of the area was recognized and random mining began. Sapphires and zircons were recovered from the river bed and small shafts were sunk in the river bank (*Figure 14*). The work soon yielded several kilograms of precious stones and word of the find spread.

One of the authors (RR) was then approached by the local dignitaries to study the area, assess the potential and give advice on exploitation of the deposit.

After some field studies an opinion had to be formed about the geological setting of the occurrence. The area is covered by thick vegetation, particularly in the valleys, and lack of funds precluded clearing of undergrowth, gridding, trenching and shaft-sinking, so the
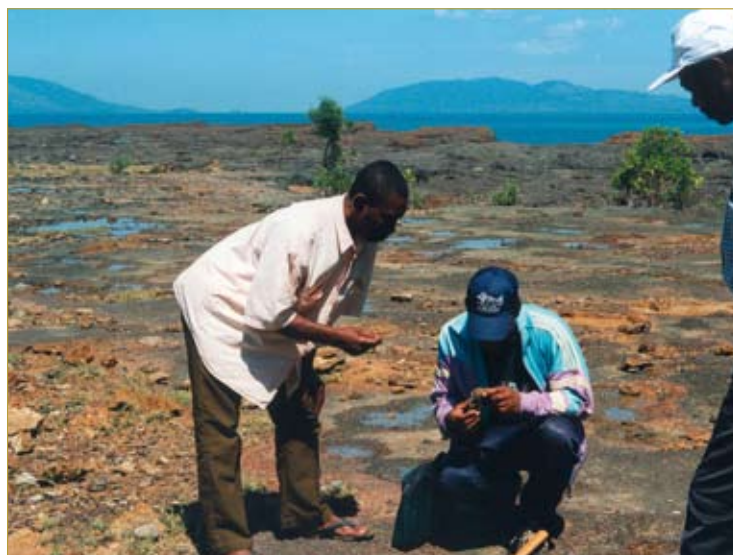
Figure 11: Andovokonko, Ambato Peninsula. Searching for sapphires on the basalt surface with calcrete crust. Nosy-Bé is in the background.

Figure 12: Ambato Peninsula Woman prising loose sapphire on basalt surface in tidal flats.

Figure 13: Searching for sapphires under granite boulders
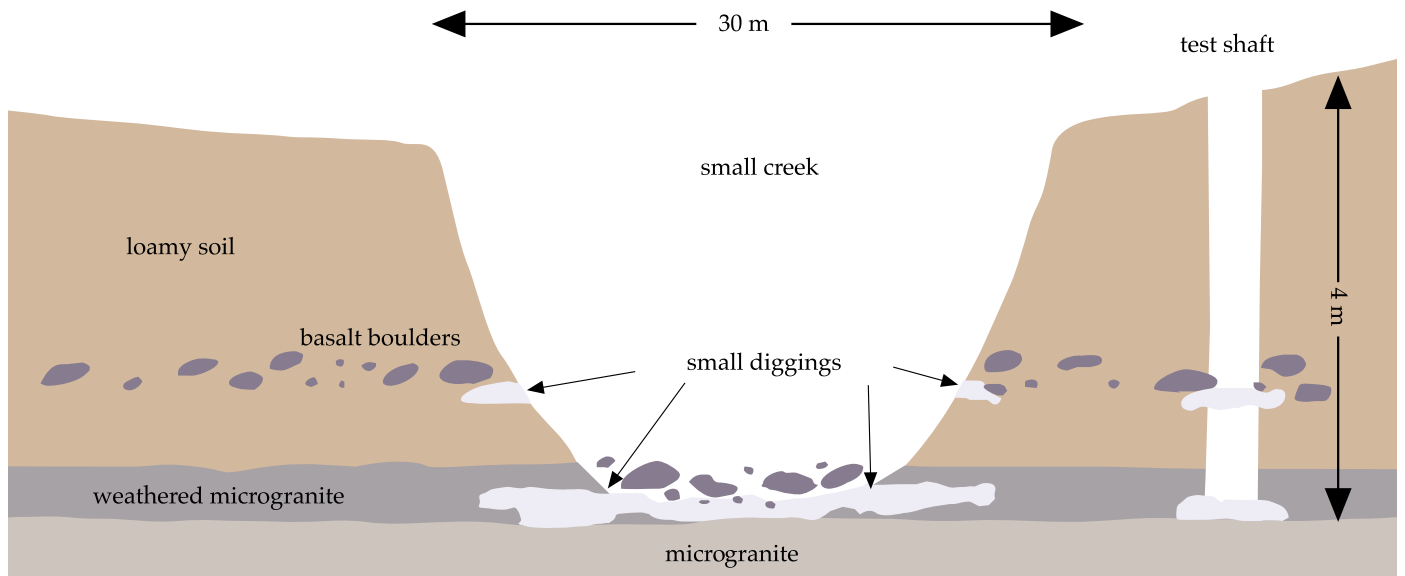
Figure 14: Cross-section of creek bed with workings for sapphire.

30 m

test shaft

4 m

small creek

loamy soil

basalt boulders

small diggings

weathered microgranite

microgranite

Section 1

scale 1: ≈ 25.000

sandstones, marls and argillaceous rocks (Lias)

intruding alkaline microgranite

Section 2

eroded surface (Tertiary)

Section 3

Quaternary (?) basalt flows and tuffs

?
?
?

Section 4

crater lake

recent surface

?
?
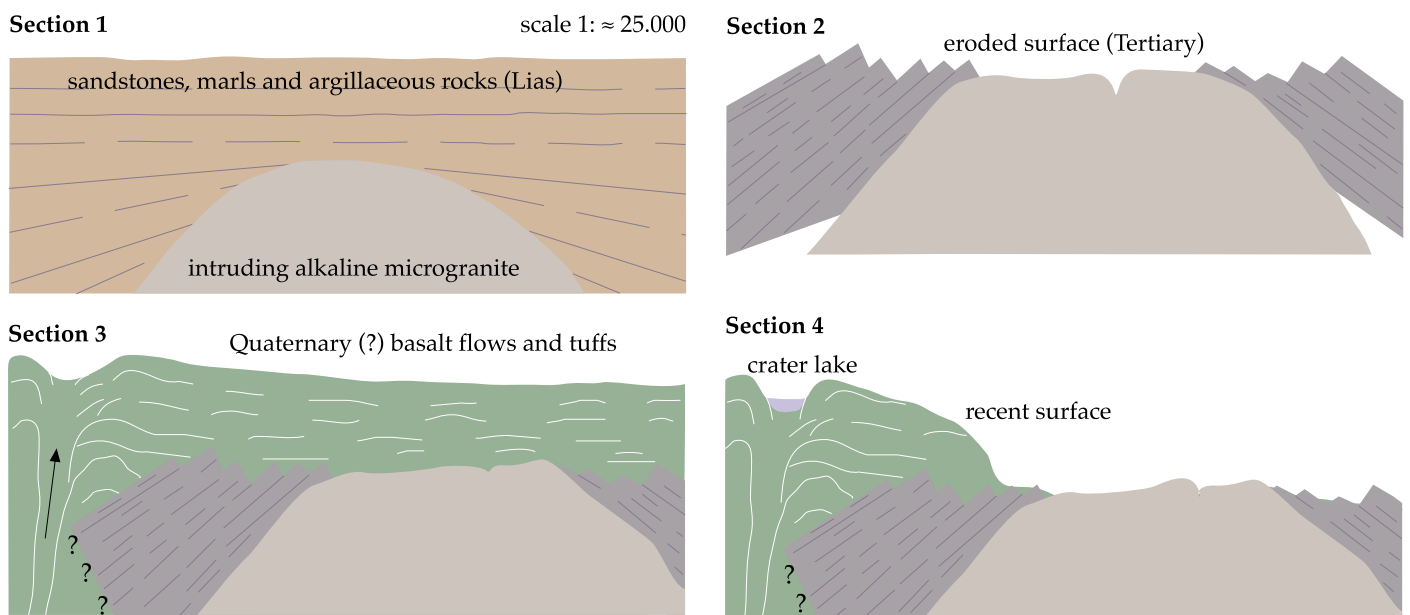
Figure 15: Sequence of cross-sections explaining the probable geological history of northern Nosy-Bé, with Section 4 representing the present day.

entire area of some 5 × 5 km was covered on foot. This gave an adequate understanding of the geology and mineral occurrences.

The 'core' of the peninsula is a (micro-) granitic batholith, overlain by Liassic sandstone, argillaceous sandstone and Tertiary to Quaternary (?) basalts (*Figure 15*). Systematic sampling of stream sediments and panning for heavy metals was done in the creeks. Corundum and zircon were found only in a few places and could not be traced to any source rock. These two minerals were also found on strongly weathered surfaces of the granite. Both minerals can also be found trapped under boulders in a clay matrix directly above the granite (*Figure 16*). The Lias sediments are steeply dipping and form small cliffs,

Figure 16: Befotaka, Nosy-Bé. Sapphire-bearing horizon above the granite.

Figure 17: Steeply dipping Lias sediments.

and they were searched for corundum and zircon, but only the heavy iron oxides were found (*Figure 17*). Based on these observations, work concentrated on the search for sapphires in the zone above the granite and on the eroded basalt platforms at sea level. This approach proved successful. In this rough terrain with its rather steep morphology, only a few river valleys and

the coastal plains have potential, and although precious stones were found quite frequently, only at one place near Befotaka, were they in significant quantities. Apparently only there was the basalt large enough for the river to do its work and concentrate sufficient stones to form a commercially viable deposit. In other areas the basalt cover might have been thinner or poorer in corundum or perhaps the valuable stones have simply been washed away. The conclusion is that commercially interesting zones are largely confined to the alluvium of one small river (*Figure 18*). Further, quantitative evaluation of the deposit must be done with suitable equipment such as a backhoe for trenching and submersible pumps for water drainage.

Commercial aspects

The prospecting for sapphires in the vicinity of Befotaka has confirmed the existence of recent placer deposits concentrated in a layer above the granite bedrock. The extent and grade of the deposits have not been assessed in the usual terms of 'certain, probable, possible' because a professional valuation would require systematic trenching, bulk sampling, sorting of sapphires and additional tests on the reaction of the stones to thermal enhancement. However, a start has been made which enables us to make the following comments regarding commercial aspects.

Samples taken randomly from the placers have contained sapphires in concentrations up to 20 ct/m^3 with stone sizes up to 15 ct. In contrast, the loamy overburden yielded <3 ct/m^3. The pisolithic gravel C – horizon above the weathered granite surface has intermediate concentrations and probably contains >10 ct/m^3.

The creek bed sand and gravel, similar in its composition to the horizon struck in the few test pits, gave comparable results. Small sapphires appeared to be randomly distributed, while larger specimens (>0.5 ct) and good quality pieces are found directly at the uneven surface of the bedrock. There the precious stones and other heavy minerals accumulate in small traps such as crevices in the bedrock and underneath boulders. The local miners are

a

sapphires (?)

basalt

Lias sandstone

weathered surface
loam, soil

b

creek bed

sapphires

granite

c   (calcrete) crust on basalt flow

sapphires

d   recent shore line

sapphires

?

?
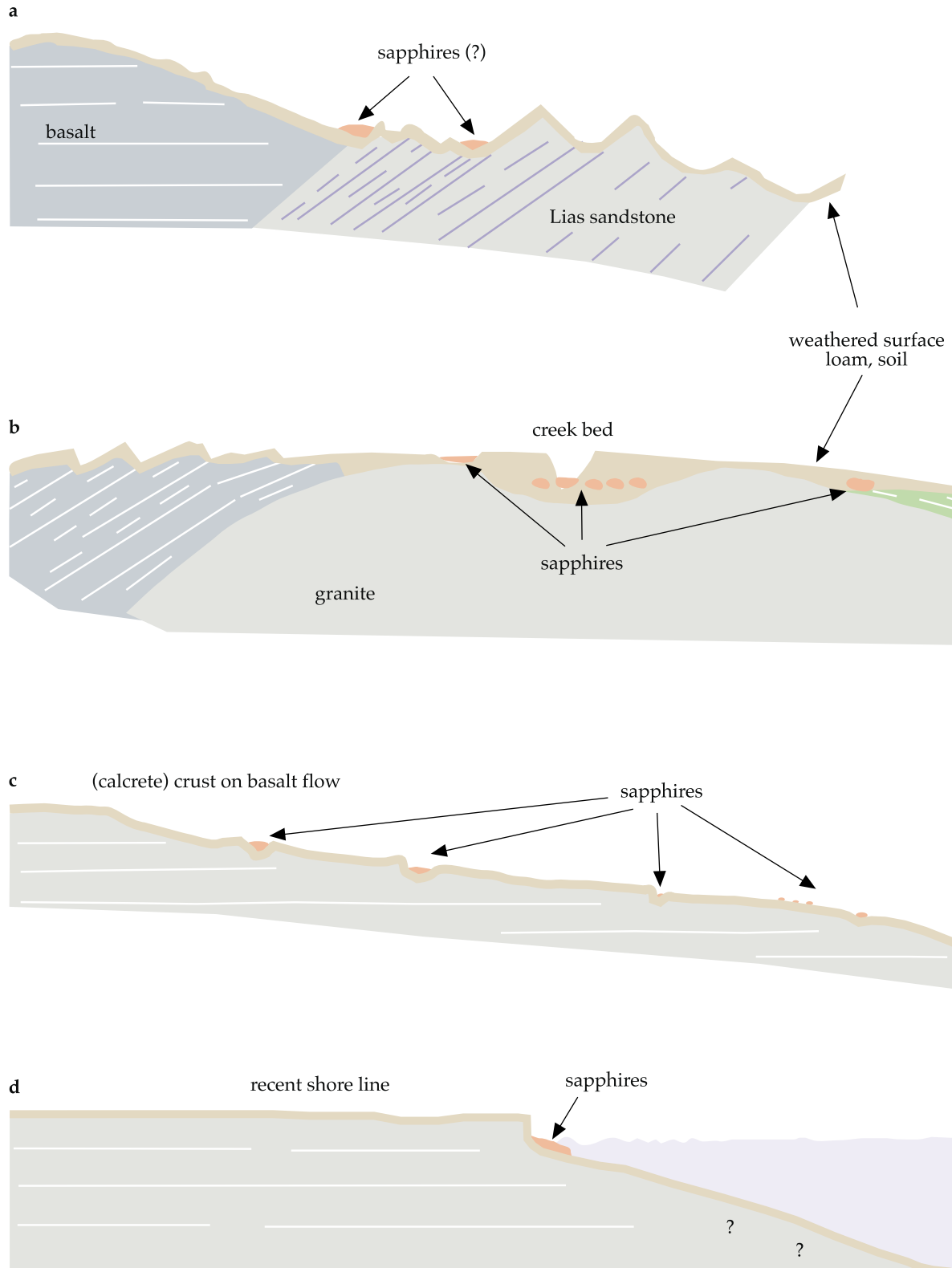
Figure 18: Schematic cross-section, showing traps and placers containing sapphires (a+b: Befotaka, Nosy-Bé, c+d: Andovokonko, Ambato peninsula).

aware of this and carefully search the creek bed for those traps, often using simple tools to prise stones from the ground. In a commercial mining operation this would be done by water jets (*Figure 19*).

The recovered corundum ranges from opaque or dark to beautiful blue and transparent. If the sapphire population is comparable to that at Ambilobe, Antsiranana Province, we can assume that to be marketable, some 90% of translucent samples require thermal enhancement. Samples with a grey, milky appearance and containing a certain amount of Ti in the form of rutile needles are best suited for this treatment. After treatment at around 1800° C under reducing conditions they should show a good sapphire blue.

To obtain more realistic figures for recovery costs it is recommended to use ct/m^2 surface rather than ct/m^3 of placer deposit. If one assumes a recovery of 20 ct/m^2, of which 8 ct (40%) can only be used for cabochons, this leaves 12 ct (60%) to be sapphire of good quality; such a proportion would justify heating to enhance their value. Of this, some 5 ct of faceted stones could be cut.

The crucial question of market value of course depends on the market, which varies, but one could estimate, based on recent experience, that the production of untreated rough stones directly from the mine should bring > 25 US$ per m^2 of mined surface.

All these are assumptions and no large or medium scale mining should be started without a proper feasibility study, based on accurate figures for reserves, grade, quality of stones, and market prices. In spite of this, a mining company has recently commenced work in the area, and one hopes that lessons learned from previous gemstone booms and sudden collapses are not ignored. As quickly as new mining centres can spring up, so can they vanish. Once surface deposits have been exploited and/or mining below the water table is required, the migrating miners move on…and with them the dealers. Left behind are ghost towns (*Figures 20* and *21*), a testament to a short-term view of local resources and, perhaps, a stimulant to thoughts of more long-term development.

Figure 19: Example of medium-sized mining and treatment operation (near Ilakaka, S Madagascar).

Figure 20: Huts for buying and selling of rich sapphire lots are quickly set up…

Figure 21: …and equally as quickly abandoned.

References

Melluso, L., and Morra, V., 2000. Petrogenesis of Late Cenozoic mafic alkaline rocks of Nosy-Bé archipelago (northern Madagascar); relationships with the Comorean magmatism. *Journal of Volcanology and Geothermal Research*, **96**, 129-42

Milisenda, C.C., Henn, U., and Henn, J., 2001. New gemstone occurrences in the south-west of Madagascar. *Journal of Gemmology*, **27**(7), 385-94

Schwarz, D., Kanis, J., and Schmetzer, K., 2000. Sapphires from Antsiranana Province, Northern Madagascar. *Gems & Gemology*, **36**(3), 216-33

Superchi, M., Donini, A., Muzzioli, D., and Roman, E., 1997. Sapphire occurrences at Ambondromifehy in the Antsiranana Province, North Madagascar. *26th International Gemmological Conference, Idar-Oberstein, Abstract volume*, 62-3

Sutherland, F.L., Hoskin, P.W.O., Fanning, C.M., and Coenraads, R.R., 1998. Models of corundum origin from alkali basaltic terrains: A reappraisal. *Contr. Min. Petrol.*, **133**(4), 356-72

Sutherland, F.L., and Schwarz, D., 2001. Origin of gem corundums from basaltic fields. *Australian Gemmologist*, **21**, 30-3

Chrysocolla quartz from the Bacan Archipelago, South Halmahera Regency, North Maluku Province, Indonesia

H.C. Einfalt[1] and H. Sujatmiko[2]

1. *Friedenstr. 46, D 75015 Bretten, Germany, Email:* hcv.einfalt@gmx.de
2. *Jalan Pajajaran 128, Bandung 40173, Indonesia, Email:* miko@melsa.net.id

Abstract: *Chrysocolla quartz from South Halmahera occurs in a series of basaltic pillow lavas as veins and small pods. A brief account is given of the geology, mining procedure and current processing facilities, supplemented by information on gemmological characteristics, mineralogical composition and internal textural pattern. The chrysocolla quartz is cut as cabochons which range in colour from sky blue to bluish green, uniform or mottled in appearance due to the proportion of chrysocolla and the intergrowth pattern with quartz and chalcedony. Apart from common opaque spots of native copper and cuprite and very little malachite, additional coloured minerals are present in the bluish green variety, of which dioptase (?) and ajoite (?) are indicated by optical and qualitative chemical data, respectively. Chrysocolla in this material seems to be largely non-crystalline because of few and very weak reflections in X-ray diffraction recordings. Some genetic aspects of the mineralization are discussed.*

Keywords: *chrysocolla quartz, petrographic texture, secondary copper minerals, small scale mining, Tertiary volcanic rocks*

Introduction

For several years, blue to greenish gemstone material has been known from the North Maluku Province, Indonesia, under the name of 'Bacan stone'. This refers to its source on the island of Bacan, situated in South Halmahera, about 2400 km east of Jakarta (*Figure 1*). In fact, the gem material originates from the island of Kasiruta, to the northwest of Bacan island (spelt Batjan in some atlases).

It occurs as chrysocolla-bearing quartz veins and small pods in volcanic rocks. Polished cabochons from this material are of very pleasing colours (*Figure 2*), and some of them resemble turquoise or chrysoprase.

Small scale mining commenced in 1988, and currently the material attracts interest from Taiwanese, South Korean and Indonesian buyers. The local government
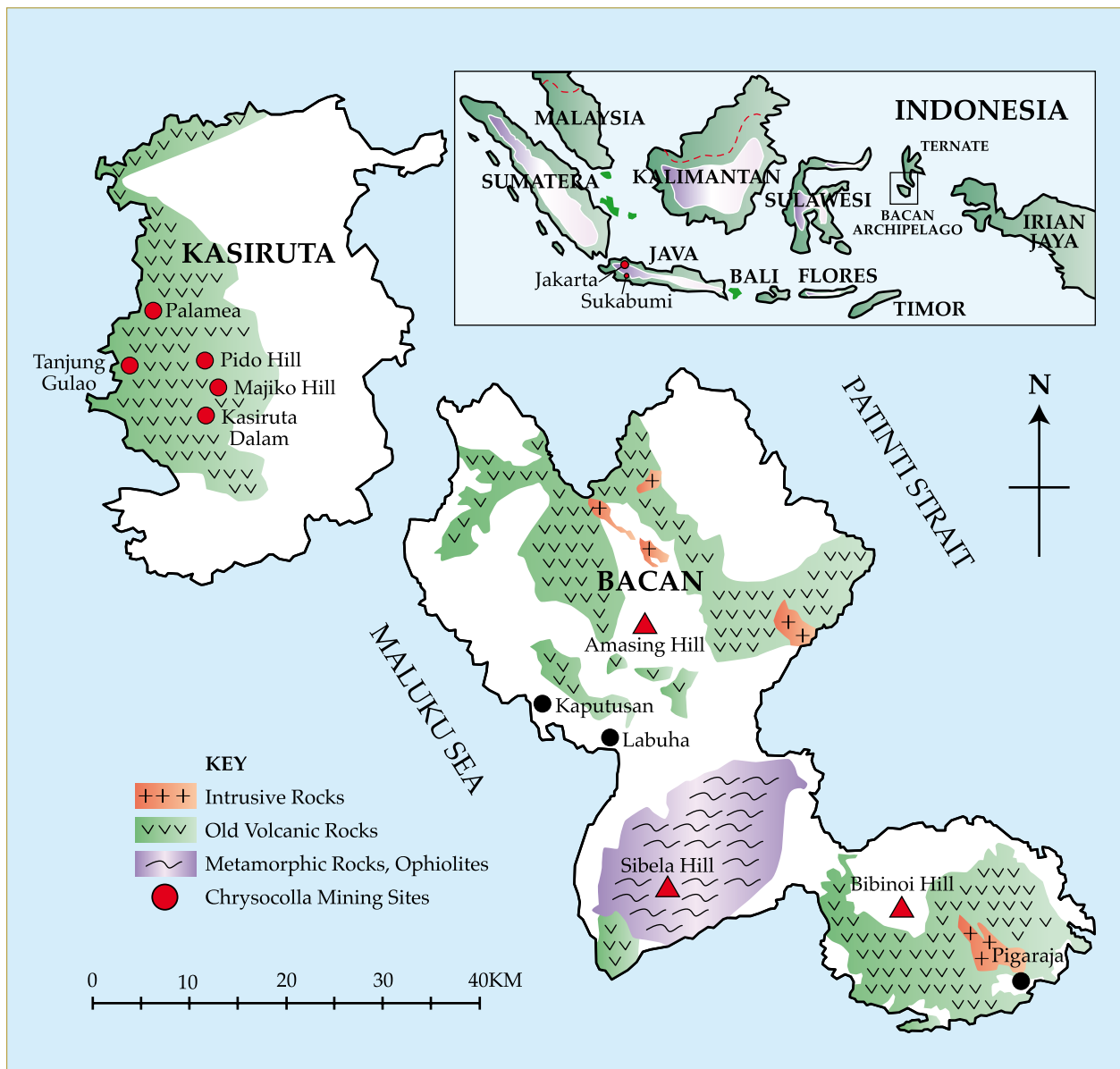
Figure 1: *Bacan archipelago is situated southwest of the island of Halmahera. The map shows the extent of the 'Older Volcanics' (the host rocks to the chrysocolla quartz) on the islands of Bacan and Kasiruta, the porphyry intrusions and the metamorphic and ophiolitic basement. Sediments and 'Younger' and 'Recent Volcanics' as well as structural elements have been omitted from the map.*

supports efforts to develop further the already existing small local gem cutting industry.

Geology

The geology of the Bacan archipelago (Hall *et al.*, 1988; Sukamto *et al.*, 1981; Yasin, 1980) is dominated by volcanic rocks of three island arcs, developed successively since the Early Tertiary, in a complex tectonic setting due to the collision of the Philippine Sea Plate (to which the Bacan Archipelago and the island of Halmahera belong) to the East and the Molucca Sea Plate to the West, forming the Molucca Sea Collision Zone (Hall *et al.*, 1995; Hall, 2000). The oldest non-metamorphic rocks of this area are the 'Older volcanic rocks' of the Philippine Sea Plate Arc volcanism, a series of basaltic pillow lavas of island arc chemistry, and volcanic breccias with local intercalations of foraminiferal limestones with an upper Oligocene age which occur on Bacan and Kasiruta islands (*Figure 1*). They are followed by 'Older sediments' composed of dominantly clastic rocks (mudstones and volcanoclastic turbidites), and reef limestones on top of this

sequence. The 'Younger Volcanic rocks' of the Neogene Halmahera Arc are composed mainly of volcanic breccias of andesitic to basaltic composition, stratigraphically followed by 'Younger sediments' possibly of a Late Tertiary to Early Quaternary age, and the youngest (up to Recent) volcanic rocks of the Present Halmahera Arc as cinder cones and tuff-volcanoes of andesitic composition. Uplifting of the Bacan archipelago during plate collisions followed by erosion has exposed the oldest rocks of this area which are ophiolitic rocks (crystalline schists and mafic to ultramafic rocks) of Jurassic age (Hall *et al.*, 1995) at Sibela Hill in the centre of Bacan.

During the Middle Miocene, the Oligocene to Miocene sequences were locally intruded by porphyritic rocks of granodioritic, dioritic and tonalitic composition with a little Cu/Au mineralization (Silitonga *et al.*, 1981), with malachite, chrysocolla, tenorite and limonite in the exposed oxide zone, and covelline and chalcosine in the core samples drilled from the cementation zone (Rammlmair *et al.*, 1985). A disseminated Cu-Ag-Au mineralization in green pillow lavas of the 'Older volcanic rocks' has been reported from the central Kasiruta island (Djaswadi *et al.*, 1990).

Figure 2: Cabochons made from Bacan stone range in colour from pale blue to a deeper blue green. Each weighs between 8 and 12 ct.

Gemstone deposits on Kasiruta island

Chrysocolla quartz together with multicoloured chalcedony is presently mined at five localities on Kasiruta island (*Figure 1*). All mining sites are situated in the pillow lavas of Oligocene age, forming the 'Older volcanic rocks'. The lavas are dark grey to near-black volcanic rocks of basalt composition with white plagioclase laths up

Figure 3: The massive chrysocolla quartz rock sample on the right weighs about 1.5 kg and was mined from vein type mineralization on Kasiruta island. The deep greenish blue stone on the left is a high quality material slice of about 300 g.

to a few millimetres long in a dense, partially glassy matrix which contains abundant microcrysts of plagioclase and clinopyroxene. Microfractures are filled with pale green palagonite as an alteration product.

The mineralization is either of *vein type*, filling fractures, fissures or joints as massive concentrations of chrysocolla and quartz (*Figure 3*), or of the *crust type*. The *vein type* crosscuts volcanic breccia and pillow lavas. Veins vary in width between a few centimetres and 30 cm, with a length of up to 10 m, and seem to be related to extension joint systems (common at Pido and Majiko hills). The *crust type* is irregular in shape, forming small pods and showing features of impregnation. It is common at the contact of

and in spaces between pillows (as at Tanjung Gulao, *Figure 4*).

Mining

Chrysocolla mining in the area was started on a very small scale in 1988 by a few groups of local miners. This so-called 'Bacan Stone' is said to have become more generally known when about 500 kg of gem-quality material was collected during a mineral assessment programme by an Indonesian exploration company and appeared on the market in Sukabumi, West Java, the centre of the gemstone industry in Indonesia. As a result, the demand for and extraction of 'Bacan stone' have increased significantly, especially since 2004.

In November 2004, 24 groups of miners consisting of three to seven persons each were involved in mining activities on Kasiruta (Sujatmiko, 2004). The main mining area was on Majiko Hill with 17 groups

Figure 4: A volcanic breccia between pillows is impregnated and cemented with chrysocolla quartz of crust type mineralization (locality: Tanjung Gulao). Gem-quality material has already been extracted from the dark cavity at the upper left.

actively working the *vein type* mineralization. None had a mining permit and there was neither guidance in extraction nor supervision by the local Government.

Mining commences where surface indications of chrysocolla are found (*Figure 5*). The *vein type* deposits are preferred as the mineralization pattern is more regular than in the more disseminated *crust type*. Hand-dug shafts with a very narrow opening

Figure 5: Small scale surface mining at Pido Hill exposes the pillow lava structure (irregular oval holes).

are sunk to a depth of 5 to 10 m, following the mineralized zone. The equipment used is very simple and includes shovel, pick, hammer and crowbar. The impact of mining on the environment at these places is usually restricted to the immediate surroundings of the small shafts and involves clearing of the vegetation, some soil removal and dumping of waste rock.

The general pattern is that each group stays at the mining site for about a week before taking a rest for a few days. During a period of three months each group collects between 20 kg to 200 kg of chrysocolla quartz, which will also contain some associated multicoloured chalcedony. Miners are mostly active in the period between the planting (September) and the harvesting (January-February) seasons. However, especially with the recent increase of prices for good quality chrysocolla quartz from Kasiruta, mining continues on a smaller scale throughout the whole year.

Home industry and gem trade

There are about ten gem cutting facilities in Labuha, the capital of South Halmahera regency, where local craftsmen process mainly the translucent chrysocolla quartz

varieties, but make little use of other gemmy material like chalcedony or coloured jasper ('picture stone'). The equipment consists mainly of grooved carborundum wheels for shaping and grinding but there have been recent government moves to introduce new machinery. Since no polishing powders are available, polishing is done with dry bamboo sticks, where the silica in the bamboo fibres gives a very good polish (*Figure 6*). Most of the chrysocolla quartz is cut as oval cabochons in the range of 6 to 20 ct, although some are heart shaped. Until recently, the only public market was a gem shop at the airport of Ternate, the capital of North Maluku province, where the cabochons were sold to visitors at prices between US$ 30 and 100 per piece of 10 to 15 ct, about 5 to 10 times the amount paid to the craftsmen in Labuha (US $5 to 20). The main selling of cut stones and also of gem rough has shifted now to Sukabumi and Jakarta in West Java and Surabaya in East Java.

Figure 7: The photograph shows the range of chrysocolla quartz rough material and cabochons investigated in this study. Although strongly coloured homogeneous material is favoured for cabochons (IC 4-7), inhomogeneous material of variable colours (IC 1, 3) can still be used for cutting of ornamental pieces. The white dotted, black pieces (IC 2) are from the volcanic host rock.

Material for examination

The gem material from the Kasiruta localities supplied for gemmological, mineralogical and chemical examination consisted of six cabochons and the remains after their cutting (*Figure 7*). The rough material is variable in mineralogical composition and colour even on a centimetre scale, requiring careful selection of pieces to be cut for even-coloured stones (*Figures 2* and *8*). On the other hand, its variation (*Figure 7*) does allow for production of stones with an ornamental character. The properties of the six cabochons are summarized in *Table I*.

Colour

The cabochons range in colour from green-blue with a moderate colour saturation through lighter colours to a dark bluish green. The blue stones are described as chrysocolla, whereas the green stones (*Figure 8*) are sold as 'chrysoprase'. In many stones, the colour is fairly homogeneous on top of the cabochon, but appears somewhat mottled in others due to clearly visible intergrowths with colourless quartz (*Figure 9*). A few small black spots are copper ore minerals. The cutter usually tries

Figure 6: A local craftsman at Labuha, Bacan island, uses simple machinery for shaping and grinding of cabochons. Polishing with dry bamboo gives a very smooth surface to the stones.

Increasingly, most of the rough gem material is sold directly at the mining site to buyers from Indonesia, South Korea, Japan and Taiwan. Prices in 2005 ranged from several tens up to two hundred US$ per kg and stand currently at about US$ 500 per kg for first grade quality. It is therefore increasingly difficult for local craftsmen to have access to gem-quality rough material at affordable prices.

Sample no.	Weight (carat)	Colour	Surface appearance	SG	Fluorescence under long- and short-wave UV
IC 4	4.8	Green blue, moderate saturation	Uniform in colour and texture, a few opaque spots	2.34	Weakly dark blue
IC 5	5.0	Green blue/turquoise, low saturation	Mottled appearance due to intergrowth with quartz	2.50	Light blue white Rough: dark blue to violet,chalcedony part bluish white
IC 6a	3.5	Bluish green, moderate saturation	Dto., small agate lined vug on lower surface	2.33	No fluorescence
IC 6b	4.2	Bluish green, strong saturation	Fairly uniform in colour, globules of blue mineral in green matrix visible with handlens	2.47	No fluorescence Rough: blue fluorescence in light blue green parts
IC 7a	3.1	Greenish blue, moderate saturation	Mottled appearance due to intergrowth with quartz, change to greenish at edge	2.38	Blue white Rough: bluish white in chalcedony parts
IC 7b	11	Greenish blue, strong saturation	Fairly uniform colour, few opaque spots, white lower surface and edge	2.44	Blue white, white lower surface with bluish white fluorescence

Table I: Summary of some properties of chrysocolla quartz cabochons and rough material from Kasiruta, North Maluku, Indonesia

Figure 8: Many chrysocolla quartz cabochons appear distinctly green and are sold locally as chrysoprase. The large cabochon weighs 21 ct, the others around 11 ct each.

Figure 9: The base of a blue green cabochon (cabochon IC 6a) appears mottled due to globules of chrysocolla in colourless quartz. A small vug is lined by pale brown chalcedony and the centre filled with quartz. Length of bar: 1 mm.

Figure 10: Immersed in water and magnified, the inhomogeneous nature of this cabochon is visible, with blue chrysocolla globules in a darker green matrix. Some black grains of ore are visible on the right, and an air bubble is visible in the vug on the left. Cabochon IC 6b, length of bar: 1 mm.
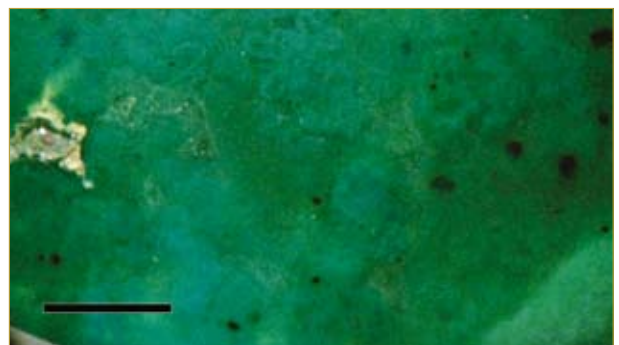
to place any patchy or inhomogeneous colour areas on the base or towards the edges of the cabochon.

Viewed with handlens or binocular microscope, even the seemingly homogeneously coloured cabochons may display a heterogeneous appearance/composition. This is due to the presence of colourless quartz and opaque minerals as well as to the uneven distribution of mineral aggregates of various intensity of blue and green colours (*Figure 10*), even more evident in thin sections cut from this material. Of the examined cabochons, only IC 4 had a perfectly homogenous surface save for several small spots of ore minerals, similar to the one in *Figure 11*.

Specific gravity

The specific gravity of the cabochons ranges from 2.34 to 2.50, reflecting the variable mixtures of quartz and chrysocolla. The highest value (2.50) outside the chryscolla range is due to a very high proportion of quartz (with its higher SG of 2.65) and chalcedony (2.58 to 2.63); this cabochon is also the faintest in colour due to the rather small amount of chrysocolla.

Hardness and refractive index

Hardness and refractive index have not been determined in a systematic way due to the heterogeneous nature of the material, but tests on some stones indicate that even the seemingly purest chrysocolla sample (cabochon IC 4) has a hardness higher than 6 due to the quartz content. Viewed with oblique incident light, the polished surface exhibits small depressions due to the hardness differences of chrysocolla and quartz. Because all investigated cabochons consist of intimate intergrowth of various minerals, no reliable measurements of the refractive index are available.

Fluorescence

Chrysocolla is not known do exhibit fluorescence under UV-light (Eppler, 1984). However, both the cabochons and the rough material exhibit variable fluorescence under long- and short-wave UV light. Details are given in *Table I*. Chalcedonic parts of the rough material and the bleached (white) base of one cabochon display a light bluish white, and the fluorescence in the samples is most likely due to their chalcedony content, perhaps modified by the presence of coloured minerals which may affect colour perception.

Durability

Mechanically, the hardness of six of the stones protects them fairly well against wear. However, they are more vulnerable to chemical attack: dilute hydrochloric acid decolorized the surface rapidly to a white 'chrysocolla', and even weak acids like citric acid, common in many household cleaning solutions, bleached the surface colour perceptibly with development of a yellowish tone after 15 min of contact with a commercial cleaning solution. This reaction revealed the

Figure 11: This fairly homogeneously coloured cabochon (similar to IC 4) is typical of the blue end of the colour range of Bacan stones. Weight: about 20 ct.

inhomogeneous mineralogical composition more clearly by developing different shades of colour. Thus, prolonged exposure to these solutions will seriously affect the colour of the chrysocolla quartz.

Surface and internal textures

When magnified, many polished cabochons show intricate patterns of water-clear quartz surrounding bluish white globular and irregularly shaped aggregates which can be interconnected with each other and even form chain-like textures. The base of one of the cabochons (IC 5) is a good example of this intergrowth pattern (*Figure 12*). Because
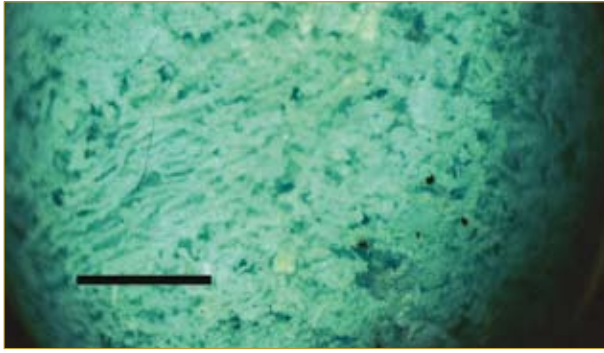
Figure 12: The rather poor quality of cabochon IC 5 on its base shows the intricate intergrowth of chrysocolla (blue green) and quartz (dark). Cabochon immersed in water, length of bar: 1 mm.

the quartz is transparent, the colour of the chrysocolla aggregates below the surface is reflected through the surrounding quartz, giving an overall blue or green colour to the stones.

A surface may be interrupted by the presence of very small vugs with fillings resembling agate and a lining of white or pale yellow chalcedony towards the massive material (*Figure 9*); some vugs also have small perfect quartz crystals protruding into free space.

Mineralogical composition

In chrysocolla quartz or chrysocolla chalcedony, the chrysocolla occurs finely dispersed within, impregnated by or encrusted by silica material. This has higher mechanical durability than pure chrysocolla and is much more suitable for use as a gem. However, when used as a trade name chrysocolla quartz or chrysocolla chalcedony often applies to quartz-chalcedony rocks coloured by widely dispersed and minute secondary Cu minerals which may include not only chrysocolla *sensu stricto*, but also a range of similar secondary Cu-silicates and Cu-sulphates such as ajoite, plancheite, shattuckite, brochantite and antlerite (see Johnson *et al.*, 1995). The trade name has also been used for any massive, globular, glassy, blue to green copper-bearing silicate mixture of minerals which has not been identified.

The true mineral chrysocolla forms layers and globules of fibrous aggregates, commonly in a radiating pattern, with the fibres not exceeding a length of 5 mm. It is a hydrous copper silicate with the formula $(Cu, Al)_2H_2Si_2O_5(OH)_4.nH_2O$, where the water content is variable and Cu can be substituted partially by Mn (Throop and Buseck, 1971), Fe and Al (Anthony *et al.*, 1995; Van Osterwyck-Gastuche, 1970). Up to 5.9 wt.% Al_2O_3 and up to 5.7 wt.% Fe_2O_3 have been reported from chrysocolla (Gaines *et al.*, 1997). Such substitutions and the presence of minerals such as (hydr)oxides of Fe, Mn and Cu can result in variable colours from pale blues and greens to black (Anthony *et al.*, 1995; Eppler, 1984; Gaines *et al.*, 1997; Webster, 1994).

Pure chrysocolla is birefringent with RIs of 1.57 - 1.60 (Gaines *et al.*, 1997), but the gem materials labelled chrysocolla generally have RIs around 1.50, indicating that they are mixtures perhaps including other copper silicates, chalcedony and opaline silica. The gem materials also have variable hardness (Mohs 2-4) and specific gravity of 2.0 - 2.4 (Klein, 2002).

The mineralogical composition of six samples typical of the gem material from Kasiruta has been examined qualitatively by X-ray diffraction (using a Siemens D 500 diffractometer, Cu KÅ radiation at 1.5405 Å, (delta lambda 0.0038 Å), a graphite monochromator, speed 0.5°/min as standard parameters between 5.0 and 65.0° 2θ) and by microscopic observations in thin section of the rough gem material from which the cabochons had been cut.

X-ray diffraction results

The diffractograms of the cabochon material all indicate quartz as the main crystalline phase. The bluish green cabochon IC 6a contains additionally a major amount of chalcedony, a deduction confirmed in thin section, and three very small peaks indicate the silica variety mogánite (Graetsch, 1994).

Non-quartz peaks are rare and very weak. In two samples, one or two reflections coincide with the main reflections of chrysocolla (Anthony *et al.*, 1997) at 1.48 and 2.90 Å d-spacings, but the other reflections

are not visible. Chrysocolla is a hydrogel or gelatinous precipitate (Klein, 2002; Webster, 1994). It is therefore commonly of low structural order, and much chrysocolla has been found to be highly disordered to non-crystalline, which explains the weak or missing reflections in XRD recordings. A few very small peaks at d = 1.509 Å (from cuprite?), 2.082 Å (from native copper?) and others of unknown origin confirm the microscopic observation of the presence of additional mineral phases.

The XRD-data of a separated vividly blue, fibrous part from the rough material from which IC 6 was cut, selected to be as free from quartz as possible, confirm the poor crystalline order of the sample material. The diffractogram (*Figure 13*) shows a rapid increase of the background level, which forms then an elevated plateau (to the end of the recorded diffraction angle), typical of material in a highly disordered state. This plateau is overtopped by quartz peaks and three very weak and indistinct peaks at d = 1.48, 2.89 and 1.60 Å, coinciding with the stronger reflections of chrysocolla, and two reflections at low angles with d = 8.5 and 16.5 Å, which are close to published d-values for chrysocolla at 7.9 and 17.9 Å (Anthony *et al.*, 1997).

Thin section observation

In thin sections (plane polarized light), some chrysocolla aggregates in the samples from Bacan are pale green but most show variable intensities of brown, either in the core or at the rim of zoned globules (*Figure 14*). Such colour variation may be explained by different Cu-, Mn- or Fe-contents, but this needs verification.

The textural pattern is variable. Chrysocolla as very fine grained fibres can be intimately intergrown with quartz (samples IC 4 and IC 5) in compact masses or forming a network of small globules
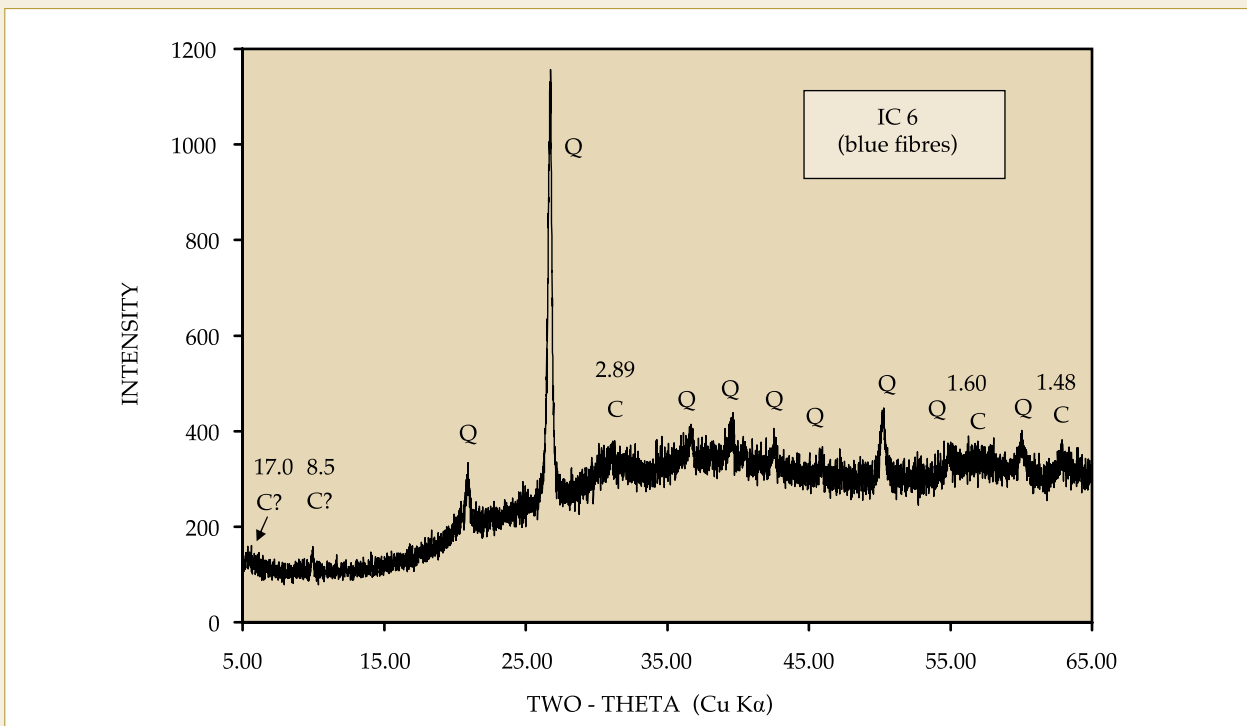
Figure 13: The X-ray diffraction recording obtained from a blue, fibrous part of rough gem material (sample IC 6) shows a markedly elevated background reading between 2θ angles of 20° and 65°, the distinctly visible peaks of quartz (Q) and a few and very low, broad peaks of chrysocolla (C). (The broad peak at d = 1.60 interferes with a very weak reflection of quartz). The elevated background and the few and indistinct chrysocolla peaks indicate a highly disordered structural state of the chrysocolla. Numbers above symbols are d-values of chrysocolla peaks.
(Two Theta values are converted to d-values by the Bragg equation: $n\lambda = 2d \sin 2\theta$, with $n = 1,2,3,..$; λ = wavelength of the applied radiation (in Å); d = distance between two parallel planes of the crystal lattice (in Å); θ = angle of reflection of the X-ray beam on the sample surface.)
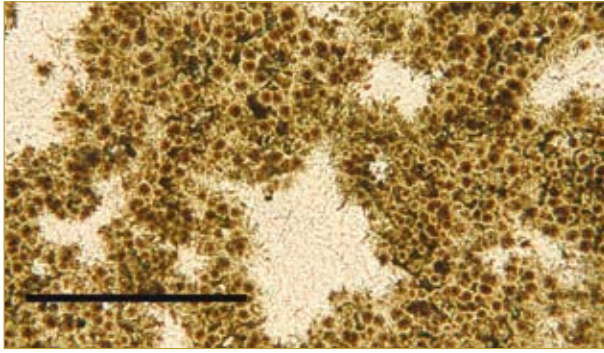
Figure 14: *Aggregates of small chrysocolla globules form a network whose gaps are filled with quartz. Sample IC 5, thin section, plane polarized light, length of bar: 1 mm.*
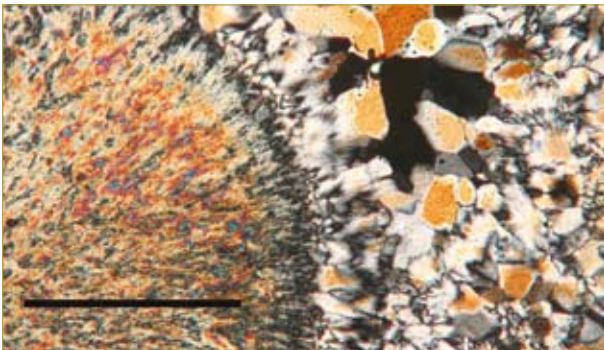
Figure 15: *A sphere of radiating chrysocolla fibres is rimmed by a thin layer of chalcedony, followed by coarser grained quartz. Sample IC 6, thin section, crossed polarizers, length of bar: 1 mm.*

Figure 16: *Thin section of IC 6 displaying the colloform banding of globules of chrysocolla with small interlayers of chalcedony and the later growth of quartz in several layers around the chrysocolla-chalcedony aggregate (upper photograph). The lower photograph, taken in cross polarized light, shows the radiating habit of the chrysocolla fibres. Length of bar: 1 mm.*

(*Figure 14*). Another textural type consists of large globules of radiating chrysocolla fibres, rimmed by a thin zone of chalcedony (*Figure 15*). A third type, prominent in IC 6 and 7, forms botryoidal aggregates of several chrysocolla layers of variable thickness, with quartz/chalcedony interlayers. Here, each chrysocolla layer consists of outwardly radiating fibre bundles and may be near-colourless or coloured in variable intensities of brown and green (*Figure 16*). Small quartz aggregates act as the nucleation centres for these semi-spherical colloform aggregates, as do copper minerals.

According to thin section observation, coloured mineral species in addition to chrysocolla are present in the Bacan material. Small 'islands' of vividly emerald to grass green and roughly colloform aggregates set in a colourless to white matrix are composed of malachite and have been found in all samples in trace amounts. Though malachite is generally a common mineral in the oxide zone of copper sulphide mineralization, it is rare in the examined material from Kasiruta.

The greenish-blue material (IC 4 and 5) consists mostly of chrysocolla with only a few specks of malachite as colouring mineral, whereas the bluish-green material (cabochons IC 6a and b) has at least two additional coloured minerals: the botryoidal chrysocolla aggregates are surrounded by a compact layer composed of a grainy mineral in tiny rectangular crystals (*Figure 17*). Its blue green colour (the cause for the overall colour of these cabochons), refractive index distinctly higher than that of quartz, high birefringence and straight extinction under crossed polarisers indicate that it is probably dioptase. Additionally, a grey-green mineral phase in small compact, embayed grains with a blue tinge in oblique incident light, which occurs also in sample IC 7, remains to be identified.

Quartz occurs in three varieties: firstly as fibrous chalcedony, forming clusters of small rosettes in quartz-rich parts, often as a thin zone of outwardly radiating fibres around chrysocolla globules (*Figure 15*), and occasionally with agate banding in

vuggy parts. Secondly, it forms a mosaic of microcrystalline quartz with increasing grain size towards the centre of the quartz-filled areas between the chrysocolla-quartz aggregates. Thirdly, quartz occurs rarely as well shaped tiny crystals in small cavities.

The layering of successive quartz crystallization (without chrysocolla intergrowth) resembles the botryoidal aggregates of chrysocolla (*Figure 16*, upper photograph), and occurs both as the outer layers around chrysocolla-quartz bodies and

Figure 17: Botryoidal aggregates of chrysocolla and chalcedony are surrounded beyond the outer dark brown layer of chrysocolla by a dense, grainy zone of an unidentified green mineral (dioptase?) in the blue green sample IC 6. Thin section, crossed polarizers, length of bar: 1 mm.

as separate, quartz-chalcedony colloform spheres. The remaining space between the spheres is filled by coarser quartz grains. The amount of this layered and gap-filling quartz determines the degree of reduction of the overall colour intensity and is the cause of a mottled appearance when present in higher concentrations, as in cabochon IC 5, where it is estimated to make up about 60 % by volume.

Copper ore minerals, all of secondary origin, are abundant in the rough gem material and are also present in very small amounts as dark spots in the cabochons. In addition to the (rare) malachite, cuprite (Cu_2O) is common as small xenomorphic grains or as grain aggregates and has been identified on the basis of its reflectance, the abundant red internal reflections and the characteristic tiny inclusions of native copper. Where coarser grained, it is dark red and commonly surrounded by another ore mineral, probably

tenorite (CuO), a common associate in chrysocolla quartz. Native copper occurs also as fillings of microfractures.

Where abundant, the ore minerals change the overall colour of the gem material to near-black with a bluish tint. They are also present as regular, chain-like linings in the banded patterns of chalcedony and as nucleation centres for chrysocolla-quartz globules (*Figure 18*).

Clusters of a needle-shaped or bladed ore mineral, opaque in thin section but dark
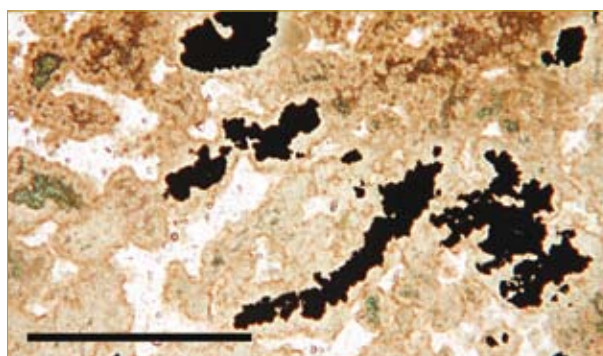
Figure 18: Cuprite and native copper (black) and malachite (green) act as nuclei for chrysocolla (pinkish brown) crystallization in sample IC 3. Quartz (colourless) fills the space between the chrysocolla aggregates. Thin section, plane polarized light, length of bar: 1 mm.

brown in thin blades, have been observed in material of sample IC 4. It has been found only in the weathered crust of rough gem material where the stone has lost its green or blue colour. It surrounds sub-spherical microcrystalline quartz aggregates, probably the remnants of the original chrysocolla-quartz globules, and is very likely derived from Fe-rich chrysocolla, the Fe being released during weathering and recrystallizing as an oxyhydroxide. Qualitative XRF analytical data support this interpretation.

Information from chemical data

Preliminary qualitative analyses have been carried out on the six cabochons using a wavelength dispersive X-ray fluorescence machine (Tracor Spectrace 5000) with a Rh-tube run at 50 KV and 0.35 mA and an Al-filter. All samples contain some Fe and Mn

and traces of Ca and Ti. Potassium is clearly present in the cabochons IC 6a and IC 6b. Other metals have not been detected (Al may be present, but was undetectable due to the use of an Al-filter). A few conclusions can be drawn from these data.

The potassium in samples IC 6a and IC 6b indicates probably the bluish green mineral ajoite $((K,Na)Cu_7AlSi_9O_{24}.nH_2O)$ as another mineral causing (together with the supposed dioptase) the more green colour of these cabochons.

The name 'chrysoprase' for the beautiful greenish translucent gem material from Kasiruta is misleading as Ni has not been detected in the examined cabochons. From the geological point of view, the association with basaltic volcanics and the Cu-dominated mineralization makes it unlikely for chrysoprase to occur in this environment.

Concerning other blue and green secondary minerals, neither phosphates (e.g.turquoise) nor sulphates (e.g. antlerite) are present because neither P nor S have been detected in the samples.

The highest copper counts were obtained from the blue cabochon IC 4 which indicates a high chrysocolla content as expected from its colour saturation and low amount of quartz.

Since no other Fe, Mn-bearing minerals have been observed in thin sections of (unweathered) rough gem material, the small amounts of Fe and Mn detected are interpreted as minor contents of the chrysocolla

Genetic aspect and conclusions

Genetically, chrysocolla is an alteration product in the oxidation zone of a copper sulphide mineralization, with quartz-chalcedony as a common co-precipitate in intimate intergrowth. This chrysocolla quartz may be accompanied by a variety of other secondary Cu-minerals, such as malachite, tenorite, ajoite, plancheite, dioptase and cuprite, which are usually not identified in the gem material as they are of lesser interest to

the gem trade. The gem material from Bacan exemplifies this variability by showing at least four different blue to green minerals of which only chrysocolla and malachite have so far been positively identified. The proportion of quartz-chalcedony to chrysocolla and its distribution as fine intergrowth with the coloured minerals or as clusters and patches affects the overall colour saturation and textural appearance of the Bacan gems.

Textural evidence points to a certain sequence of mineral precipitates during the process of supergene alteration of the primary mineralization which is related to the progressive oxidation of sulphides and dissolution of primary mineral species. A generalized sequence involves the following steps, probably replacing the primary texture or being superimposed onto its relics:

• crystallization of cuprite, native copper, malachite and tenorite from Cu-bearing aqueous solutions, derived from the oxidation and dissolution of primary or secondary Cu-sulphides,

• change in precipitation from Cu-oxides and Cu-carbonate to Cu-silicates: chrysocolla-quartz intergrowths or botryoidal, layered chrysocolla-chalcedony sequences from still Cu-bearing, but strongly siliceous aqueous solutions or gels due to dissolution of primary quartz during an advanced process of mineral dissolution, crystallize around nucleation centres of the secondary Cu-minerals,

• growth of a rim of chalcedony or microcrystalline quartz around chrysocolla aggregates from a Cu-depleted siliceous solution or gel, or of other Cu-silicates like dioptase (?) or ajoite (?) as in the bluish green material if Cu is still present in the gel/solution.

The later precipitates are:

• quartz or chalcedony in separate globular aggregates with radiating patterns which may be partially contemporary with the crystallization of the outer quartz-chalcedony layers around chrysocolla-quartz aggregates, followed by

• coarser grained quartz without systematic orientation of the crystals (this

quartz type, however, may be a relic of the primary texture) and rarely, by

- late chalcedony or quartz crystals in vugs.

This sequence reflects the comparatively easy and early oxidation and dissolution of the Cu-sulphides, followed by a rapid decrease of Cu supply with time to the zone of secondary mineral precipitation, and the development of siliceous, increasingly Cu-depleted solutions or gels due to dissolution of primary quartz during prolonged near-surface weathering or in the zone of fluctuating groundwater levels (Cuadra C., P. and Rojas S., G., 2001).

The chrysocolla quartz and other secondary copper minerals on Kasiruta island owe their formation to mineralization processes during Tertiary magmatic activities. The primary mineralization in the volcanic rocks may have been a porphyry-related epigenetic Cu mineralization of Middle Miocene age already known in the Bacan archipelago (Djaswadi *et al.*, 1990; Rammlmair *et al.*, 1985), or a small and locally occurring syngenetic Cu mineralization in the Oligocene pillow basalt lavas, or both. The small occurrences of the *crust type* chrysocolla between pillows are a strong indication for the latter type of primary mineralization, whereas the *vein type* chrysocolla could be derived from porphyry. In terms of prospecting for further occurrences, if the chrysocolla were derived from a porphyry, one would expect new finds to be in the vicinity of known occurrences, but if it originated in the pillow lavas, it could show a wide and unsystematic distribution, also of low volume at each occurrence. In view of the widespread occurrence of the Older Volcanics both on Kasiruta and on Bacan island (where no chrysocolla quartz mineralization is yet known), the potential of gem-quality rough material might be considerable.

Acknowledgements

References

Anthony, J.W., Bideaux, R.A., Bladh, K.W., and Nichols, C., 1997. *Handbook of Mineralogy, Volume II - Silicates*. Mineral Data Publishing, Tucson, Arizona; also www.minsocam.org/msa/Handbook/

Cuadra C., P., and Rojas S., G., 2001. Oxide mineralization at the Radomiro Tomic porphyry copper deposit, Northern Chile. *Economic Geology*, **96**, 387-400

Djaswadi, S., Tjahjono, B., and Sudharto, T., 1990. Penjajagan Mineral Logam di Maluku Utara (Reconnaissance of Metallic Minerals in North Maluku). *Proceedings PIT XIX Ikatan Ahli Geologi Indonesia, Bandung*, 11-13 December 1990, 302-24

Eppler, W.F., 1984. *Praktische Gemmologie*. 2nd edn. Rühle-Diebener-Verlag, Stuttgart, 504pp

Gaines, R.V., Skinner, H.C.W., Foord, E.E., Mason, B., and Rosenzweig, A., 1997. *Dana's new mineralogy*, 8th edn. John Wiley & Sons, Inc., New York, 1561pp

Graetsch, H., 1994. *Structural characteristics of opaline and microcrystalline silica minerals*. In: Heaney, P.J., Prewitt, C.T., and Gibbs, G.V. (eds). *Silica: physical behaviour, geochemistry and materials application*. Washington D.C. Min. Soc. America, *Reviews in Mineralogy*, **29,** 209-32

Hall, R., 2000. Neogene history of collision in the Halmahera region, Indonesia. *Proceedings of the Indonesian Petroleum Association 27th Annual Convention*, 487-93

Hall, R., Ali, J.R., Anderson, C.D., and Baker, S.J., 1995. Origin and motion of the Philippine Sea Plate. *Tectonophysics*, **251**, 229-50

Hall, R., Audley-Charles, M.G., Banner, F.T., Hidayat, S., and Tobing S.L., 1988. Late Paleogene-Quaternary geology of Halmahera, Eastern Indonesia: initiation of a volcanic island arc. *J. Geol. Soc., London*, **145**, 577-90

Johnson, M.L., McClure, S.F., and DeGhionno, G., 1995. Azurite and antlerite rock. Gem Trade Lab Notes, *Gems & Gemology*, **31**(2), 120

Klein, C., 2002. *The 22nd Edition of the Manual of Mineral Science*. John Wiley & Sons, New York. 647pp

Rammlmair, D., Kippenberger, C., Kaestner, H., and Bering, D., 1985. *Exploration at the Cu-Au-porphyry Kaputusan (Bacan Island, Northern Moluccas)*. Federal Institute for Geosciences and Natural Resources, Hannover/FRG; unpubl. internal report

Silitonga, P.H., Pudjowalujo, H., and Mollat, H., 1981. *Geological Reconnaissance and Mineral Prospecting on Bacan Island (Moluccas, Indonesia).* In: Barber, A.J., and Wiryosuyono, S. (eds) *The Geology and Tectonics of Eastern Indonesia. Geological Research and Development Centre,* Bandung, Indonesia; Special Publication, **2**, 373-81

Sujatmiko, H., 2004. *Laporan kajian potensi bahan baku batu mulia di Bacan, kabupaten Halmahera Selatan, propinsi Maluku Utara (Report on the gem stone potential on Bacan, South Halmahera regency, North Maluku province).* Internal report for the Provincial Government of North Maluku, Industry and Trade Office, in collaboration with the Gem-AFIA group

Sukamto, R., Apandi. T., Supriatna, S., and Yasin, A., 1981. *The Geology and Tectonics of Halmahera Island and Surrounding Areas.* In: Barber, A.J., and Wiryosuyono S. (eds). *The Geology and Tectonics of Eastern Indonesia. Geological Research and Development Centre,* Bandung, Indonesia; Special Publication, **2**, 349-62

Throop, A.H., and Buseck, P.R., 1971. Nature and origin of black chrysocolla at the Inspiration Mine, Arizona. *Economic Geology,* **66**, 1168-75

Van Osterwyck-Gastuche, M.C., 1970. La structure de la chrysocolla. *C. R. Acad. Sci.,* Paris, **271, sér. D**, 1837-40

Webster, R., 1994. *Gems - their sources, descriptions and identification.* 5th edn. Revised by P. G. Read; Butterworth-Heinemann Ltd. Oxford. 1026pp

Yasin, A., 1980. *Geological map of the Bacan quadrangle, North Maluku, Scale 1/250.000.* Geological Research and Development Centre, Bandung, Indonesia

Comment: The publications of the Geological Research and Development Centre, Bandung, can be obtained as photocopies (payment for costs of photocopies and postage/transmission required) from: Ir. H. Sujatmiko, Secretary General of the Indonesian Gemmological Society/AFIA, Jalan Pajajaran 128, Bandung 40173 / Indonesia.

Crowning glory: the identification of gems on the head reliquary of St Eustace from the Basle Cathedral Treasury

Louise Joyner[1*], Ian Freestone[1*] and James Robinson[2]

1. Department of Conservation, Documentation and Science, The British Museum, Great Russell Street, London, WC1B 3DG
2. Department of Prehistory and Europe, The British Museum, Great Russell Street, London, WC1B 3DG

* Now at School of History and Archaeology, Cardiff University, Humanities Building, Colum Drive, Cardiff, CF10 3EU, Wales

Abstract: *The gems on a thirteenth-century reliquary of St Eustace have been examined non-destructively using Raman microspectroscopy with a horizontal laser attachment and X-ray fluorescence spectrometry. Nine of the gems are composed of varieties of quartz (rock crystal, chalcedony, amethyst and carnelian), two of aragonite (pearl and mother of pearl), one of obsidian and six of synthetic glass. The compositions of five glass stones suggest that they represent re-used Roman glass, while the intaglio on the obsidian and a drill hole in the pearl also suggest the re-use of old material. One glass stone has a medieval glass composition.*

Introduction

The head reliquary of St Eustace (British Museum M & ME 1850,11-27,1) is a container for holy relics, dating to the early thirteenth century (see *Figure 1*). It has two parts, one carved out of wood in the shape of a man's head in which unlabelled fragments of a skull thought to be that of St Eustace were kept with various other labelled relics; the other, a metal covering of silver gilt which is decorated with a diadem encrusted with gems. The metal covering was made some time after the wooden head, possibly to enrich this holy artefact. The reliquary was originally kept in the treasury of Basle Cathedral and was acquired by *The British Museum* in 1850 (Cherry, 2001; Husband and Chapuis, 2001). Many ornate holy relics dating from the early eleventh through to the sixteenth centuries AD formed the treasury at Basle Cathedral. The collection was subsequently split up when the Canton of Basle was divided in 1833 (Hänni *et al.*, 1998; Reiche *et al.*, 2004). The city of Basle

Figure 1: *Photograph of the head reliquary of St Eustace. The reliquary is 33.5 cm high*

Figure 2: *Part of an engraving of the conversion of St Eustace to Christianity by Albrecht Dürer, AD 1501. A print is in the British Museum (1868-8-22-183)*

kept part and the rest of the collection was auctioned off in 1836 to various museums in Berlin, London, New York, Paris, St Petersburg, Vienna and Zurich (Hänni *et al.*, 1998; Reiche *et al.*, 2004).

According to legend, Eustace was a general under the Roman Emperor Trajan who reigned from AD 98 to 117. He converted to Christianity while out hunting on Good Friday, after seeing a vision of a stag with a luminous crucifix between its antlers (see *Figure 2*) (described in approximately 1260 by de Voragine, 1993 translation). Some time later, after a victorious battle, he refused to participate in the thanksgiving to the Roman gods, and was burnt to death with his wife and two sons inside a bronze bull. After

three days the family was removed from the bull, and their dead bodies were found to be miraculously undamaged.

Sixteen gems are set around the diadem of the head reliquary of St Eustace, all equally spaced. In addition, two of 20 original gems set on the top corners of the base pedestal survive. A study of the stones on the head reliquary of St Eustace had previously been carried out in the Research Laboratory of the British Museum in 1957 using traditional gemmological methods. This examination left a number of issues unresolved and it became apparent, during the preparation of a recent catalogue that several of the identifications were questionable, and a re-examination was therefore undertaken.

Analytical methods

The gems are set into the diadem and base pedestal in closed-back settings, and it was not permitted to remove them for examination using standard gemmological methods. Instead the gems were examined using a 10× loupe, then investigated using Raman microspectroscopy. For other studies using this method to identify ancient gems, see Smith and Robin (1997), Calligaro *et al.* (2002), Clark and van der Weerd (2004), Smith (2005) and Kiefert *et al.* (2005). Selected stones and all those identified as paste, were then examined using air-path X-ray fluorescence spectrometry (XRF). These are non-destructive methods which allowed the identification of the stones *in situ*. The surface of each gem was wiped with a clean soft cloth prior to analysis to remove any contamination due to handling.

Horizontal Raman microspectroscopy

The Raman microspectroscope in the Department of Conservation, Documentation and Science at the British Museum is a Dilor LabRam Infinity model equipped with a Nd: YAG green laser at 532 nm and a near-infrared diode laser at 784 nm. It has a conventional microscope stage and objectives as well as an open-beam horizontal microscope attachment. As the head reliquary is too large to permit examination under a conventional Raman microspectroscope, the horizontal beam attachment was used with a ×50 long working distance objective (see *Figure 3*). In this way the Raman microspectroscope was used to analyse the gems while they were still in the diadem and base pedestal. The gem to be analysed was positioned directly in front of the laser beam, for count times between 5 and 20 seconds for 6 accumulations. The maximum power of the lasers used was 4 mW. It was possible to identify each of the gems from its Raman spectrum, by comparison with an internal British Museum database of reference Raman spectra of gems. These British Museum internal reference gems were analysed using both the green and near infrared lasers, and their identifications were confirmed using standard gemmological techniques

Figure 3: The British Museum Raman microspectroscope with an open-beam horizontal microscope attachment showing how spectra were obtained from the gems on the head reliquary of St Eustace. A close-up image of part of the diadem is visible in the screen on the right.

and X-ray diffraction. These internal reference Raman spectra are consistent with other published gemstone spectra (Pinet *et al.*, 1992; Huang, 1999). The accuracy of the Raman peak positions in measuring and assigning them is +/- 2 cm^{-1}.

X-ray fluorescence spectrometry

In situ XRF analysis of the surfaces of the unprepared gems was carried out in air, using a molybdenum X-ray tube operated at 35 kV and 0.4 mA. Spectra were accumulated for 500 seconds and count rates were typically 500 per second. XRF was used to identify the types of glass (paste) gems. The glass compositions were calculated by comparison with the spectra of Corning Museum standard glasses (Brill, 1999). There are a number of limitations to this method. Important light elements in glass such as sodium, aluminium and magnesium cannot be detected, while the error on silicon is high. In addition, the geometry of the analysis cannot be well controlled, and surface analysis of glass is likely to have included some corroded material. For these reasons, the analyses are, at best, approximations of the true composition of the glasses, and are considered semi-quantitative. However, even semi-quantitative data are very useful in that the compositional ranges of early glasses were quite restricted, and the XRF analyses allow the glass gemstones to be placed in specific compositional categories which have certain cultural affiliations.

Gems

The head reliquary of St Eustace contains a variety of gems, including colourless, white, purple, orange, black, grey, red and blue stones. Most of the stones are cabochons which are common in medieval reliquaries (Clark, 1986), but four have facets: one is a dark orange rectangular table cut stone, one is a white opaque gem with a table facet, one is an intaglio of a hippocamp, while another resembles a nicolo with an intaglio fish motif. All the gems are mounted in closed-back rub-over settings, and for this study have been numbered Gem 1-18, starting with the milky white gem at the front of the diadem and moving sequentially round the head as indicated in *Figure 4*. Gems 17 and 18 are on the base pedestal.

In the following sections the results are collated and summarized under species headings and compared with the results of the previous (1957) study in *Table I*. Some of the gemstone identifications corroborate the earlier identifications, but some have been revised. In particular, the number of gems that are identified as glass (paste) is greater than was previously recognized. The other gems include rock crystal (quartz), amethyst, carnelian, chalcedony, obsidian, mother-of-

pearl and pearl. Furthermore, XRF analysis has allowed identification of the glass types used.

Rock crystal

There is just one rock crystal (quartz) gemstone on the head reliquary: Gem 10, an oval cabochon. It is colourless, transparent and contains few inclusions. The main peak on the Raman spectrum occurs at *c.* 463 cm^{-1} with subsidiary peaks at *c.* 206 cm^{-1} and *c.* 353 cm^{-1} (see *Figure 5a*). This spectrum matches the reference spectrum for quartz.

Amethyst

There are two amethysts set in the diadem, Gem 2 and Gem 5, which are located on the true left of the head. Gem 2 is a square cabochon and Gem 5 is a rectangular cabochon. They are purple and appear slightly cloudy, both containing feathers (healed fractures) (see *Figure 6a*). Both gems gave similar Raman spectra with the main peak at *c.* 464 cm^{-1}, and other peaks at *c.* 207 cm^{-1}, *c.* 354 cm^{-1}, *c.* 401 cm^{-1} and *c.* 807 cm^{-1} (see *Figure 5b*). The reference spectrum for quartz matches the spectra obtained from these gems, and as they are purple in colour they are identified as amethyst.

Table I: Gems in the head reliquary of St Eustace.

Gem No.	Colour	1957 identification	Present identification
1	milky white	chalcedony	pale blue-grey chalcedony
2	purple	amethyst	amethyst
3	orange-brown	paste	orange-brown soda-lime-silica glass – Roman glass
4	black intaglio	black jasper	obsidian
5	purple	amethyst	amethyst
6	white opaque	mother-of-pearl	mother-of-pearl (aragonite)
7	red	paste	red potash-lime-silica glass – medieval glass
8	milky white	chalcedony	pale blue-grey chalcedony
9	colourless with blue backing	paste	colourless soda-lime-silica glass – Roman glass
10	colourless	crystal	rock crystal
11	grey cloudy	chalcedony	pale blue-grey chalcedony
12	orange	agate or onyx	carnelian
13	grey milky	chalcedony	pale blue-grey chalcedony
14	top opaque pale blue-grey, base dark brown	nicolo or paste	soda-lime-silica glass imitation of nicolo – Roman glass
15	grey	pearl	baroque pearl bead (aragonite)
16	orange	sard	carnelian
17	pale blue	crystal	pale blue soda-lime-silica glass – Roman glass
18	pale blue	crystal	pale blue soda-lime-silica glass – Roman glass

Carnelian

There are two gems identified as carnelian in the diadem, Gem 12 and Gem 16. Gem 12 is an orange oval cabochon and Gem 16 is a dark orange rectangular table cut stone, and both are translucent (see *Figure 6b*). The Raman spectra of these two gems are very similar and match the British Museum reference spectrum for microcrystalline quartz. Both show main peaks at *c.* 463 cm⁻¹ with a subsidiary peak at *c.* 501 cm⁻¹ which is the characteristic peak for moganite, a silica polymorph which commonly occurs in microcrystalline quartz (Kingma and Hemley, 1994). The other peaks occur at *c.* 207 cm⁻¹ and *c.* 354 cm⁻¹. As these gems are orange in colour and are very fine grained, they are identified as carnelian.

Chalcedony

Four gems in the diadem have been identified as pale blue-grey chalcedony: Gems 1, 8 and 13 are all oval cabochons while
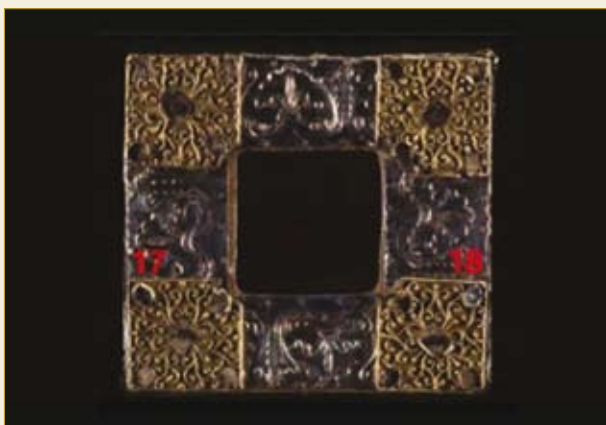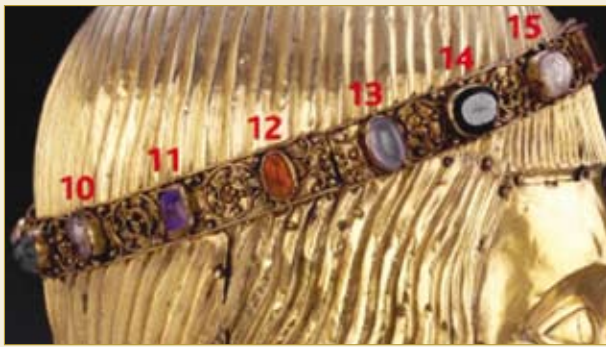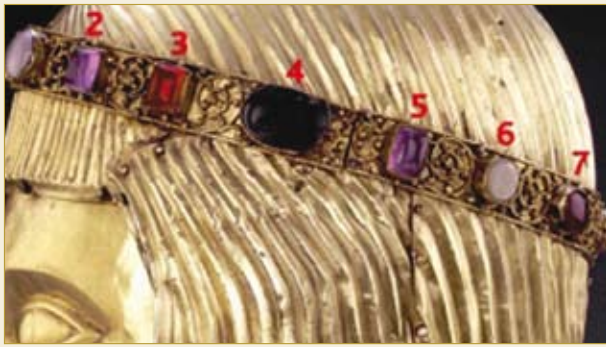
Figure 4: The gems in the diadem and base pedestal of the head reliquary of St Eustace. The gem numbers correspond to those in Table I.

Gem 11 is a square cabochon. They generally have a milky or cloudy translucent appearance (see *Figure 6c*). The Raman spectra for all these gems are similar. They all have their main peaks at *c.* 463 cm^{-1} with a subsidiary peak at *c.* 501 cm^{-1}, the characteristic peak for moganite (see Carnelian above) and other peaks at *c.* 207 cm^{-1} and *c.* 354 cm^{-1}. As these gems are translucent and have a very fine grained texture, they are identified as pale blue grey chalcedony.

Baroque pearl

A large baroque pearl bead complete with a drill hole has been set into the front of the diadem, Gem 15 (see Figure 6d). The Raman spectrum for this pearl has its main peak at c. 1085 cm^{-1} with minor peaks at c. 207 cm^{-1} and c. 704 cm^{-1}, a combination which matches that of reference Raman spectra for aragonite (see Figure 5c) and which confirms that it is a pearl. Calcite can be discounted as its main peak positions lie at 1089 cm^{-1}, 713 cm^{-1}, 284 cm^{-1} and 155 cm^{-1} (Williams, 1995). This large pearl contains a drill hole which is unnecessary in its closed setting in the diadem and which suggests that the pearl may originally have been worn as a bead or on a string. Its setting into the diadem is possibly an example of the re-use of a gem from antiquity.

Mother-of-pearl

There is just one gem fashioned from mother-of-pearl and that is Gem 6. It is round with a table facet and has lost most of its iridescent nacreous layer. The Raman spectrum for this gemstone matches the reference spectrum for aragonite with peaks at *c.* 1085 cm^{-1} and *c.* 705 cm^{-1} (see *Figure 5d*) and this together with the iridescent layer confirms identification of this gem as mother-of-pearl.

Synthetic glass (paste): compositional categories

A number of the gems in the diadem and those from the base pedestal of the head reliquary were found to be made of synthetic glass or paste. Most of these glasses did not give Raman bands significantly above background, probably due to surface alteration and contamination effects.
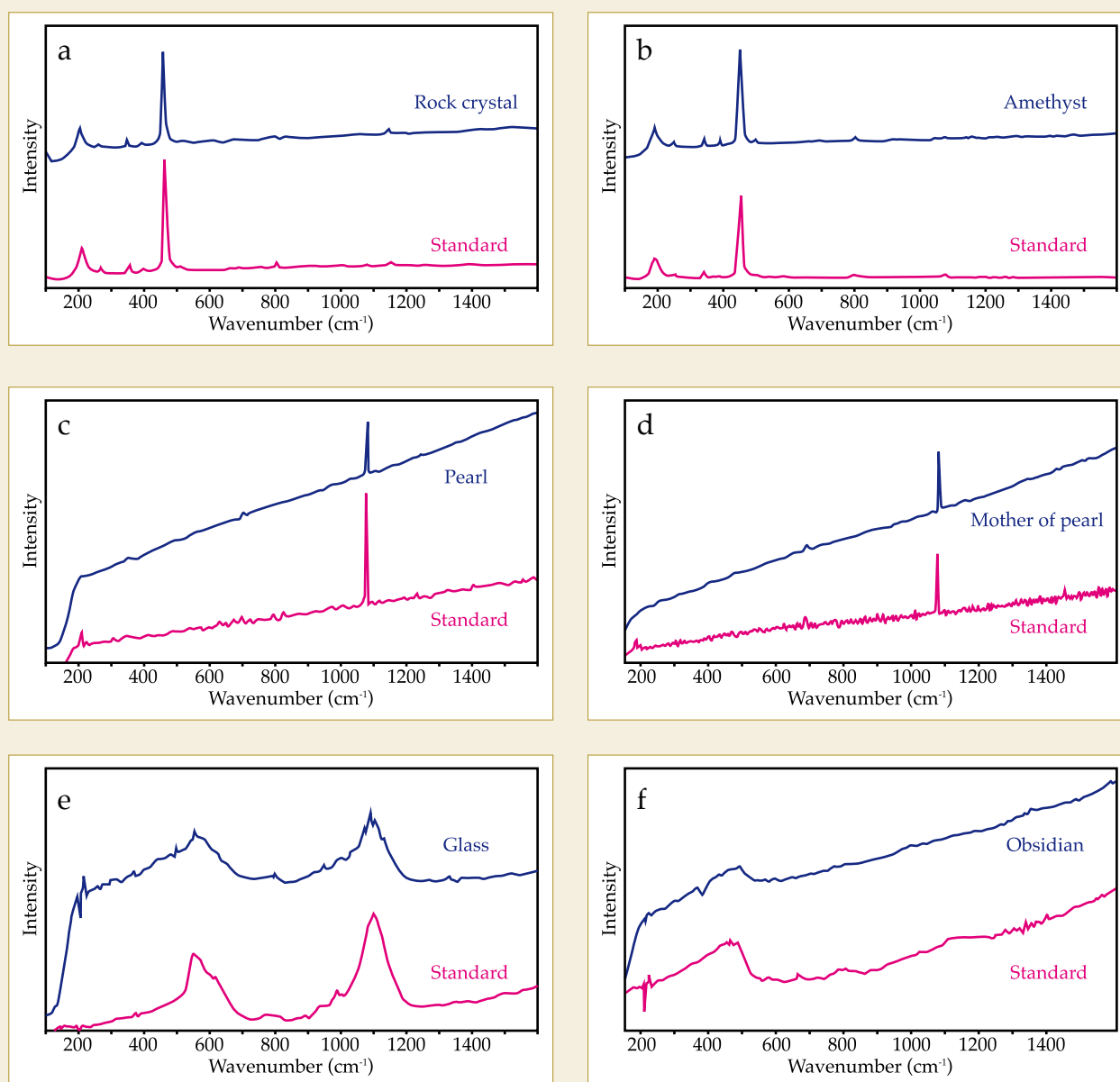
Figure 5: Raman spectra of some of the gems on the head reliquary of St Eustace using the Nd:YAG green laser (532 nm):

a) Raman spectra of Gem 10 rock crystal (blue) and the British Museum reference sample for quartz (pink).
b) Raman spectra of Gem 2 amethyst (blue) and the British Museum reference sample for quartz (pink).
c) Raman spectra of Gem 15 baroque pearl (blue) and the British Museum reference sample for pearl (pink).
d) Raman spectra of Gem 6 mother-of-pearl (blue) and the British Museum reference sample for aragonite (pink).
e) Raman spectra of Gem 3 orange-brown glass (blue) and the British Museum reference sample for glass (pink).
f) Raman spectra of Gem 4 obsidian (blue) and the British Museum reference sample for Obsidian (pink)

However, the orange-brown glass (Gem 3) gave a spectrum with two broad peaks, one at *c.* 559 cm^{-1} and the other at *c.* 1087 cm^{-1} with the green laser, which coincide with the bands for a glass reference sample (see *Figure 5e*) and correspond to the Si-O bending and stretching modes respectively (see Columban *et al.,* 2003).

Of the six synthetic glasses identified and analysed by XRF, five (Gems 3, 9, 14, 17 and 18) showed lime (CaO) contents of the order of 10%

with very small amounts of potash (K_2O *c.*1%). The moderate lime and low potash contents of these glasses mean that they are almost certainly soda-lime-silica glasses (Bowman and Freestone, 1997). Sayre and Smith (1961) recognized two types of soda-lime-silica glass to be prevalent in the pre-industrial world, one with low potash and magnesia (ie. below about 1.5 % each), and the other with higher concentrations of these components. Recent work has confirmed this basic subdivision

Figure 6: Photographs of some of the gems on the head reliquary of St Eustace:

a) Amethyst (Gem 5) showing feathers.

b) Carnelian (Gem 16).

c) Pale blue-grey chalcedony (Gem 1).

d) Baroque pearl (Gem 15) with the end of a drill hole just visible at the right-hand side. The drill hole has no purpose in this setting and indicates a previous use for the pearl.

e) Orange-brown transparent glass (Gem 3) showing bubbles characteristic of glass.

f) Glass nicolo simulant with a fish motif (Gem 14). Surface-reaching bubbles can be seen in the opaque pale grey table.

g) Colourless glass with opaque blue glass(?) globules forming a backing (Gem 9).

h) Obsidian (Gem 4) with a hippocamp intaglio on the table.

which is attributed to the use of different types of soda as raw material (Henderson, 1985; Wedepohl, 1997; Freestone and Gorin-Rosen, 1999). The high lime/potash ratios of the present glasses strongly suggest that they are all of the low-potash, low-magnesia category and they are considered to have been made using a naturally-occurring evaporitic source of soda, such as that found in the Wadi Natrun, Egypt.

In contrast, the glass Gem 7 has a quite different composition, with high concentrations of both potash and lime, around 20%. This type of potash-lime-silica glass was produced using the ashes of beech trees and ferns as sources of alkali, and is commonly termed 'woodash glass' or 'forest glass' (Henderson, 1985; Wedepohl, 1997).

Orange-brown transparent glass: Represented as the square cabochon, Gem 3, contains swirls and bubbles typical of glass (see *Figure 6e*). It is a soda-lime-silica type glass, containing around 1% iron oxide and a minor amount of manganese oxide which are the colourants. Also present is antimony in the order of 1% antimony oxide (see *Figure 7a*), which was used as a decolourant in the production of ancient glass (Sayre, 1963).

Red transparent glass: Gem 7 is a transparent red glass oval cabochon containing large bubbles, and is the sole representative of potash-lime-silica or woodash glass, typical of glasses made in medieval times. It contains low amounts of iron (tenths of a percent) but around 0.2% copper (see *Figure 7b*), which

might be just enough to precipitate copper crystallites, giving rise to a copper ruby glass. Alternatively (and more likely), the red tone may be due to the manganese oxide (*c.* 0.5%) in the glass.

Pale blue-grey opaque and dark brown glass:
It was originally unclear if Gem 14, with an opaque dark brown pavilion and an opaque pale blue-grey crown with a fish motif carved into the table, was a nicolo or a paste imitation (see *Figure 6f*). However, bubbles are visible in both parts of the stone and

these are indicative of synthetic glass. The pavilion of Gem 14 proved to be a soda-lime-silica glass coloured brown by *c.* 2-3% manganese oxide; also approximately 1% of antimony oxide is present, which makes it opaque. The crown is opacified by a relatively high concentration of antimony oxide (*c.* 5-10%), probably present as calcium antimonate (see for example Freestone, 1991). The pale-blue-grey coloration appears to be due to the presence of small quantities of cobalt and copper in solution (approximately 0.1% each),
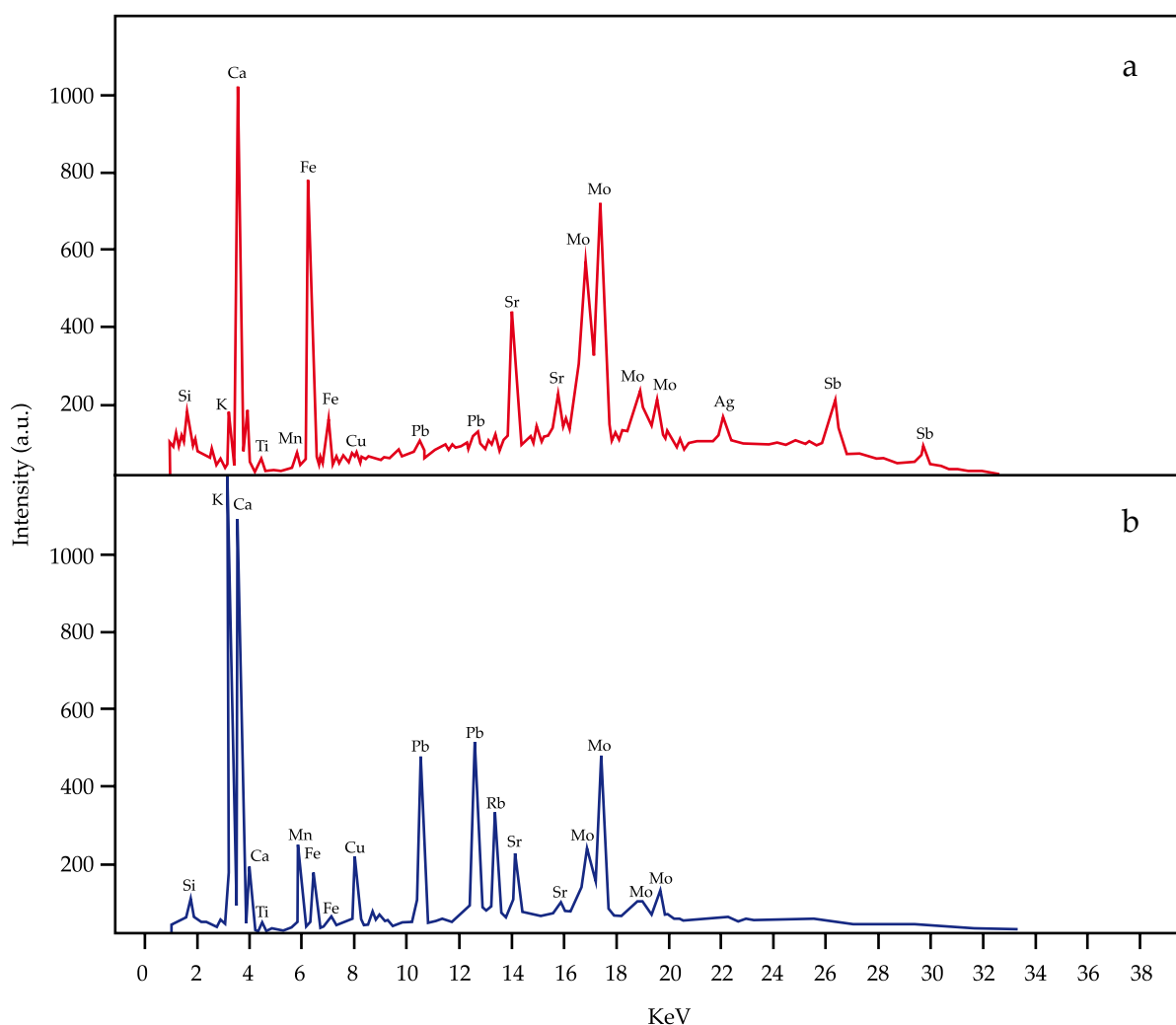
Figure 7: *X-ray fluorescence (XRF) spectra showing qualitative elemental composition of synthetic glasses (paste). The main elemental peaks are labelled by chemical symbol. The molybdenum peak (Mo) on each spectrum is derived from the X-ray target used.*

a) XRF spectrum of the orange-brown transparent glass (Gem 3). This glass is a silica glass with a high lime (Ca) to potash (K) ratio, high iron (Fe) content and low manganese (Mn) content. It is a Roman glass. The small silver (Ag) peak is probably due to contamination from the silver gilt mount.
b) XRF spectrum of the red transparent glass (Gem 7). This glass is a typical medieval glass with a high potash (K) content. It is a potash lime silica glass.

perhaps modified by the presence of *c*.5-10% lead oxide.

Colourless glass with blue backing and pale blue transparent glasses: Three oval cabochons, Gem 9 on the diadem, and the smaller Gems 17 and 18 set on the top of the base pedestal, are of pale blue, transparent, soda-lime-silica glass. Gem 9 is made from a colourless glass, bubble-rich, with rounded blue globules of what look like an ultramarine blue-coloured opaque ?glass at the base of the stone (see *Figure 6g*). Gems 17 and 18 were originally identified as crystal but their compositions and Raman spectra indicate that they are glass. Apart from the presence of a small amount of copper (*c.* 0.1%) which is insufficient to cause a strong coloration, in Gem 18 there appeared to be no deliberately added blue colourant (copper, cobalt). Instead, these glasses appear to owe their weak blue coloration to ferrous iron (c.f. Brill, 1988), which was incorporated incidentally as a component of the sand when the glass was originally made. Antimony, commonly added to ancient glass as a decolourant, is present in Gem 9, while all three glasses contain tenths of a percent of manganese, the typical decolourant of soda-lime-silica glass from the Roman period on.

Obsidian

An opaque black oval wheel-cut intaglio with a hippocamp (sea-horse) on the table facet (Gem 4), originally identified as jasper, proved to be glass (see *Figure 6h*). However, it gave a Raman spectrum unlike those of the other glasses, with a small broad band visible at *c.* 487 cm^{-1} using the green laser (see *Figure 5f*). XRF results indicated the presence of iron, potassium and low levels of calcium (*c.* 2% CaO); the low level of calcium and the fact that it is subordinate to potassium (*c.* 5%) suggests that this stone is probably the natural volcanic glass, obsidian.

Discussion

Nine of the 18 gems were identified as a varieties of quartz (including rock crystal,

amethyst, carnelian and chalcedony), six were identified as glass paste, two were organic gems (baroque pearl and mother-of-pearl) and one was obsidian.

The procurement of gems in the medieval period has been discussed by Stratford (1993: 22). He notes the high value attributed to rock crystal, as well as the passion for Antique cameos and intaglios, which were recycled in large numbers. Only one of the gems on the Basle Head is of rock crystal, and this may be taken as a reflection of the rarity of, or demand for, this material. Rock crystal does not appear to have been mined systematically and specifically in Europe before the nineteenth century and this stone may represent a chance European find (as a by-product of metal mining or in a river bed), a material imported from the East, or a re-ground Roman stone (Stratford, 1993: 22). Rock crystal sources include the Alps, Cyprus, Egypt, Hungary, Kharga Oasis, Spain and Turkey (Ogden, 1982). The obsidian intaglio (Gem 4) is likely to be a recycled Roman object, given its subject-matter and its composition; obsidian was not widely used in the medieval period, and the most accessible sources were in the Mediterranean region. The pearl bead clearly represents re-use of a gem that was originally part of another object, although its antiquity is uncertain. It is well-known that pearls were very popular during the Roman period (Clark, 1986), and it may well be possible that the pearl bead here is recycled Roman, in keeping with the re-use of Antique gems in this period. Pearls were seen as 'symbols of regeneration' in Christian iconography and were frequently used to adorn the crowns of sovereigns in Europe (Clark, 1986). The origins of the other natural stones are unclear; they might have been recently mined and traded items, or ground down from Antique (Roman) materials. The re-use of Roman gems for the Basle treasury reliquaries is possible as there was a Roman city in Basle and another close by, located on important trade routes. There are other examples of the re-use of Antique and other gems in medieval objects (e.g. Gray, 1989; Hänni *et al.*, 1998; Kiefert *et al.*, 2005). Gems

decorating reliquaries were probably chosen for their symbolic qualities of beauty, value, rarity and religious significance (Clark, 1986).

More informative as to origin are the glass stones, which were frequently used in the medieval period as gems (Bimson and Freestone, 2000; Dandridge, 2002), particularly in reliquaries and other sacred objects (Merrifield, 1849). The low-potash, soda-lime-compositions of the majority are at variance with the composition of northern European medieval glass which was typically a potash-lime-silica variety. There is a wide consensus that soda-lime-silica glasses of the low-potash type are likely to have gone out of production by the tenth century (Freestone and Gorin-Rosen, 1999; Henderson, 2002; Whitehouse, 2002). These factors, coupled with the common presence of antimony, indicate a Roman affinity for most of the glasses, and probably indicate the re-use of old Roman glass. The nicolo simulant, for example, is likely to represent a Roman cased (layered) cameo glass; analysis has shown that the pale overlays of these glasses were commonly opacified with calcium antimonate, accompanied by an elevated lead content (Freestone, 1990). Indeed, closely similar synthetic nicolos, with similarly rather crudely engraved intaglios, were widely used in the Roman finger rings (Johns, 1996). The re-use of Roman glass on this scale is not surprising. Writing early in the twelfth century, Theophilus in his book *De Diversis Artibus* tells us that glass mosaic tesserae from old Roman buildings were used to enamel metalwork (Hawthorne and Smith, 1963). Analysis of twelfth-century enamels confirms this statement (Freestone, 1992, 1993). Written some time before the twelfth century, Eraclius describes in his book *De Coloribus et Artibus Romanorum* how Roman glass was used to mould glass gems (Merrifield, 1849). An exception in the present case is the red cabochon, Gem 7, which appears to represent a contemporary medieval glass. Interestingly, the red glasses of the enamelwork of the Mosan region (the valleys of the Meuse and the Rhine in what is now Belgium and the Rhineland) are also exceptional in a similar way, in that while all of the other colours appear to be re-used Roman glasses, the reds (in the case of the enamels, opaque rather than translucent reds) are clearly medieval (Freestone, 1993). The reasons for this are not completely clear but may relate to the relative rarity of red glass in general and translucent red glass in particular, in the ancient world. It was very difficult to produce, and we now know that it requires the presence of extreme reducing conditions in the glass for copper red or very oxidizing conditions for manganese red. Once the medieval glass workers had learned how to produce red glass on a large scale for ecclesiastical 'stained' glass windows, it is likely to have become widely available.

Comparisons with previous analyses of gems in medieval reliquary treasures

Raman microspectroscopy has also been used to analyse the gems adorning other objects from the Basle Cathedral Treasury, the Reliquary cross and the Dorothy monstrance, both believed to have been manufactured around 1440 (Hänni *et al*., 1998). Hänni *et al*. (1998) identified rock crystal, amethyst, smoky quartz, citrine, quartz-topped doublets, turquoise and glass (paste) in the Reliquary cross, and rock crystal, amethyst, black chalcedony, carnelian, agate, quartz-topped doublets, glass doublet, peridot, sapphire, garnet, spinel and glass (paste) in the Dorothy monstrance. A carnelian intaglio of a goat and an agate cameo of a woman's head, both set in the Dorothy monstrance, suggested to Hänni *et al*. (1998) the re-use of either Greek or Roman engraved gems, a common practice in the medieval era. The other possibility they mooted was that they were made at the same time as the objects in which they are found, coinciding with a resurgence of interest in engraved gems in the fifteenth century. Raman spectral analysis of the gems in the cross of the church of St Clara and the Agnus Dei monstrance, also part of the Basle Cathedral Treasury, by Kiefert *et al.* (2005) identified sapphires. Both objects contain sapphires with drill holes. In the first, an oval

cabochon sapphire was observed to have a drill hole from end to end along its length, and in the second a light blue sapphire had two drill holes. This again illustrates the re-use of gems in medieval reliquaries.

Reiche *et al.*'s (2004) non-destructive analysis of the gems in the early eleventh-century reliquary Heinrich's cross, also part of the Basle Cathedral Treasury, was made using a mobile Raman microscope. They identified most of the gems as glass paste or varieties of quartz (including rock crystal, amethyst, carnelian and chalcedony), but also found some garnets (almandine, spessartine and almandine-spessartine varieties), sapphires and rubies. It is interesting to note the relatively high use of varieties of quartz and synthetic glass on reliquaries from the Basle Cathedral Treasury (see *Table II*). Unfortunately, the glass paste compositions were not further investigated by either Hänni *et al.* (1998) or Reiche *et al.* (2004), so no detailed comparisons can be made with the glass gems on the head reliquary of St Eustace. However, using XRF and open-architecture X-ray diffraction, Dandridge (2002) did identify the compositions of the glass used for gems in the late twelfth-century Romanesque reliquary cross from Limoges, France, as being consistent with both Roman glass and Romanesque enamels. He also identified rock crystal in the cross.

The identifications of the gems set in the reliquary objects relate only to those currently in place, which may or may not be original, as also noted by Reiche *et al.* (2004). There is no way of knowing if some or all of the gems on the reliquary head of St Eustace have been replaced since it was made.

Conclusions

The use of the Raman microspectroscope with a horizontal laser attachment, in combination with X-ray fluorescence spectrometry and a 10× loupe, has allowed the identification of the full range of stones adorning the head reliquary of St Eustace. It has been possible to correct a number of the earlier identifications and in some cases update the terminology used. In particular, glass or paste is seen to be much more abundant in the assemblage. Furthermore, the use of X-ray fluorescence analysis, coupled with a modern understanding of the chemistry of early glass, has allowed the identification of the majority of glass stones as re-used Roman glass. There is also good evidence that several of the natural gems (obsidian, pearl) were re-used, probably Antique. Thus the present investigation emphasizes the extent to which the re-use of old materials to decorate metalwork was embedded in the practices of the medieval goldsmith. Recent research suggests that the re-use of old Roman glass tailed off in the thirteenth century (Biron *et al.*, 1996). However, a fetish for Roman intaglios and engraved stones continued through to relatively modern times, and it was only with their removal from circulation into public museums and private collections of antiquities that the processes of re-use, reworking or incorporation into new objects were reduced on any significant scale.

Acknowledgements

Table II: Proportions of gem varieties in reliquaries from the Basle Cathedral Treasury.

Gemstone type	Head reliquary of St Eustace	Hänni *et al.* (1998)	Reiche *et al.* (2004)
Quartz varieties	50%	40%	22%
Glass (paste)	33%	30%	46%
Other gemstone varieties	17%	30%	32%
Total number of gems	18	47	68

Rome programme. Janet Ambers and Mike Hughes kindly helped with the Raman microspectroscopic analysis, and Mike Cowell with the XRF. Tony Milton took the photographs of the Basle head reliquary. Tony Simpson is thanked for his help with the graphics. We would also like to thank the referees for their suggestions and comments on this paper.

References

Bimson, M., and Freestone, I.C., 2000. Analysis of some glass from Anglo-Saxon jewellery. In: J Price (Ed.), *Glass in Britain and Ireland, AD 350-1100*. British Museum, London, Occasional Paper 127, 131-6

Bowman, S.G.E., and Freestone, I.C., 1997. Early 14th century enamelwork: a technical examination of the Hanap cover of All Souls College, Oxford. *TECHNE, 6*, 41-7

Biron, I., Dandridge, P., and Wypiski, M., 1996. Techniques and materials in Limoges enamels. In: B.D. Boehm and E. Taburet-Delahaye (Eds), *Enamels of Limoges 1100-1350.* Metropolitan Museum, New York. 48-62

Brill, R. H., 1988. Scientific investigations. In: G.D. Weinberg, *Excavations at Jalame: site of a glass factory in Late Roman Palestine.* University of Missouri, Columbia. 257-94

Brill, R. H., 1999. *Chemical analyses of early glasses*, volumes 1 and 2. Corning Museum of Glass, Corning, NY

Calligaro, T., Colinart, S., Poirot, J.-P., and Sudres, C., 2002. Combined external-beam PIXE and µ-Raman characterization of garnets used in Merovingian jewellery. *Nuclear Instruments and Methods in Physics Research B, 189*, 320-7

Cherry, J., 2001. 13. Kopfreliquiar des hl. Eustachius. In: *Der Basler Munsterschatz*, Meles, B. with Historisches Museum Basel, Bayerisches Nationalmuseum, Metropolitan Museum of Art, New York, Christoph Merian Verlag

Clark, G., 1986. *Symbols of excellence: precious materials as expressions of status*. Cambridge University Press, Cambridge

Clark, R.J.H., and van der Weerd, J., 2004. Identification of pigments and gemstones on the Tours Gospel: the early 9th century Carolingian palette. *Journal of Raman Spectroscopy, 35*, 279-83

Columban, Ph., March, G., Mazerolles, L., Karmous, T., Ayed, N., Ennabli, E., and Slim, H., 2003. Raman identification of materials used for jewellery and mosaics in Ifriqiya. *Journal of Raman Spectroscopy, 34*, 205-13

Dandridge, P., 2002. Reconsidering a Romanesque reliquary cross. *Met Objectives, 4*(1), 5-7

de Voragine, J., 1993. *The golden legend: readings on the Saints*. Translated by W.G. Ryan, Princeton University Press, Princeton

Freestone, I.C., 1990. Laboratory Studies of the Portland Vase. *Journal of Glass Studies, 32*, 103-7

Freestone, I., 1991. Looking into Glass. In: S. Bowman (Ed.), *Science and the past.* British Museum Press, London, 37-57

Freestone, I.C., 1992. Theophilus and the composition of medieval glass. In: P.B. Vandiver, J.R. Druzik, G.S.,Wheeler and I.C. Freestone (Eds), *Materials Issues in Art and Archaeology III. Materials Research Society Symposium Proceedings, 267*, 739-46

Freestone, I.C., 1993. Compositions and origins of glasses from Romanesque champleve enamels. In: N. Stratford (Ed.), *Catalogue of Medieval enamels in the British Museum. Volume II: Northern Romanesque enamel.* British Museum Press, London. 37-45

Freestone, I.C., and Gorin-Rosen, Y., 1999. The great glass slab of Bet Shearim - an early Islamic glass-making experiment? *Journal of Glass Studies, 41*, 105-16

Gray, A., 1989. A fourteenth century crown. *Journal of Gemmology, 21*(7), 431-2

Hänni, H.A., Schubiger, B., Kiefert, L., and Häberli, S., 1998. Raman investigations on two historical objects from Basel Cathedral: The Reliquary cross and Dorothy monstrance. *Gems & Gemology, 34*(2), 102-25

Hawthorne, J.G., and Smith, C.S., 1963. *On divers arts: the treatise of Theophilus translated from the medieval Latin*. University of Chicago Press, Chicago

Henderson, J., 1985. The raw materials of early glass production. *Oxford Journal of Archaeology, 4*, 267-91

Henderson, J., 2002. Tradition and experiment in first millennium AD glass production – the emergence of early Islamic glass technology in Late Antiquity. *Accounts of Chemical Research, 594-602

Huang, E., 1999. Raman Spectroscopic Study of 15 Gem Minerals. *Journal of the Geological Society of China, 42*, 301-18

Husband, J., and Chapuis, J., 2001. *The Treasury of Basel Cathedral*. The Metropolitan Museum of Art, Yale University Press, New Haven

Johns, C.M., 1996. *The Jewellery of Roman Britain*. UCL Press, London

Kiefert, L., Chalain, J-P., and Häberli, S., 2005. Case Study: diamonds, gemstones and pearls: from the past to the present. In: H.G.M. Edwards and J.M. Chambers (Eds.), *Raman spectroscopy in archaeology and art history*. RSC Analytical Spectroscopy Monographs, The Royal Society of Chemistry

Kingma, K.J., and Hemley, R.J., 1994. Raman spectroscopic study of microcrystalline silica. *American Mineralogist, 79*, 269-73

Merrifield, M.P., 1849. *Original treatises on the arts of painting*, Volume I. John Murray, London

Ogden, J., 1982. *Jewellery of the Ancient World*. Trefoil Books, London

Pinet, M., Smith, D.C., and Lasnier, B., 1992. Utilité de la Microsonde Raman pour L'Identification Non Destructive des Gemmes. In: *La microsonde Raman en gemmologie*. Association Française de Gemmologie

Reiche, I., Pages-Camagna, S. and Lambacher, L., 2004. *In situ* Raman spectroscopic investigations of the adorning gemstones on the reliquary *Heinrich's Cross* from the Treasury of Basel Cathedral. *Journal of Raman Spectroscopy, 35*, 719-25

Sayre, E. V., 1963. The intentional use of antimony and manganese in ancient glasses. In F. R. Matson and G. E. Rindone (Eds.) *Advances in glass technology, Part 2.* Plenum Press, New York. 263-82

Sayre, E.V., and Smith, R. W., 1961. Compositional categories of ancient glass. *Science,* **133**, 1824-6

Smith, D.C., 2005. Overview: jewellery and precious stones. In: H.G.M. Edwards and J.M. Chambers (Eds.) *Raman spectroscopy in archaeology and art history.* RSC Analytical Spectroscopy Monographs, The Royal Society of Chemistry

Smith, D.C., and Robin, S., 1997. Early Roman Empire intaglios from 'rescue excavations'. In: Paris: an application of the Raman microprobe to the non-destructive characterization of archaeological objects. *Journal of Raman Spectroscopy*, **28**, 189-93

Stratford, N., 1993. *Catalogue of Medieval enamels in the British Museum. Volume II: Northern Romanesque enamel.* British Museum Press, London

Wedepohl, K.H., 1997. Chemical composition of medieval glass from excavations in West Germany. *Glastech. Ber. Glass Sci. Technol.,* **70**, 246-55

Whitehouse, D., 2002. The transition from natron to plant ash in the Levant. *Journal of Glass Studies,* **44**, 193-6

Williams, Q., 1995. Infrared, Raman and Optical Spectroscopy of Earth Minerals. In: T.J. Ahrens (Ed.) *A Handbook of Physical Constants: Mineral Physics and Crystallography.* AGU Reference Shelf Volume 2, American Geophysical Union

The orientation and symmetry of light spots and asterism in rose quartz spheres from Madagascar

Dr Karl Schmetzer[1] and Dr Michael Krzemnicki[2]

1. Taubenweg 16, D-85238 Petershausen, Germany
2. SSEF Swiss Gemmological Institute, Falknerstr. 9, CH-4001 Basel, Switzerland

Abstract: *The orientation of light spots on the surface of four asteriated rose quartz spheres from Madagascar is described. The up to 50 different light spots form similar patterns on all samples examined with respect to their orientation, but are somewhat different according to their relative intensity. They are represented by the poles of six groups of symmetry equivalent quartz crystal forms, related to prismatic, rhombohedral and basal crystal faces. The phenomenal light spots are caused by reflection at plane phase boundaries with an orientation parallel to crystal faces of the rose quartz host and are due to inclusions of tiny minerals or negative crystals and/or oriented reflecting plane fluid cavities or mineral platelets.*

Introduction

Phenomenal quartzes are known from various localities. Specimens with needle-like inclusions orientated parallel to one direction are known as quartz cat's-eyes. Asteriated quartzes or rose quartzes with six-rayed stars reveal three groups of needle-like inclusions orientated in a plane perpendicular to the *c*-axis. Rarely twelve-rayed stars are seen which show six groups of needles in the same plane. Multi-star quartzes revealing numerous stars on the surface of cabochons or complete spheres come mainly from Sri Lanka. The multi-star network is due to numerous intersecting light bands which are caused by various groups of needle-like inclusions (Kumaratilake, 1997; Schmetzer and Glas, 2003).

Occasionally, asteriated rose quartzes reveal – in addition to the three ordinary light bands forming the six-rayed star – several more or less sharp light spots. Such additional light spots have already been described by Goldschmidt and Brauns (1911) and by Kalkowsky (1915) in rose quartz spheres from Brazil and Madagascar as 'Lichtknoten' (light knots). This optical phenomenon has rarely been mentioned in gemmological textbooks (see for example Bauer and Schlossmacher, 1932).

On asteriated rose quartz spheres or cabochons seen on various occasions at mineral or gem shows, the authors have also observed such additional light spots, mainly in material from Brazil or

Madagascar. The present study, however, started when we received two extraordinary rose quartz spheres, weighing 421 and 159 grams, diameters about 6.7 and 4.9 cm. The specimens originated from Madagascar and were submitted by the Swiss gem merchant A. Leuenberger to the SSEF Swiss Gemmological Institute, Basel, Switzerland. Leuenberger had noticed that in addition to their ordinary six-rayed asterism, the rose quartz spheres showed numerous light spots distributed over the complete surface, a phenomenon that he had not seen in any of the numerous spheres he had cut or seen in the past.

Stimulated by the initiative of Mr Leuenberger, the authors examined a large number of asteriated and non-asteriated rose quartz spheres that were offered by several Malagasy dealers at the Munich mineral fair. Most of these samples showed only the ordinary six-rayed star of asteriated quartz *(Figure 1)*. However, we were able to select two additional spheres of 138 and 113 grams in weight, diameters 4.6 and 4.3 cm, respectively, for the present study, which showed the optical phenomenon mentioned above. Rose quartz is found in many localities on the island of Madagascar and at all of these is of pegmatitic origin (Pezzotta, 2001). Such pegmatitic origin has also been reported for Brazilian asteriated and non-asteriated rose quartz by Cassedanne and Roditi (1991).

Visual appearance and macroscopic observation

All four rose quartz spheres showed a similar phenomenal pattern consisting of a complete six- or twelve-rayed star and additional light spots. The central star in spheres A,C and D (see a summary of observed light effects in *Table 1*) revealed three intersecting light bands and was not very strong *(Figures 2a, 4, 5a)*. In B, three additional, even weaker light bands were present forming, together with the three somewhat more intense light bands, a twelve-rayed central star *(Figure 3a)*. The

intersection points of these stars are called north and south poles of the spheres.

In all four spheres, it was possible to follow the six arms of the star (in B to follow the six stronger arms of the twelve-rayed star) from the north to the south poles of the spheres. Turning the spheres to follow these light bands along the arms of the star, i.e. from the first intersection point (north

Figure 1: Ordinary six-rayed asterism in a rose quartz from Madagascar. This sphere weighs 81 grams and measures 3.9 cm in diameter; the light spot left of the intersection point of the six arms of the star is the reflection of the fibre optic spot light used for illumination.

pole) to the second intersection point (south pole), five additional light spots are located on each of these light bands *(Figures 2b, 3b)*. From the positions of these light spots, i.e. from the pole distances of the different spots on the arms of the star, it is obvious that these light spots form symmetry equivalent groups (designated groups 1,3 and 4 in *Table 1, column 1*). The light spots designated as group 1 were located at a distance of 90° to the poles of the spheres, i.e. at the equator of all samples *(Figure 2b)*. The light poles of groups 3 and 4 were on the upper and lower hemispheres of the rose quartz spheres *(Figure 3b)*. It was also observed that the patterns of spots observed on the upper and lower half of the spheres are identical with respect to pole distances and intensities. A schematic drawing of all the patterns of light bands and light spots observed on the four spheres is given in *Figure 6*.

Table 1: Phenomenal light effects in four rose quartz spheres from Madagascar.

Sphere						A	B	C	D
Weight [grams]						138	113	159	421
Diameter [cm]						4.6	4.3	4.9	6.7
Central star						six-rayed	twelve-rayed	six-rayed	six-rayed
Other light bands									$[0\bar{1}11]$
Group of faces	**Designation of faces**	**Symbol**	**Miller indices (hkil)**	**Angle of light spots versus c-axis**	**Number of symmetry equivalent crystal faces and light spots**	**Intensity of light spots, relation to the central star***			
1	hexagonal prism	m	$(10\bar{1}0)$	90°	6	strong	strong	moderate	strong
2	trigonal prism	a	$(11\bar{2}0)$	90°	3	weak	moderate	n.o.	weak
		a'	$(2\bar{1}\bar{1}0)$		3				
3	rhombohedron	r	$(10\bar{1}1)$	51.8°	2x3	strong	strong	moderate	strong
		z	$(01\bar{1}1)$		2x3				
4	rhombohedron	π	$(10\bar{1}2)$	32.4°	2x3	weak	moderate	moderate	weak
		π'	$(01\bar{1}2)$		2x3				
5	trigonal dipyramid	s	$(11\bar{2}1)$	65.6°	2x3	moderate	strong	moderate	moderate
		s'	$(2\bar{1}\bar{1}1)$		2x3				
6	basal pinacoid	c	(0001)	0°	2x1	moderate	strong	strong	moderate

* Light spots related to the arms of the central six- or twelve-rayed star are indicated in blue, light spots not related to the central star are indicated in red.   n.o. = not observed.

Following the arms of the central stars from the north pole to the south pole, on spheres A and D (see again *Figure 6*), the sequences of light spots on the arms of the star showed the following intensities: a first spot of low intensity (group 4), three subsequent light spots of high intensity (belonging to group 3, to group 1 and again to group 3) and another light spot of low intensity (again group 4). As already mentioned, the middle light spot of high intensity (group 1) was located exactly half way between the north and south poles of the sphere, i.e. at its equator. In spheres B and C, the same sequence and position of light spots belonging to groups 1, 3 and 4 was observed, although with different relative intensities (*Table 1*).

Rotating spheres A and D to view their virtual equators, the six intense light spots (group 1) on the six arms of each star were clearly visible. In addition, six more light spots of lower intensity (group 2) were observed, equidistant from the light spots on the arms of the six-rayed star. Consequently, a total of 12 light spots (six of higher intensity on the arms, group 1, and six of the lower intensity, group 2) were located at the equator of the sphere. Finally, between each light spot of low intensity at the equator and the north
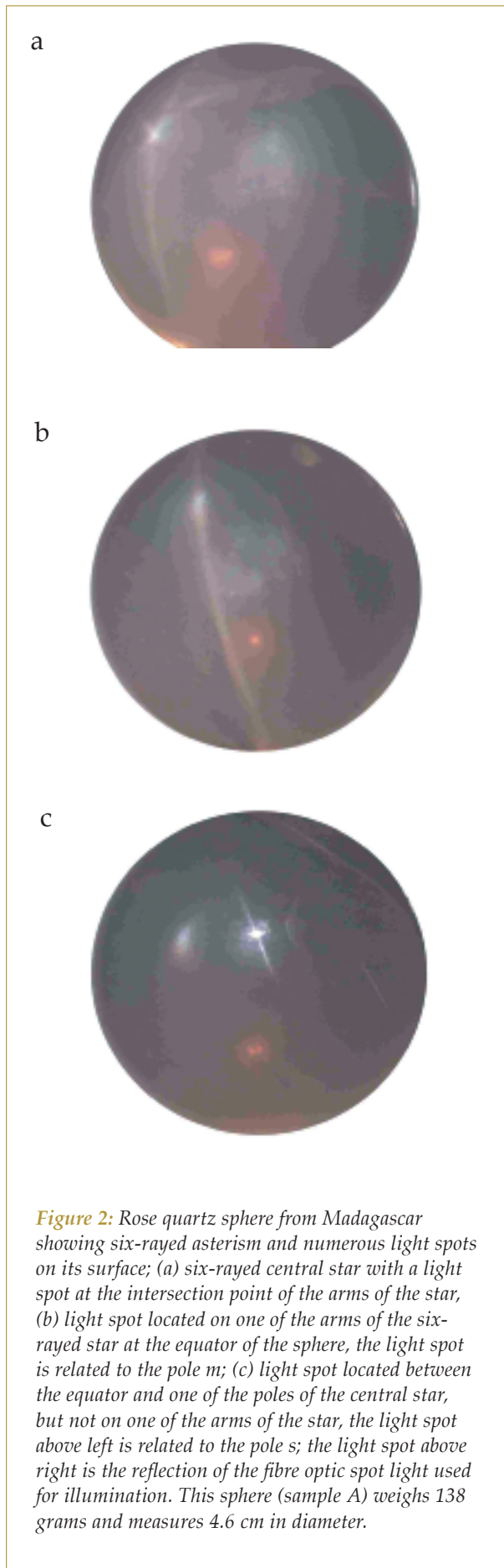
Figure 2: *Rose quartz sphere from Madagascar showing six-rayed asterism and numerous light spots on its surface; (a) six-rayed central star with a light spot at the intersection point of the arms of the star, (b) light spot located on one of the arms of the six-rayed star at the equator of the sphere, the light spot is related to the pole m; (c) light spot located between the equator and one of the poles of the central star, but not on one of the arms of the star, the light spot above left is related to the pole s; the light spot above right is the reflection of the fibre optic spot light used for illumination. This sphere (sample A) weighs 138 grams and measures 4.6 cm in diameter.*
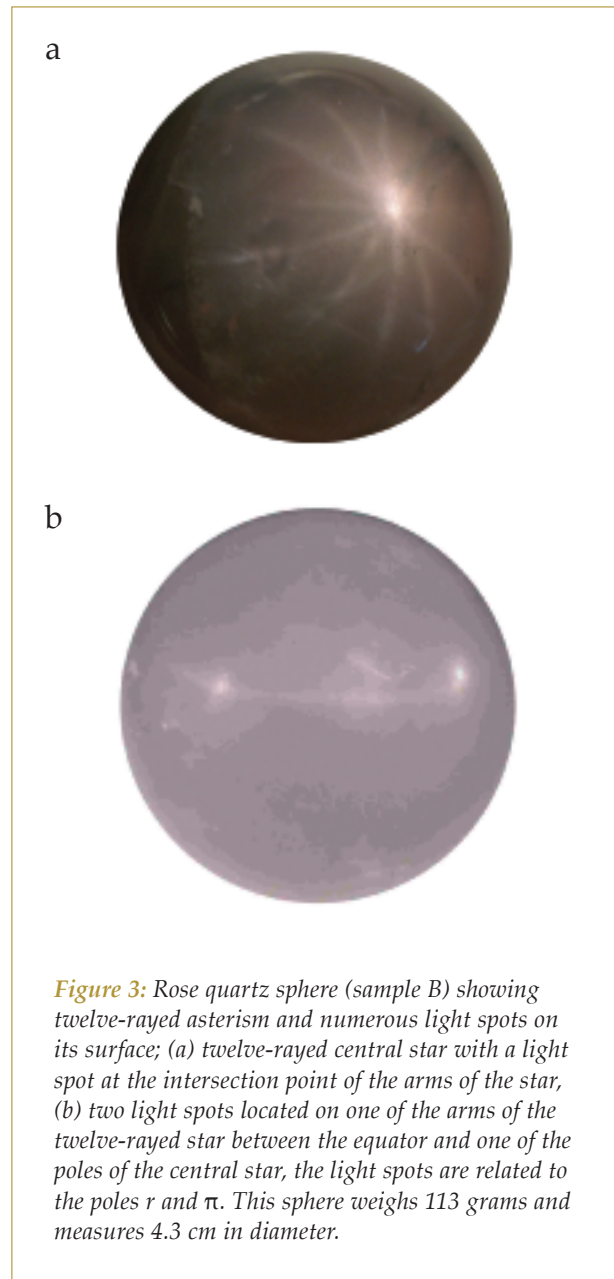
Figure 3: *Rose quartz sphere (sample B) showing twelve-rayed asterism and numerous light spots on its surface; (a) twelve-rayed central star with a light spot at the intersection point of the arms of the star, (b) two light spots located on one of the arms of the twelve-rayed star between the equator and one of the poles of the central star, the light spots are related to the poles r and π. This sphere weighs 113 grams and measures 4.3 cm in diameter.*

and south poles of the sphere, one additional light spot of moderate intensity is present (*Figures 2c, 5c*). These symmetry equivalent light spots are designated as group 5.

In spheres B and C, in addition to the different relative intensities of the light spots belonging to groups 1, 3 and 4, the following differences were observed. In B, the light spots belonging to groups 2 and 5 were stronger in intensity than in A and D. They lie on the additional six light bands of the twelve-rayed central star (see *Figure 3a*). In sphere C, there was no evidence for 6 light spots of low intensity at the equator (group 2). The 12 light spots between the arms of the star (group 5),

Figure 4: Rose quartz sphere (sample C) showing six-rayed asterism with a light spot at the intersection point of the arms of the star; the light spot at the right is the reflection of the fibre optic spot light used for illumination. This sphere weighs 158 grams and measures 4.9 cm in diameter.

however, were present (see again *Table 1*).

In all four spheres, additional light spots are present at the intersection points of the central star, i.e. at the north and south poles of the spheres (*Figures 2a, 3a, 4* and *5a*). They are of different sizes and intensities but this variation cannot be explained by intersection of the arms of the six- or twelve-rayed stars alone.

Sphere D contains distinct light bands forming the arms of the six-rayed central star, and additional light bands of low intensity (see *Figure 5b*), but it was extremely difficult to follow these light bands over the surface of the complete sphere. However, they appear to form a network between at least some of the light spots described above. The other three spheres, did not appear to show any similar networks of light bands.

Crystallographic orientation of light spots

Using the stereographic projection, a quick overview of the number and position of the various groups of light spots in relation to the six- or twelve-rayed central star is obtainable (*Figure 6*). In total, 48 light spots belonging to five groups (6 + 6 + 12 + 12 + 12 spots of groups 1 to 5) were observed (*Table 1*). If we add the two spots at the north and south pole (group 6), the sphere shows 50 light spots distributed over its surface.

It is evident that the positions of the spots at the equator (two groups with 6 spots each) are identical with the poles of the hexagonal prism *m* (group 1) as well as with the trigonal prisms *a* and *a'* (group 2) of quartz. The light spots at the intersection points of the central stars represent the position of the basal pinacoid *c*.

With this basic information, the angles between the remaining light spots which are not located at the equator of the sphere (three groups of 12 spots each) and the poles of the spheres were estimated. Using these data, the positions of the spots were found to be identical with the positions of the poles of four different rhombohedra, *r*, *z*, *π* and *π'* (groups 3 and 4), and two trigonal dipyramids *s* and *s'* (group 5). In summary, the positions of all 50 light spots observed on the surface of the sphere are represented by the pole positions of six groups of symmetry equivalent quartz crystal forms, namely basal pinacoid, prism, rhombohedron and dipyramid. Consequently, the oriented light spots are represented by the pole positions of known quartz crystal faces.

Crystallographic orientation of additional light bands

On the surface of sphere D, several light bands of low intensity were observed forming a special type of network. Although these weak reflections did not form complete light bands over the surface of the sphere, one network of six symmetry equivalent light bands was clearly established. Following one of these light bands from the equator at a light spot belonging to a pole of a trigonal prism (*a* or *a'*), this light band connects one light spot belonging to the pole of a first rhombohedron (*r* or *z*) with a light spot belonging to the pole of a second rhombohedron (*π* and *π'*) and a light spot belonging to the pole of a third rhombohedron (again *r* or *z*), running through the equator at a second prism (*a* or *a'* ; see *Figure 6D*). These light bands are inclined to the *c*-axis and are represented by the crystallographic zone symbol [0111]. The angle of these six light bands to the *c*-axis is calculated as 32.4°. Consequently, the needle

axis of elongated particles forming these light bands is inclined at an angle of 57.6° to the *c*-axis.

Two of this group of six equivalent light bands intersect at each rhombohedral light spot belonging to a pole of group 3 (*r* or *z*) (*Figure 5b*). Combined with one light band of the central star, each rhombohedral light spot related to poles of group 3 also becomes the centre of a weak six-rayed star. In addition, the light spots belonging to poles of groups 2 and 4 become centres of weak four-rayed stars (see *Figure 6*).

Other groups of symmetry equivalent light bands (caused by additional groups of needle-like inclusions in different orientation) may also be present, but their intensity was too low to determine any orientation.

Microscopic observation

Without destroying the rose quartz spheres we were able to observe at high magnification extremely thin needles in all samples, especially by means of fibre optic illumination. These sets of needles are responsible for the six- or twelve-rayed asterism and for the additional light bands of sphere D. Such thin needles are commonly described as oriented rutile needles in quartz host crystals.

In C, we found numerous extremely small reflecting particles in all orientations of the sphere, in which distinct light spots were seen on the surface. However, we were unable to resolve the individual particles and to determine if they were mineral inclusions or negative crystals. We were also unable to determine if individual particles reflect only in one orientation of the host crystal or if individual particles were related to several reflections and light spots.

In D, reflecting particles were present that were large enough to be resolved with the gemmological microscope. In detail, we observed a dense pattern of oriented reflecting plane faces, some hexagonally or trigonally outlined and commonly elongated parallel to a particular crystallographic direction (*Figure 7a, b*). This specific pattern of reflecting, mostly elongated plane faces was seen in each of the numerous orientations of the sphere in which a

a

b

c
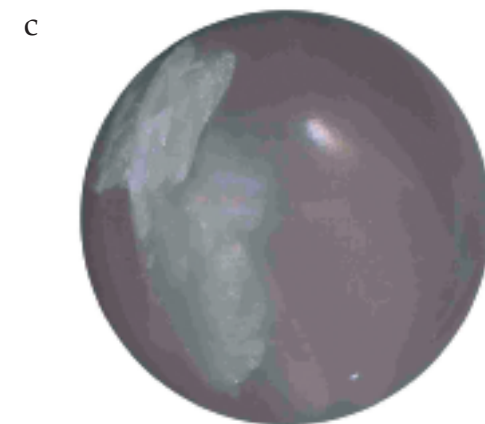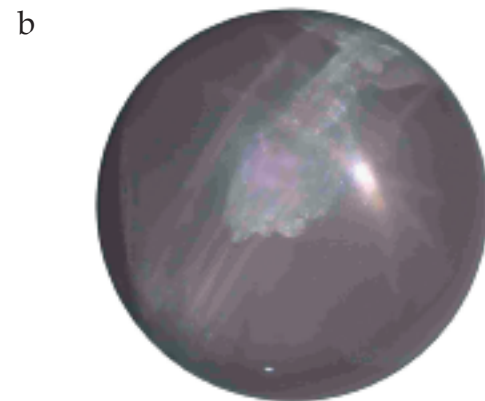
Figure 5: Rose quartz sphere (sample D) showing six-rayed asterism, numerous light spots and light bands on its surface; (a) six-rayed central star with a light spot at the intersection point of the arms of the star, (b) light spot located at the intersection point of one of the arms of a six-rayed star with two additional weak light bands, the light spot is related to the pole r; (c) light spot located between the equator and one of the poles of the central star, but not on one of the arms of the star, the light spot is related to the pole s. This sphere weighs 421 grams and measures 6.7 cm in diameter.
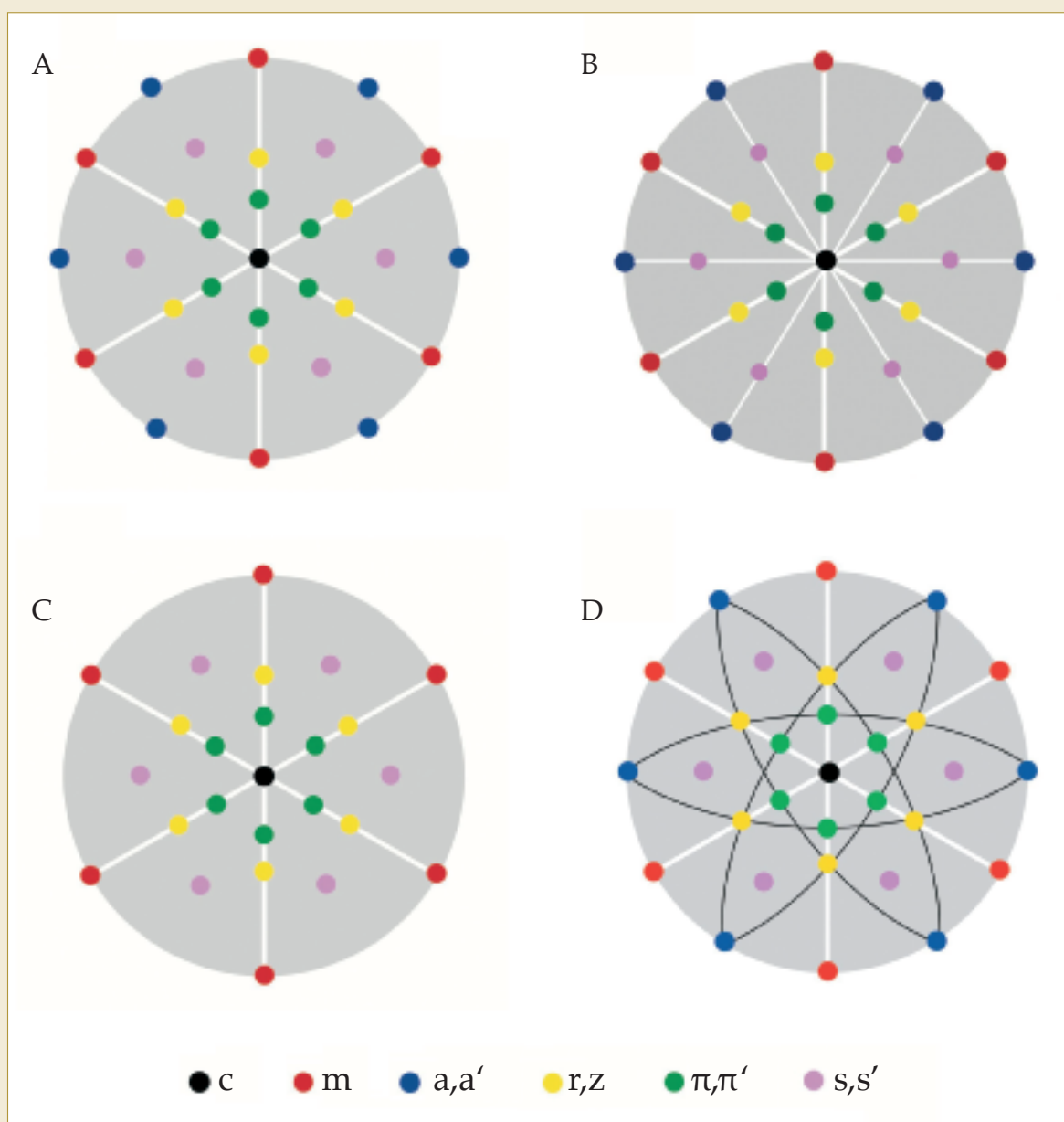
Figure 6: Stereographic projection of light poles on the surfaces of rose quartz spheres (samples A,B,C and D) from Madagascar and their orientation relative to the light bands of the central six- or twelve-rayed stars (only the upper hemispheres of the projection spheres are drawn). The light spots are related to several groups of symmetry equivalent poles of quartz crystal faces. In sample D, additional light bands perpendicular to $[0\bar{1}11]$ form four- and six-rayed stars at the positions of rhombohedral and prismatic light spots. Symbols at the bottom represent Groups 1-6 of faces detailed in Table 1.

somewhat larger light spot (compared to C with the extremely small particles) was seen on the surface. Due to microscopic examination it is, however, not clear if these reflecting plane faces represent solid or fluid-containing thin platelets or if they represent the surfaces of larger solid or fluid inclusions (mineral inclusions or fluid-filled negative crystals).

An investigation of the larger inclusions

in sphere D by micro-Raman spectroscopy did not lead to any conclusive results. We obtained only the spectrum of the quartz host but no additional lines which could help to further identify the inclusions.

Spheres A and B contain both reflecting small particles and the somewhat larger plane faces that are present in C and D respectively. In A and B, however, the
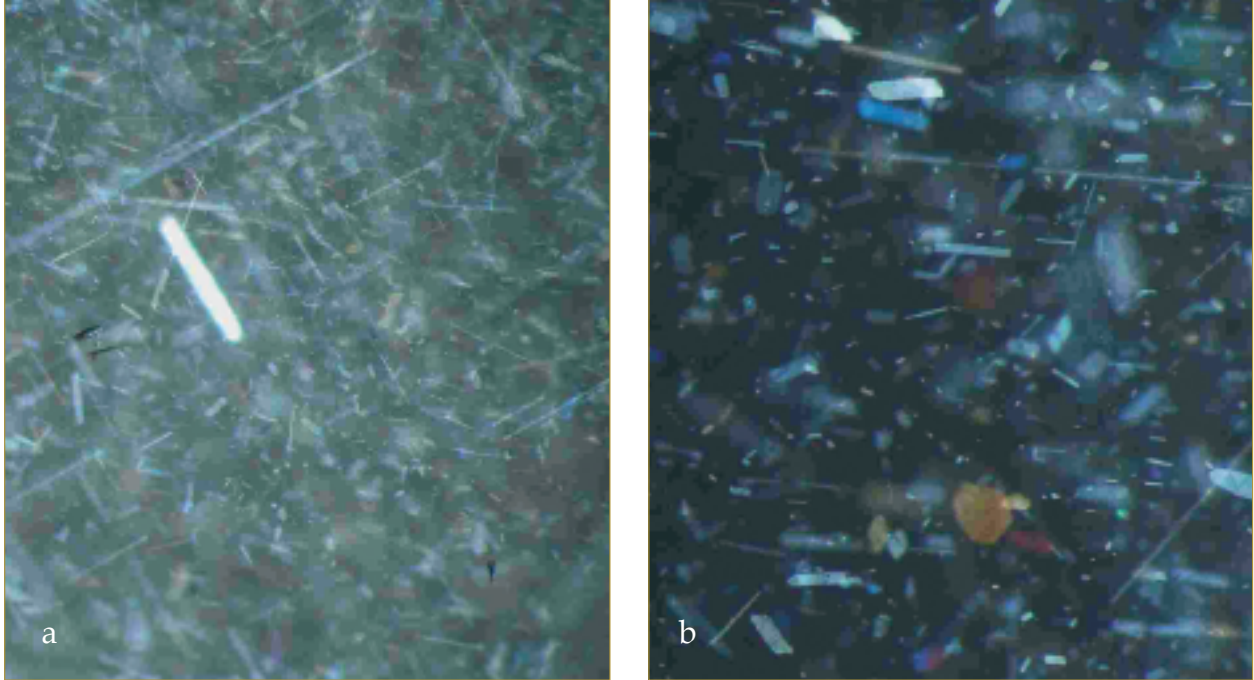
Figure 7: Numerous reflecting plane faces, some hexagonally or trigonally outlined and mostly elongated parallel to a specific crystallographic direction were seen in sample D in each orientation of the sphere in which light spots were seen on its surface; (a) magnified 40 ×, (b) magnified 80 × (photo 7b by H. A. Hänni).

reflecting plane faces are smaller. At present we are unable to decide if we have one distinct type of inclusion with different sizes or if we really have two different types of inclusion present in the rose quartz spheres – in addition to the series of extremely thin needles which are assumed to cause the light bands of the more or less intense six- or twelve-rayed stars.

Further research is needed to identify all types of inclusion in rose quartz spheres showing asterism and additional light spots. This could be done with oriented thin sections (cut from similar phenomenal spheres) using a combination of microscopy, electron microscopy, electron diffraction, micro-Raman spectroscopy and electron microprobe analysis. This is a complex problem which was beyond the resources of the present study.

Discussion

The above orientations of light spots related to crystal faces of rose quartz spheres were determined at the beginning of the twentieth century by Goldschmidt and Brauns (1911) and Kalkowsky (1915), and they further indicated that the light forming the light spots is reflected from the faces of negative crystals within the rose quartz host or from series of oriented light-reflecting platelets of unknown nature. From our study of spheres A, B, C and D, it is evident that the different light spots are caused by reflected light originating from phase boundaries or planes which are orientated parallel to six different forms of symmetrically equivalent quartz crystal faces. In contrast, Maier (1943) suggested that the light spots in rose quartz originate from intersecting light bands, even if there are no intersecting light bands or no light bands at all are visible.

In seeking the reasons to explain our observations on four rose quartz spheres from Madagascar, especially

• the intensities of light spots related to light bands of the central stars,
• the intensity of isolated light spots not related to light bands of the central stars and
• the microscopic proof of light reflecting particles and/or platelets of different size.

The suggestion of Maier (1943) seems unrealistic. In particular, there is an absence of any distinct light spots (poles) at the intersections of light bands as described in detail for quartzes from Sri Lanka (Schmetzer and Glas, 2003) and this makes it unlikely that intense light spots could be caused by two or three intersecting, but invisible light bands. Consequently, the idea that the observed light spots (related to the poles of quartz crystal faces) are caused by

reflection of light from plane faces of negative crystals and/or oriented mineral platelets within the rose quartz single crystal is more likely. This schematic model is consistent with the visual observation of the numbers and positions of all light spots. The dominant orientations of the reflecting faces are parallel to the dominant faces of quartz, e.g. parallel to the hexagonal prism *m* as well as the rhombohedra *r* and *z*, and produce the brightest spots. Light spots of lower intensity represent subordinate faces of quartz, i.e. the rhombohedra π and π' as well as the trigonal prisms *a* and *a'*.

However, the nature of the inclusions responsible for the light spots is not clear so far. It is evident that reflected light indicates phase boundaries between the host rose quartz crystal and additional solid or liquid phases. The solid phases might be mineral inclusions or mineral platelets. The liquid phases might be fluid-filled platelets or negative crystals outlined by the number of quartz crystal forms mentioned above. It is also not clear if there is any connection with the fibrous nanoinclusions of dumortierite (?), which were determined recently in rose quartzes originating from different deposits all over the world (see Goreva *et al.*, 2001).

The different intensities of light spots on the surface of different spheres could be caused by either liquid or solid inclusions. Different concentrations of the light reflecting faces of negative crystals would result in different concentrations of light reflecting mineral platelets in different rose quartz host crystals. The different sizes of the observed light spots might be due to different sizes of light-reflecting phase boundaries.

The rose quartz spheres contain also one or two groups of needle-like inclusions with an orientation perpendicular to the *c*-axis of the host crystals. These rutile (?) needles are responsible for the central six- or twelve-rayed stars of the samples. The larger sphere D contains at least one additional group of needle-like inclusions inclined to the *c*-axis, thus forming the six additional light bands which are, consequently, also inclined to the *c*-axis.

Acknowledgements

References

Bauer, M., and Schlossmacher, K.,1932. *Edelsteinkunde. 3rd edn*. Verlag Bernhard Tauchnitz, Leipzig

Cassedanne, J.P., and Roditi, M.,1991. Crystallized and massive rose quartz deposits in Brazil. *Journal of Gemmology*, **22**(5), 273-86

Goldschmidt, V., and Brauns, R., 1911. Über Lichtkreise und Lichtknoten an Kristallkugeln. *Neues Jahrbuch für Mineralogie, Geologie und Paläontologie*, **31**. Beilage-Band, 220-42

Goreva, J.S., Ma, C., and Rossman, G.R., 2001. Fibrous nanoinclusions in massive rose quartz: The origin of rose coloration. *American Mineralogist*, **86**(4), 466-72

Kalkowsky, E., 1915. Opaleszierender Quarz. *Zeitschrift für Krystallographie und Mineralogie*, **55**(1), 23-50

Kumaratilake, W.L.D.R.A., 1997. Gems of Sri Lanka: a list of cat's-eyes and stars. *Journal of Gemmology*, **25**(7), 474-82

Maier, W., 1943. Experimenteller Asterismus. *Neues Jahrbuch für Mineralogie, Geologie und Paläontologie Abhandlungen, Abt. A*, **78**(3), 283-380

Pezzotta, F., 2001. Madagascar. A mineral and gemstone paradise. *ExtraLapis English No.1*, 51 pp

Schmetzer, K., and Glas, M., 2003. Multi-star quartzes from Sri Lanka. *Journal of Gemmology,* **28**(6), 321-32

Polish up your diamond knowledge with Gem-A's

DIAMOND DAYS

Diamond Buying Guide

This workshop will bring you up to speed on the 4 Cs - carat weight, clarity, colour and cut. Suitable for jewellery sales' staff, jewellery designers or customers who want to hone their skills before buying. We'll show you how to assess a stone based on the 4 Cs and reveal just how different two stones of similar size and weight can be.

Tuesday 6 March

Price: £138.00 (Gem-A members £125.00)

Six-Day Diamond Practical Course

An intensive course plus Certificate Exam which places the greatest emphasis on the use of the 10x lens, still the industry standard, but will also include:

• Clarity grading

• Colour grading with emphasis placed on grading by eye

• Aspects of cut including symmetry and proportions

• Simulants and treatments

• Description of rough crystals

Wednesday 21 to Wednesday 28 February; exam Thursday 1 March*
Wednesday 9 to Wednesday 16 May; exam Thursday 17 May*

* weekdays only – excludes weekends

Price £900.00

Three-day Advanced Diamond Grading Course

A concentrated course for holders of the Gem Diamond Diploma or Diamond Grading Certificate, which will cover key areas of advanced diamond grading, including:

• Use of the microscope to clarity grade and plot diamonds

• Colour grading and master stones

• Fluorescence grading

• Cut - measurements, proportions, symmetry and polish

A basic knowledge of modern treatments, simulants and synthetics currently available is required.

Wednesday 25 to Friday 27 April

Price: £695.00

DIAMOND DAYS are held at our London Headquarters in the Hatton Garden area.
The hours are 10:00 a.m. to 4:30 p.m.

Apply soon – all courses are hands-on and so numbers are limited.

To book or for further details:
www.gem-a.info/education/londonWrkShops.cfm
or contact Claire by email claire@gem-a.info or phone 020 7404 3334.

Rings image © Hatah London

Identification of the horse origin of teeth used to make the Japanese 'kakuten' using DNA analysis

Hironaga Kakoi [1], Masahiko Kurosawa [1], Hiroshi Tsuneki [2] and Ikuko Kimura [3]

1. Laboratory of Racing Chemistry, Tsuruta-machi 1731-2, Utsunomiya, Tochigi 320-0851, Japan
2. Department of Clinical Pharmacology, Graduate School of Medicine and Pharmaceutical Sciences, University of Toyama, 2630 Sugitani, Toyama 930-0194, Japan
3. Department of Food and Nutrition Science, Toyama College, 444 Gankaiji, Toyama 930-0193, Japan

Address correspondence to Dr Hiroshi Tsuneki, E-mail: *htsuneki@pha.u-toyama.ac.jp*

Abstract: *'Kakuten' is a kind of 'ojime', an ornamental craft product of the Edo era in Japan. There are worldwide collectors of this item owing to its magical and exotic motif and refined craftsmanship. 'Kakuten' has also attracted the particular interest of collectors because its material has been believed to consist of the red crown of the Japanese crane. Recently, the texture and composition of the 'kakuten' were investigated under high magnification and by microarea Fourier transform infrared spectroscopy, and it was clarified that the 'kakuten' is made from the tooth of a grass-eating animal. In the present study, the species of the animal has been identified using analysis of the DNA sequence of mitochondrial cytochrome b gene (CYTB) including the species-specific region. Nucleotide sequence data indicate that the 'kakuten' is very similar to and has a close phylogenetic relationship to a horse; thus, we conclude that 'kakuten' artefacts are fashioned from the teeth of a horse.*

Key words: *horse cytochrome b, kakuten, nucleotide sequence, ojime, species identification*

Introduction

'Netsuke' and 'ojime' are small ornamental craft products of the Edo era and have been regarded as Japanese magical jewels by collectors[1]. 'Ojime' is used to tighten the connecting strings between a cylindrical container of a khsier (a tobacco pipe) and a

pouch for shredded tobacco leaves (*Figures 1a,b* and *c*), or between a 'netsuke' and an 'inroh' (*Figures 1d* and *e*). An ornamental ring containing many 'kakuten' is shown in *Figure 1f*. These items have attracted worldwide interest owing to their exotic motifs and delicate craftsmanship. Among the various products, 'kakuten', a kind of 'ojime', has been highly praised not only for being a magical ornament but also for its interesting origin. The literal translation for 'kakuten' is a head (red crown) of a Japanese crane and the word 'ho-ten' or 'ho-ting' used instead of 'kakuten' in the old literature means a casque of an extinct bird, the

helmeted hornbill [2]. However, gemmological tests of specific gravity and refractive index gave different results for the material of 'kakuten' and that of these birds. It is thus interesting to clarify the origin of this craft product, and identification of its material may allow us to continue the tradition of its manufacture.

For the identification of the origin of 'kakuten', Sunagawa *et al.* [3, 4] investigated its texture under high magnification and its composition by microarea Fourier transform infrared spectroscopy (FTIR), and concluded that 'kakuten' is made from the tooth of

Figure 1: Photographs of 'kakuten' artefacts inserted between a cylindrical container for tobacco pipe and a pouch of shredded tobacco leaves (a, b and c), on a woven rope between 'netsuke' and 'inroh' (d and e, a rear view), and in f, 91 pieces of 'kakuten' tied in a ring. The sizes of 'kakuten' are: 2.0 cm in a, 1.9 cm in d, 1.9 cm in e and in the range 1.8-3.0 cm in f.

a grass-eating animal [3]. This observation revealed valuable gemmological information because ornamental objects made from the teeth of animals are very rare. However, the animal species could not be identified in their study. On the basis of their conclusion that 'kakuten' is made from a part of an animal tooth, several further biological studies were possible, and one appropriate one to determine the animal species was deoxyribonucleic acid (DNA) analysis.

The sequence variation of the mitochondrial cytochrome b gene (*CYTB*) has been widely studied as it provides a powerful basis to resolve phylogenetic relationships in a wide range of animal species and is often used to identify species of animals in forensic investigations (e.g., Hsieh *et al.*[5]). Therefore, one should be able to determine the animal species from which the materials of 'kakuten' originate using phylogenetic data on the basis of *CYTB* variation. In this study, we have carried out a nucleotide sequencing analysis for *CYTB* from 'kakuten' samples by polymerase chain reaction (PCR). Furthermore, by comparing the nucleotide sequences of *CYTB* between 'kakuten' and other animals, the origin of 'kakuten' artefacts has been clarified.

Identification of the horse origin of teeth used to make the Japenese 'kakuten' using DNA analysis

Materials and methods

Two 'kakuten' samples, 'kakuten' -1 and 'kakuten' -2, were analysed in the present study, 'kakuten' -1 being the sample used in our previous studies [3, 4]. To extract total DNA, 1 g of the 'kakuten' was milled to a fine powder and suspended with 20 ml of 0.5 M EDTA (pH 8.0) for five days for decalcification. The DNAs from decalcified samples were extracted using a DNA extraction kit and NucleoSpin DNA Trace (Macherey-Nagel, Dueren, Germany) following the supplier's protocol, and the DNA was eluted in 100 μl of sterile water. Additionally, total DNAs (20 ng/μl) were isolated from horse (thoroughbred) and cattle (Holstein) blood samples using an automated DNA extractor (MagExtractor System MFX-2000, Toyobo, Osaka, Japan), and were also used for comparison in the present analysis.

Terminology used in DNA studies

Polymerase Chain Reaction (PCR):

PCR is a molecular biological technique for amplifying a specific DNA fragment with a pair of primers. The purified PCR products can be used for sequencing.

Base pair (bp):

A unit of length for the double-strand DNA fragments. Each DNA nucleotide is composed of a base (adenine, A; thymine, T; guanine, G; or cytosine, C), a phosphate molecule, and a sugar molecule (deoxyribose).

Bootstrap analysis:

Statistical technique to evaluate the reliability of each node in a phylogenetic tree. High bootstrap values support the validity of the clustering.

To obtain the nucleotide fragments of *CYTB* from the extracted DNAs, we designed an available primer pair by referring the *CYTB* sequence data of the horse (accession number, AY584828), cattle (V00654), elephant (AJ224821) and camel (X56281) from GenBank (http://www.ncbi.nlm.nih.gov/GenBank). The primer sequences were as follows: forward, 5'TCAGCAATTCCCTACATCGGCAC3'; and reverse, 5' CGGAATATTATGCTTCGTTG3'. PCR amplification of the *CYTB* fragment of 503 base pairs (bp) (nucleotide position, nt, 451-953) was performed in a total volume of 15 μl of the following mixture: 2 μl of DNA solution, 15 pmol of each primer, 2.5 mM MgCl$_2$, 0.33 mM dNTPs, 1.5 μl of 10× reaction buffer (Applied Biosystems, Foster City, CA, U.S.A.) and 1.5 U of AmpliTaq Gold (Applied Biosytems). Thermal reactions were carried out using a GeneAmp PCR System 9700 (Applied Biosystems) with initial denaturation at 95°C for 10 min, followed by 33 cycles of 94°C for 30 secs, 55°C for 1 min and 72°C for 30 sec and a final step at 72°C for 10 min. To check whether the fragments were amplified, PCR products were subjected to electrophoresis using a 2.0% agarose gel. Direct sequencing of PCR products purified using GFX™ PCR DNA and Gel Band Purification kits (Amersham Biosciences, Piscataway, NJ, U.S.A.) was performed on both strands using BigDyeTerminator Cycle Sequencing kit (Applied Biosystems). The sequencing products were loaded in to an automated DNA sequencer ABI PRISM 3100 (Applied Biosystems). A sequence of 460 bp (nt 474-933) was determined using a sequencing analysis software (Applied Biosystems).

The sequence data from the 'kakuten', horse and cattle DNAs were compared with those of six animal species, namely, the horse, cattle, elephant, camel, pig (Z50107) and mouse (V00711) species, taken from GenBank using multiple sequence alignment in GENETYX-Mac software package programme Ver 11.0 (Software Development, Tokyo, Japan), and a neighbour-joining tree was constructed with nucleotide variation on the basis of these sequencing data.

Results and discussion

Figure 2 shows the electrophoretic patterns of PCR-amplified fragments obtained from the 'kakuten', horse and cattle DNAs. Single bands were observed for each sample and each PCR product showed the expected band 503 bp. On the other hand, there were no bands for the PCR blanks. These results indicate that *CYTB* fragments can be amplified successfully without producing artefacts or cross-contamination during the PCR.

Nucleotide sequence data of 460 bp were obtained from these PCR products. These sequences are shown in *Figure 3* with the sequences of the six animal species from GenBank. The horse and cattle DNA sequences obtained from our measurements were completely identical to the horse (AY584828) and cattle (V00654) data in GenBank, respectively. Both the 'kakuten' -1 and 'kakuten' -2 sequences had notable homology (71.7 -79.1%) with the cattle, elephant, camel, pig, and mouse sequences in GenBank. A sequence homology of more

Figure 2: Electrophoretic patterns of PCR-amplified fragments from 'kakuten', horse and cattle DNAs. The molecular sizes (50-2000 bp) are indicated on the left side. PCR blank, control (-), is the amplified product using sterile water as a template.

than 99% was found between the 'kakuten' and the horse sequences. 'Kakuten' -1 and 'kakuten' -2 sequences had homologies of 99.57% (458/460) and 99.78% (459/460) to the horse data, respectively. Two nucleotide

Figure 3: Comparison of partial sequences of CYTB (460 bp) among 'kakuten', horse and cattle DNAs, and those of six animals from GenBank. Dots indicate concordance with the sequence of the horse (AY584828).

substitutions (C⟷T at nt 618 and G⟷A at nt 810) were observed between the 'kakuten' -1 and horse sequences and one nucleotide substitution (T⟷C at nt 549) was observed between the 'kakuten' -2 and horse sequences. Since they were synonymous ('silent') substitutions, no differences are predicted between the primary structures of cytochrome b of the 'kakuten' and the horse. Moreover, it was found that the data of 'kakuten' -1 was completely identical to another *CYTB* sequence of the horse, D32190, in GenBank. From these data, it was considered that the observed variation between the 'kakuten' and horse sequences was due to a difference within the same species. In addition, 'kakuten' -1 and 'kakuten' -2 can be classified into the horse group and they are clearly distinct from other animal groups in the phylogenetic tree constructed using the sequences of the 'kakuten', horse, and cattle DNAs and those of the six animals mentioned above (*Figure 4*). Since this region of the horse CYTB sequence (AY584828) has homology of 71.4% with that of the Japanese crane sequence (U27550) (not shown), it is unlikely that the 'kakuten' is fashioned from crane material.

The 'kakuten' has been used for producing near-spherical shapes of 'ojime' (*Figures 1a, c, d* and *e*). The 'haori' is a traditional jacket of Japanese men and can be tied with silk strings attached with 'kakuten' ornaments. The larger 'kakuten' with globular shapes up to 30mm in diameter have also been hung as side weights for a 'kakejiku' (a Japanese painting decorated in the corners, a 'tokonoma' of a Japanese guest room). However, because the molar tooth of the adult horse (thoroughbred) measured in this investigation was only 19-21 mm x 30-32 mm, it is probable that some 'kakuten' artifacts are composed of more than one piece of molar glued together.

In conclusion, it is clear that on the basis of DNA analysis of the species-specific *CYTB* sequence, the material from which 'kakuten' originates is the horse, in particular, the tooth of the horse. This result also means that 'kakuten' ornaments may be manufactured today using material similar to that used in the Edo period.
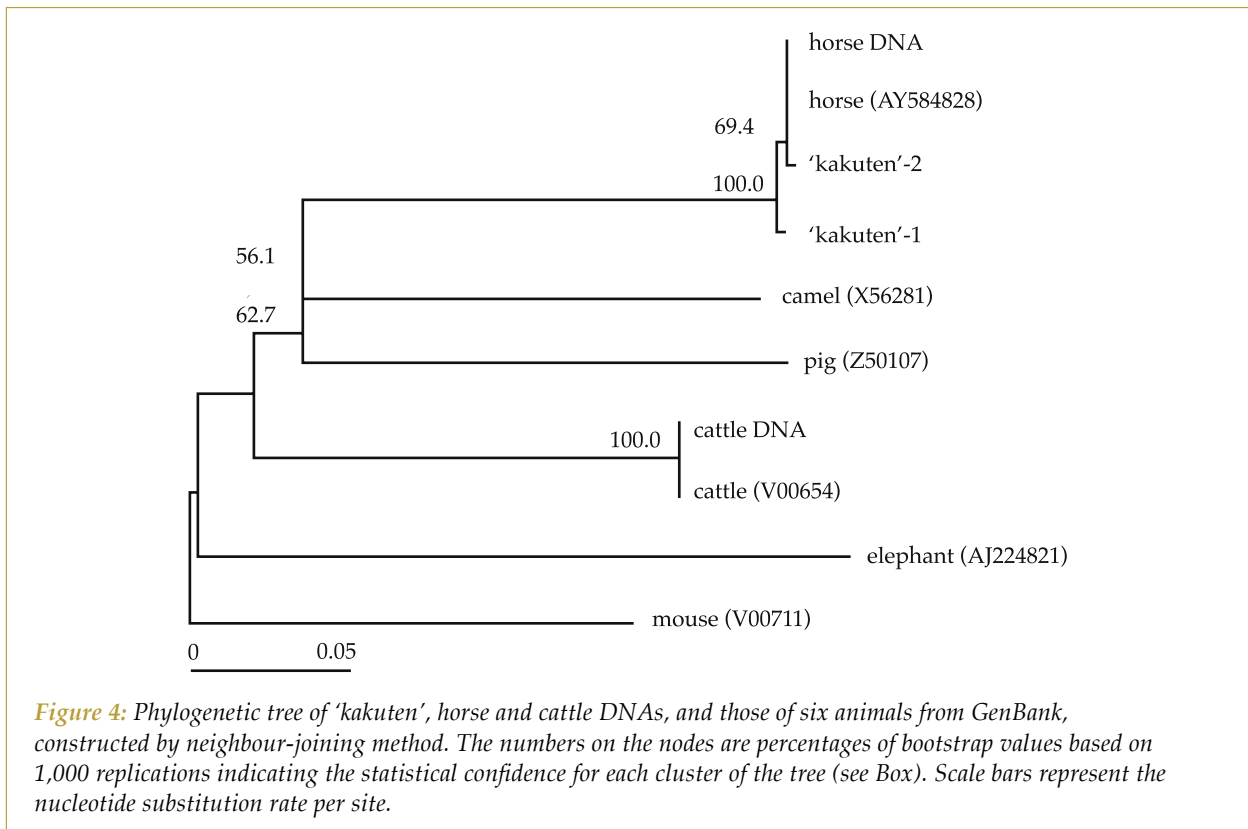
Figure 4: Phylogenetic tree of 'kakuten', horse and cattle DNAs, and those of six animals from GenBank, constructed by neighbour-joining method. The numbers on the nodes are percentages of bootstrap values based on 1,000 replications indicating the statistical confidence for each cluster of the tree (see Box). Scale bars represent the nucleotide substitution rate per site.

Acknowledgements

References

1. Kinsey, R.O., 1991. *Ojime, magical jewels of Japan*. H.N. Abrams Inc., New York

2. Inaba, S.T., 1781. *Soken-Kisho* (highly praised ornamental craft products for swords). Vols. 7 and 8 (in Japanese). Shisuikan, Osaka, Japan

3. Sunagawa, I., Takahashi, Y., Kimura, I., I, Suzuki, K., and Sakae, T., 2002. Micro FT-IR analysis of 'Kakuten', an ornamental object fashioned from tooth of herbivorus animal. *Nihon Univ. J Oral Sci.* **28**, 102-167 (in Japanese)

4. Sunagawa, I., Takahashi, Y., Kimura, I., and Sakae, T., 2002. 'Kakuten' (crane crown), an 'ojime' made from the tooth of a grass-eating animal. *J. Gemm.*, **28**(1), 33-40

5. Hsieh, H.M., Chiang, H.L., Tsai, L.C., Lai, S.Y., Huang, N.E., Linacre, A., and Lee, J.C., 2001. Cytochrome b gene for species identification of the conservation animals. *Forensic Sci. Int.*, **122**(1), 7-18

A colorimetric study of a tourmaline from Mozambique which shows a reverse alexandrite effect

Yan Liu[1] and B. A. Fry[2]

1. Liu Research Laboratories, South El Monte, California 91733, U.S.A.
2. P.O. Box 724, Mars, Pennsylvania 16046, U.S.A.

Abstract: A tourmaline from northern Mozambique shows a reverse alexandrite effect. It appears a greenish-blue colour under incandescent light and purple under daylight. An advanced colorimetric study confirmed the reverse colour change of the tourmaline between incandescent light and daylight. The traditional alexandrite effect theory attributes the colour change to two transmission bands in the visible wavelength range, but the colours observed in the Mozambique tourmaline do not correspond to the transmission bands. The reverse alexandrite nature of the Mozambique tourmaline also cannot be explained by the traditional theory. A new alexandrite effect theory attributes the colour change to a combination of chromatic adaptations and colour responses of the human visual system to the incoming visible light from the gemstone under different light sources.

Keywords: alexandrite effect, colour change, hue angle, tourmaline

Introduction

Alexandrite effect gemstones normally display warm colours, such as orange and purple, under incandescent light, and cool colours, such as blue and green, under daylight. Traditionally, this alexandrite effect has been explained by two transmittance bands in the visible wavelength range of its spectrum (Gübelin and Schmetzer, 1982). Recently one author (B.A.F.) obtained a 5.68 ct colour-change tourmaline from Moiane, northern Mozambique, which shows a greenish-blue colour under incandescent light, and purple under daylight. This colour change is a reverse alexandrite effect (Wentzell 2004; Wentzell *et al.*, 2005).

Liu *et al.* (1994, 1995, 1999) used an advanced colorimetric method to study the alexandrite effect of many gemstones in detail. They found that not only gemstones with two prominent spectral transmittance bands, essential for the traditional alexandrite effect theory, but also other gemstones with
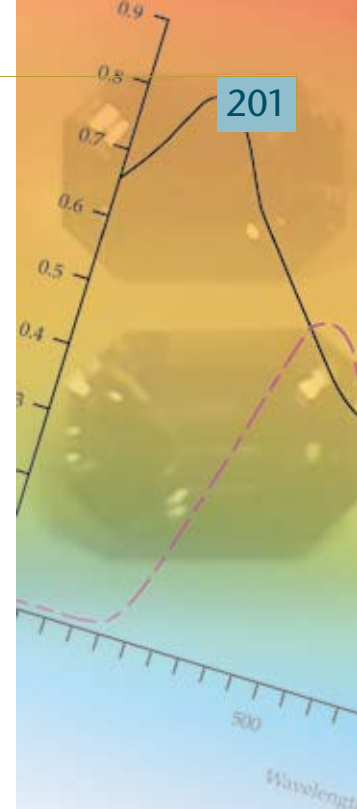
multi-bands and step bands demonstrated the alexandrite effect. Generalizing on these findings led to proposing a new theory to account for the alexandrite effect. This consists of a combination of chromatic adaptations of the human visual system to different light

Figure 1: The 5.68 ct tourmaline from Mozambique under incandescent light (a) and under daylight (b).

sources, and the vision system response to the spectral distribution reflected by the colour change gemstones when they are illuminated by the different light sources.

Based on a study of the appearance change of Munsell chips under different light sources (Helson *et al.*, 1952) and their alexandrite effect experiments with all available alexandrite effect samples, Liu *et al.* (1994) determined that a 20° absolute hue-angle in the CIELAB colour space is the 'empirical' criterion for judging the alexandrite effect, since all the hue-angle changes of the colour chips are smaller than 20° and all the hue angle changes of alexandrite effect gemstones are greater than 20°. If a gemstone shows a hue-angle change more then 20°, it would qualify as displaying the alexandrite effect. If the hue-angle is smaller than 20°, a small hue shift may be observed, but it would not be recognized by colour memory.

Four categories of colour change can be distinguished among alexandrite effect gemstones according to the pair of illuminants used (Liu *et al.*, 1994). The type 1 alexandrite effect gemstones change colour between daylight and incandescent as well as fluorescent daylight and incandescent light, but do not change colour between daylight and fluorescent daylight. Alexandrite is a typical type 1 colour change gemstone. The type 2 alexandrite effect gemstones change colour between daylight and fluorescent daylight as well as fluorescent daylight and incandescent light, but not between daylight and incandescent light. Colour change glass is a typical type 2 colour change material. Type 3 alexandrite effect gemstones change colour between the three pairs of light sources. Some colour change sapphires are typical type 3 colour change gemstones. Type 4 alexandrite effect gemstones only change colour between fluorescent, daylight and incandescent light. Some garnets are typical type 4 colour change gemstones.

In this study, we use the colorimetric method (see Liu *et al.*, 1999) to measure spectral transmittance and to calculate the colorimetric data. Liu's theory (1994) will be used to offer an explanation for the reverse nature of the alexandrite effect demonstrated by the tourmaline reported on here.

Material

The tourmaline used for this study is a 5.68 ct emerald-cut stone (11.63 × 8.67 × 7.48 mm). Its colour is greenish-blue (see *Figure 1a*) under incandescent light and purple (*Figure 1b*) under daylight. This colour change is a reverse alexandrite effect. A 'normal' alexandrite effect would appear purple under incandescent light and bluish green under daylight. This tourmaline is the first gemstone to demonstrate the reverse alexandrite effect and, at the time of writing (May 2006), is unique.

An Ocean Optics USB-2000 spectrometer with an integrating sphere was used to measure the spectral transmittance of the tourmaline with the light beam perpendicular to the table facet.

Table I: Colour changes of the tourmaline.

Observed hue			Calculated hue-angle		
Incandescent	Daylight	Fluorescent daylight	A	D65	F7
greenish blue	purple	purple	225	315	314

Note: Metamerism index MIv is the CIE standard method of assessing the spectral quality of daylight simulators in the visible wavelength range. Metamerism index MIv of a daylight simulator must be B or better for colour grading of gemstones.

Results

The transmittance spectrum (*Figure 2*) of the tourmaline shows two transmittance bands in the visible wavelength range. One is centred at about 430 nm and the other at about 570 nm.

The transmittance spectrum of alexandrite is shown in *Figure 2* (dotted line) for comparison. Alexandrite has a transmittance band centred at about 490 nm, and another at a longer wavelength that extends from 570 nm into the near infrared range. It is clear that the two transmittance bands of the tourmaline are positioned at significantly shorter wavelengths than those of the alexandrite.

Table I shows the calculated colorimetric data from the transmittance spectrum of the tourmaline under CIE standard illuminants
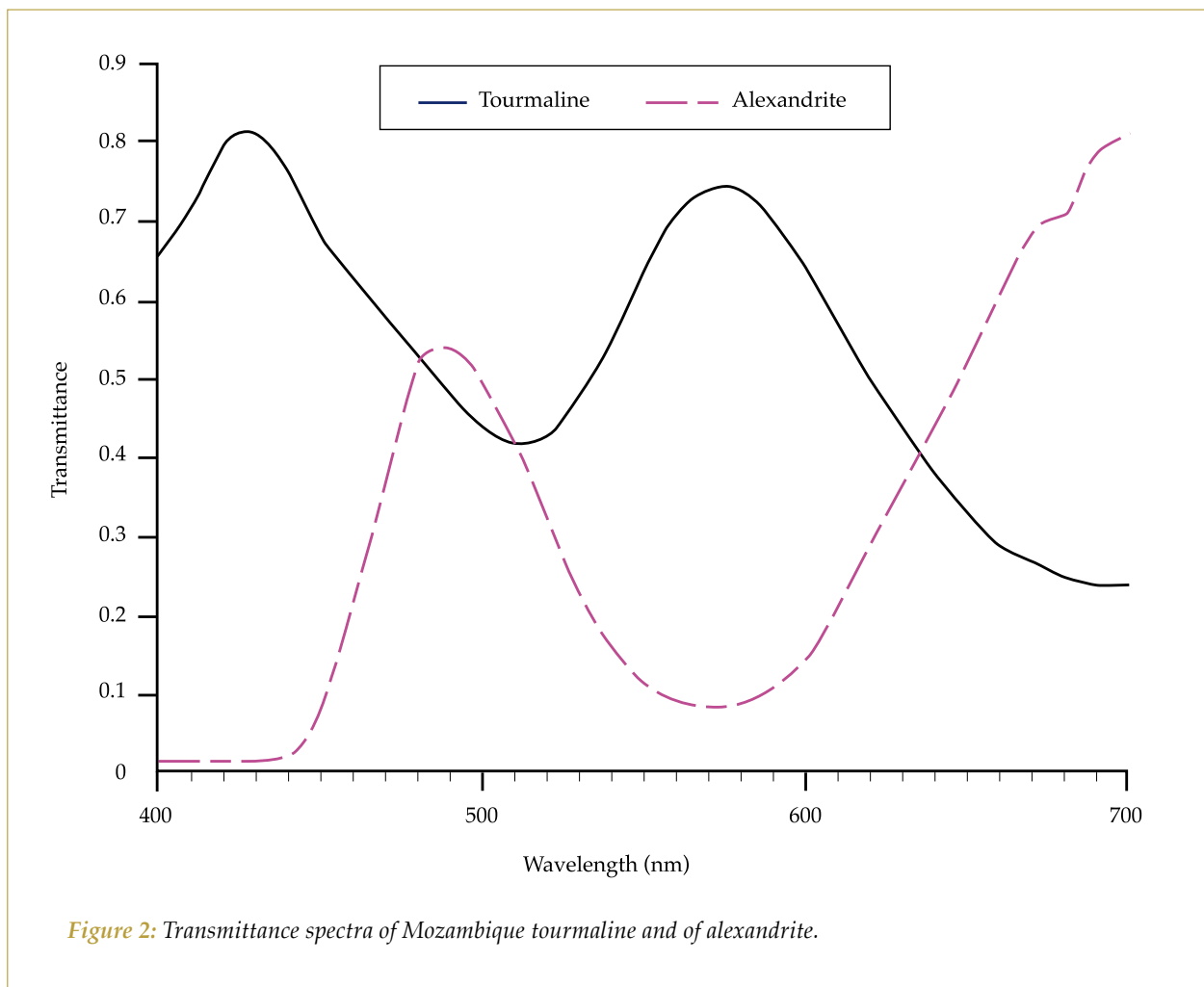

Figure 2: Transmittance spectra of Mozambique tourmaline and of alexandrite.

A, D65 and F7, and the observed hues are under an incandescent light with a colour temperature at about 2856 K, a D65 daylight simulator at about 6500 K with a metamerism index MIv A in the visible wavelength range, and a fluorescent daylight lamp with a colour temperature at about 6500 K.

Discussion

The CIELAB colour space is a near-uniform colour space, and any hue-angle represents the hue of a colour (see, for example, Liu *et al.,* 1999). *Figure 3* shows the hue-angle changes of the tourmaline in the CIELAB colour space. The calculated hues of the tourmaline under the three CIE standard illuminants A, D65, and F7 agree with the observed
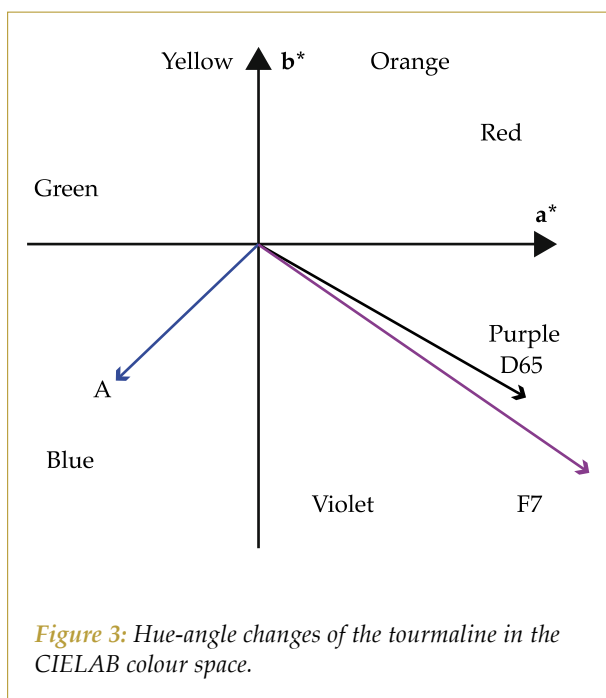

Figure 3: Hue-angle changes of the tourmaline in the CIELAB colour space.

hue under the three corresponding light sources: an incandescent light, a D65 daylight simulator, and a 6500 K fluorescent lamp. The hue-angle of 225° under CIE standard illuminant A represents a greenish blue hue, and the observed hue is greenish blue under incandescent light. The hue-angle of 315° under CIE standard illuminant D65 represents a purple hue, and the observed hue is purple. The hue-angle of 314° under F7 fluorescent daylight lamp at 6500 K is also a purple hue, and the observed hue is the same purple.

The hue-angle change in the CIELAB colour space is used to evaluate the degree of the alexandrite effect. All colours may change to some degree between different light sources but unless the hue angle change exceeds 20°, such shifts do not qualify as an alexandrite effect. All purple colours, for example, show significant colour shifts between incandescent light and daylight, but not sufficient to produce an alexandrite effect. The strength of the alexandrite effect is classified into four categories as shown in *Table II.*

The observed hue change of the tourmaline between CIE standard illuminants A and D65 is 90°, and the calculated hue-angle change between A and D65 is 89°, thus the tourmaline is an alexandrite effect gemstone in the alexandrite effect category of 'strong'.

Based on the classification of the alexandrite effect proposed by Liu *et al.* (1994), the tourmaline shows a type 1 colour change, i.e. it changes colour between daylight and incandescent light and between fluorescent daylight and incandescent, but shows no change between daylight and fluorescent daylight.

Both colour observations and colorimetric calculations confirm that the tourmaline displays a reverse alexandrite effect. The reverse alexandrite effect of the tourmaline cannot be explained by the traditional theory. According to the traditional theory, this tourmaline should appear a warm colour with long wavelengths dominant under incandescent light, and a cool colour

Table II: The categories of alexandrite effect.

Hue-angle change	Category
20° - 45°	moderate
45° - 90°	intense
90° - 135°	strong
135° - 180°	very strong

with short dominant wavelengths under daylight. From *Figure 2*, it is apparent that the tourmaline should show a yellow-orange colour under incandescent light (long

wavelength transmittance band is centred at about 580 nm) and blue under daylight (short wavelength band is centred at about 430 nm). In fact, it appears purple under daylight and greenish blue under incandescent light. Thus, the reverse colour change of the tourmaline demonstrates that the traditional theory of the alexandrite effect is inadequate.

The theory proposed by Liu *et al.* (1994) argues that the alexandrite effect is caused by a combination of both chromatic adaptation and the visual system responses to the spectral distribution of the light from an alexandrite effect gemstone under different light sources. The principles of colour perception dictate that the visual system will adapt to illumination with incandescent light by becoming less sensitive to the long wavelength range of red and orange. Likewise the visual system will adapt to illumination with sunlight by becoming a little less sensitive to the short wavelength range and slightly more sensitive to the longer wavelengths. These chromatic adaptations are not dependent on the object illuminated.

When this tourmaline is viewed under an incandescent light several effects occur to produce its observed colour of greenish blue. The chromatic adaptation reduces the human visual system's sensitivity to the long wavelength range of orange and red. The tourmaline's relatively low transmittance of the long wavelength range, that can be seen in *Figure 2*, further reduces the visual system's perception of the orange and red hues. The high spectral transmittance of the tourmaline, in the short wavelength band centred on about 430 nm combines with the previous effects to produce a greenish-blue colour. The tourmaline's high spectral transmittance centred about 570 nm contributes a little green to complete the tourmaline's observed colour of greenish-blue under incandescent light.

When the tourmaline is viewed under daylight several effects occur to produce its observed colour of purple. The chromatic adaptation will reduce but not eliminate the contribution from the high spectral transmittance band centred on 430 nm to the tourmaline's colour. Also, chromatic adaptation will increase the long wavelength contribution to the tourmaline's colour, despite the tourmaline's relatively low transmittance of the long wavelength range. The contributions of the 430 nm and the 570 nm transmittance bands combine to produce a purple colour.

Colour constancy is a very fundamental colour vision phenomenon. In the wider field of colour science in general, the alexandrite effect, which is a non-colour-constancy phenomenon, is very unusual. Traditional explanations relied heavily on the two transmittance bands in alexandrite's visible spectrum, but newer theories were put forward by Liu *et al.* (1994) to explain anomalies. The discovery of this tourmaline from Mozamibque with its particular colour behaviour has meant more difficulties for the traditional theory, but support for the theories of Liu *et al.* (1994).

Conclusions

At the time of writing, all the alexandrite effect gemstones which have been previously studied have shown colour changes from warm hues under incandescent light to cool hues under daylight. The tourmaline is the first gemstone found that shows a reverse alexandrite effect from greenish blue under incandescent light to purple under daylight. Our advanced colorimetric study of the tourmaline confirms this reverse alexandrite effect. The colour change behaviour (alexandrite effect) of the tourmaline is type 1, and its hue change category is strong at about 90° between the CIE standard illuminants A and D65.

The reverse alexandrite effect of the studied tourmaline cannot be explained by traditional theory of the alexandrite effect, but it does provide more evidence for Liu's explanation. The alexandrite effect is a non-colour-constancy phenomenon caused by a combination of chromatic adaptations to the different light sources and vision system responses to the spectral distribution of the light emitted by the alexandrite effect gemstones illuminated by the corresponding light sources.

References

Gübelin, E., and Schmetzer, K., 1982. Gemstones with alexandrite effect. *Gems & Gemology*, **18**(4), 197-203

Helson, H., Judd, D., and Warren, M., 1952. Object-color change from daylight to incandescent filament illumination. *Ill. Eng.* 47, 1952

Liu, Y., Shigley, J., Fritsch, E., and Hemphill, S., 1994. The "alexandrite effect" in gemstones. *Color Research and Application*, **19**(3), 186-91

Liu, Y., Shigley, J., Fritsch, E., and Hemphill, S., 1995. Relationship between the crystallographic orentation and the "alexandrite effect" in synthetic alexandrite. *Mineralogical Magazine,* **59**(1), 111-14

Liu, Y., Shigley, J., Fritsch, E., and Hemphill, S., 1999. A colorimetric study of the alexandrite effect in gemstones. *Journal of Gemmology*, **26**(6), 371-85

Wentzell, C., 2004, Copper-bearing color change tourmaline from Mozambique. *Gems & Gemology,* **40**(3), 250-1

Wentzell, C., Fritz, E., and Muhlmeister, S., 2005. More on copper-bearing color-change tourmaline from Mozambique. *Gems & Gemology*, **41**(2), 173-5

Fuchsite quartzite as an imitation of emerald

Pedro Luiz Juchem[1], Tania Mara Martini de Brum[1],
Adriane Comin Fischer[2], Naira Maria Balzaretti[3],
Adolpho Herbert Augustin[4]

1. Gemmological Laboratory (LABOGEM) – Universidade Federal do Rio Grande do Sul (UFRGS). Caixa Postal 15.001; CEP 91540-000 – Porto Alegre, Rio Grande do Sul, Brazil. Email: labogem@ufrgs.br
2 LABOGEM and Universidade de Brasilia (UnB). Email: adriane.fischer@ufrgs.br
3. Instituto de Fisica (UFRGS). Email: naira@if.ufrgs.br
4. LABOGEM and Programa de Pós-Graduação em Geociências (UFRGS). Email: ahaugustin@yahoo.com.br

Abstract: *Ten parcels of pre-shaped green stones were identified mostly as emerald, but some were fuchsite quartzite. Both emerald and quartzite stones had been treated with a filling substance to improve their clarity, identified as paraffin oil. Since the fuchsite quartzite has a deeper green colour than usual for this rock, it is possible that the impregnating oil was also green.*

Keywords: *Emerald, fissure fillers, infrared spectroscopy, oil treatment, quartzite, Raman spectroscopy*

Introduction

Rough and cut gemstones have been used in the last few years in Brazil as a guarantee for public and private debts. To increase the security of this kind of transaction, certificates describing such stones are commonly sought from the Gemological Laboratory (LABOGEM) at the Universidade Federal do Rio Grande do Sul (UFRGS).

Ten parcels of pre-shaped green stones, declared as emerald by the owner, were examined at LABOGEM for certification. Standard mineralogical investigations indicated that most stones were indeed emerald, but there were some stones with slightly different characteristics from emerald. These stones were identified as fuchsite quartzite, and this paper summarizes its properties to enable recognition of material that is probably traded as emerald in the gemstone market.

Both emerald and fuchsite quartzite stones in the parcels were impregnated with a filling substance, whose residue was noticed inside the plastic package and which was also greasy to the touch. This treatment probably increased both colour and clarity in the fuchsite quartzite, because its green hue is closer to emerald than expected for this rock. So, the fuchsite quartzite and emerald look similar at first glance in the parcels. However, when looked at in more detail, emerald and quartzite do show differences due to their internal textures. These differences are reported in detail below.

Analytical procedures

Standard mineralogical and gemmological tests, petrographical examination and electron microscopy with energy-dispersive analysis (SEM-EDS) were performed to characterize the emeralds and their imitations. Some advanced investigation techniques were used to identify the filling substance, including infrared and Raman spectroscopy. The analyses were performed at LABOGEM, at the Physics Institute and the Electron Microscopy Centre, all at the Federal University (UFRGS) in Porto Alegre.

Mineral data were obtained with a *Schneider* 10x hand lens, dichroscope, polariscope and gemmological microscope, an *Olympus* stereomicroscope, a *Topcon* refractometer and a *Leitz* petrographic microscope. Specific gravity (SG) was determined with an A200CT *Marte* hydrostatic balance to a precision of 0.001 g, in distilled water at room temperature. *Krüss* ultraviolet lamps of short and long wavelengths were used in order to observe fluorescence.

Petrographic analysis of the quartzite stones was done with the permission of the owner. The aim of quartzite petrography was to obtain a complete description of the mineralogy and textures of this rock to determine its provenance.

A *Jeol JSM 5800* SEM with an energy dispersive system (EDS) for semi-quantitative chemical analyses was used to identify minerals in the quartzite. The samples were coated with a thin layer of carbon to prevent charge build-up. Fourier Transformation Infrared (FTIR) transmission analyses were performed using a *Bomem* (*Hartmann & Braun*) spectrometer in the Attenuated Total Reflectance (ATR) mode, in the range 2500 to 3400 cm^{-1}. Micro-Raman spectroscopy was performed on emeralds and quartzite samples using a *Jobin Yvon HR 320* monochromator system equipped with a CCD detector and a He-Ne laser beam (632.8 nm) coupled with an *Olympus* microscope, in the range 400 to 2500 cm^{-1}.

Results and discussion

Ten parcels of pre-shaped stones weighing approximately 200 g each were submitted to authenticity tests. The shapes of the stones include oval, rectangular, marquise, pear, triangular, rounded and free-form, ranging between 7 and 30 mm in size.

Two groups of stones were distinguished on the basis of general characteristics. The larger group was composed of opaque to translucent stones, with light-green, greyish-green and yellowish-green colours; irregular colour distribution and colour zoning were observed. A weak dichroism was observed in some translucent stones, with twin colours varying from yellowish green to bluish green. Some stones contain grey to black surface inclusions, identified as biotite and matrix rock fragments. These preliminary mineralogical observations indicate emerald of low gem quality.

The smaller group of stones was characterized by a strikingly homogeneous green, which was quite distinct from the colours of the emeralds, even to the naked eye (*Figure 1*). This material did not exhibit inclusions and dichroism was absent.

Under a long wavelength ultraviolet lamp, emerald showed a dark red or a yellowish-green glow, while the unknown material was inert (*Table I*). Observed under magnification, this unknown material showed wavy bands with slightly different green hues, in patterns different from the colour zoning seen in emerald, and its structure was granular, resembling a crystalline aggregate. Under the polariscope, this material remains light during 360° rotation, which is typical of aggregates. With combined transmitted and incident light, it was possible to see granular quartz crystals and platy mica crystals. Euhedral to subhedral pyrite and orange-red subhedral crystals, probably corundum, were also identified.
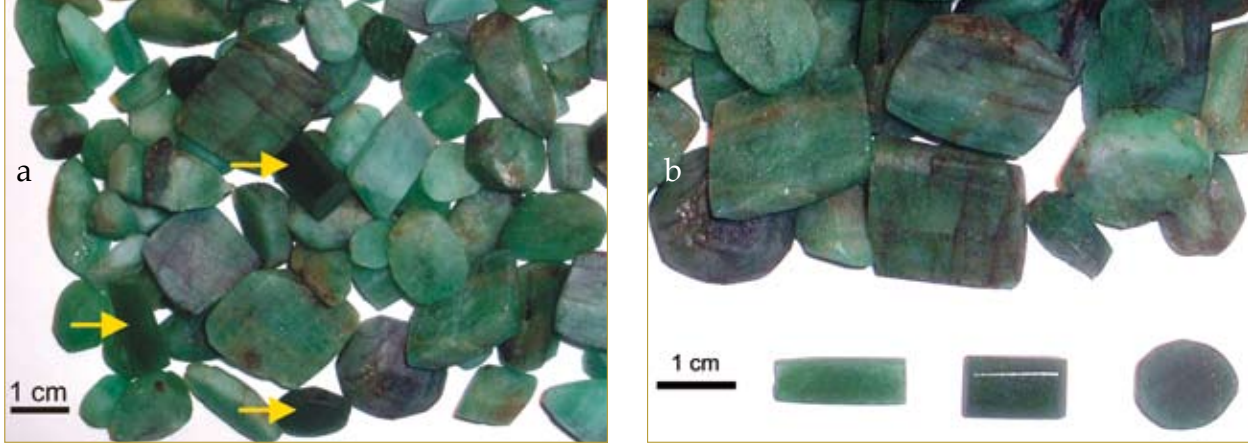
Figure 1: One parcel of pre-shaped green stones. (a) Some quartzite stones (arrowed) among emeralds. (b) A detailed view of three homogeneous green quartzites are shown at the bottom below rather poor quality emeralds with irregular colour distribution and grey to black inclusions.

The refractive indices (RI), despite the difficulty related to the polycrystalline structure, were approximately $N_o = 1.540$ and $N_e = 1.550$ (*Table I*), characteristic of quartz. However, the SG of this material was higher than that of quartz but similar to the analysed emerald.

Microscopic observation of thin sections confirmed that the unknown material was quartzite (*Figure 2*) with the following composition and textures:

- anhedral quartz with wavy extinction in a granoblastic texture;
- oriented light-green mica crystals with weak pleochroism, in a lepidoblastic texture;
- euhedral to subhedral opaque crystals, previously identified as pyrite using a stereomicroscope;
- euhedral to subhedral corundum;
- reddish-brown patches of iron oxides (Bard, 1985; Klein and Hurlbut, 1993).

SEM/EDS analyses of the mica crystals revealed the presence of Cr (*Figure 3*) which is consistent with their green colour and indicates their identification as fuchsite (Kerr, 1959; Klein and Hurlbut, 1993). The pyrite and corundum identifications were confirmed by SEM/EDS analyses and some small zircon crystals, about 40 µm long, were also found.

Table I: Some standard properties of the analysed emerald and quartzite stones.

Properties	Analysed materials	
	Emerald	Fuchsite quartzite
colours	light-green, greyish green, yellowish green	green
colour distribution	irregular distribution; parallel zoning	wavy bands
transparency	opaque to translucent	translucent
dichroism	weak; from yellowish green to bluish green	absent
SG	2.65 – 2.70	2.67
360° rotation on polariscope	four dark and light positions	constant transmission, remains light
RI	1.570-1.583	1.540-1.550
fluorescence under UV light	dark red and yellowish green	inert
internal features	inclusions of biotite and matrix rock fragments	grain boundaries of quartz and flakes of fuchsite mica
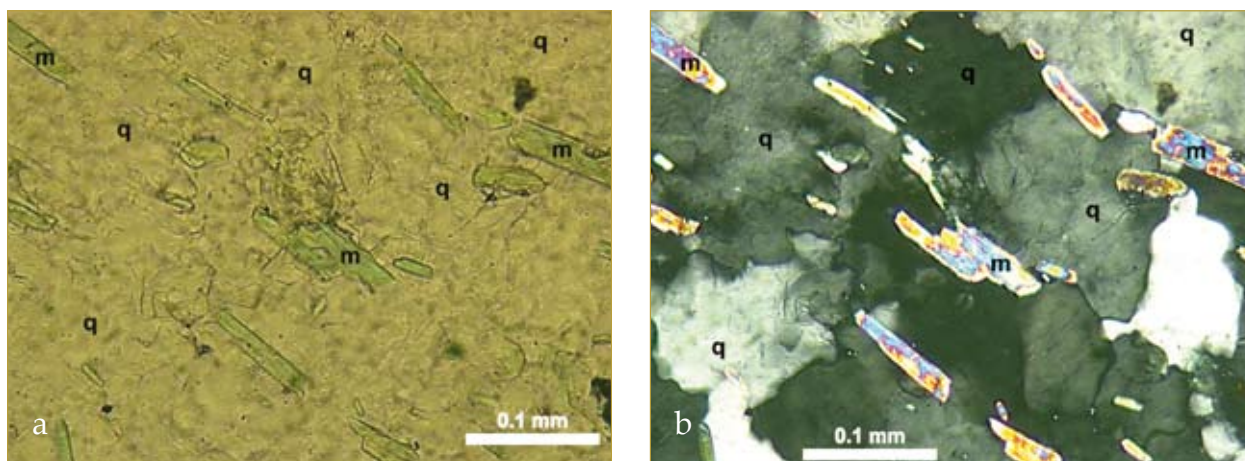
Figure 2: *A thin section of fuchsite quartzite observed under a petrographic microscope in ordinary illumination (a) and using crossed polars (b), showing granoblastic quartz (q) with wavy extinction and light-green Cr-muscovite (fuchsite) crystals (m) in a lepidoblastic texture.*
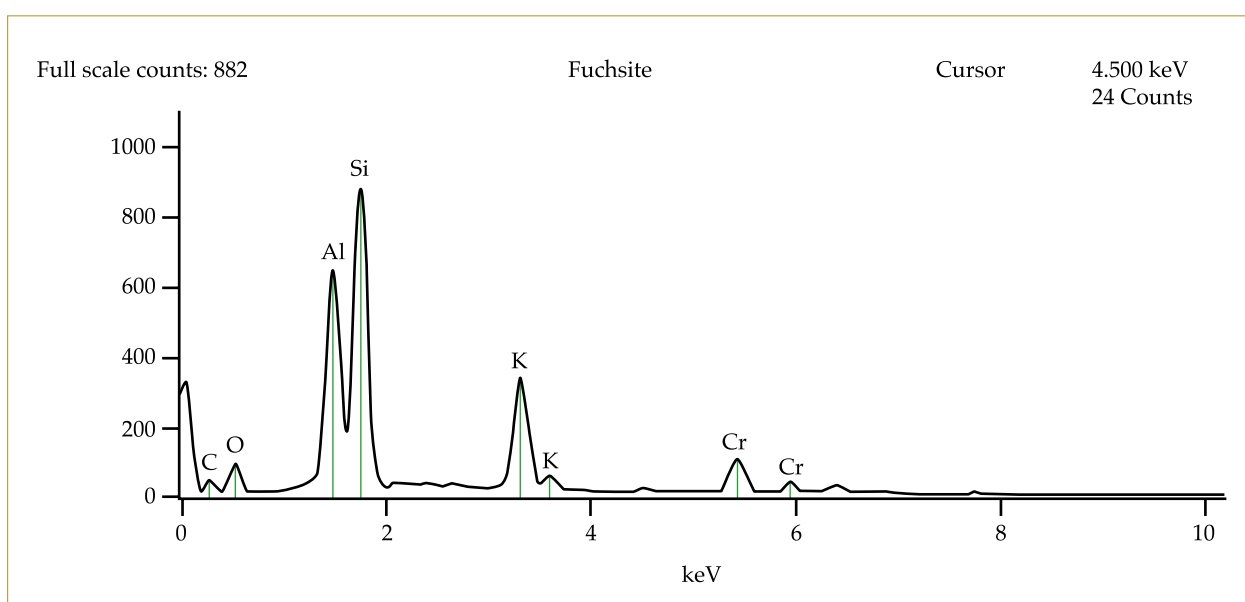
Figure 3: *Spectrum showing the presence of the major elements of muscovite (K, Al, Si) and a small but significant content of Cr which is the cause of the green colour and the reason for the varietal name fuchsite. Carbon content is due to coating applied to the specimen to disperse electrical charge.*

Fillers were not detected either in emerald fissures or in pores in the quartzite, under magnification or using UV light (see Johnson *et al.*, 1999 and Kiefert *et al.*, 1999). This is probably because the stones were not treated under vacuum to introduce the filling substance into fissures or pores, and is consistent with the fact that Brazilian dealers of rough and pre-shaped emerald only wet the emerald surface with the treatment substances. Sometimes these substances may be heated to reduce their viscosity so that they flow into surface fissures more easily than at room temperature. However, this treatment improves the clarity only at the surface of the stones and further treatment may be done after the stones have been cut.

Raman spectra were obtained from both emerald and fuchsite quartzite samples but Cr content in both caused considerable fluorescence. Backgrounds were so high that no peaks could clearly be attributed to fillers even between 1200-1700 cm^{-1}, the better region to characterize filling substances according to Kiefert *et al.* (1999). However, there is a clear peak at 467 cm^{-1} in the fuchsite quartzite stones due to the quartz content (*Figure 4*).
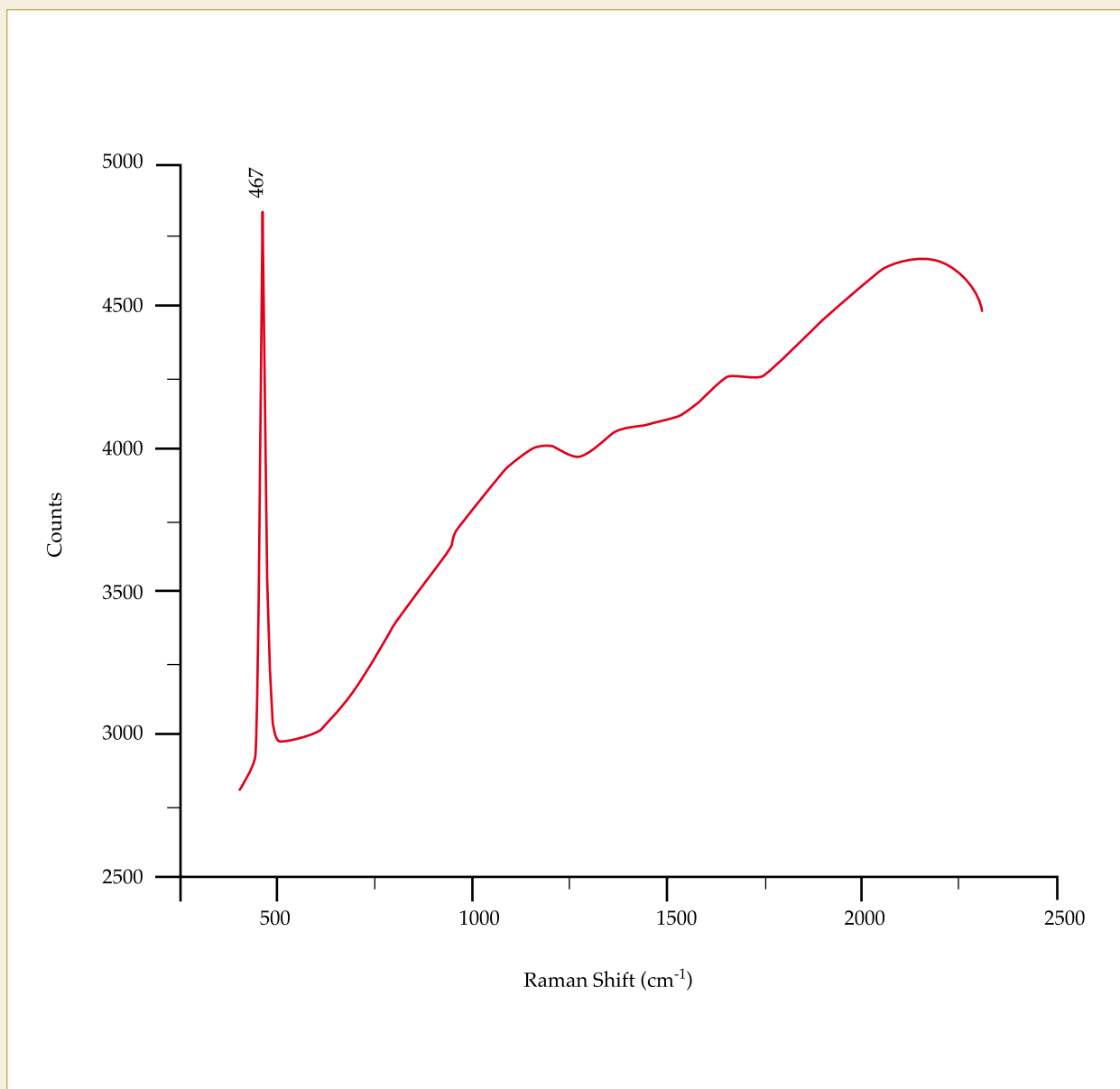
Figure 4: *A Raman spectrum of the quartzite, with strong fluorescence from 500-2500 cm^{-1}, due to Cr content in fuchsite crystals. The peak observed at 467 cm^{-1} is due to quartz (Nyquist et al., 1997;* Handbook of minerals Raman spectra*).*

FTIR spectra obtained from emeralds and quartzites in the ATR mode proved to be the best method of identifying any impregnating substances in the analysed stones. FTIR spectra of oils and artificial resins show that the main absorption bands lie in the 2800 to 3000 cm^{-1} range, corresponding to C-H vibration bonds present in many organic compounds; bands between 3000 and 3100 cm^{-1} are only present in the spectra of resins (Kiefert *et al.*, 1999). In this work, FTIR spectra from several samples of emerald and quartzite showed absorption bands in the 2600 to 3000 cm^{-1} range. In addition to the characteristic absorption bands of emerald and quartzite, both stones consistently showed absorption bands in the range 2600 to 3000 cm^{-1}. *Figure 5* shows two representative spectra from the quartzite (A and B), and one representative spectrum of emerald (*Figure 5 C*), where two main absorption bands can be observed at approximately 2850 cm^{-1} and 2920 cm^{-1}, with a shoulder at ± 2953 cm^{-1}. These peaks are also present in universal oil (*Figure 5 D*) at 2854 cm^{-1} and 2925 cm^{-1}, with a shoulder at 2955 cm^{-1} and agree with data shown by Kiefert *et al.* (1999). A comparison with the FTIR spectra for
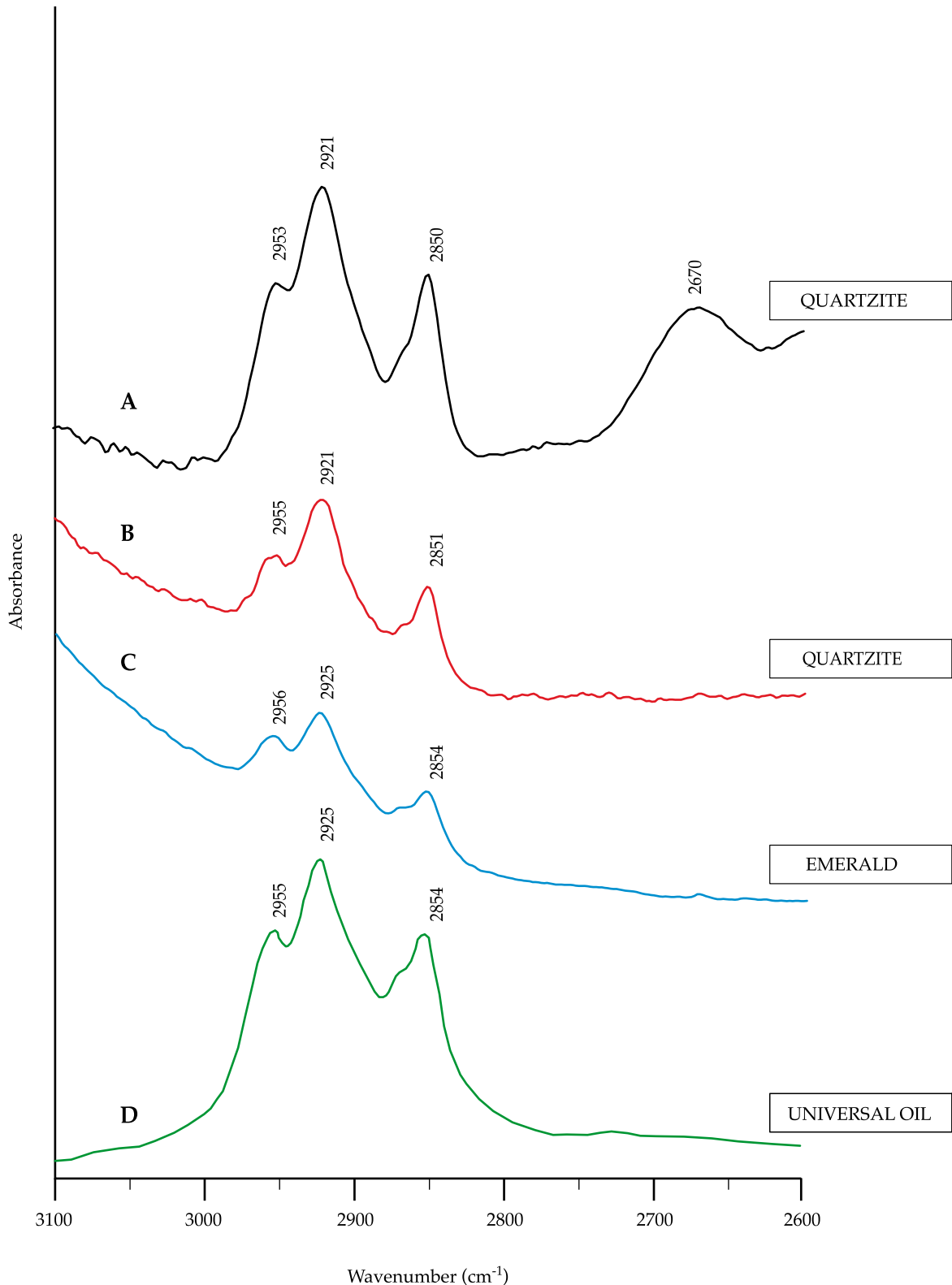
Figure 5: *FTIR spectra of two fuchsite quartzite stones (A and B), one emerald (C) and of universal oil (D) as described by Kiefert* et al. *(1999), in the range 3100-2600 cm⁻¹. The comparison of these four spectra show that absorption bands are very similar in the 2850-2956 cm⁻¹ area, indicating that universal oil could be the filling substance used in emerald and in quartzite. The absorption band in A at 2670 cm⁻¹, was observed in only one quartzite sample (A).*

filling substances presented by Johnson *et al.* (1999) shows a similarity between these results and the 'group B' filling substances, as shown in *Figure 6*. This group is represented by substances like paraffin oil and wax, Joban oil and HXTAL resin. The results obtained in the present research are most closely matched by the spectrum of paraffin oil. According to Gardner *et al.* (1978) and Kiefert *et al.* (1999), paraffin oil and universal oil are the same substance and Budavari *et al.* (1996) describes the name 'Nujol' as one of the trade marks used for this product. The broad absorbance peak observed in the quartzite spectrum at 2670 cm^{-1} in *Figure 5 A*, is reported neither by Kiefert *et al.* (1999) nor by Johnson *et al.* (1999) for paraffin oil. However, there are small peaks in this region for paraffin wax, as shown in Figure 6 B, spectrum h. An absorbance band with a wave number near this value (2670 cm^{-1}) was reported by Scholl (1983) for paraffin oil and this band was obtained also from a Nujol drop, made and distributed in Brazil by Schering-Plough Chemical Industry.

Conclusions

The precise identification of emerald as well as the identification of any filling substances is very important in order to avoid damage to consumer confidence. Basic gemmological tests can provide information sufficient to distinguish emerald from its imitations, but to obtain data on any treatments or filling substances it is necessary to use advanced techniques like SEM/EDS, Raman and FTIR spectroscopy (Farmer, 1974; Gadsen, 1975; McMillan and Hofmeister, 1988; Johnson, *et al.*, 1999).

Fracture filling is commonly used to enhance the clarity and even the colour of emeralds. Impregnation with different types of oil and resins has been used for decades and is accepted in the trade nowadays. However, major coloured stone trade organizations recommend that such gemstone treatment should be disclosed with details of the products used for this treatment (Levy, 1997; Johnson *et al.*, 1999; Kiefert *et al.*,
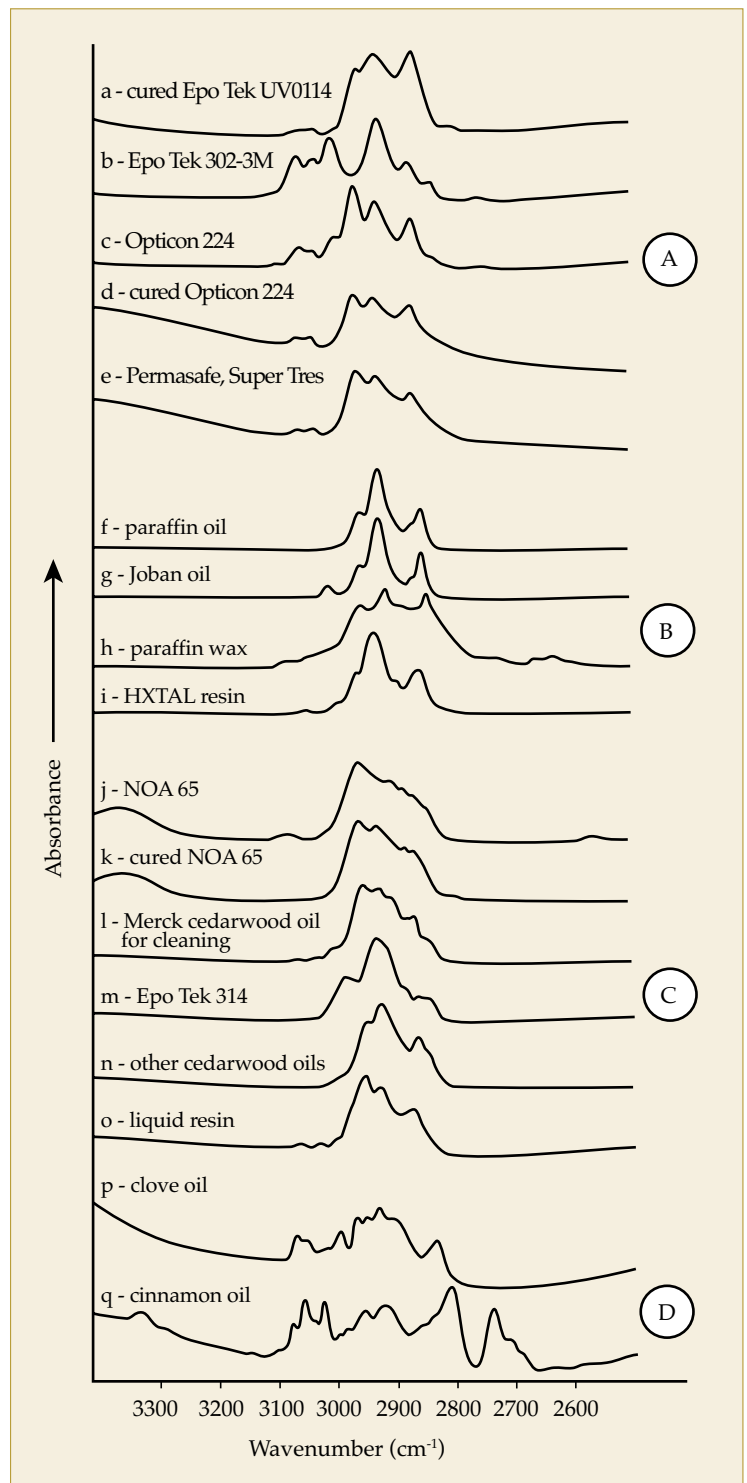
Figure 6: Infrared spectra of 17 filling substances arranged in four groups based on their spectra in the range 3400-2500 cm^{-1}, according to Johnson et al. *(1999). The infrared spectra from emerald and quartzite obtained in this research are most similar to group B.*

1999). In the stone parcels described in the present study, both emeralds and quartzites were submitted to treatment and as a result, looked very similar at first glance. FTIR spectra show that the filling substance used

was either paraffin oil or something very similar. Paraffin is also known as universal oil which is colourless and on the market in Brazil with the trade mark Nujol; it is commonly used by local gemstone dealers to improve clarity in emerald. However, on closer inspection, the quartzite showed a deeper green than would be expected if only the green fuchsite were causing the colour and, according to Ringsrud (1983), colourless fillers can improve the colour appearance of an emerald. The oily residue on the plastic packages containing the stones was colourless, but it is possible that some green substance was added to the Nujol used to treat the quartzite. According to Polli (2001), oils with green dyes are commonly used in countries like India and Brazil to impregnate gemstones such as quartz or beryl in order to obtain emerald imitations.

As yet the presence of any green dye has not been detected using FTIR, and it is possible that Joban oil, which is moderately green and has a paraffin-like spectrum, was used rather than Nujol or pure paraffin.

Mixing of the treated fuchsite-quartzite cut stones with emerald in gem parcels is a threat to consumer confidence, but the degree of occurrence and how serious this fraud is has not yet been determined. The work will continue in seeking the origins of the quartzite and treatments.

Acknowledgement

References

Bard, J.P., 1985. *Microtexture de roches magmatiques et métamorphiques.* Masson, S.A. Paris. 181 pp

Budavari, S., O'Neil, M.J., Smith, A., Heckelman, P.E., and Kinneary, J.F. (Eds), 1996. *The Merck Index. An encyclopedia of chemicals, drugs, and biologicals.* 12th Edn. Merck Research Laboratories Division of MERCK & CO., Inc. Whitehouse Station, NJ

Farmer, V.C., 1974. *The infrared spectra of minerals.* Mineralogical Society monograph IV. Bartholomew Press, London. 549 pp

Gadsden, J.A., 1975. *Infrared spectra on minerals and related inorganic compounds.* Butterworths, London, 277 pp

Gardner, W., Cooke, E.I., and Cooke, R.W.I., 1978. *Handbook of chemical synonyms and trade names.* CRC Press Inc. Boca Raton, Florida. 769 pp

Johnson, M.L., Elen, S., and Muhlmeister, S., 1999. On the identification of various emerald filling substances. *Gems & Gemology*, **35**(2), 82-107

Handbook of minerals Raman spectra. 2000-2004, Lyon, ENS-Laboratoire de Sciences de La Terre. Available at http://www.ens-lyons.fr/LST/Raman accessed on 10/12/2005

Kerr, P.F., 1959. *Optical Mineralogy.* 4th Edn. McGraw-Hill Book Company, New York. 492 pp

Kiefert, L., Hänni, H.A., Chalain, J-P., and Weber, W., 1999. Identification of filler substances in emeralds by infrared and Raman spectroscopy. *Journal of Gemmology*, **26**(8), 501-20

Klein, C., and Hurlbut Jr., C., 1993. *Manual of Mineralogy.* After J.D. Dana. 21st Edn. J. Wiley and Sons, Inc. New York. 681 pp

Levy, H., 1997. Accepted trade practice. *Gem & Jewellery News*, **6**(2), 19-22

McMillan, P.F., and Hofmeister, A.M., 1988. *Infrared and Raman spectroscopy.* In: Hawthorne, F.C. (Ed.), 1988. *Spectroscopic Methods in Mineralogy and Geology. Reviews in Mineralogy, 18.* Chapter 4, 99-159. Min. Soc. America, Washington, DC

Nyquist, R.A., Putzig, C.L., and Leugers, M.A., 1997. *Infrared and Raman Spectral Atlas of Inorganic Salts* (a 4-volume set). The Dow Chemical Company, Midland, Michigan. Academic Press, San Diego. 224 pp

Polli, G.O., 2001. Preenchimento de fraturas em esmeraldas. In: Castañeda, C., Addad, J.E., Liccardo, A. (Eds), *Gemas de Minas Gerais,* Chapter 4, 74-99. Sociedade Brasileira de Geologia, Núcleo de Minas Gerais

Ringsrud, R., 1983. The oil treatment of emeralds in Bogotá, Colombia. *Gems & Gemology*, **19**(3), 149-56

Scholl, F., 1983. *Atlas of Polymer and Plastic Analysis. 2nd Edn – Additives and processing aids. Spectra and methods of Identification.* Carl Hanser Verlag, Munich, **3**, 456 pp

Characterization of omphacite jade from the Po valley, Piedmont, Italy

Ilaria Adamo[1], Alessandro Pavese[1,2], Loredana Prosperi[3], Valeria Diella[2], David Ajò[4,5], Monica Dapiaggi[1], Carlo Mora[6], Franco Manavella[7], Franco Salusso[8] and Valter Giuliano[9]

1. *Dipartimento di Scienze della Terra, Sezione Mineralogia, Università degli Studi di Milano, Via Botticelli 23, 20133 Milano, Italy*
2. *Istituto per la Dinamica dei Processi Ambientali (I.D.P.A.), Consiglio Nazionale delle Ricerche (C.N.R), Sezione di Milano, Via Botticelli 23, 20133 Milano, Italy*
3. *Istituto Gemmologico Italiano (I.G.I.), Viale Gramsci 228, 20099 Sesto San Giovanni, Milano, Italy*
4. *Istituto di Chimica Inorganica e delle Superfici (I.C.I.S.), Consiglio Nazionale delle Ricerche (C.N.R.), Corso Stati Uniti 4, 35127 Padova, Italy*
5. *Gruppo di Coordinamento per la Ricerca sui Materiali Gemmologici, Progetto Finalizzato Materiali Speciali per Tecnologie Avanzate II, Consiglio Nazionale delle Ricerche (C.N.R.), Italy*
6. *Agenzia Formativa Scuola Professionale per Orefici E.G. Ghirardi, Via San Tommaso 17, 10121 Torino, Italy*
7. *Via Pinerolo, 10060 Macello, Torino, Italy*
8. *Via Papa Giovanni XXXIII 11, 10060 Bricherasio, Torino, Italy*
9. *Protezione della natura, parchi e aree protette, Assessorato della Cultura, Provincia di Torino, Torino, Italy*

Abstract: *A dark green jade has been discovered recently in secondary alluvial deposits which are widespread in the Po valley, between Cuneo and Turin (Piedmont, Italy). Traditional gemmological tests have been combined with advanced analytical techniques (X-ray powder diffraction, chemical composition determination, absorption and photoluminescence spectroscopy) and thin section examinations to provide full characterization of this material and reveal that it is mainly composed of omphacite pyroxene.*

Introduction

Jade has a rich history dating back thousands of years, due to its use as a precious and enchanting gemstone (see, for example, Hughes *et al.*, 2000). A dark green jade has been discovered recently by Franco Manavella and Franco Salusso as pebbles in secondary alluvial deposits in the Po valley (Piedmont, north Italy). This material is suitable for cutting into small cabochons or slabs. Other deposits have been discovered in nearby areas, and a geological map of recoveries is being compiled. However, a full characterization of this dark green jade and its correct mineralogical composition have still to be established. The present study aims to provide a detailed description of this dark green jade from the Po valley, so as to (i) determine whether it consists of a single mineral phase or of an assemblage, (ii) establish its relationship to a given family of minerals and (iii) provide a set of features to enable distinction of this Po valley jade from other jades. Interest in the dark green jade in question is also motivated by paleo-ethnological implications, as this jade has been mined and used since prehistoric times by local populations to manufacture a variety of articles (D'Amico *et al.*, 1995).

Materials and methods

The dark green jade from the alluvial deposits of the Po valley has been characterized on the basis of the observations gathered from a suite of eight samples (see *Figure 1*), kindly provided by Carlo Mora.

Seven of the eight specimens (nos. 1, 2, 3, 4, 5, 6, 7) are cabochon-cut with (i) either an oval or a drop shape (five of these have a hollow inside so as to improve the colour transparency), (ii) weight ranging from 0.93 to 3.67 ct and (iii) size within $10.5\text{-}17.7 \times 6.1\text{-}12.1 \times 1.2\text{-}2.6$ mm; the only rough sample studied (specimen A) weighs 6.31 ct, with dimensions of $14.3 \times 11.4 \times 2.1$ mm.

All samples were first investigated by traditional gemmological methods, to determine their optical and physical properties. Polished thin sections were obtained from specimens 1 and A, and investigated in transmitted light mode by means of a traditional microscope and using a Cambridge Stereoscan 360 scanning electron microscope (SEM). The SEM is equipped with an Oxford Isis 300 energy dispersive spectrometer (EDS), and this enabled study of exsolution textures and compositional zoning in the same thin sections.

X-ray powder diffraction measurements were then carried out on two specimens (1 and A), to determine the mineralogical composition of the dark green jade. Data collections were performed at normal temperature and pressure by means of a Panalytical X'Pert-PRO MPD X'Celerator X-ray powder diffractometer, using CuKα radiation (λ=1.518 Å) and a beam of 40 kV, 40 mA. X-ray powder diffraction patterns were collected over 5-117° 2θ, with steps of 0.008° 2θ, a counting time of 25 sec/step and NBS-Si as an internal calibrant. This has enabled the lattice parameters to be calculated by the Rietveld method using the GSAS software package (Larson and Von Dreele, 2000) to treat the experimental 2θ-profiles.

The chemical composition of the dark green jade has been quantitatively determined using an Applied Research Laboratories electron microprobe fitted with five wavelength dispersive spectrometers (WDS) and a Tracor Northern energy dispersive spectrometer (EDS) (accelerating voltage of 15 kV; sample current on brass of 15 nA; counting time of 20 sec on peaks and 5 sec on backgrounds). Natural kaersutite (for Na, Mg, Al, Si, K, Ca, Ti, Fe), rhodonite (for Mn) and chromite (for Cr) have been used as standards; the results have been corrected for matrix effects using a conventional PAP routine of the SAMx series of

programs. Proportional formulae and Fe^{2+}/Fe^{3+} partitioning have been calculated on the basis of the method described in Cawthorn and Collerson (1974). Measurements have been carried out on two thin sections, obtained from specimens 1 and A.

The following equipment was used for spectroscopic investigations:

(i) a Nicolet NEXUS FTIR spectrometer, operating both in transmission mode (the beam passing through a sample, for all the specimens, and through pellets composed of a blend with a 1:100 sample to KBr ratio, for specimens 1 and A, only) and in reflectance mode [by means of a diffuse reflectance accessory (DRIFT); all samples were studied], to investigate the 4000-400 cm^{-1} infrared range, with a resolution of 4 cm^{-1};

(ii) a UNICAM UV-Vis 500 spectrometer, operating in reflectance mode, equipped with an integrating-sphere and tungsten and deuterium lamps, to study the 190-900 nm ultraviolet-visible-near infrared range;

(iii) a custom-made instrument equipped with frequency-doubled Nd:YAG laser (λ=532 nm, Casix CDPL-1100T), a monochromator (Jobin Yvon HR640) with reciprocal dispersion of 24 Å/mm and a photomultiplier tube (Hamamatsu R6357), to record photo-luminescence (PL) spectra at room temperature for three samples (nos. 1, 2 and 3).

Particular attention has been paid to spectroscopic techniques because they provide non-destructive analytical methods, except for the IR-measurements in transmission mode using KBr compressed pellets.

Gemmological properties

The gemmological features of the dark green jade from the Po valley are shown in *Table I*. All samples are translucent with a dark green hue. They exhibit refractive indices and specific gravities ranging over 1.67-1.68 and 3.35-3.36, respectively. These values are slightly higher than those common for jadeite jade (R. 1.65-1.66; SG 3.32-3.33), from different geographic localities (Hargett, 1990; Fritsch *et al.*, 1992; Htein and Naing, 1995; Ou Yang and Li Hansheng, 1999; Ou Yang and Qi, 2001). The specimens are inert under short- and long-wave UV radiation, appear dark green under a Chelsea colour filter and have a hardness of 6½ on the Mohs scale. Gemmological microscopy observations reveal the cabochons to have a microcrystalline to a porphyroblastic texture with black and green veins and spots, fractures, and some prismatic, transparent and colourless crystals..

In agreement with Hargett (1990); Ou Yang *et al.* (2003) and Harlow *et al.* (2004), the results of the gemmological testing of the jade from the Po valley suggest an omphacite-like composition. Omphacite jade has recently grown in importance in the gems market [see for instance the inky black omphacite jade from Hong Kong and China (Ou Yang *et al.*, 2003) and the blue omphacite from Japan and Guatemala (Harlow, 2003; Harlow *et al.*, 2004)] and this has boosted much interest in the dark green jade from the Po valley as a gemmological material.

Figure 1: Six of the eight omphacite jades (0.93-3.67 ct and 6.1-17.7 mm) from the Po valley, examined in this study. Photo by Ilaria Adamo.

Thin sections examination

Thin section observations using a traditional petrographic microscope and a scanning electron microscope show a randomly

Table I: Gemmological properties of omphacite jade from the Po valley, Piedmont (Italy).

Colour	dark green
Transparency	translucent
RI*	1.67-1.68
SG	3.35-3.36
UV fluorescence	short-wave: inert long-wave: inert
Chelsea colour filter	dark green
Mohs hardness	6½
Microscopic features	microcrystalline texture; black and green veins and spots; fractures; prismatic, transparent and colourless crystals
* By the distant vision method	

oriented microcrystalline to a porphyroblastic texture *(Figure 2)*, composed almost totally of omphacite. SEM-EDS measurements reveal some compositional zoning, or micro exsolution within the omphacite grains *(Figure 3)*. The lighter areas (20-80 μm across) contain relatively more Ca, Mg and Fe than the darker areas which are richer in Na and Al. This suggests that lighter patches have more of the diopside-hedenbergite end-members while the darker areas (30-100 μm size) are closer to pure jadeite.

X-ray powder diffraction

An X-ray powder diffraction pattern of the jade from the Po valley *(Figure 4)* indicates that it consists of a single phase consistent with an Fe-bearing omphacite, in agreement with the results from gemmological analysis. The very small angular step used in the scan and the modest instrumental contribution (the Full Width at Half Maximum of LaB6 over the whole angular range explored is never larger than 0.02° 2θ) means that the presence of any other phases would have been recorded. During the refinement, the cell parameter of the internal standard was

kept fixed in order to correctly evaluate the zero-point correction of the goniometer. The refined cell parameters of the dark-green jade [a = 9.5791(3), b = 8.7588(2), c = 5.2554(3) Å, α = γ = 90° and β = 106.918(2)° with monoclinic cell setting and $C2/c$ space group] are typical of omphacite [Edgar *et al.*, 1969; Ogniben, 1968; Deer *et al.*, 1978; Rossi *et al.*, 1983; see, in particular, Camara *et al.* (1998) who report a detailed study of a large suite of Fe-rich omphacite samples].

Chemical composition

The results of chemical analyses of jade specimens 1 and A are summarized in *Table II* and indicate an omphacitic composition, in agreement with previous observations. The valence state of iron has been investigated and on the basis of crystal-chemical considerations and relying on the model of Cawthorn and Collerson (1974) both Fe^{3+} and Fe^{2+} are present, in keeping with the compositions of omphacite samples reported by Deer *et al.* (1978). The Fe^{3+} / Fe^{2+} ratio of >1 is consistent with the high Na-content, which is commonly accompanied by relatively high ferric iron. The chromium contents
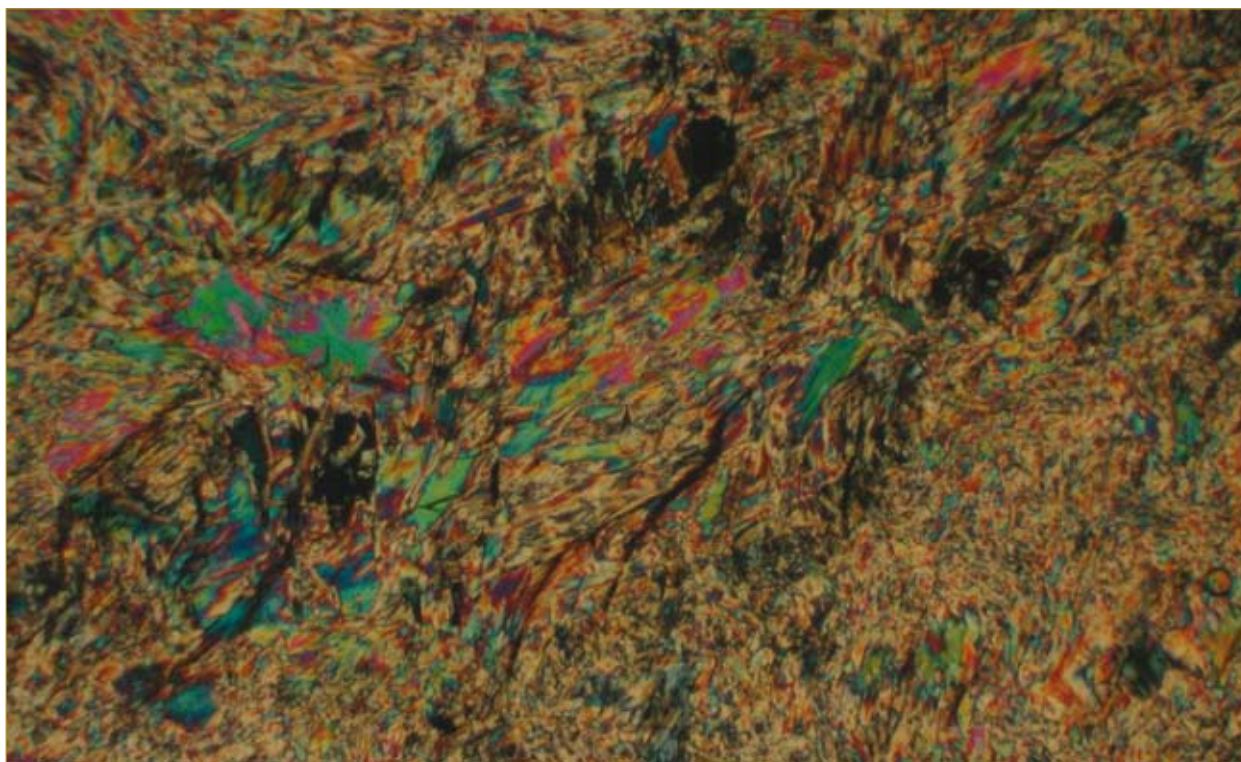
Figure 2: Thin section of omphacite jade (specimen 1) from the Po valley, showing a porphyroblastic texture. Cross polarized light; magnification 9x. Photo by Illaria Adamo.

Figure 3: Back-scattered electron image of omphacite jade from the Po valley. The darker areas are richer in jadeite while the paler areas have higher contents of diopside-hedenbergite. Photo by Agostino Rizzi.
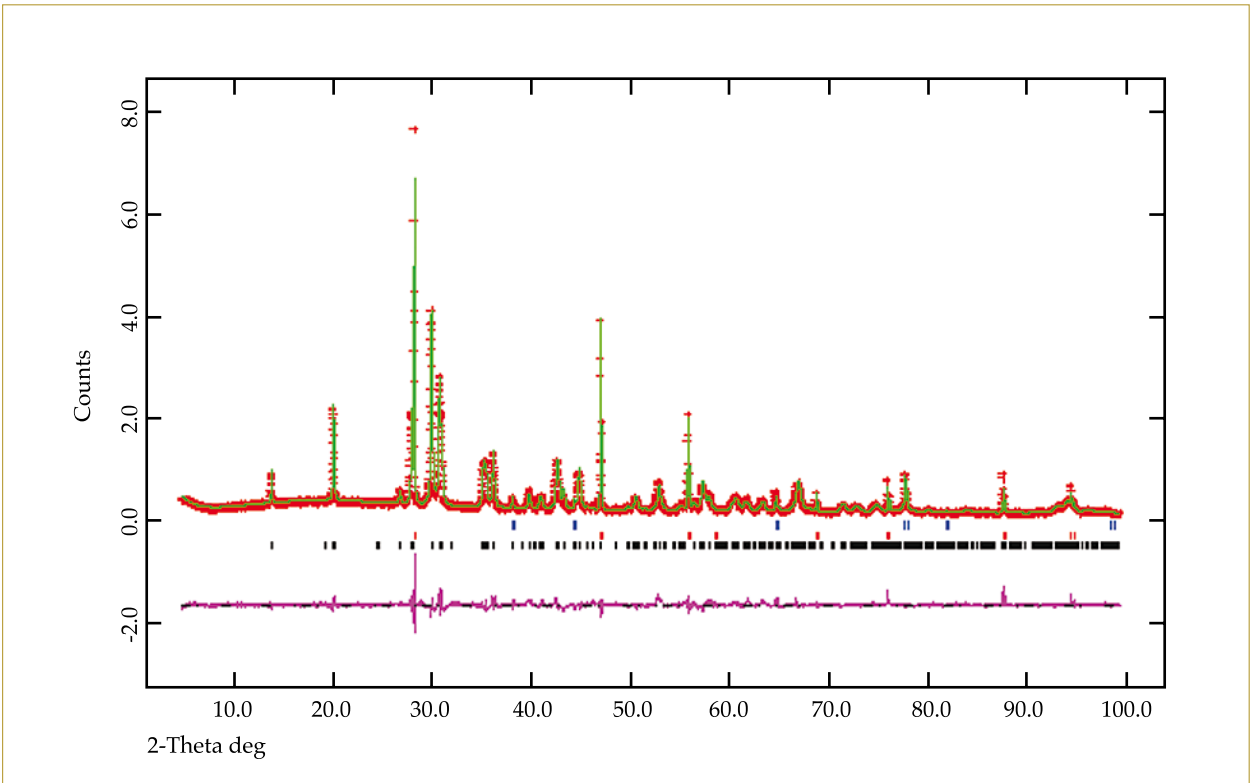
Figure 4: *Rietveld refinement of the X-ray powder diffraction pattern (5 -100° 2θ-angle range) of the omphacite jade from the Po valley. The lower pattern represents the residuals between calculated and experimental curves.*
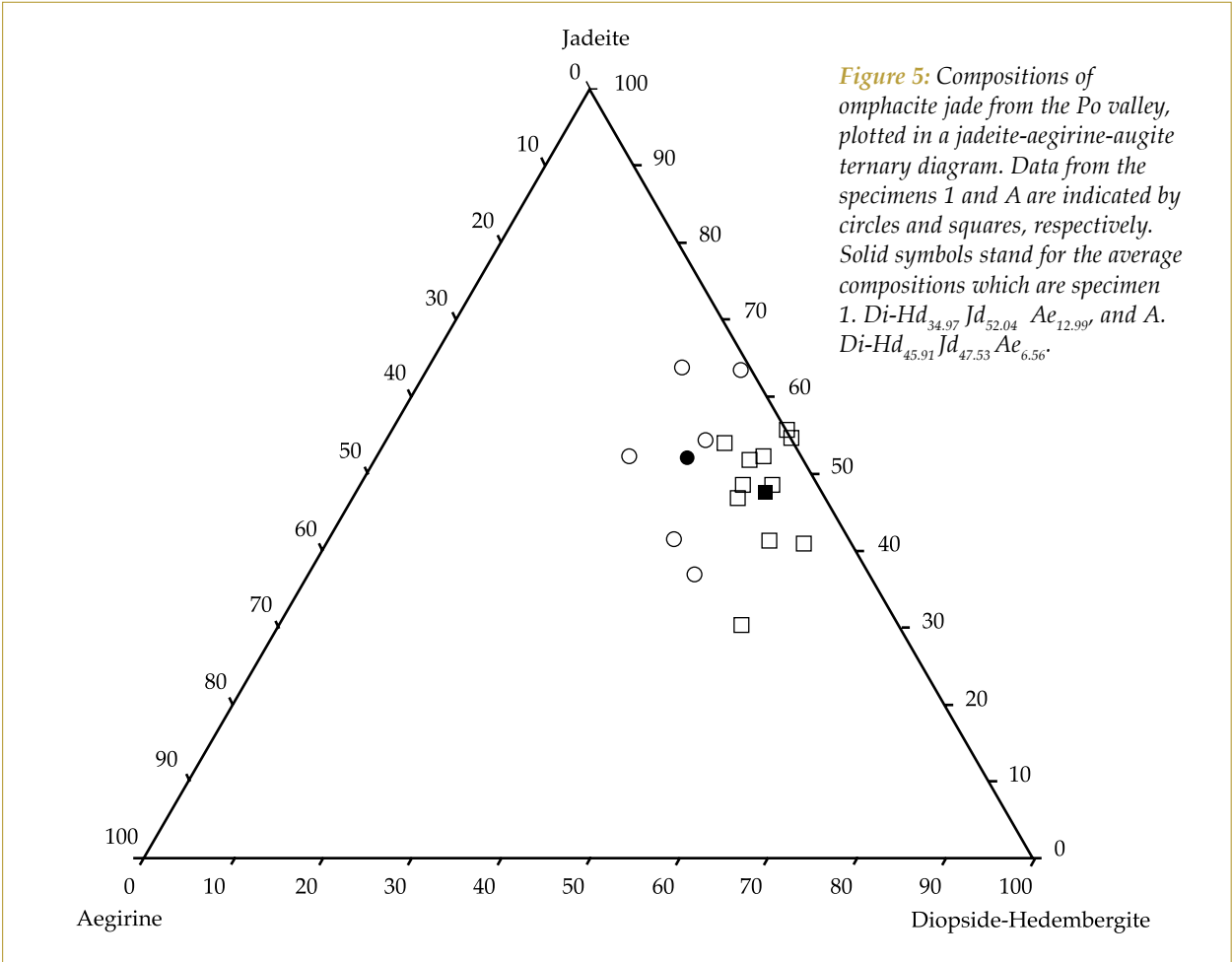
Figure 5: *Compositions of omphacite jade from the Po valley, plotted in a jadeite-aegirine-augite ternary diagram. Data from the specimens 1 and A are indicated by circles and squares, respectively. Solid symbols stand for the average compositions which are specimen 1. $Di-Hd_{34.97} Jd_{52.04} Ae_{12.99}$, and A. $Di-Hd_{45.91} Jd_{47.53} Ae_{6.56}$.*

Table II: Chemical composition of omphacite jade from the Po valley.

Oxide (wt.%)	Specimen 1 (mean of 6 analysis points)	Specimen A (mean of 12 analysis points)	Cations calculated on the basis of six oxygens		
			Element	Specimen 1	Specimen A
SiO_2	55.86	55.44	Si	1.965	1.965
TiO_2	0.22	0.14	Ti	0.006	0.004
Al_2O_3	13.23	11.96	Al	0.549	0.500
Cr_2O_3	0.17	0.29	Cr	0.005	0.008
Fe_2O_3	5.17	2.60	Fe^{3+}	0.137	0.069
FeO	1.14	1.38	Fe^{2+}	0.034	0.041
MnO	0.13	0.12	Mn	0.004	0.004
MgO	6.38	8.37	Mg	0.335	0.442
CaO	8.27	11.22	Ca	0.312	0.426
Na_2O	9.94	8.29	Na	0.678	0.570
K_2O	0.01	*	K	-	-
			Na/(Na + Ca)	0.685	0.572
Total	100.52	99.81	$Al/(Al + Fe^{3+})$	0.800	0.879

* Below detection limit (0.01 wt.%)

(average 0.23 wt.%; 0.007 atoms per formula unit) are probably responsible for the very attractive green colour (Rossman, 1980). These conclusions are substantiated by spectroscopic observations, discussed in the next section.

The results in *Table II* agree with the omphacite compositional field (Morimoto, 1988) defined by the Na/(Na + Ca) and Al/(Al + Fe^{3+}) ratios, lying within $0.2 \leq Na / (Na + Ca) \leq 0.8$ and $Al /(Al + Fe^{3+}) > 0.5$ (see also: Clark and Papike, 1968; Deer *et al.*, 1978; Ou Yang *et al.*, 2003). The chemical composition of omphacite is expressed through its formula unit, *i.e.* $(Ca,Na)(Mg,Fe^{2+},Fe^{3+},Al)(Si_2O_6)$ and, being a solid solution of the pyroxene group, can be formulated in terms of the four end-members: $CaMgSi_2O_6$ (diopside, Di), $CaFe^{2+}Si_2O_6$ (hedenbergite, Hd), $NaAlSi_2O_6$ (jadeite, Jd) and $NaFe^{3+}Si_2O_6$ (aegirine or acmite, Ae) In *Figure 5* the measured compositions of jade from the Po valley are displayed on a ternary diagram as a function of Di-Hd, Jd and Ae. The analysis points exhibit some scatter, which suggests some degree of chemical inhomogeneity or microscopic zoning.

Mn and Ti are present in quantities comparable to Cr and provide a full compositional characterization of the omphacite jade from the Po valley.

Spectroscopic features

Infrared spectroscopy

A typical omphacite-like mid-infrared spectrum over the 1500-400 cm^{-1} range obtained in transmission mode from our jade samples (KBr-pellet method) is shown in *Figure 6*, along with that of pure jadeite for comparison (see also the results of Ou Yang *et al.*, 2003, on inky black omphacite jade). Both transmission and reflectance IR patterns are characterized by a broad band at about 3530 cm^{-1} (*Figure 7*), due to OH incorporated in the pyroxene structure and this is consistent with recent studies (see, for example, Skogby *et al.*, 1990;
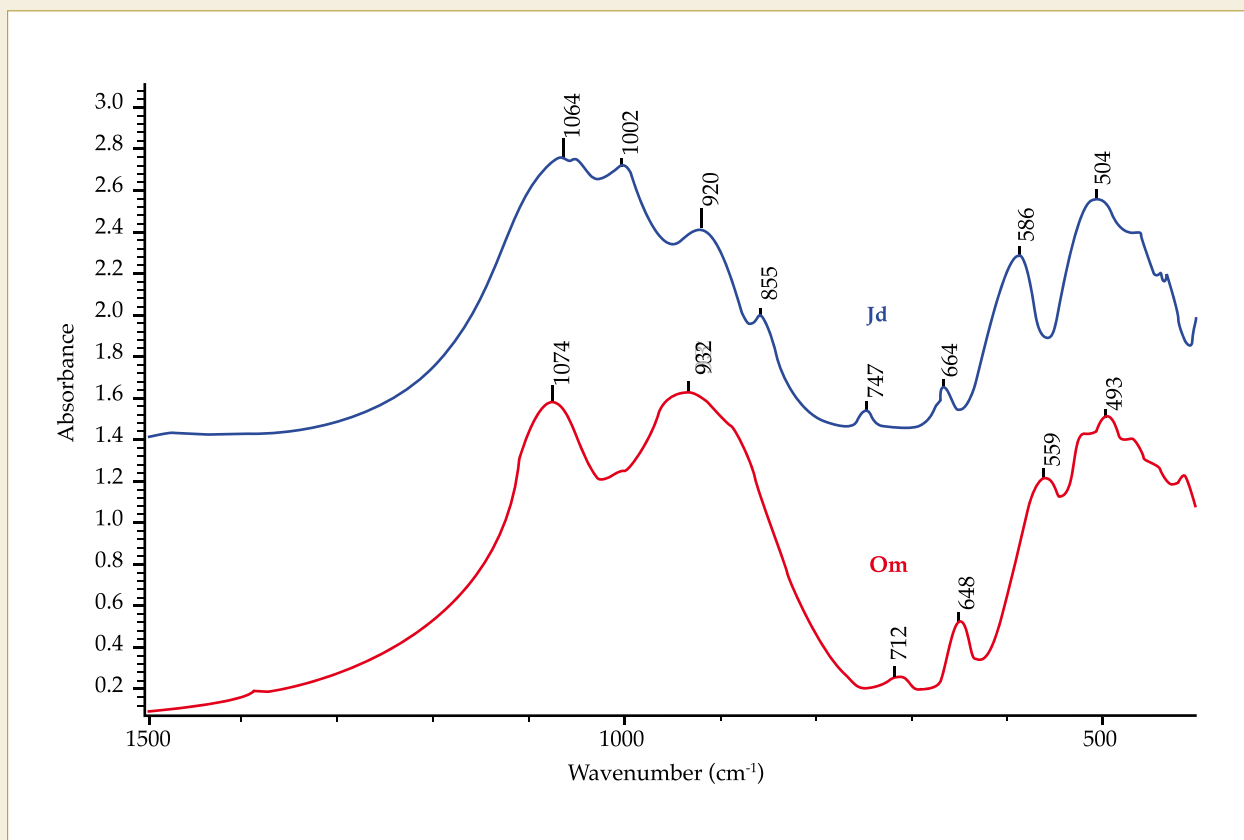
Figure 6: Infrared spectrum (1500-400 cm⁻¹) in transmission mode (KBr-pellet technique) of omphacite jade (Om), compared with a typical spectrum of jadeite jade (Jd). The spectra are offset for clarity.
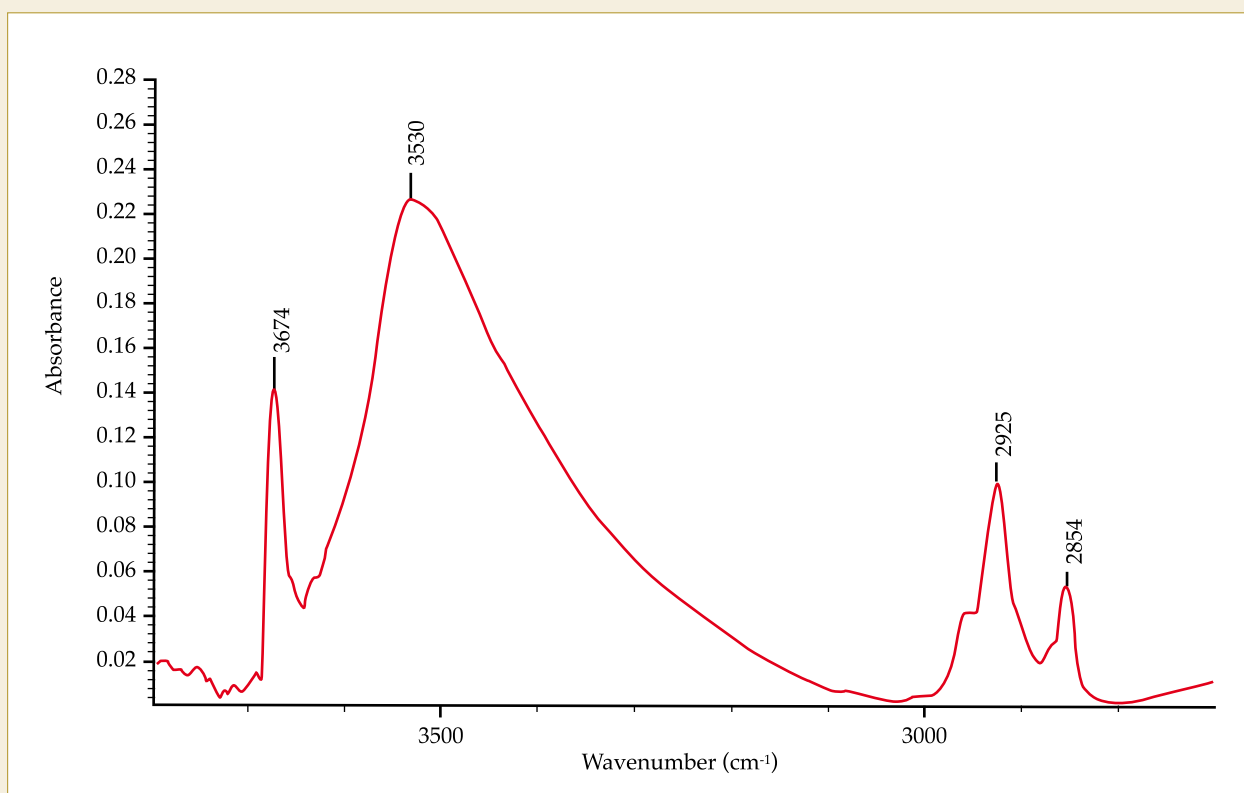
Figure 7: Infrared spectrum (3800-2700 cm⁻¹) in transmission mode (obtained with the beam passing through the sample) of the omphacite jade. Peaks attributed to hydroxyl groups (3674 and 3530 cm⁻¹) and residues of organic matter (2925 and 2854 cm⁻¹) are visible.
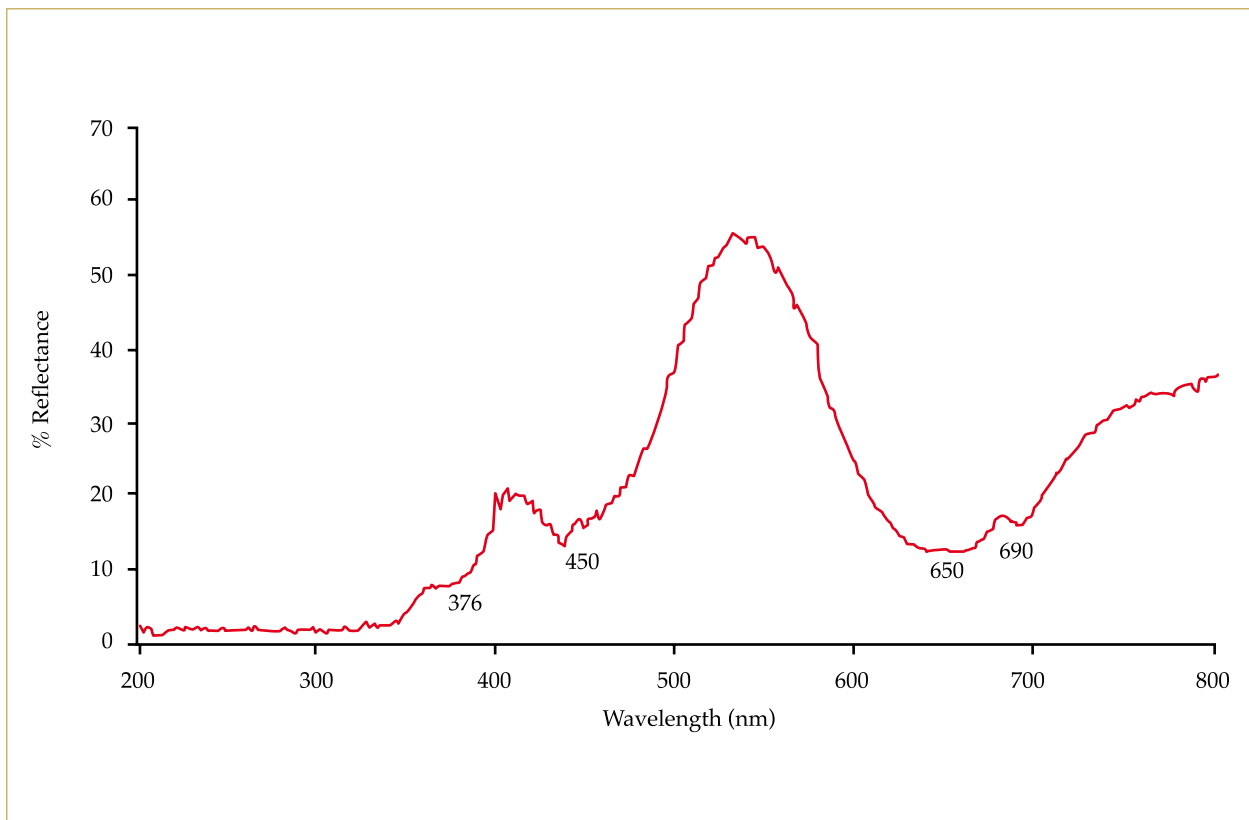
Figure 8: Reflectance spectrum in the range 200-800 nm of omphacite jade (specimen 1) from the Po valley. Broad absorption bands near 450 nm and 650 nm and a narrow band at 690 nm are typical of Cr^{3+}.

Katayama and Nakashima, 2003; Koch-Müller *et al.*, 2004). Some spectroscopic features due to the hydroxyl group can also be related to the occurrence of inclusions in omphacite jade, such as a sharp band at 3674 cm^{-1}, clearly observable in both transmission and reflectance IR spectra (see again *Figure 7*), and attributable to thin sub-microscopic amphibole (probably tremolite) lamellae (Ingrin *et al.*, 1989; Skogby *et al.*, 1990; Hawthorne *et al.*, 2000, Ishida *et al.*, 2002; Jenkins *et al.*, 2003; Koch-Müller *et al.*, 2004). The presence of pyroxene-amphibole intergrowths, due to alteration processes is common in omphacite (Veblen and Buseck, 1981; Skogby *et al.*, 1990; Koch-Müller *et al.*, 2004) and can readily be detected by IR spectroscopy.

Weak absorption peaks near 2920 cm^{-1} and 2850 cm^{-1} in both transmission and reflectance mode (see *Figure 7*) are probably due to residues of organic material used after polishing to improve the shine of the jade (Fritsch *et al.*, 1992; Tan *et al.*, 1995; Quek and Tan, 1997, 1998).

Ultraviolet-visible-near infrared spectroscopy

A non-polarized spectrum over the ultraviolet-visible energy range (200-800 nm) of omphacite jade from the Po valley is displayed in *Figure 8*. Consistent with the microprobe analyses, the spectrum exhibits features typical of Cr^{3+}, i.e. two broad absorption bands at 450 and 650 nm, with a narrow band at 690 nm, that are located either side of the transmission window near 530 nm (Khomenko and Platonov, 1985; Rossman, 1980, 1988; Burns, 1993; Harlow *et al.*, 2004). The absorption peaks at 376 nm and 438 nm due to Fe^{3+} are barely detectable because of Cr^{3+} absorption (see Rossman, 1974, 1980, 1988; Khomenko and Platonov, 1985; Burns, 1993; Harlow, 2003; Harlow *et al.*, 2004) and this confirms that the dark green hue is due mainly to Cr^{3+}.

Photoluminescence spectroscopy

The photoluminescence (PL) spectrum over the 550-850 nm energy range (*Figure 9*) contains a band or a shoulder at about 690 nm and confirms the presence of Cr^{3+}.
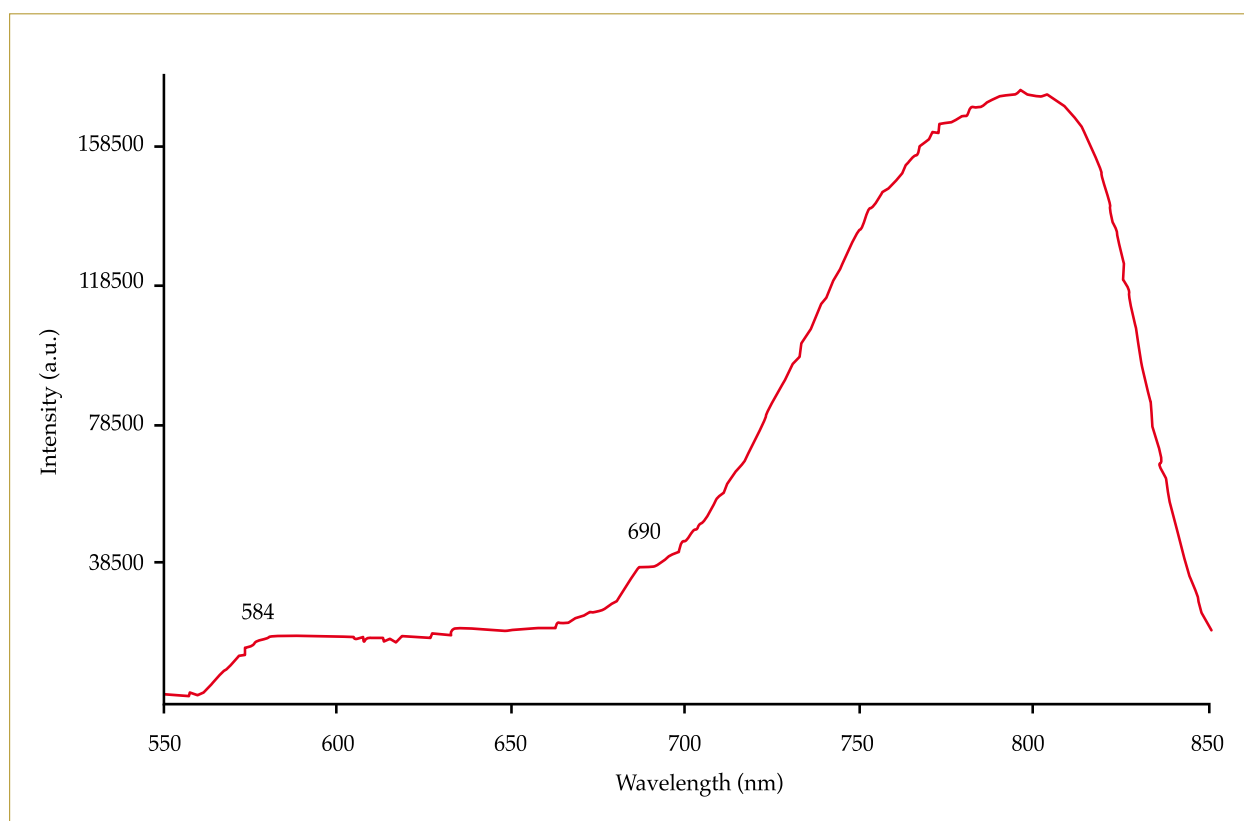
Figure 9: Photoluminescence spectrum over the 550-850 nm range of the omphacite jade (specimen 1) from the Po valley. Note the peak/shoulder at about 690 nm, due to Cr^{3+}; the emission band at 584 nm, related to Mn^{2+}; and the wide photoluminescence band on the longer wavelength side (centred about 800 nm) attributed to Fe^{3+}.

A wide emission band at 584 nm (see again *Figure 9*) is attributed to Mn^{2+} (Tarashchan, 1978; Walker, 1985; Blasse and Grabmaier, 1994; Zharikov and Smirnov, 1997), while Fe^{3+} is probably responsible for the broad PL band at longer wavelengths. However, for iron, determination of the band maximum is hindered by the decrease of sensitivity of the photo-multiplier passing from the visible to the infrared energy region. The attribution of this band to Fe^{3+} is further supported by the PL spectrum recorded with a germanium detector (Walker and Glynn, 1992; Carbonin *et al.*, 2005), which also brings to light a series of narrow lines at high wavelength, related to Fe^{2+} (Walker and Glynn, 1992).

Distinctive features of the dark-green jade from the Po valley

The omphacite jade from the Po valley may be readily distinguished from jadeite jades and from their simulants by means of traditional gemmological testing, in particular by determining their RI (1.67-1.68) and SG (3.35-3.36).

Determination of the Fe^{3+}, Fe^{2+}, Ti^{4+}, Cr^{3+} and Mn^{2+} contents by chemical analyses, UV-Vis and PL spectroscopy, and of the possible presence of hydroxyl groups and residues of organic matter applied after polishing using IR spectra, should be carried out to characterize this dark green jade from the Po valley.

Conclusions

On the basis of the results from gemmological testing and advanced analytical methods, the dark green jade from secondary alluvial deposits in the Po valley (Piedmont, Italy) consists mainly of omphacite pyroxene with some micro exsolution and some compositional zoning. The dark green colour is mainly attributable to trivalent Cr, which is present along with comparable amounts of Mn and Ti. The luminescent properties of the

dark-green jade of the Po valley are related to Mn^{2+}, Fe^{2+}, Fe^{3+} and Cr^{3+}. Promotion and distribution of this material on the Italian gemstone market are planned for the near future.

Acknowledgements

References

Blasse, G., and Grabmaier, B.C., 1994. *Luminescent Materials*, Springer-Verlag, Berlin

Burns, R.G., 1993. *Mineralogical applications of crystal field theory, 2nd edn. Cambridge Topics in Mineral Physics and Chemistry*. Cambridge University Press, Cambridge

Camara, F., Nieto, F., and Oberti, R., 1998. Effects of Fe^{2+} and Fe^{3+} contents on cation ordering in omphacite. *European Journal of Mineralogy*, **10**(5), 889-906

Carbonin, S., Visonà, D., Rizzo, I., Favaro, M.L., Pozza, G., and Ajò, D., 2005. Optical properties and composition of corundum and of synthetic and mineral related materials. *Institute of Physics, Conf. Ser.*, **152** (Section G), 827-30

Cawthorn, R.G., and Collerson, K.D., 1974. The recalculation of pyroxene end-member parameters and the estimation of ferrous and ferric iron content from electron microprobe analyses. *American Mineralogist*, **59**(11/12), 1203-8

Clark, J.R., and Papike, J.J., 1968. Crystal-chemical characterization of omphacites. *American Mineralogist*, **53** (5/6), 840-68

D'Amico, C., Campana, R., Felice, G., and Ghedini, M., 1995. Eclogites and jades as prehistoric implements in Europe. A case study of petrology applied to cultural heritage. *European Journal of Mineralogy*, **7**(1), 29-41

Deer, W.A., Howie, R.A., and Zussman, J., 1978. *Rock-forming minerals, single-chain silicates*, 2A (2nd edn), Longman, London

Edgar, A.D., Mottana, A., and Macrae, N.D., 1969. The chemistry and cell parameters of omphacite and related pyroxenes. *Mineralogical Magazine*, **37**(285), 61-74

Fritsch, E., Shun-Tien Ten Wu., Moses, T., McClure, S.F., and Moon, M., 1992. Identification of bleached and polymer-impregnated jadeite. *Gems & Gemology*, **28**(3), 176-81

Hargett, D., 1990. Jadeite of Guatemala: a contemporary view. *Gems & Gemology*, **26**(2), 134-41

Harlow, G.E., 2003. Blue omphacite in jadeitites from Guatemala and Japan: Crystal chemistry and chemistry and color origin. *Geological Society of America Annual Meeting, Seattle, Washington, November 2-5, 2003, http://gsa.confex.com/gsa/2003AM/finalprogram/abstract_65497.htm.m*

Harlow, G.E., Quinn, E.P., Rossman, G.R., and Rohtert, W.R., 2004. Gem News International: Blue omphacite from Guatemala. *Gems & Gemology*, **40**(1), 68-70

Hawthorne, F.C., Welch, M.D., Della Ventura, G., Liu, S., Robert, J-L., and Jenkins, D.M., 2000. Short-range order in synthetic aluminous tremolites: an infrared and triple-quantum MAS NMR study. *American Mineralogist*, **85**(11/12), 1716-24

Htein, W., and Naing, A.M., 1995. Studies on kosmochlor, jadeite and associated minerals in jade of Myanmar. *Journal of Gemmology*, **24**(5), 315-20

Hughes, R.W., Galibert, O., Bosshart, G., Ward, F., Thet Oo, Smith, M., Tay Thye Sun and Harlow, G.E., 2000. Burmese jade: the inscrutable gem. *Gems & Gemology*, **36**(1), 2-26

Ingrin, J., Latrous, K., Doukhan, J-C., and Doukhan, N., 1989. Water in diopside: an electron microscopy and infrared spectroscopy study. *European Journal of Mineralogy*, **1**(3), 327-41

Ishida, K., Hawthorne, F.C., and Ando, Y., 2002. Fine structure of infrared OH-stretching bands in natural and heat-treated amphiboles of the tremolite-ferro-actinolite series. *American Mineralogist*, **87**(7), 891-8

Jenkins, D.M., Bozhlov, K.N., and Ishida, K., 2003. Infrared and TEM characterization of amphiboles synthesized near the tremolite-pargasite join in the ternary system tremolite-pargasite-cummingtonite. *American Mineralogist*, **88**(7), 1104-14

Katayama, I., and Nakashima, S., 2003. Hydroxyl in clinopyroxene from the deep subducted crust: evidence for H_2O transport into the mantle. *American Mineralogist*, **88**(1), 229-34

Khomenko, V.M., and Platonov, A.N., 1985. Electronic absorption spectra of Cr^{3+} ions in natural clinopyroxenes. *Physics and Chemistry of Minerals*, **11**, 261-5

Koch-Müller, M., Matsyuk, S.S., and Wirth, R., 2004. Hydroxyl in omphacites and omphacitic clinopyroxenes of upper mantle to lower crustal origin beneath Siberian platform. *American Mineralogist*, **89**(7), 921-31

Larson, A.C., and Von Dreele, R.B., 2000. General structure analysis system (GSAS). *Los Alamos National Laboratory Report LAUR 86-748*

Morimoto, N., 1988. Nomenclature of pyroxenes. *Bullettin Mineralogique*, **11**, 535-50

Ogniben, G., 1968. Il pirosseno onfacitico di Cesnola-Tavagnasco (Piemonte). *Periodico di Mineralogia*, **37**(I), 1-12 (in Italian)

Ou Yang, C.M., and Li Hansheng, 1999. Review of recent studies on black jadeite jade. *Journal of Gemmology*, **26**(7), 417-24

Ou Yang, C.M., and Qi Li Jian, 2001. Hte long sein - a new variety of chrome jadeite jade. *Journal of Gemmology*, **27**(6), 321-7

Ou Yang, C.M., Qi Li Jian, Li Hansheng, and Kwok, B., 2003. Recent studies on inky black omphacite jade, a new variety of pyroxene jade. *Journal of Gemmology*, **28**(6), 337-44

Quek, P.L., and Tan, T.L., 1997. Identification of B jade by diffuse reflectance infrared Fourier transform (DRIFT) spectroscopy. *Journal of Gemmology*, **25**(6), 417-27

Quek, P.L., and Tan, T.L., 1998. Identification of polystyrene in impregnated jadeite. *Journal of Gemmology*, **26**(3), 168-73

Rossi, G., Smith, D.C., Ungaretti, L., and Domeneghetti, M.C., 1983. Crystal-chemistry and cation ordering in the system diopside-jadeite: a detailed study by crystal structure refinement. *Contributions to Mineralogy and Petrology*, **83**, 247-58

Rossman, G.R., 1974. Lavender jade. The optical spectrum of Fe^{3+} and $Fe^{2+} \rightarrow Fe^{3+}$ intervalence charge transfer in jadeite from Burma. *American Mineralogist*, **59**(7/8), 868-70

Rossman, G.R., 1980. Pyroxene spectroscopy. *Pyroxenes, Reviews in Mineralogy*, **7**, Mineralogical Society of America, Washington DC, 93-115

Rossman, G.R., 1988. Optical spectroscopy. In Hawthorne, F.C. (Ed.), *Spectroscopic Methods in Mineralogy and Geology, Reviews in Mineralogy*, 18, Mineralogical Society of America, Washington DC, 207-54

Skogby, H., Bell, D.R., and Rossman, G.R., 1990. Hydroxide in pyroxene: variations in the natural environment. *American Mineralogist*, **75**(7/8), 764-74

Tan, T.L., Tay, T.S., Loh, F.C., Tan, K.L., and Tang, S.M., 1995. Identification of bleached wax and polyner-impregnated jadeite by X-ray photoelectron spectroscopy. *Journal of Gemmology*, **24**(7), 475-83

Tarashchan A.N., 1978. *Lüminescentija Mineralov*, Naukova Dumka Publishing House, Kiev, 66-75 (in Russian)

Veblen, D.R., and Buseck, P.R., 1981. Hydrous pyriboles and sheet silicates in pyroxenes and uralites: intergrowth microstructures and reaction mechanisms. *American Mineralogist*, **66**(11/12), 1107-34

Walker, G., 1985. Mineralogical applications of luminescence techniques. In Berry, F.J., and Vaughan, D.J. (Eds), *Chemical bonding and spectroscopy in mineral chemistry*. Chapman and Hall, London, 103

Zharikov, E.V., and Smirnov, V.A., 1997. Luminescent dopants. *Wide-gap luminescent materials: Theory and Applications*, Kluwer Academic Publishers, Boston/Dordrecht

Dyed polymer-impregnated jadeite jade: identification by light-induced autofluorescence spectroscopy

T. L. Tan, P. L. Chong and K.Y. Seah

Natural Sciences and Science Education, National Institute of Education, Nanyang Technological University, 1, Nanyang Walk, Singapore 637616, Singapore

Abstract: *Dyed polymer-impregnated jadeite jade is collectively known as grade B+C jade, while grade A jadeite jade is natural and untreated. In this work, autofluorescence spectra in the visible light range from 400 to 700 nm have been measured for six samples of grade A jade and six samples of grade B+C jades, and strong autofluorescence in the green-blue region (450-550 nm with maxima near 505-520 nm) was observed in the spectra of all samples of grade B+C jade. In contrast, weak autofluorescence was found throughout the whole visible region for all grade A jade samples and the method is thus effective in differentiating grade B+C jade from grade A jade. The strong green-blue autofluorescence in grade B+C jades can be explained by the presence of dyes and polymers used to treat them. Infrared spectra of all jade samples were recorded to confirm the grades and the presence of polymers in grade B+C jades. Autofluorescence spectroscopy has been found useful for identifying dyed polymer-impregnated jade particularly where it is thick or completely enclosed in jewellery mounts.*

Keywords: *autofluorescence spectroscopy, jade grades B and C, jadeite jade, treated jade*

Introduction

Nephrite jade has been prized in China for thousands of years, yet some of the finest jade is jadeite which has been a part of the Chinese culture only since the late eighteenth century, when the mines in what is today north-central Myanmar were opened (Schumann, 1997). The most desirable jadeite is natural, untreated and of fine colour, but of course, supply is limited, and many jadeite jades in the market today, especially since the 1980s have been treated to improve their aesthetic attraction, hence the importance of grading (Fritsch *et al.*, 1992; Hurwit, 1989). Jadeite jades (basically $NaAlSi_2O_6$) are generally classified according to their treatment process under three broad grades, A, B and C. The grading scheme we refer to in this paper with categories A, B and C,

relates to the treatment of a jade item and not to how beautiful or ugly an item may be. Grade A jadeite jade is natural and untreated. Its surface is usually waxed with beeswax to improve lustre after polishing (Quek and Tan, 1997). Grade B jadeite jade is bleached, and polymer-impregnated jade (Fritsch *et al.*, 1992; Fritsch, 1994). The polymer resin not only covers the open fractures but also significantly improves its transparency and colour by covering the jadeite with a hard and clear plastic-like coating. Grade B+C jadeite jade is subjected to a combination of treatment such as bleaching, dyeing and staining, and polymer-impregnation (Liddicoat, 1971; Wu, 2001). Webster (1994, pp 685-6) mentioned that greyish-white jadeite can be stained to an 'imperial jade' colour by the use of a combination of organic yellow and blue dyes. Also, white jadeite is stained to a strong mauve colour which is deeper in hue than any natural mauve or 'lavender' jadeite.

Fritsch and McClure (1993) mentioned that more sensitive detection methods are critical for differentiating between the different grades of jadeites as the skill of doctoring of jadeite by impregnation of polymers improves. This distinction of jade grades has become an intense area of interest for both gemstone dealers and gemmologists. Since natural jadeite jade (grade A) has been difficult to locate in the market, gemmologists have used sophisticated methods of studying these jades to determine what type of treatment it may have undergone. Polymer-impregnation and use of dyes in jades will no doubt cause a definitive change in some physical and chemical properties although some basic tests are unreliable, such as refractive index measurement, visible absorption spectrum using the hand-held spectroscope, and ultraviolet luminescence (Fritsch *et al.* 1992), or even, inconclusive, like specific gravity (Quek and Tan, 1997). Infrared spectroscopy was successfully used to distinguish grade B from grade A jade (Fritsch *et al.*, 1992). Other sophisticated techniques in identifying grade B jades such as X-ray photoelectron

spectroscopy (Tan *et al.*, 1995; Quek and Tan, 1998); infrared fibre-optic probe (Gao and Zhang, 1998); and diffuse reflectance infrared Fourier transform (DRIFT) spectroscopy (Quek and Tan, 1997) have also been reported.

In this work, light-induced autofluorescence spectroscopy is used for the first time to obtain conclusive evidence of dye and polymer impregnation in grade B+C jadeite jade and thereby provide a useful means of distinguishing it from grade A jade. However, this technique cannot at present be used to detect dyed jadeite. The autofluorescence technique is already well established in studies on biological tissues (Chang *et al.*, 2002), and dental research (Amaechi and Higham, 2002; Pretty *et al.*, 2004). Furthermore, luminescence or fluorescence spectroscopy (Rendell, 1987), as it is generally known, has been used to study minerals and materials (Gaft *et al.*, 2005), paintings (Wainwright, 1989), and gemstones (Hoover and Theisen, 1993; Harding, 1994; Moroz *et al.*, 1998).

Materials and experimental methods

Six samples of natural untreated jadeite jade (grade A jade) are shown in *Figure 1*. They are light to dark green with white patches and contain fine fissures on their polished surfaces. Six samples of polished dyed polymer-impregnated jadeite jade (grade B+C jade) are shown in *Figure 2*; these are light to dark green. Four of the samples are carved into symbolic animals, while two are parts of different bangles. All twelve samples originated from Myanmar (formerly Burma). The samples were thoroughly rinsed in propanol immediately before all measurements and blow-dried to remove any organic contaminant on their surfaces due to handling.

Refractive index values were obtained for all samples using the spot method on a gemmological refractometer. The samples have a surface polish which is good enough

Figure 1: Six natural untreated jadeite jades, grade A, used in this study. The dimensions of the cabochon are about 2 cm × 1.5 cm.

Figure 2: Six treated jadeite jades, grades B+C, used in this study. The dimensions of the jade at the centre of the bottom row are 4.5 cm × 1 cm.

for reliable measurements. Specific gravity measurements were made using the hydrostatic weighing method (Klein, 2002, pp 33-5). An electronic balance with sensitivity of 0.01 g was used to determine the weights of the samples.

In the transmission Fourier transform infrared (FTIR) spectroscopic work, a Perkin-Elmer Spectrum One spectrometer with a resolution of 2 cm^{-1} in the useful wavenumber range of 2000 to 4000 cm^{-1}, was used to record the spectra of all samples. The infrared measurements are non-destructive. Taking into account the spectrometric resolution of 2 cm^{-1}, and other possible errors in the experiments, the position (in cm^{-1}) of an absorption peak is accurate to ± 3 cm^{-1}.

All the jade samples were further tested using the light-induced autofluorescence spectroscopic technique with the Shimadzu RF-5301PC spectrofluorophotometer. A typical schematic diagram of the configuration of the spectrofluorophotometer

is shown in *Figure 3*. This instrument is used to irradiate a sample with excitation light and measure the fluorescence emitted from the irradiated sample for qualitative or quantitative analysis. The excitation of a molecule due to absorption of light energy to a high-energy state and the subsequent fall to a lower energy level results in emission of (fluorescent) light that has a wavelength longer than that of the incident light (Rendell, 1987; Schulman,1985). The excitation light wavelength of 405 nm was selected using an excitation monochromator placed next to the 150W xenon discharge lamp. This excitation wavelength has been used in studies on organic substances (Guilbault, 1990) and stimulates fluorescence in the visible region of 405-700 nm. The emission monochromator selectively receives fluorescence emitted from the sample and its photomultiplier tube measures the intensity of the fluorescence. The term autofluorescence describes materials which fluoresce by themselves

Figure 3: Schematic diagram of the light-induced autofluorescence spectrofluorophotometer system.

Light Source (Xenon arc lamp 150W) → Excitation Monochromator → Sample → Emission Monochromator → Detector (Photomultiplier tube) → PC & Printer
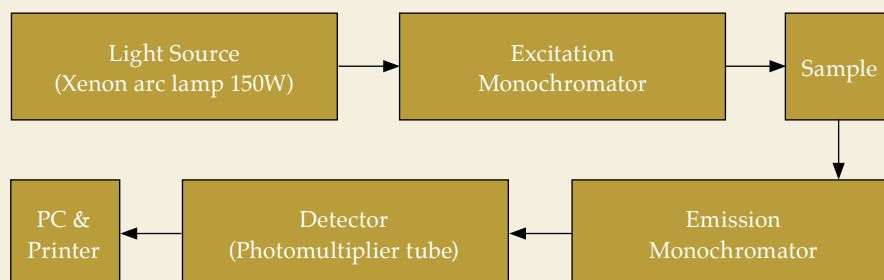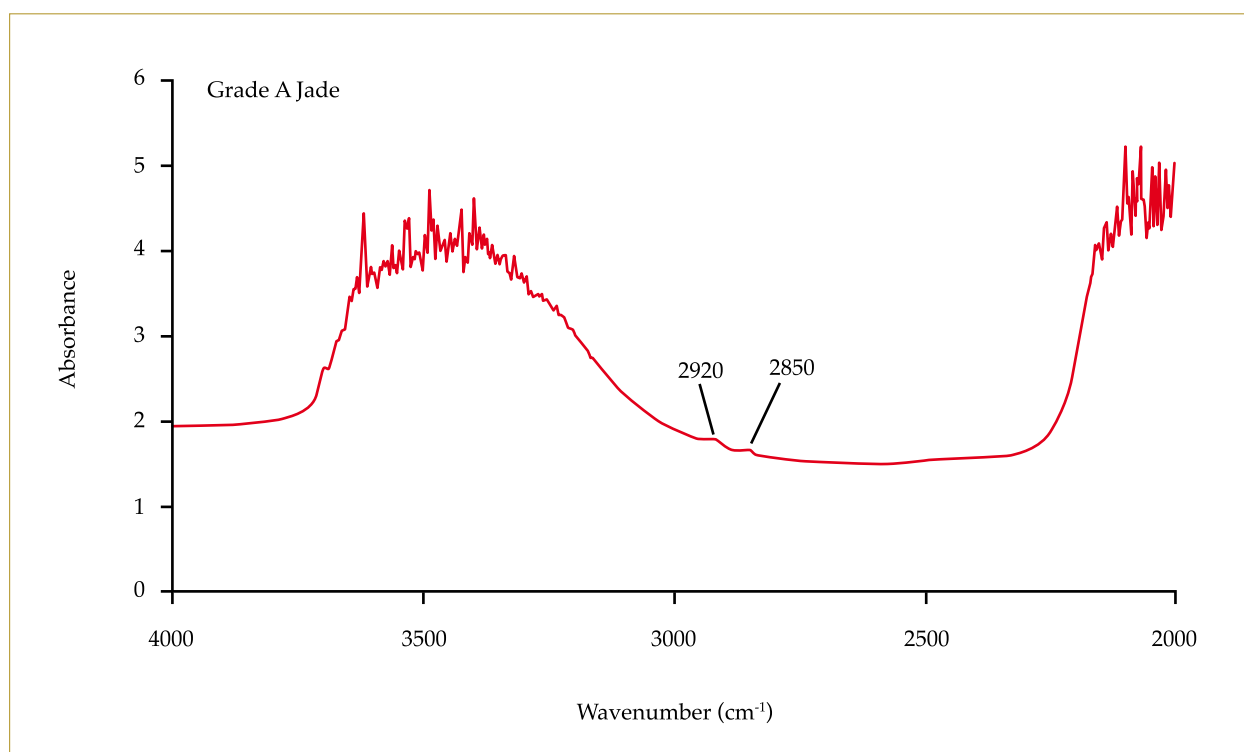
Figure 4: *Typical Fourier transform infrared (FTIR) absorption spectrum of grade A jadeite jades. The infrared peaks due to wax on the jade samples are at 2850 cm^{-1} and 2920 cm^{-1}.*

without the introduction of fluorescent reagents. Autofluorescence spectra of intensity versus wavelength in the 400-700 nm region were measured in all 12 jade samples.

Results and discussion

The refractive index measurements for all six grade A jades gave a mean of 1.66 ± 0.01, while for all six grade B+C jades, a mean of 1.65 ± 0.01 was obtained. Within experimental error, there is no significant difference between these refractive index measurements. These measurements agree with the typical value of 1.65-1.66 for jadeite jade (Fritsch *et al.*, 1992), and the value of 1.652-1.688 given in Schumann (1997).

Specific gravity (SG) measurements of grade A jades were found to be in the range of 3.30 to 3.36, giving a mean of 3.32 ± 0.02. Measurements of grade B+C jades lay in a wider range of 3.09 to 3.26, with a mean of 3.18 ± 0.08. These measurements agree well with 3.04 to 3.27 for grade B jades, measured by Fritsch *et al.* (1992). Although it may appear from the present measurements that SG can be used to differentiate grade

A from grade B+C jade, Fritsch *et al.* (1992) reported that some bleached and polymer-impregnated jades sank in 3.32 SG liquid, their behaviour depending on the type of polymers used in impregnation.

In the Fourier transform infrared (FTIR) transmission studies, the jade samples were virtually opaque to infrared radiation in the 400-2000 cm^{-1} region, and therefore the useful region of study was restricted to 2000-4000 cm^{-1}. *Figure 4* shows the typical spectrum of grade A jades. Weak infrared absorption peaks at 2850 cm^{-1} and 2920 cm^{-1} indicate the presence of small quantities of wax used in buffing the jade surface and not in impregnation (Fritsch *et al.*, 1992; Quek and Tan, 1997, 1998). For grade B+C jades, strong infrared absorption was typically found in the 2880-3060 cm^{-1} region, as shown in *Figure 5*. The strong peaks at 2880, 2930, 2970, 3040 and 3060 cm^{-1} indicate a high concentration of C-H bonds, found in organic materials including polymers. Polymers such as epoxy resin and polystyrene have been commonly used for impregnation (Fritsch *et al.*, 1992; Quek and Tan, 1998), and strong infrared absorption of similar pattern has been found in this region. The infrared absorption in the 2880-3060 cm^{-1}
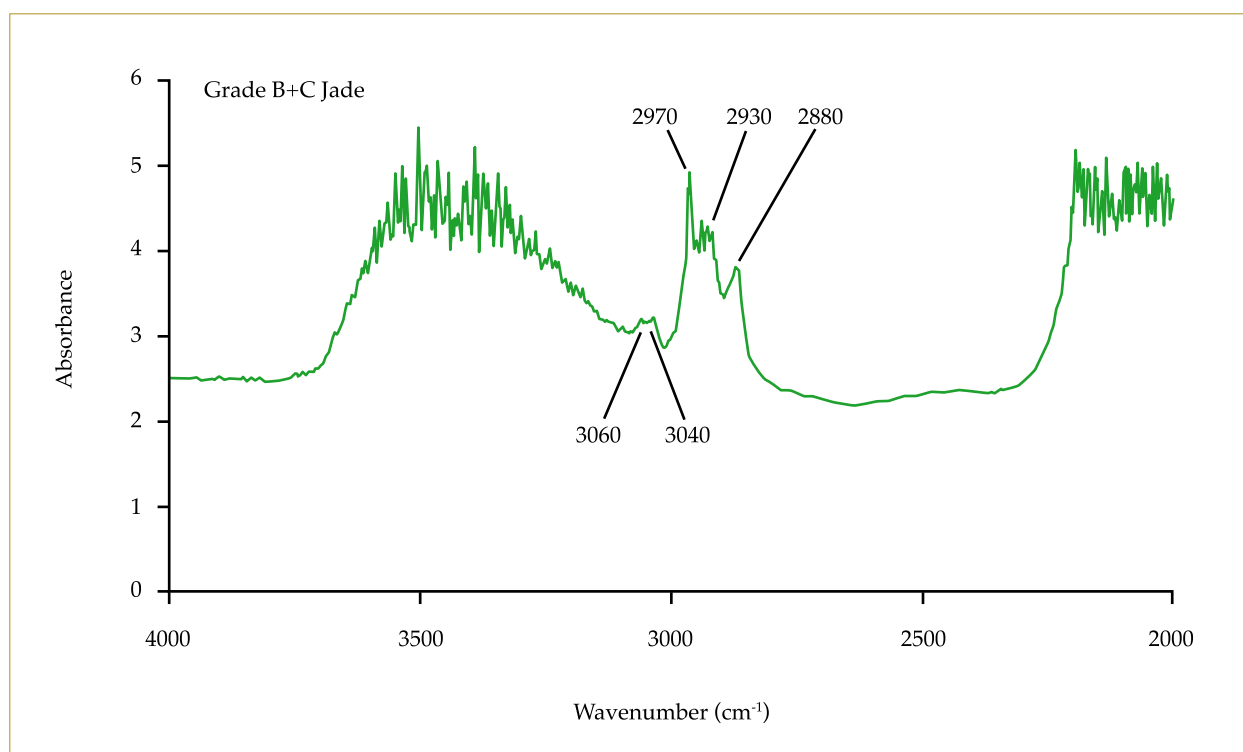
Figure 5: Typical Fourier transform infrared (FTIR) absorption spectrum of grade B+C jadeite jades. The infrared peaks due to an organic substance in the jade samples are at 2880 cm^{-1}, 2930 cm^{-1}, 2970 cm^{-1}, 3040 cm^{-1}, and 3060 cm^{-1}.

region can also be the result of the presence of organic substances used in dyes in grade B+C jades. Organic dyes used in staining jades have been reported, and one example concerned two organic dyes, one yellow and the other blue, which were combined to turn a greyish-white jadeite into an 'imperial jade' colour (Webster, 1994). Dyed and/or polymer-impregnated jades have been in the jade market for quite some time (Liddicoat, 1971; Fritsch *et al*., 1992; Schumann, 1997; Wu, 2001).

The two typical autofluorescence spectra of grade A and grade B+C jades in the 400-700 nm wavelength region are shown *Figures 6* and *7*. The spectra effectively cover the whole visible light region. All six grade A jade samples show weak fluorescence of relatively uniform intensity up to five arbitrary units in the 400-600 nm region, which decreases to zero at 650 nm. This means that there is minimum fluorescence in the yellow–orange-red region. As a whole, this would result in a relatively blue fluorescence. The broad gradual peaks found in the 450-500 nm region may further add to the overall weak blue fluorescence in grade A jade. However, Schumann (1997) reported that in pale green natural jadeites, very weak fluorescence of 'whitish glimmer' was observed. The weak blue

fluorescence observed in grade A jades could be due to the presence of wax in small quantity, as organic substances such as wax and polymers tend to fluoresce in the blue region (Fritsch *et al*., 1992). The weak fluorescence could also be caused by trace transition metals (iron and chromium) present in jades (Nassau, 2001).

From the autofluorescence spectra typical of all six grade B+C jades shown in *Figures 6* and *7*, it can be observed that strong fluorescence of about 40 to 55 arbitrary units, occurred in the 450-550 nm wavelength region when excited by violet-ultraviolet light of 405 nm. This is a factor of about ten times more than that of grade A jades in the same region. With strong fluorescent peaks occurring in the range of 505 nm to 520 nm, and near zero fluorescence in the 600-700 nm region, the dominant colour in grade B+C jades is green-blue. The strong fluorescence in the 450-550 nm region could be explained by the presence of organic compounds found in organic dyes and polymers used in the treatment of grade B+C jades. Organic compounds such as those used in polymer-impregnation of jadeites were found to have bluish white to yellowish green, or chalky blue fluorescence (which covers the 400-600 nm region) when subjected to long-wave ultraviolet radiation (Fritsch *et al*., 1992; Quek and Tan,
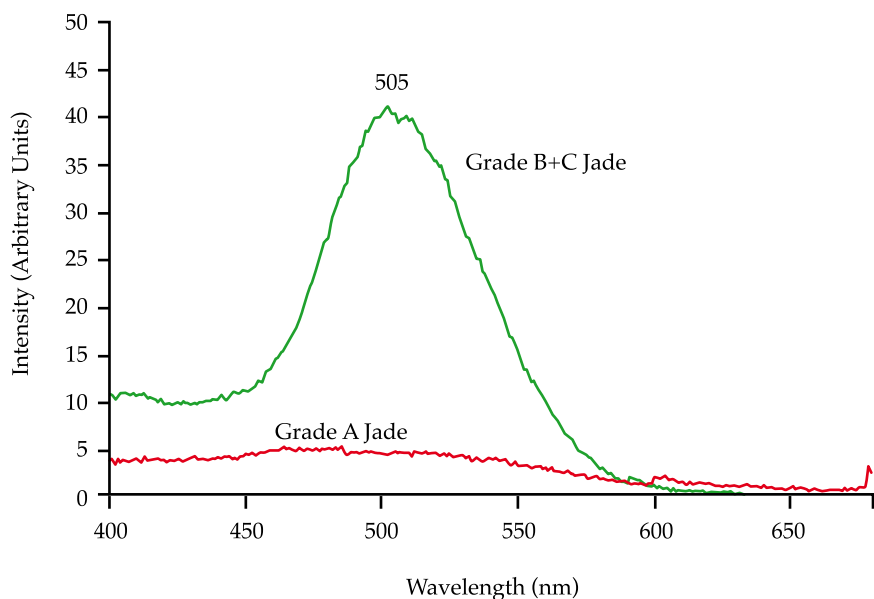
Figure 6: Typical light-induced autofluorescence spectra of grade A and grade B+C jadeite jades. The spectral peak for grade B+C jadeite jades is at 505 nm.
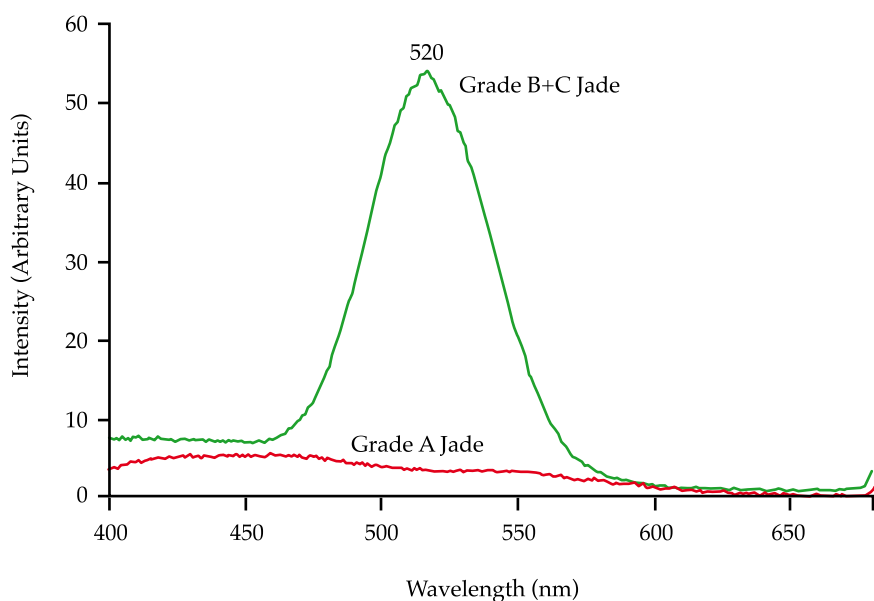
Figure 7: Typical light-induced autofluorescence spectra of grade A jade (no obvious peak) and grade B+C jade (peak at 520 nm).

1997, 1998). Strong green-blue fluorescence in the 450-600 nm region was typically observed in limestone samples containing bitumen, by Wang *et al*. (1997), who found that bitumen was the cause of this fluorescence. Organic dyes such as the 'coumarin dye' were excited to fluoresce in the 500-580 nm region by violet light and ultraviolet

radiation, as reported in Nassau (2001). An extensive list of types of organic dyes and their fluorescence bands are provided in Guilbault (1990). All the organic dyes were found to fluoresce strongly in the 450-650 nm region. Results from this autofluorescence spectroscopic work show that the strong fluorescence in the 450-550 nm region in all grade B+C jade samples caused by organic dyes and polymers in them can be used to differentiate them from grade A jades. However, this method cannot at present be used to detect grade C jade (dyed jade).

Conclusion

Dyed polymer-impregnated jadeite jade known in the gem trade as grade B+C jade cannot be differentiated from the natural untreated (grade A) jadeite jade using refractive index measurements. Specific gravity measurements do show that our samples of grade B+C jades have slightly lower values than those of grade A jades. However, the specific gravity readings are not significantly different and are highly dependent on the concentration and type of materials used to treat these jades. So such differences are not a reliable guide to identity. In this work, light-induced autofluorescence spectroscopy has been found to be effective in differentiating grade B+C jade from grade A jade. Strong autofluorescence in the green-blue (450-550 nm) region was observed in the spectra of all samples of grade B+C jade. In contrast, weak autofluorescence of about 10 times less that of grade B+C jade, was found throughout the whole visible region for all grade A jade samples. The strong green-blue autofluorescence in grade B+C jades is attributed to the presence of organic dyes and polymers used in their treatment. Fourier

transform infrared (FTIR) spectra of all jade samples were recorded to confirm the presence of organic substances in grade B+C jades. The use of autofluorescence spectroscopy which is a non-destructive surface technique, for identifying dyed polymer-impregnated jadeite jade from natural jadeite jade is found to be effective and accurate. It is particularly useful for thick jade samples on which transmission infrared measurements are impossible, and for jade close-mounted in jewellery.

References

Amaechi, B.T., and Higham, S.M., 2002. Quantitative light-induced fluorescence: a potential tool for general dental assessment. *J. Biomed. Opt.,* **7**, 7-13

Chang, H.P., Qu, J.Y., Yuen, P.W., Sham, J., Kwang, D., and Wei, W.I., 2002. Light-induced autofluorescence spectroscopy for detection of nasopharyngeal carcinoma in vivo. *Applied Spectroscopy,* **56**, 188-93

Fritsch, E., 1994. Type-B jadeite: new polymers and estimating the amount of wax. *Jewellery News Asia,* **123**, 106-10

Fritsch, E., and McClure, S.F., 1993. Polymer impregnated jadeite. ICA Laboratory Alert, **75**

Fritsch, E., Wu, S.T.T., Moses, T., McClure, S.F., and Moon, M., 1992. Identification of bleached and polymer-impregnated jadeite. *Gems & Gemology,* **28**, 176-87

Gaft, M., Reisfeld, R., and Panczer, G., 2005. *Modern Luminescence Spectroscopy of Minerals and Materials.* Springer Publishing, New York, USA

Gao, Y., and Zhang, B.L., 1998. Identification of B jade by FTIR spectrometer with near-IR fibre-optic probe accessory. *Journal of Gemmology,* **26**(5), 302-7

Guilbault, G.G., 1990. Assay of Organic Compounds. In: *Practical Fluorescence*, edited by G.G. Guibault. Marcel Dekker, New York, USA, 249-53

Harding, R.R., 1994. Luminescence. In: *Gems*, by R. Webster, edited by P.G. Read. Butterworth-Heinemann, Oxford, U.K., 837-53

Hoover, D.B., and Theisen, A.F.,1993. Fluorescence excitation-emission spectra of chromium-bearing gems: an explanation for the effectiveness of the crossed filter method. *Australian Gemmologist,* **18**, 182-7

Hurwit, K., 1989. Gem trade lab notes: Impregnated jadeite jade. *Gems & Gemology,* **25**, 239-40

Klein, C., 2002. *Mineral Science.* John Wiley & Sons, New York, USA, 646 pp

Liddicoat, R.T., 1971. Dyed light-violet jade. *Gems & Gemology,* **13**, 323-4

Moroz, I., Panczer, G., and Roth, M., 1998. Laser-induced luminescence of emeralds from different sources. *Journal of Gemmology,* **26**(5), 316-20

Nassau, K., 2001. *The physics and chemistry of color – the fifteen causes of color. 2nd edn.* John Wiley & sons, New York, USA, 290-5, 364-6

Pretty, A.I., Edgar, W.M., and Higham, S.M., 2004. The validation of quantitative light-induced fluorescence to quantify acid erosion of human enamel. *Arch. Oral Biol.* **49**, 285-94

Quek, P.L., and Tan, T.L., 1997. Identification of B jade by diffuse reflectance infrared Fourier transform (DRIFT) spectroscopy. *Journal of Gemmology,* **25**(6), 417-27

Quek, P.L., and Tan, T.L., 1998. Identification of polystyrene in impregnated jadeite. *Journal of Gemmology,* **26**(3), 168-73

Rendell, D., 1987. *Fluorescence and Phosphorescence.* John Wiley Publishing, New York, USA, 419 pp

Schulman, S.G., 1985. *Molecular Luminescence Spectroscopy, Methods and Applications.* John Wiley Publishing, New York, U.S.A, 526 pp

Schumann, W., 1997. *Gemstones of the world*. Sterling Publishing, New York, USA, 154-7

Tan, T.L., Tay, T.S., Loh, F.C., Tan, K.L., and Tang, S.M., 1995. Identification of wax- and polymer-impregnated jadeite by x-ray photoelectron spectroscopy. *Journal of Gemmology,* **24**(7), 475-83

Wainwright, I.N.M., 1989, Examination of paintings by physical and chemical methods. *Proceedings of a seminar for curators and conservators*. National Gallery of Canada, Ottawa, Canada, 79-102

Wang, J., Wu, X., and Mullins, O.C., 1997. Fluorescence of Limestones and Limestone Components. *Applied Spectroscopy,* **51**, 1890-5

Webster, R., 1994. *Gems: their sources, descriptions , and identification. (5th edn.)* Edited by P.G. Read. Butterworth-Heinemann, Oxford, 1026 pp

Wu, R., 2001. A new jadeite imitation B+C quartzite. *Jewelry Circles,* **59**, 53

Abstracts

Diamonds

A gemological study of a collection of chameleon diamonds.

T. Hainschwang, D. Simic, E. Fritsch, B. Deljanin, S. Woodring and N. DelRe. *American Journal of Science*, **41**(1), 2005, 20-35.

A report is given of a unique collection of 39 cut chameleon diamonds, ranging from 0.9 to 1.93 ct, which exhibited temporary changes in colour when heated to ~ 150°C, and, for some, after prolonged storage in the dark (i.e. thermochromic and photochromic colour changes, respectively). Most changed from olive green to brownish yellow or yellow, but some changed from light yellow to a more intense greenish yellow; the first group are typical of the 'Classic' chameleons, whereas the purely thermochromic change shown by the second group was the 'Reverse'. These two groups showed different spectroscopic and UV fluorescence characteristics, but all show strong long-lasting phosphorescence after short-wave UV excitation. Using this combination of reaction to UV radiation and spectroscopic properties, a gemmologist can separate chameleon from other green diamonds without recourse to heat.   R.A.H.

Lab Notes.

T.H. Moses and S.F. McClure (Eds). *Gems & Gemology,* **42**(2), 2006, 160-8.

Items noted include extensive circular brown or green radiation stains on two cut diamonds, an intense pink colour of three diamonds as a result of a surface coating and a 1.03 ct cut diamond containing several blue inclusions that proved to be sapphire.   R.A.H.

The Cullinan diamond centennial: a history and gemological analysis of Cullinans I and II.

K. Scarratt (ken.scarratt@gia.edu) and R. Shor. *Gems & Gemology,* **42**(2), 2006, 120-32.

The year 2005 marked the centenary of the discovery of the largest gem diamond ever found: the 3106 ct Cullinan. Eight decades after it was mined, at the Premier mine (renamed the Cullinan mine for its centenary in 2003), 25 km east of Pretoria, South Africa, a team of British gemmologists conducted the first modern examination of the two largest diamonds cut from the rough, the 530 ct Cullinan I and the 317 ct Cullinan II, which have been part of the British Crown Jewels since their presentation to King Edward VII in 1908. This article traces the history of this diamond and presents the full details of the examination and grading of these two approximately D-colour, potentially flawless, historic diamonds. This examination took place in the vault below the Waterloo Barracks in the Tower of London. Photographs are presented of both stones dismounted from their settings, and details not given in the earlier two-volume set *The Crown Jewels: the History of the Coronation Regalia in the Jewel House of the Tower of London* [M.A. 99M/1248] include the UV spectra confirming that these stones are type II diamonds, and their colour grading.   R.A.H.

High-pressure-high-temperature treatment of gem diamonds.

J.E. Shigley (jshigley@gia.edu). *Elements**, **1**(2), 2005, 101-4.

The annealing of gem-quality diamonds at very high pressures (> 5 GPa) and temperatures (> ~ 1800°C) can produce significant changes in their colour. Treatment under these high pressure high temperature (HPHT) conditions affects certain optically active defects and their absorptions in the visible spectrum. In the jewellery industry, laboratory-treated diamonds are valued much less than those of natural colour. Polished diamonds are carefully examined at gemmological laboratories to determine the 'origin of the colour' as part of an overall assessment of their quality. Currently, the recognition of HPHT-treated diamonds involves the determination of various visual properties (such as colour and features seen under magnification), as well as characterization by several spectroscopic techniques. HPHT-treated diamonds were introduced into the jewellery trade in the late 1990s, and despite progress in their recognition, their identification remains a challenge. While some detection methodologies have been established, the large number of diamonds requiring testing with sophisticated scientific instruments poses a logistical problem for gemmological laboratories.   R.A.H.

* Elements *is a new magazine published jointly by the Mineralogical Society of Great Britain and Ireland, the Mineralogical Association of Canada, the Geochemical Society, the Clay Minerals Society, the European Association for Geochemistry, the International Association of GeoChemistry, the Mineralogical Society of America, the Société Française de Mineralogie et de Cristallographie, the European Mineralogical Union and the International Mineralogical Association, and is provided as a benefit to members of these societies. Ed.*

Synchrotron micro-X-ray fluorescence analysis of natural diamonds: first steps identification of mineral inclusions *in-situ*.

H. Sitepu, M.G. Kopylova (mkopylov@eos.ubc.ca), D.H. Quirt, J.N. Cutler and T.G. Kotzer. *American Mineralogist*, **90** (11-12), 2005, 1740-7.

Synchrotron micro-X-ray fluorescence analytical data yielded the first high-resolution maps of Ti, Cr, Fe, Ni, Cu and Zn for natural diamond grains, along with quantitative μSXRF analyses of select chemical elements in exposed kimberlite indicator mineral

grains. The distinction of diamond inclusions inside the natural diamond host, both visible and invisible using optical transmitted-light microscopy, can be mapped using synchrotron μXRF analysis. Overall, the relative abundances of chemical elements determined by μSXRF elemental analyses are broadly similar to their expected ratios in the mineral and therefore can be used to identify inclusions in diamonds *in-situ*. Accurate estimates are given by synchrotron μXRF analysis of Cr of exposed polished minerals when calibrated using the concentration of Fe as a standard; corresponding Cr *K*-edge μXANES analyses on selected inclusions yield unique information about the formal oxidation state and local coordination of Cr.   R.A.H.

Diamond cut grading: unintended consequences and solutions.

S. Sivovolenko, G. Holloway, Y. Shelementiev and J. Mistry. *Australian Gemmologist,* **22**(10), 2006, 447-54, 12 figs.

The threats to creative and innovative diamond cutting by diamond grading labs who now grade the cut quality of stones are explored.
                                    L.J.

Gems and Minerals

"Paraíba"-type copper-bearing tourmaline from Brazil, Nigeria and Mozambique: chemical fingerprinting by LA-ICP-MS.

A. Abduriyim (ahmadjan@gaaj.zenhokyo.co.jp), H. Kitawaki, M. Furuya and D. Schwartz. *Gems & Gemology,* **42**(1), 2006, 4-21.

Gem-quality bright blue to green 'Paraíba'-type Cu-bearing tourmaline is now known from deposits in Nigeria and Mozambique, in addition to three commercial localities in Brazil. The Nigerian and Mozambique tourmalines show saturated blue-to-green colours and cannot be distinguished from the Brazilian material by standard gemmological tests or on the basis of semi-quantitative chemical data obtained by EDXRF. However, quantitative chemical data from laser ablation-ICP-MS show that tourmalines from the three countries can be differentiated by plotting (Ga + Pb) vs. (Cu + Mn), the Pb/Be ratio vs. (Cu + Mn) and Mg-Zn-Pb. Analytical results are tabulated together with physical properties for six variously coloured samples from Brazil and for five each from Nigeria and Mozambique. In general, the Nigerian tourmalines contain greater amounts of Ga, Ge and Pb, whereas the Brazilian stones have more Mg, Zn and Sb. The new Cu-bearing tourmalines from Mozambique show enriched contents of Sc, Ga, Pb and Bi, but lacked Mg. All are elbaites.
                                    R.A.H.

Problems that may be encountered when identifying gemstones in antique jewellery: some practical tips.

R. Bauer. *Australian Gemmologist,* **22**(10), 2006, 455-59, 11 images.

The identification of various gemstone types used in antique jewellery are discussed. The use of the 10x lens is advocated, together with other simple techniques. Examples used include discriminating rose-cut diamonds from rose-cut zircons, synthetic doublets, imitation pearls, turquoise, coral, opal doublets, amber and diamonds with old style cuts.   L.J.

Pseudomorphesen und Polyederbildungen im Amethystgang von Wiesenbad, Sachsen.

W. Beck and T. Treffurth. *Lapis*, **31**(5), 2006, 22-3.

Pseudomorphism is discussed with special reference to amethyst from Wiesenbad, Saxony, Germany.   M.O'D.

Torrington and its gemstones.

H. Bracewell. *Australian Gemmologist,* **22**(11), 2006, 479-84, 1 map, 17 figs.

This paper describes the location and geology of Torrington, an old tin mining village in New South Wales. The geology comprises a granite plateau which is richly mineralized, including deposits of tin, tungsten, quartz, topaz and emerald. The history of the mining activity at Torrington from the late nineteenth century to the present day is described.   L.J.

Vulcanite or gutta-percha that is the question.

G. Brown. *Australian Gemmologist*, **22**(10), 2006, 460-5, 10 figs, 1 table.

A description of the physical and chemical properties of vulcanite and gutta-percha, both long chain polymers made from sap-like exudates or latex is given. A history of these two synthetic gem materials is detailed, and their use in jewellery from the mid century is discussed. The features used to discriminate between vulcanite and gutta-percha are specified, together with a recommended testing sequence.
                                    L.J.

The Devonshire mineral collection of Chatsworth House: an 18th century survivor and its restoration.

M.P. Cooper. *Mineralogical Record,* **36**(3), 2005, 239-72.

A fascinating account is given of the reassembly, restoration and recataloguing of this mineral collection assembled nearly 200 years ago. Details are included of the 'Duke's Emerald' from Muzo, Colombia; this weights 1383.95 ct, is a terminated prism 5 cm in diameter and was for long renowned as the largest and finest uncut emerald in existence. It is a superb deep green, but although it is perfectly transparent in places, it is heavily flawed in others. A colour photograph is presented.   R.A.H.

Occurrence of *in-situ* corundum in Kegalle District, Sri Lanka.

T.S. Dharmaratne, R. Chandrajith and S. Weerawarnakula. *Gemmologie. Z. Dt. Gemmol. Ges.,* **54**(1), 2005, 21-34. 3 maps, 8 photographs, 1 table, bibl. (English with German abstract.)

Recently discovered *in-situ* corundum occurrences in two

locations are described; they are known as Ballapana and Galapitamada in the Kegalle district, Sri Lanka. The *in-situ* corundum mineralization in the area occurs in structurally controlled biotite gneiss rocks. The corundum-bearing rocks of Ballapana are variably weathered and lateritized. The texture of the gneiss suggests a reaction between biotite and sillimanite that has produced corundum and K-feldspar. The corundum crystals from Galapitamada contain higher amounts of Fe_2O_3 compared to other locations.   E.S.

Geologie und Petrographie des Saphir- und Rubinvorkommens van Chimwadzulu Hill, (W-Malawi).

H.G. DILL. *Gemmologie. Z. Dt. Gemmol. Ges.*, **54**(1), 2005, 7-20. 1 map, 16 photographs, 1 table, bibl. (German with English abstract.)

Corundums are widely found in the Proterozoic belt extending over Eastern Africa from Kenya, to Tanzania and Malawi into Madagascar. The Chimwadzulu Hill deposit is in the Kirk range in Malawi and forms part of the corundum belt together with deposits near the north of Lake Malawi and in the Mwanza district in the south of the country. A great variety of gem and sub-gem corundum crystals is concentrated in an eluvial placer deposit and is intermittently mined in open cast operations on the Kirk plateau. Hydration and desilication of basic igneous rocks abundant in anorthite led to Al-enriched minerals like corundum and zoisite. Amphibolites enriched with zoisite and garnet are taken as an 'ore guide' to the primary corundum mineralization.   E.S.

Petrographische und gemmologische Untersuchungen der Chalcedon-Lagerstätte Finishi Village in den Stormberg-Vulkaniten (Malawi).

H.G. DILL AND U. HENN. *Gemmologie. Z. Dt. Gemmol. Ges.*, **55**(1/2), 2006, 25-38. 1 map, 25 photographs, 1 graph, bibl. (German with English abstract.)

In south west Malawi along the border with Mozambique, large areas are covered with layers of tholeiitic basalts intruded by doleritic dykes and sills. This igneous activity climaxes during the lower Jurassic and its igneous rocks were attributed to the Stormberg series. High contents of Fe and Cr in the basaltic magma led to the formation of spinels such as magnetite and chrome picotite. Later the igneous rocks were subjected to auto-hydrothermal alteration resulting in calcite and chalcedony filled amygdules in the basalt cavities along subhorizontal joints and druses in the breccia zones. The blue chalcedony from Malawi is found in either geodes or clefts and shows thinly layered interbedding of blue chalcedony and milky quartz in some cases with rock crystal and calcite. RI, birefringence and density are typical of chalcedony. The blue colour is caused by the Tyndall effect (selective reflection of the light by sub-microscopic particles and/or pores).   E.S.

Sérandit aus Aris, Namibia.

H.V. ELLINGSEN. *Mineralien Welt*, **17**(3), 2006, 51.

Sérandite is briefly reported from Aris, Namibia.   M.O'D.

Gold, opal und Wein-Mineraliensammeln im Zemplen- und Slanske-Gebirge in Ungarn und der Slowakei.

D. GROLIG. *Mineralien Welt*, **17**(3), 2006, 52-62.

General account, with maps, of gold and opal-bearing sites in Hungary and Slovakia.   M.O'D.

The characterisation of tortoise shell and its imitations.

T. HAINSCHWANG (thomas.hainschwang@gia.edu) and L. LEGGIO. *Gems & Gemology*, **42**(1), 2006, 36-52.

Tortoiseshell reached the height of its popularity as an ornamental gem material during the 18th, 19th and early 20th centuries, but the advent of plastic imitations and new laws protecting sea turtles have led to a drastic reduction in the amounts of tortoise shell in the market. Proper identification is important and this paper summarizes the gemmological properties of tortoiseshell and its imitations, including the results of several spectroscopic tests; transmission and specular reflectance infrared spectroscopy were found to be of particular value.   R.A.H.

Keshi Perlen – ein erklärungsbedürftiger Begriff.

H.A. HÄNNI. *Gemmologie. Z. Dt. Gemmol. Ges.*, **55**(1/2), 2006, 39-50. 8 photographs, 1 table, bibl. (German with English abstract.)

The original term 'Keshi pearls' describes tiny mantle pearls which have developed without tissue transplant during the production of Akoya cultured pearls. The term is now frequently used for gonad-grown cultured pearls which have formed from the mantle tissue grafts after a bead has been rejected. The correct term for these should be 'beadless cultured pearls'. Bead rejection may occur in gonad-grown as well as mantle-grown cultured pearls, in freshwater as well as seawater. Recent examination of Chinese freshwater cultured pearls with beads suggest that they have been formed in mantle pearl sacs which have previously produced beadless pearls. The non-beading or bead rejection of such mantle pearl sacs may lead to large flattened baroque beadless cultured pearls.   E.S.

Gemmologische Kurzinformationen. Skapolith-Katzenaugen aus Indien.

H. HENN. *Gemmologie. Z. Dt. Gemmol. Ges.*, **54(1)**, 2005, 55-8. 4 photographs, 1 table, bibl. (German with English abstract.)

Scapolite cat's-eyes from India show brownish-orange to yellow-brown to brown as well as grey colours. RI = 1.559-1.579, DR 0.020, density 2.74-2.75. The brownish-orange and yellow-brown hues are due to hematite inclusions. Browns and greys are caused by dark crystal inclusions, and the cat's-eye effect is caused by parallel oriented dark crystal needles.   E.S.

Gemmologische Kurzinformationen. Roter, klar durchsichtiger Andesin aus dem Kongo.

U. HENN. *Gemmologie. Z. Dt. Gemmol. Ges.*, **54**(1), 2005, 53-55. 4 photographs, 1 graph, bibl.

The red transparent andesine feldspar from the Congo showed RIs of 1.554-1.562, DR 0.008, SG 2.69. Tiny inclusions with metallic lustre and lamellar twinning were observed.   E.S.

Chatoyance und Asterismus bei Feldspat aus Tansania.

U. HENN, C.C. MILISENDA AND T. HÄGER. *Gemmologie. Z. Dt. Gemmol. Ges.*, **54**(1), 2005, 43-46. 5 photographs, 1 table, 1 graph, bibl. (German with English abstract.)

Yellow-brown aventurescent feldspar cat's-eyes and star feldspars from Tanzania were shown to be alkali feldpsars with distinct perthitic structure. Chatoyancy and asterism were caused by oriented needle-shaped hematite inclusions.   E.S.

U. HENN AND C.C. MILISENDA. *Gemmologie. Z. Dt. Gemmol. Ges.*, 54(4), 2005, 121-202.

This is an issue completely devoted to the treatment of gemstones. It is subdivided into treatment methods and resulting changes of their properties, with an introduction by Th. Lind on the nomenclature of and trade in treated gem material. Lind discusses the laws governing declaration of treatment, and the general rule to classify gems as natural, enhanced or treated.

Methoden der künstlichen Eigenschaftsveränderungen bei Edelsteinen, setting out methods of artificial alteration of the properties of gemstones, occupies pp. 127-34, with 4 photographs, 1 graph and a bibliography. Heat treatment can produce changes in the colour and colour intensity, improve transparency, but might result in fissures. Various types of heat treatment are discussed. The authors then describe diffusion treatment and irradiation, bleaching, impregnation with colourless organic substances and fracture filling with glass as well as dyeing. The surface of a stone can be covered by deposition of a thin film; foiling has been known for 2000 years, but engraved foils can also produce asterism or chatoyancy.

Edelsteine und ihre künstlichen Eigenschaftsveränderungen on pp 135-202, with 2 tables and 74 photographs, presents gems and the artificial alteration of their properties in alphabetical order. For each gem, there are descriptions of the treatments available, the results produced, possible identification accompanied by photographs and bibliography for the more important stones from agate to zoisite and 'Zugperle' (cultured pearl). It is a very comprehensive summary, as much as is possible within 70 pages.
                                                         E.S.

Steckbrief Spinel.

R. HOCHLEITNER AND S. WEISS. *Lapis*, **31**(11), 2006, 8-11.

Update of spinel finds with mineralogical data.   M.O'D.

Smaragde selbstgessamelt: die Fundstelle Minnesund in Norwegen.

P. IMFELD AND S. WEISS. *Lapis*, **31**(5), 2006, 32-5.

Emerald is described from Minnesund, Norway. The local geology and mineralization are noted. Some specimens were found during panning for gold.   M.O'D.

Herkunftsbestimmung von Süsswasserzuchtperlen mit Laser Ablations ICP-MS.

D.E. JACOB, U. WEHRMEISTER, T. HÄGER AND W. HOFMEISTER. *Gemmologie. Z. Dt. Gemmol. Ges.*, **55**(1/2), 2006, 51-8. 1 map, 9 photographs, 1 table, 1 graph, bibl. (German with English abstract.)

It has become increasingly difficult to differentiate between freshwater cultured pearls from Lake Kasimigaura in Japan and those coming from China. The authors present a new objective method to determine origin using trace elements in the composition of the pearls. Tiny holes (10 μm maximum) are drilled by laser close to the drill hole of the pearl. The method is practically non-intrusive and requires minimum sample preparation. The measured Ba/Sr ratios clearly distinguish Kasimigaura cultured pearls by their low values from the higher and more variable Ba/Sr values of the Chinese freshwater pearls.   E.S.

Neue 'Holzopale' vom Wintermühlenhof im Siebengebirge.

E. KLEIN, F. HÖHLE AND H. LORENZ. *Mineralien Welt*, **17**(4), 2006, 38-42.

Common opal known locally as 'wood opal' and occurring in white through yellow to brown is described from the Wintermühlenhof area of the Siebengebirge, Germany.   M.O'D.

Haüyn, Titanit und Apatit aus Niedermendig.

H.-J. KOLZEM. *Lapis*, **30**(3), 2005, 25-7.

Gem quality crystals of blue transparent hauyne, pink apatite and yellow-brown titanite are described from the Niedermendig area of the Eifel, Germany.   M.O'D.

Gem News International.

B.M. LAURS (ED.) (blaurs@gia.edu). *Gems & Gemology*, **42**(1), 2006, 62-80.

Items noted at the 2006 Tucson show include a 62.81 ct tsavorite from Tanzania, a fine-grained muscovite ~ 7 cm across (EPMA given) represented as rose quartz, a series of cut stones of greenish-yellow sillimanite from India and yellowish-brown cut titanites (up to 6.21 ct) from Pakistan. Mention is also made of a 2.2 ct step-cut vayrynenite from northern Pakistan and a convincing moonstone doublet consisting of a grey labradorite base with a glass top.   R.A.H.

Gem News International.

B.M. LAURS (ED.) (blaurs@gia.edu). *Gems & Gemology*, **42**(2), 2006, 169-88.

Mention is made of a 9.50 ct faceted euclase with an intense greenish-blue colour, a 10 ct faceted fluorite exhibiting a distinct colour change from blue in daylight or fluorescent light to purple in incandescent light, and jeremejevite from Sri Lanka and Myanmar. Details are given also of cabochons and faceted stones of yellowish green to yellow prehnite from the Northern Territory, Australia, and from Mali, and of a cabochon (14.97 ct) and faceted stone (3.70 ct) of triploidite from China (probably the tin-polymetallic sulphide deposits near Dachang, Guangxi).   R.A.H.

Die Achate aus dem Rhyolith vom Rehberg bei Sailauf im Spessart.

J. LORENZ. *Lapis*, **31**(6), 2006, 13-20.

Good-quality ornamental agates are described from rhyolites at Rehberg near Sailauf, Spessart, Germany, some specimens showing a green fluorescence. Associated minerals are noted. M.O'D.

Identification and durability of lead glass-filled rubies.

S.F. McCLURE, C.P. SMITH, W. WANG AND M. HALL. *Gems & Gemology,* **42**(1), 2006, 22-34.

Since 2004, large quantities of rubies which have had numerous fractures filled with high lead-content glass, making them appear very transparent, have been reaching international markets. This dramatic treatment is not difficult to identify with a standard gemmological microscope, since it shows flash effect, gas bubbles, etc. Locating filled cavities in reflected light, however, is more challenging, as the surface lustre of the filler is close to that of the ruby. The filling material appears to be very effective in reducing the appearance of fractures, and is fairly resistant to heat exposure during jewellery repair procedures, but does react readily with household solvents. R.A.H.

Elephant pearls true or false?

B. MANN. *Australian Gemmologist,* **22**(11), 2006, 503-7, 9 figures, 1 table.

Elephant pearls are spherical calcified concretions of dentine that come from the soft tissue of growing tusks of mammoths and modern elephants. Ten suspected elephant pearls were investigated and found to come from the molar teeth of Asiatic elephants that have been fashioned by man. The elephant pearls were tested by standard gemmological methods and X-radiography. Evidence of surface working was found on all the pearls, and six had been dyed (red, blue and purple). The history of elephant pearls is given. L.J.

Almandin und Andalusit von Neualbenreuth, Bayern.

S. MEIER. *Lapis*, **30**(3), 2005, 31-4.

Almandine crystals of apparently gem or ornamental quality are described from Neualbenreuth, Bavaria, Germany where they occur in a mica schist. Crystals of andalusite in quartz are described from the same area. M.O'D.

[Colorimetry of coloured gemstones: Comparative study of the colorimeter with the visual colour sensation of gemstones.]

K. MIKI AND Y. TAKAHASHI. *Journal of Gemmological Society of Japan*, **24**(1-4), 2004, 3-12, 7 figs, 5 tables. (in Japanese with English abstract).

By a combination of a set of LEE filters and multi-colorimeter measurements, statistical data on how personal visual sensitivity varies depending on the colours of gemstones have been processed. It was found that small differences are more easily detected in some colours than in others. The green and pale colours of yellow, orange, pink, blue and violet are easier to distinguish than dark colours of red, blue and bluish violet. The results show that general colour sensation fits in with perceived colour of gemstones. Faceted gemstones display several colours due to the presence of many facets, and a range of bright and more shadowy colours. Detailed colour sensations from such stones were analysed by visual tests of three colour differences. It was demonstrated that most human colour sensation recognises the medium bright colour as the defining colour of such faceted gemstones. I.S.

Aquamarine aus neuen Vorkommen in Brasilien.

C.C. MILISENDA AND H. BANK. *Gemmologie. Z. Dt. Gemmol. Ges.,* **54**(1), 2005, 47-51. 6 photographs, bibl. (German with English abstract.)

The new occurrence is situated at Padre Paraiso, about 80 km north of Teofilo Otoni in the state of Minas Gerais in Brazil. It produces large transparent crystals weighing up to 80 kg. Faceted specimens are pastel-coloured greenish blue and may exceed 100 ct. Intense blue aquamarines have been found near the famous Santa Maria de Itabira deposit at Tatu; faceted stones range from 1 to 10 ct. A third new find is near Jacutinga, 60 km south of Pocos de Caldas and 10 km east of the border of the Sao Paulo state. Faceted specimens are small, seldom more than 3 ct, but show an intense blue colour rarely seen in small aquamarines. E.S.

Neues Vorkommen kupferführender Turmaline in Mosambik.

C.C. MILISENDA, Y. HORIKAWA, K. EMORI, R. MIRANDA, F.H. BANK AND U. HENN. *Gemmologie. Z. Dt. Gemmol. Ges.,* **55**(1/2), 2006, 5-24, 30 photographs, 1 table, 4 graphs, bibl. (German with English abstract.)

A new occurrence in the region of Alto Ligonha in the north of Mozambique produces purple to violet, pink, blue, violet-blue, green-blue, yellow-green and green tourmalines, the colour being caused by trace elements of manganese and/or copper, comparable with the Paraíba tourmalines from Brazil. Purple-violet and violet-blue stones can be heat treated to result in a turquoise blue colour. The chemical composition indicates that it is the lithian tourmaline elbaite. The lively blue and green tourmalines have been very successful on the gem market and have led to the discussion as to whether the name 'Paraíba touramalines' should refer to their origin or composition. E.S.

Rubin emit bleihaltigen Gläsern gefüllt.

C.C. MILISENDA, Y. HORIKAWA AND U. HENN. *Gemmologie. Z. Dt. Gemmol. Ges.,* **54**(1), 2005, 35-42. 12 photographs, 3 graphs, bibl. (German with English abstract.)

The filling of fractures in rubies with glass has been known for a long time. These glass substances usually had borax as a basis. As these treatments are undertaken at a temperature of 1500°C, the original fracture is altered and the treatment can easily be verified. The new filling material used is a lead-containing glass with a higher RI which can be applied at a lower temperature (1000°C), so the original fissure is not altered too much. Magnification reveals characteristics such as flash

effect and bubble-like inclusions. At present the majority of such treated stones come from Andilamena (north central Madagascar). This treatment can be applied to all corundums. E.S.

Gemmologische Kurzinformationen. Gelb-grüne, facettierte Sillimanite aus Orissa (Indien).

C.C. Milisenda and M. Wild. *Gemmologie. Z. Dt. Gemmol. Ges.,* **55**(1/2), 2006, 59-61. 4 photographs, bibl. (German with English abstract.)

Transparent yellow-green to green-yellowish sillimanites come from a new find in Orissa. The faceted stones resemble chrysoberyl and weigh between 2.85 and 10.63 ct with RIs of 1.658-1.681, DR 0.020-0.021 and SG of 3.26. The absorption spectra showed lines at 460, 440, 412 and 360, which can be attributed to trivalent iron. Microscopic examination showed parallel orientated, fibrous mineral inclusions and parallel orientated needle-like inclusions and hollow tubes. E.S.

Lab Notes.

T.M. Moses and S.F. McClure (Eds). *Gems & Gemology,* **42**(1), 2006, 54-61.

Notes are given on a diamond with 'fingerprint' inclusions (common in rubies and sapphires, but extremely rare in diamonds) and a pink diamond with etch channels at the intersection of glide planes. Two of the emerald crystals in a mineral specimen 'assembled' from genuine Colombian material were found to show internal descriptions in Arabic; the crystals apparently had been core drilled from the bottom and a rolled up piece of paper inserted into the drill holes which were then filled with a resin. R.A.H.

Kolonne bei Embilipitya auf Sri Lanka-eine interessante Fundstelle für Olivin, Hornblende und Spinelle.

H.D. Müller and S. Jahn. *Mineralien Welt,* **17**(4), 2006, 44-51.

Finds of olivine, hornblende and spinel are described from the Embilipitya area of Sri Lanka. Other species mentioned include schorl and allanite. Some of the olivine appears to be of gem quality. M.O'D.

Smaragd 2004, Anatas 2005: Kristallfestival im Habachtal.

H. Neutkins. *Lapis*, **31**(6), 2006, 26.

Recently-discovered and attractive specimen-quality emerald crystals are described from the Habachtal, Austria. M.O'D.

Das Smaragd-Vorkommen von Byrud (Eidsvoll) in Süd-Norwegen.

F.S. Nordrum and G. Raade. *Mineralien Welt,* **17**(4), 2006, 52-64.

Emerald crystals, some of gem quality, are described from the southern Norwegian deposit at Byrud (Eidsvoll). The local geology and other species found are also described. M.O'D.

Mineral and melt inclusions in sapphires as an indicator of conditions of their formation and origin (Primorsky region of the Russian Far East).

V. Pakhomova, B. Zalishchak, V. Tishkina, M. Lapina and N. Karmanov. *Australian Gemmologist*, **22**(11), 2006, 508-11, 3 figs.

The authors have studied the sapphires from the Nezametnoye corundum deposit in Russia to investigate the physico-chemical conditions of corundum formation. They studied the mineral and primary melt inclusions that are syngenetic with the corundum using XRF, thin section petrography and electron microprobe analysis. From the mineral and melt inclusion data, they suggest that corundum crystallized from a quartz-syenite melt within a temperature range from 780° to 820°C, and pressure range from 1.7 to 3 kbar, involving both magmatic and metasomatic processes. These results contradict previous theories that the Nezametnoye corundum formed in alkali basalts. L.J.

Spessartin- und Dioptas Mineralisationen im Kaokoland, Namibia.

A. Palfi. *Mineralien Welt,* **16**(4), 2005, 49-61.

Spessartine and diopside mineralization is described from

Kaokoland in north-west Namibia. Some of the fine transparent orange spessartine crystals have been faceted. A mineral list is given. M.O'D.

Characteristic spectral features of iron as a gemstone chromophore.

G. Pearson. *Australian Gemmologist,* **22**(10), 2006, 430-46, 35 figs, 1 table.

UV-Visible spectrophotometry has been used to determine the absorption spectra of gemstones that contain iron including sapphire, beryl, chrysoberyl, spinel and peridot. The spectra determined differed from those found in the gemmological literature. A single absorption band found between 400-460 nm was present in all, as was a pair of absorption bands in the UV region between 360-390 nm, not visible with a gemmological spectroscope. L.J.

The variation of gemmological properties and chemical composition of gem-quality taaffeites and musgravites from Sri Lanka.

K. Schmetzer, L. Kiefert, H-J. Bernhardt and M. Burford. *Australian Gemmologist,* **22**(11), 2006, 485-92, 8 figs, 2 tables.

The physical and chemical properties of three taaffeites and one musgravite from Sri Lanka are described. They are beryllium-magnesium-aluminium oxides. The gems were analysed using standard gemmological methods, non-polarized UV-VIS spectrometry, Raman microspectroscopy and electron microprobe. The greyish violet colour of the taaffeites is ascribed to iron and the purple-red colour of one taaffeite to traces of chromium and moderate iron levels. The variations in chemical composition result in variations in the gemmological properties. However there are overlaps in the gemmological properties of the taaffeites and musgravites. L.J.

Ein 'Lapis' aus den Jahre 1903.

H.-P. Schröder. *Lapis,* **31**(11), 2006, 13-16.

Describes and illustrates Rudolf Zimmermann, Monatsschrift Mineralien-Geseins-und Petrefakantensammler. Some colour plates from the original are reproduced. M.O'D.

A guide to mineral localities in China.

B. Smith, C. Smith, G. Liu and B. Ottens. *The Mineralogical record*, 2005, **36**, 87-101.

The guide is arranged in alphabetical order of location and includes type (mining district, mine, etc), geographical coordinates, province and type of mineral. A number of species yielding gem-quality specimens are included. A country map is provided.   M.O'D.

My other collection.

B. Sneyd. *Australian Gemmologist*, **22**(10), 2006, 466-9, 16 figs.

Various types of postcards illustrating aspects of gemstones and gemmology collected by the author are described.   L.J.

Ammolith-ein opalisiererender Muschelmarmor aus dem Karwendelgebirge, Tirol.

M. Strasser. *Lapis*, **31**(11), 2006, 37-40.

A fossilized ammonite with an opal-like play-of-colour is described from the Karwendelgebirge, Tirol, Austria. The trade name ammolite has been used for ornamental quality material.   M.O'D.

Gemstone mining and exploration in Australia.

F.L. Sutherland. *Australian Gemmologist,* **22**(11), 2006, 496-502, 2 maps, 6 figs.

An overview of the significant gem deposits in Australia that are currently being worked, including precious opal, diamond, sapphire, nephrite, chrysoprase, agate, silicified ornamental materials and pearls. 2005 saw the start of new ruby mining in Eastern Australia, and recent finds of amber have been found in the Cape York Peninsula.

L.J.

A SIMS study of the transitional elemental distribution between bands in banded Australian sedimentary opal from the Lightning Ridge locality.

P.S. Thomas (paulthomas@uts.edu.au), L.D. Brown, A.S. Ray and K.E.

Prince. *Neues Jahrbuch for Mineralogie Abhandlungen*, **182**(2), 2006, 193-9.

The distribution of trace elements in banded Australian sedimentary opal from the Lightning Ridge region was investigated with secondary ion mass spectrometry (SIMS) using both spot and spatial analysis by stepping incrementally across the sample in line-scan mode. The opal was found to be fairly homogeneous within bands, but it showed a relatively sharp change in trace element contents at the interface between bands for such elements as Ti, V, Co, Cu, Zn and Y. A number of elements (Na, Mg, Al, K, Ca, Mn and Fe), however, did not vary significantly between bands, which is taken to suggest that the adjacent bands in the opals were formed at the same time. These observations are consistent with earlier reported laser ablation ICP-MS results, and support the solution depletion sedimentation model proposed as the mechanism for band formation in banded opal. R.A.H

Old opal fields revisited at Coober Pedy.

I.J. Townsend. *Australian Gemmologist*, **22**(11), 2006, 475-8, 5 figs, 3 maps.

A South Australian Government financed initiative to subsidize drilling projects to locate new opal fields at Coober Pedy was begun in 2004. As a result new opal bearing deposits have been located. In addition High Resolution Resistivity has been tested on known opal bearing areas at Coober Pedy with good results.   L.J.

The effects of heat treatment on zircon inclusions in Madagascar sapphires.

W. Wang (wuyi.wang@gia.edu), K. Scarratt, J.L. Emmett, C.M. Breeding and T.R. Douthit. *Gems & Gemology,* **42**(2), 2006, 134-50.

A study of zircon inclusions in gem-quality sapphires showed that progressive decomposition and chemical reactions between zircon and the host sapphire occurred at 1400-1850°C. In unheated sapphires, transparent zircon inclusions displayed slightly elongated forms and clear interfaces with their corundum host; most were confined within the host at relatively high pressures (up to 27 kbar), and showed evidence of natural radiation-related damage metamictization. Subsolidus reactions

of some zircon inclusions started at as low as 1400°C, as shown by the formation of baddeleyite (ZrO_2) and a SiO_2-rich phase. Differences in the degree of pre-existing radiation damage are the most likely cause for the decomposition reactions at such relatively low temperatures. Melting of zircon and dissolution of the surrounding sapphire occurred in all samples at 1600°C and above. From these observations, a systematic sequence of both modification and destruction of zircon inclusions with increasing temperature was compiled. This may be useful as a gemmological aid in determining whether a zircon-bearing ruby or sapphire has been heated and to provide an estimate of the heating temperature.   R.A.H.

Gemmology, geology and origin of the Sanawana emerald deposits, Zimbabwe.

J.C. Zwaan. *Scripta Geologica,* **131**, 2006, 212.

The emeralds from the Sandawana deposits, Zimbabwe, have relatively high refractive indices (ε 1.584 – 1.587, ω1.590 – 1.594) and specific gravity (2.74 – 2.77), with evenly distributed colour ranging from medium to dark green and with yellowish-to bluish-green dichroism. They contain inclusions of actinolite and cummingtonite needles and long prismatic laths of albite and apatite, as well as phlogopite, calcite, dolomite, quartz and ilmenorutile; partially healed fissures are also seen. Electron microprobe analyses were performed on four gem-quality, medium to dark green rough emeralds and one light green emerald extracted on pegmatite, all from the Zeus mine. Probe analyses are also reported for 23 amphibole inclusions and for 20 other inclusions; trace element contents of 22 emeralds were also measured. These emeralds have relatively high contents of Cr, Na, Mg, Li and Cs, and are readily distinguished from emeralds from most other localities by traditional gem-testing techniques. These emerald deposits occur at the contacts between the Mweza greenstones and REE-bearing granitic pegmatites emplaced during a main 2600 Ma deformation event at the southern end of the Zimbabwe craton. Late-stage Na rich 'solution-melt' containing F, P,

Li, Be and Cr caused albitization and phlogopitization in the greenstone wall-rock. Synkinematic growth of phlogopite was accompanied by emerald, fluoropatite, holmquistite and chromian ilmenorutile, indicating Na-K metasomatism in the emerald-bearing shear zone. Further data on emeralds and associated minerals and the mining methods employed are included in the main text, along with illustrations, diagrams and electron micrographs.

R.A.H.

Instruments and Techniques

Applications of laser ablation-inductively coupled plasma-mass spectrometry (LAICP-MS) to gemology.

A. Abduriyim (ahmadjan@gaaj-zenhokyo.co.jp) and H. Kitawaki. *Gems & Gemology,* **42**(2), 2006, 98-118.

The authors have applied the minimally destructive LA-ICP-MS technique to gemology to take advantage of its high spatial resolution, rapid and direct analysis of gemstones (whether loose or mounted), and precise measurement of a wide range of elements – even in ultra-trace amounts. The principles of LA-ICP-MS are summarized and the application of this technique to the detection of Be diffusion treatment in corundum and the identification of the geographic origins of emeralds. The method is significantly less expensive than secondary ion mass spectrometry (SIMS) and more sensitive than laser-induced breakdown spectroscopy (LIBS), which is the least costly of these three techniques.

R.A.H.

Test case for the refractometer – olivine or sinhalite?

A Hodgkinson. *Australian Gemmologist,* **22**(11), 2006, 493-5, 9 figs, 1 table.

Brown iron-rich olivine is similar in appearance to sinhalite. The refractometer can, with care, be used to differentiate brown olivine from sinhalite by detecting the position of beta which is nearer to gamma in sinhalite. Magnetism can be used to detect the more magnetic olivine. Absorption spectra are useful in some instances, as is the use of thermal conductivity and crossed filters.

L.J.

Re-surfacing a refractometer prism.

T. Linton. *Australian Gemmologist,* **22**(10), 2006, 470-1, 2 figs.

The potential effects of repolishing a refractometer prism are detailed, including inaccurate readings of RI.

L.J.

Faceting transparent rhodonite from Broken Hill, New South Wales, Australia.

P.W. Millsteed (paulmilsteed@hotmail.com). *Gems & Gemology,* **42**(2), 2006, 151-8.

Because of its perfect cleavage and brittle nature, rhodonite is notoriously difficult to facet. A technique has been developed through experiments on eight crystals from the North mine at Broken Hill, via a systematic structural, crystallographic and optical analysis and the use of a non-conventional faceting approach – the 'greasy lap'. This method uses a mixture of petroleum jelly and diamond grit to charge a non-embedded lap, allowing the diamond grit to 'roll free' during the lapping process.

R.A.H.

Synthetics and Simulants

A study on the identification of turquoise by FTIR.

Y-C. Kim. *Journal of the Korean Crystal Growth and Crystal Technology,* **14**(6), 2004, 272-6 (Korean with English abstract).

Natural turquoise can be distinguished easily from its common substitutes using infrared spectroscopy in the range 2000~450 cm-1, especially by features in the mid-infrared. Gilson turquoise exhibits a significantly smoother pattern when compared with natural turquoise, due to a different state of aggregation. Infrared spectra of natural, treated synthetic and imitation turquoise (gibbsite, calcite) are shown and compared.

I.S.

Prospects for large single crystal CVD diamonds.

S.S. Ho, C.S. Van, Z. Liu, H.K. Mao and R.J. Hemley. *Industrial Diamond Review,* **66**, 2006, 28-32.

A description is given of chemical vapour deposition (CVD) techniques for fabricating large single-crystal diamond at very high growth rates (up to > 100 J-lm/h). Single crystals more than 1 cm in thickness and weighing more than 10 ct can now be produced with a range of optical and mechanical properties for different applications. This diamond can be tailored to possess high fracture toughness, and high-pressure/high-temperature annealing can increase its hardness significantly. The size of the diamonds can be further enlarged by successive growth on different faces. The process has been optimized to produce diamond with improved optical properties in the ultraviolet to infrared range, opening prospects for new technological and scientific applications. Illustrations are given of a 5 ct single-crystal CVD diamond (without seed), 12 mm high and 6.7 mm diameter, cut from a 10 ct block using a computer-controlled YAG laser system, and of a 0.2 ct brilliant cut diamond produced from a 1 ct block.

R.A.H.

Abstractors

R.A. Howie   R.A.H.   L. Joyner   L.J.   M. O'Donoghue   M.O'D.   E. Stern   E.S.   I . Sunagawa

Book Reviews

Gems of Sri Lanka (6th revised edn).

D.H. Ariyaratna, 2006. Ariyaratna, London. 177 pp, illus. in colour. Softcover. ISBN 955-95494-4-8. £14.95.

This sixth edition describes gem prospecting and mining, and the polishing and trading of Sri Lankan gemstones. There are introductory chapters on gem varieties and identification, but the style is generally non-technical, with appendices including a glossary of Sri Lankan terminology and tables of gemmological data.

It is an interesting book which contains a great deal of local information, together with sound advice for non-professional gem buyers. The quality of reproduction of some photographs could have been improved, and more useful proof reading would have been beneficial. Some technical details are open to criticism. It is implied, for example, that all emerald appears reddish through the Chelsea Colour Filter, and some birefringence values given in the tables are open to criticism. Overall, however, the book gives an interesting account of Sri Lankan methods of gem recovery, production and trading, and should appeal to those who are interested in the industry, especially if they intend to visit the country.   P.J.E.D.

Mineralogical studies on luminescence in diamond, quartz and corundum.

J. Lindblom, 2005. Turun Yliopisto, Turku, Finland. (Annales Universitatis Turkuensis. Sarja-Ser. All, tom.183.)

A collection of papers by Lindblom and other authors. The texts are of considerable interest to gemmologists. The titles, following a general introduction, are: Differentiation of natural and synthetic quality diamonds by luminescence properties; Luminescence study of defects in synthetic as-grown and HPHT diamonds compared to natural diamonds; Details of intense light-green luminescence in quartz; Luminescence of thermally enhanced and beryllium-diffused rubies. Each paper has its own list of references and some illustrations are in colour. M.O'D.

Gems (6th edn).

M. O'Donoghue (Ed.), 2006. Elsevier: Butterworth/Heinemann, Oxford. xxx + 874 pp. ISBN 0-75-065856-8 (hardback). £90.00.

This new edition has been considerably updated and expanded since the fifth edition (1994). Michael O'Donoghue is both the editor and principal contributor, having been responsible for seventeen of the thirty-one chapters. In Part I, there are two useful introductory chapters, the first by Roger Harding being on the geological sources of gems, introducing the three main categories of rocks and the processes that formed them, before touching on the ages of gems, gem regions and gem recovery methods. This chapter ends with a useful note on the word 'origin' in certificates of authenticity: 'geological source' or 'geographical locality' may be preferable. The second chapter is by Ian Mercer on crystalline gem materials, introducing the crystal systems, the varying sizes of atoms and the concepts of habit, polymorphism, twinning, etch marks and the importance of directional properties (while avoiding the complications of face indices).

Part II deals mainly with individual gem species opening with two chapters on diamond, the first covering a general survey of diamond from the various regions of the world, before describing the effects on it of light and other radiation, and the appearance in the market of synthetic moissanite and other simulants. The second diamond chapter is by Alan Collins, and starts by reminding us that, on average, approximately 1 tonne of rock from a diamond mine must be processed to yield each carat of diamond–and even then less than 25 per cent is of gem quality. The methods used to produce synthetic diamonds are fully described, including chemical vapour deposition, and the origin of colour in diamond is fully explored, with details of colour enhancement by high-pressure-high-temperature annealing and a discussion on the colour change process. The chapter on ruby and sapphire takes full account of modern developments, with useful details on absorption spectra, and on the importance of Cr, V, Fe and Ti in the coloration of these gem minerals; the various methods of synthesis and simulation are described. The beryl chapter deals mainly with emerald, noting that Cr must be present if a green beryl is named as emerald, whereas green beryl coloured by vanadium should be termed green beryl. This section is followed by descriptions of chrysoberyl and alexandrite, spinel, topaz, tourmaline, the garnet family (with a sub-section on nomenclature), feldspars, zircon, peridot, quartz, opal, turquoise, lapis lazuli and jade. The remaining chapters deal with less common species (I found it odd to see cavansite described as resembling turquoise), natural glasses, simulants, synthetic gemstones, composite stones, plastics and pearls, and with the various cuts of gemstones and methods of value enhancement. There are appendices listing birthstones, a glossary of unusual and often misleading names, and a list of famous diamonds. This book builds on the foundations laid by previous editions, but gives a lot of space to the occurrences and localities of some of the species, e.g. topaz and feldspar. It is well illustrated with line diagrams and black-and-white photographs, together with an inset of 31 colour plates. It is unfortunate, however, that many of the captions for the numerous photographs illustrating the first chapter were apparently written in the expectation of them appearing in colour, making the references to interference colours, red garnets, green mica and pale brown glass, somewhat superfluous. In addition, the caption for Figure 1.7 is entirely wrong (it should be that of Figure 1.8a) and Figure 1.8b is a repeat of Figure 1.24 but with an inappropriate caption.   R.A.H.

The Smale Collection: beauty in natural crystals.

S. SMALE, 2006. Lithographie Inc., East Hampton, Connecticut. 204 pp, illus. in colour. Hardcover, ISBN: 9780971537187. €40.00.

Opening this magnificent book, I was reassured that the soul of the great mineral/crystal album was only sleeping and not moribund. This is exactly what the title and subtitle indicates – one man's collection (or a part of it) showing the pieces closest to his heart. The front cover with two crystals depicted introduces the fortunate reader to some of the finest photographs I have seen in handling most of the major gem and mineral books published for the past 40 years. Many of the photographs are of gem minerals: each caption gives the specimen size, where found and provenance. There is a short bibliography.

The author and noted photographer Jeff Scovil are to be congratulated on a most inspiring production.   M.O'D.

Gemstones. Understanding – Identifying – Buying.

K. WALLIS, 2006. Antique Collectors' Club, Woodbridge, Suffolk. 127 pp, illus. in colour. Hardcover. ISBN 1-85149-494-4. £15.95.

Gemstones is an ideal reference book for the gem collector, hobbyist and student gemmologist, its profuse high quality colour illustrations also enabling the identification by comparison of a range of gem materials. Written for the layperson as an introduction to the fascinating world of gemstones and jewellery, the first few pages of *Gemstones* lists the qualities which go to make up a desirable gem. These pages also contain explanations of some of the more technical gemmology terms together with descriptions of basic low-cost instruments for the identification of stones, both subjects of special interest to the author.

The history, myths and legends associated with gemstones are then covered before the book launches into its first major section, 'Precious stones', which deals with diamond, emerald, ruby and sapphire. The following section entitled 'The gemstones' includes a selection of the less well known inorganic stones ranging from andalusite to zircon. A third section 'Organic gems' features amber, ammolite, coral, horn, ivory, jet, pearl and shell. Samples of these gemstones and gem-mounted jewellery are illustrated in colour in all three sections, and this part of the book concludes with 'A selection of minor gemstones' which lists both rare and collectors' stones.

Practical cautionary advice is given in 'Buying gemstones', a section which includes information on the current types of enhancement treatments, on synthetics and simulants, and on gemstone collection. This is followed by notes on the metals and hallmarks used in jewellery mounts. The book continues with 'Gemstones around the world' which gives further useful advice on where to buy and what to avoid in various parts of the world. A final section 'Gems on the internet' warns of risks in buying loose stones and gem-set jewellery from unfamiliar websites. However, several useful and informative sites are listed in this section.

Printed on good quality paper, which further enhances the colour illustrations, the book concludes with a useful set of appendices (Glossary; Rainbow of colours; Specific gravity and refractive index of gemstones; Translations – gem names in English, French, German, Italian and Spanish; Tanzanite values; Diamond values; Comparative gem values; Further reading).   P.G.R.

Khibiny.

V. YAKOVENCHUK, G. IVANYUK, Y. PAKHOMOVSKY AND Y. MEN'SHIKOV, 2005. Laplandia Minerals Ltd in association with the Mineralogical Society of Great Britain and Ireland, Apatity and London. 466 pp, illus. in colour. ISBN 5-900395-48-0. €149.00.

This is one of the welcome surveys of a celebrated mineral area with which gemmologists with an interest in the wider world of minerals should be aware and ready to learn from. In any case, the profuse colour photographs, bibliography and well laid out text should be an example to those attempting similar depth of coverage of other classic deposits.

Khibiny is the largest nepheline syenite intrusion on Earth and more than 470 mineral species have been found there – around 88 for the first time. Gemmologists quite fairly will want to know about minerals with ornamental potential; while some blue sapphire crystals are illustrated, Khibiny is not a classic gemstone source. None the less, some species may one day turn up in a state appropriate for fashioning. I noted that sérandite, already known as most beautiful (and rare) crystals from Mt St. Hilaire, Quebec, is also reported from Khibiny, though as an inadequately characterized mineral or species of doubtful report.

The micromounter will have a more fruitful visit (if such are possible) encountering attractive crystals of rhodochrosite, eudialyte, cancrinite, villiaumite and mangan-neptunite.

The text is arranged in traditional chemical order and follows a description of the main mineral localities. Photographs give the size of the specimen depicted and the individual mineral descriptions, and the bibliography occupies 15 A4-sized pages.

For this reviewer, the best feature of the book was the opportunity to see examples of species known (if remembered) from reports of new mineral species (often from Russia and vicinity) in the less illustrated journals.   M.O'D.

Proceedings of the Gemmological Association and Gem Testing Laboratory of Great Britain and Notices

Gem-A Awards

Gem-A Examinations were held worldwide in June 2006. In the Examinations in Gemmology 221 candidates sat for the Diploma Examination of whom 119 qualified, including six with Distinction and 30 with Merit. In the Foundation Gemmology Examination, 227 candidates sat of whom 174 qualified. In the Gem Diamond Examination 67 candidates sat of whom 33 qualified, including two with Distinction and six with Merit.

The **Tully Medal** for the candidate who submits the best set of answers in the Gemmology Diploma examination which, in the opinion of the Examiners, are of sufficiently high standard, was awarded to **Dr Catherine Appleyard of Lewes**, East Sussex. Dr Appleyard was also awarded the **Anderson Bank Prize** for the best non-trade candidate of the year in the Diploma in Gemmology examination.

The **Christie's Prize for Gemmology** for the best candidate of the year in the Diploma examination who derives her main income from activities essentially connected with the jewellery trade, has been awarded to **Nicola Sherriff** of Verdun, Quebec, Canada.

The **Anderson Medal** for the candidate who submitted the best set of answers in the Foundation Certificate examination which, in the opinion of the Examiners, are of sufficiently high standard, was awarded to **Kay Harris** of Penang, Malaysia.

The **Hirsh Foundation Award** for the best candidate of the year in the Foundation Certificate Examination was awarded to two candidates, **Kay Harris** of Penang, Malaysia, and **Simon Dowden** of Chadds Ford, Pennsylvania, U.S.A.

The **Deeks Diamond Prize** for the best candidate of the year in the Diploma in Gem Diamond examinations was awarded to **Perry Huck** of Harare, Zimbabwe.

The **Bruton Medal** was not awarded.

EXAMINATIONS IN GEMMOLOGY

Gemmology Diploma

Qualified with Distinction
Appleyard, Catherine, Lewes, East Sussex
Sherriff, Nicola, Verdun, Quebec, Canada
Wang Ling, Guilin, Guangxi, P.R. China
Wang Yu, Wuhan, Hubei, P.R. China
Westlake, Ingrid, Chamonix, France
Yu Heyu, Guilin, Guangxi, P.R. China

Qualified with Merit
Bell, Lucy Kate, Stirchley, Birmingham, West Midlands
Bergeron, Elise, Montreal, Quebec, Canada
Borg, David, Paola, Malta
Carrel, Leigh, Preston, Lancashire

Gem-A Awards

Chan Wing Sze, Herleva, Kowloon,
Hong Kong
Chen, Ying Chen, Taipei, Taiwan,
R.O. China
Chui Yee Man, Tseung Kwan O,
New Territories, Hong Kong
Han Keng Siew, Aloysius, Singapore
Huen Lai-Kei, Sheree, Richmond, British
Columbia, Canada
Hui Wan Man, Kowloon, Hong Kong
Jiang Junjie, Wuhan, Hubei, P.R. China
Khan-Farrukh, Nayer, Washwood Heath,
West Midlands
Larsson, Carl Niclas, Öregrund, Sweden
Larsson, Jacqueline, Amsterdam,
The Netherlands
Lin, Jui-Yi, Taipei, Taiwan, R.O. China
Luzuriaga Alvarez, Martha Gladys, Laval,
Quebec, Canada
Ma Yuli, Wuhan, Hubei, P.R. China
Mak Kim Yiu Keung, Ma On Shan,
New Territories, Hong Kong
Matoba, Akiko, Nara City, Nara Pref.,
Japan
Murray, Helen Claire, Sutton Coldfield,
West Midlands
Ni Ziqian, Guilin, Guangxi, P.R. China
Okuyama, Muneyuki, Kohoku-ku,
Yokohama, Japan
Randrianantoandro, Minoarisoa Michelle,
Ampandrianomby, Antananarivo,
Madagascar
Razakarivony, Aina Anthony,
Ampandrianomby, Antananarivo,
Madagascar
Retsin d' Ambroise, Laura, Paris, France
Slovak, Kate, Leicester
Sun Yuan, Guilin, Guangxi, P.R. China
Surawy, Laura Katherine, London,
Yiu Ka Wah, Tokwawan, Kowloon,
Hong Kong
Zhou Huijuan, Guilin, Guangxi, P.R. China

Qualified
Akiyama, Claire Nozomi, Saitama-Ken,
Japan
Anderson, Nicola M., Edinburgh, Scotland

Bellec, Marion, Ergue-Gaberic, France
Butt, Andrew, Toronto, Ontario, Canada
Callaway, Heather, Stone, Staffordshire
Chan Lai Fong, Tuen Mun,
New Territories, Hong Kong
Chandra, V. Subash, Krishnagiri,
Tamil Nadu, India
Chang Mei-Yen, Karen, Taipei, Taiwan,
R.O. China
Chen Shioulin, Taipei, Taiwan, R.O.
China
Chen Li, Guilin, Guangxi, P.R. China
Cheung Man Yi, Kowloon, Hong Kong
Chiu Fong Ting, Tuen Mun, Hong Kong
Chow Wai Lam, Fan Ling, New Territories,
Hong Kong
Coene, Helena, Brussels, Belgium
Danjo, Keiji, Kofu City, Yamanashi Pref.,
Japan
Deeley, Philippa, Etchingham, East Sussex
Dunn, Andrew Charles, Reading, Berkshire
Dunn, William A., Los Angeles, California,
U.S.A.
Ellison, Armelle, Woking, Surrey
Forsberg, Erika, Bandhagen, Sweden
Furuya, Satoshi, Bunkyo-ku, Tokyo, Japan
Gauci, Karen Elizabeth, Burnaby,
British Columbia, Canada
Geormas, Emmanuel, Byron, Greece
Gogna, Sanjeev, Una, Himachal Pradesh,
India
Gouros, Arte, Coulsdon, Surrey
Hartley, Pauline, Woodkirk, West Yorkshire
Hayashi, Kinya, Tokushima City,
Tokushima Pref., Japan
Haythornthwaite-Shock, Lucy,
Mangotsfield, Bristol, Avon
Heywood, Natalie Louise, Enfield, Middlesex
Hu Kaifan, Wuhan, Hubei, P.R. China
Jiang Jingxia, Shanghai, P.R. China
Jones, Gary, Dudley, West Midlands
Jones, Jason Matthew, Beverley,
East Yorkshire
Kidachi, Masanobu, Sagamihara City,
Kanagawa Pref., Japan
Ko Hoi Fu, Shamshui Po, Kowloon,
Hong Kong

Gem-A Awards

Kronis, Tamara Lynne, Toronto, Ontario, Canada
Kweon, Ji Eun, Suseong-Gu, Daegu, Korea
Kwok Mei Yee, Sindy, Ap Lei Chau, Aberdeen, Hong Kong
Lam Mei Hei, Cally, Shatin, New Territories, Hong Kong
Lam Siu Kuen, Hazel, Tseung Kwan O, Kowloon, Hong Kong
Latham, Elizabeth, Wallingford, Oxfordshire
Lee, Marian, Taipei, Taiwan, P.R. China
Leung Shiu Lok, Sam, Taipo, Hong Kong
Leung Shun Lok, Kowloon Bay, Hong Kong
Li Ling, Wuhan, Hubei, P.R. China
Li Mei, Guilin, Guangxi, P.R. China
Liao Dan, Wuhan, Hubei, P.R. China
Lin Wenyan, Wuhan, Hubei, P.R. China
Liu, Hongmei, Toronto, Ontario, Canada
Low, H. San, Chatham, Kent
Luo Xuan, Wuhan, Hubei, P.R. China
Meng Wenxiang, Shanghai, P.R. China
Morsink, Cornelis E., Stirling, Ontario, Canada
Nagao, Saeko, Kooriyama City, Fukushima Pref., Japan
Ogata, Etsuko, Osaka, Japan
Okano, Makoto, Iwatsuki City, Saitama Pref., Japan
Pan Pai, Guilin, Guangxi, P.R. China
Pang Yufei, Guilin, Guangxi, P.R. China
Parkes, Gabriella, London
Peng Daoming, Wuhan, Hubei, P.R. China
Razafindrasolo, Toky Ny Aina, Ampandrianomby, Antananarivo, Madagascar
Ren Chan, Wuhan, Hubei, P.R. China
Robichaud, Emilie Gould, London
Singh, Priti, Jaipur, India
Sourendre, Shah Rupal, Ampandrianomby, Antananarivo, Madagascar
Tam Tin Sang, Daniel, Richmond, British Columbia, Canada
Tanaka, Yumi, Toyonaka City, Osaka, Japan
Tang Yin Tung, Chai Wan, Hong Kong

Thiebaut, Ivane, London
Tonkin, Claire Louise, Stratford, London
Tsoi Mei Yu, Fanling, New Territories, Hong Kong
Tsui Wing Sze, Yuen Long, New Territories, Hong Kong
Van Spaendonk, Ann, Kalmthout, Belgium
Wang Wei, Guilin, Guangxi, P.R. China
Wang Yuchao, Wuhan, Hubei, P.R. China
Widmer, Danielle Helene, Mississauga, Ontario, Canada
Wong Mars, Ma On Shan, New Territories, Hong Kong
Wong Yuen Kwan, Annie, North Point, Hong Kong
Xue Lilin, Wuhan, Hubei, P.R. China
Xue Xiaoxin, Wuhan, Hubei, P.R. China
Ye Mengqian, Guilin, Guangxi, P.R. China
Zhu Cheng, Guilin, Guangxi, P.R. China
Zou Jin, Guilin, Guangxi, P.R. China

Gemmology Foundation Certificate
Qualified
Ahn, Su Jin, Seoul, Korea
Amicone, Maria, La Salle, Quebec, Canada
Aung Myo Oo, Kamayut Township, Yangon, Myanmar
Baker, David Mark, Bath, Somerset
Bellec, Marion, Ergue-Gaberic, France
Booth, Eveline Violet, London
Bove, Bertrand, Vitry Sur Seine, France
Bracey, Anne Christine, Birmingham, West Midlands
Caulton, David, Dore, Sheffield, South Yorkshire
Cederholm, Jenny, Stockholm, Sweden
Chan Kai Chi, Seeheim-Jugenheim, Germany
Chan Che Min, Tsuen Wan, Hong Kong
Chan Tak Kit, Emily, Kowloon, Hong Kong
Chan Tsz Yan, Yuen Long, New Territories, Hong Kong
Chan Wing Kwok, Hong Kong
Chan Yuet Ngai, Taikoo Shing, Hong Kong
Chau Kit Ying, Lily, San Francisco, California, U.S.A.

Gem-A Awards

Chen Cui, Guilin, Guangxi, P.R. China

Cheung, Nelly, Tai Koo Shing,
Hong Kong

Cheung Chi Shing, Peter, Lam Tin,
Kowloon, Hong Kong

Cheung Ching Ping, Candy, Tseung
Kwan O, Kowloon, Hong Kong

Chien Lien Chin, Taichung, Taiwan, R.O.
China

Chin Suet Ying, Kwai Chung, New
Territories, Hong Kong

Cho, Hee Jeong, Anyang-Si, Gyunggi-Do,
Korea

Choi, Jae Jin, Seoul, Korea

Chu Kong Ting, Hong Kong

Chu Shuk Man, Carmen, Shatin,
New Territories, Hong Kong

Chung Man Yin, Phoenix, Tuen Mun,
Hong Kong

Clark, Denise A., London

Claydon, Louise, Morden, Surrey

Conway, Mark, Northampton

Corser, Elizabeth, Wellington, Shropshire

Cote, Gaetan, St. Lambert, Quebec,
Canada

Craddock, Natalie, Bridport, Dorset

Cui, Xianzhong, London

de Josselin de Jong, Joris, Amsterdam,
The Netherlands

Dowden, Simon, Chadds Ford,
Pennsylvania, U.S.A.

Doyle, Helen Anne, Weymouth, Dorset

Driscoll, Brian John, New York, U.S.A.

Drummond, Jean, Farnham, Surrey

Ferneyhough, Ella, Henley-in-Arden,
Warwickshire

Fletcher, Alison Jane, Birmingham,
West Midlands

Fontaine, Clotilde, Versaille, France

Freidericos, Nikitas, Athens, Greece

Fung Kei Yan, Apleichau, Hong Kong

Gosden, Paul Jeremy, London

Gourlet, Agnes, Chartres, France

Guter, Danielle, Solna, Sweden

Halabi-Lenvenyte, Urte, London

Harris, Kay, Penang, Malaysia

Hassey, Lauren Adriana, London

Heit, Liesbeth, London

Henderson, Rheanan, Edinburgh,
Scotland

Holley, Deborah, Trowbridge, Wiltshire

Horn, Chandra Leah, Montreal, Quebec,
Canada

Hsiao, Pei Ying, Taichung, Taiwan,
R.O. China

Hu, Helen, London

Huang, Lei, Smethwick, Staffordshire

Huang Ching-Ping, Shanghai, P.R. China

Hudson, Joanne, Victoria Falls, Zimbabwe

Hui Man Kwong, Kwai Chung,
New Territories, Hong Kong

Hui Wing Hing, Kowloon, Hong Kong

Jeavons, James, Geebung, Queensland,
Australia

Johnson, Belinda, Birmingham,
West Midlands

Joshi, Sumit D., Pune, Maharashtra, India

Katayama, Shinko, Colombo, Sri Lanka

Khaing, Htite Htite, Ahlone Township,
Yangon, Myanmar

Kim, Hyoung Suk, Seoul, Korea

Kim, Seul Gi, Gwangju, Korea

Kim, Ji Eun, Chungbuk-Do, Korea

Kobayashi, Taisuke, Tokyo, Japan

Kong Yang, Guilin, Guangxi, P.R. China

Koundouraki, Evagelia, Athens, Greece

Lam Shu Wing, Kwun Tong, Hong Kong

Lee Joo Yeon, Daegu, Korea

Lee Min Sook, Seoul, Korea

Lee Cheuk Ming, Kowloon, Hong Kong

Lee Oi Yan, Christine, Tai Po,
New Territories, Hong Kong

Leung Kee Yun, Tin Shui Wai,
New Territories, Hong Kong

Li Kam Tim, Quarry Bay, Hong Kong

Li Qianhe, Guilin, Guangxi, P.R. China

Lilley, Samantha, Fyfton, Leicestershire

Lim, Joon Suk, Seoul, Korea

Lin, Chun Hsien, Taipei, Taiwan, R.O.C.

Liu Mei-Chun, Bianca, Fanling,
New Territories, Hong Kong

Liu Zijian, Guilin, Guangxi, P.R. China

Gem-A Awards

Lo, Sunny, Kowloon, Hong Kong

Lui Chi Kong, Matthew, Shatin,
New Territories, Hong Kong

Luzuriaga Alvarez, Martha Gladys, Laval,
Quebec, Canada

Ma Tsz Kwan, Hong Kong

McFadden, Robin, Birmingham,
West Midlands

Machefert, Jean-Michel, Cormeilles
En Parisis, France

Mahesh M. Babu, Palai, Kottayam, Kerala,
India

Mansell, Melanie, Plymouth, Devon

Mareso, Daniele, Brockley, London

Matsuura, Miho, Yokohama City,
Kanagawa Pref., Japan

Menekodathu Remanan, Amarnath,
Surat, Gujarat, India

Meng Wenxiang, Shanghai, P.R. China

Miller, Me'Shell, North Highlands,
California, U.S.A.

Mok Chiu Fai, Kwai Chung,
New Territories, Hong Kong

Mok So Yiu, Tsuen Wan, Hong Kong

Naito, Ayako, Tokyo, Japan

Nakagawa, Yumi, Kitakatsuragi-gun,
Nara Pref., Japan

Nakanishi, Nobuo, Ikeda City, Osaka,
Japan

Ng Sheung Kan, Quarry Bay, Hong Kong

Nicolson, Louise, London

O'Connor, Darla Jo, Citrus Heights,
California, U.S.A.

Okabe, Yuichi, Kawasaki City, Kanagawa
Pref., Japan

Parhi, Chinmayee, Surat, India

Park, Hyun Jin, Daegu, Korea

Park, Ji Min, Daegu, Korea

Peng Chih Pin, Taipei, Taiwan, R.O. China

Preston, Paula, London

Prickett, Sydney James, Brisbane,
Queensland, Australia

Puniani, Geeta, Surat, Gujarat,
India

Qin Xue, Shanghai, P.R. China

Rafferty, Frank, Ambrieres-Les-Vallees,
France

Raimundo Da Silva, Aldina, Verdun,
Quebec, Canada

Raj, Kara, Ampandrianomby,
Antananarivo, Madagascar

Rajak, Mohamad Zakaria Bin Abdol,
Yangon, Myanmar

Rakotobe, Vanessa, Ampandrianomby,
Antananarivo, Madagascar

Rebmann, Olivier, Geneva, Switzerland

Rodjanagosol, Anothai, Bangkok, Thailand

Rutanatumsri, Kunthida, Bangkok,
Thailand

Said, Ibrahim, Grangetown, Cardiff,
Wales

Sakata, Yuko, Kanazawa City, Ishikawa
Pref., Japan

Sawamura, Tsukasa, Tokyo, Japan

Sek Kam Yin, Kwun Tong, Kowloon,
Hong Kong

Shah, Arti, South Harrow, Middlesex

Shah Bhavin Kirtikumar, Surat, India

She Pak Yu, New Territories, Hong Kong

Shi, Huadan, Shanghai, P.R. China

Shimizu, Maki, Oyama City, Tochigi Pref.,
Japan

Singh, Priti, Jaipur, India

Smith, Laura Sian, Reading, Berkshire

Sritunayothin, Pattra, Bangkok, Thailand

Stevens, Janet Connors, Bellevue,
Washington, U.S.A.

Stevens, Laura Ann, Bewdley,
Worcestershire

Tai Ai Hwa, Taipei, Taiwan, R.O. China

Tanvangi, Pragya, Surat, India

Tarner, Charles B., Sacramento, California,
U.S.A.

Tidd, Lauren, Churchdown, Gloucester

To Wing See, Tuen Mun, Hong Kong

Tong Sen Yue, Sandy, Central, Hong Kong

Tsang, Fiona T.Y., Aberdeen, Hong Kong

Uchiyama, Mio, Ichikawa City, Chiba Pref.,
Japan

Veenhoven, Taletta, Amsterdam,
The Netherlands

Wang Hao, Guilin, Guangxi, P.R. China

Wang Qi, Guilin, Guangxi, P.R. China

Wang Wenqi, Guilin, Guangxi, P.R. China

Gem-A Awards

Watson, Jennifer, Sutton Coldfield, West Midlands

Webster, Penny A., Creston, California, U.S.A

Wen, Wen Chi, Taichung, Taiwan, R.O. China

Wilkinson, June, Warmington, Peterborough, Northamptonshire

Wong Chi Kin, Mid-Levels, Hong Kong

Wong Ho Ming, Kowloon, Hong Kong

Wong Kin Ching, Tai Po, New Territories, Hong Kong

Wong Ling Ling, Tseung Kwan O, New Territories, Hong Kong

Wootton, Sophie Louise, London

Wright, Peter, Chaddesley Corbett, Worcestershire

Wu Zhao Min, Kowloon, Hong Kong

Xie Yi, Shanghai, P.R. China

Yadanar Lwin, Sanchung, Myanmar

Yamada, Masashi, Tokyo, Japan

Yang Chung Mei, Judy, Tsing Yi, New Territories, Hong Kong

Yau Wai Yee, Kowloon, Hong Kong

Yen Kwan, Humphrey, Central, Hong Kong

Yoon, Yoo Jin, Daegu, Korea

You Jia, Shanghai, P.R. China

Yun Mao, Shanghai, P.R. China

Zhang Jinying, Guilin, Guangxi, P.R. China

Zhao Lisha, Guilin, Guangxi, P.R. China

Zhuo Jun Xu, Shanghai, P.R. China

GEM DIAMOND EXAMINATION

Qualified with Distinction
Braham, Adrian David, Reigate, Surrey
Li, Kehan, Enfield, Middlesex

Qualified with Merit
Chown, Philip, Sevenoaks, Kent
Chiu Wai Yu, Yuki, Sheung Shui, New Territories, Hong Kong
Goodwille, Zoe, Battersea, London
Gregory, Kerry Honor, St Mellons, Cardiff, Wales
McKellar, John, Hereford
Wong Lai Yin, Kowloon, Hong Kong

Qualified
Belsham, Lesley, Great Dunmow, Essex
Branting, Andreas, London
Chan Wai Fong, Wah Fu Estate, Hong Kong
Fellows, Andrew Simon, Walsall, West Midlands
Fong Po Yi, Kowloon, Hong Kong
Garcia, Victoria, Sydenham, London
Haythornthwaite-Shock, Lucy, Mangotsfield, Bristol, Avon
Hui Ming Yan, Ray, Tseung Kwan O, New Territories, Hong Kong

Hui Tsz Yin, Kowloon, Hong Kong
Jezova, Olesia, London
Keung Wing Fun, Kowloon, Hong Kong
Lee Wah Ho, Yuen Long, Hong Kong
Leung Hang-Fai, Henry, Kowloon, Hong Kong
Marlow, Joseph Stephen, Sutton Coldfield, West Midlands
Qin Si, Wuhan, Hubei, P.R. China
Rice, Danielle, Halsham, East Yorkshire
Sheehy, Matthew James, Burnham, Berkshire
Tulo, Karen, Ludwigshafen, Germany
Wang Ligeng, Wuhan, Hubei, P.R. China
Watson, Jennifer, Sutton Coldfield, West Midlands
Webb, Stephen Charles, Nelson, New Zealand
Williams, John, London
Wong Ka Lai, Kowloon, Hong Kong
Wong Lai Wa Lever, Kowloon, Hong Kong
Wong Yuen Ching, Winnie, Kowloon, Hong Kong

Members' Meetings

London

A private viewing of the exhibition 'Fabergé and the Russian Jewellers' was held at Wartski's, Grafton Street, London W1, on 16 May.

On 11 October a group visit to the exhibition 'Bejewelled by Tiffany' at the Gilbert Collection, Somerset House, London SW1, was arranged, preceded by a lecture by the exhibition's curator Clare Phillips.

The 2006 Annual General Meeting was held on 27 June at Sotheby's, New Bond Street, London W1 (see report p.251). The AGM was followed by a Private Viewing of Sotheby's June sale 'Jewels: Antique, Period and Contemporary'. Joanna Hardy, Daniela Mascetti and Alexandra Rhodes of Sotheby's Jewellery Department spoke about selected items from the sale.

Gem Discovery Club Specialist Evenings

The Gem Club meets every Tuesday evening at the Gem-A London headquarters when Club members have the opportunity to examine a wide variety of stones.

Once a month gem and mineral specialists bring along items from their own collections; short introductory talks are followed by hands-on sessions under the guidance of the guest specialist. The April guest was Jason Williams of G.F. Williams & Co., of Hatton Garden, who gave a presentation on the cutting of synthetic gemstones in Southern China. In May Dr Jack Ogden took a look at the history of spurious and treated gemstones from ancient Egypt and Western Asia, through Roman imitations to heat treatment of corundum in sixteenth-century Ceylon, in his presentation 'Fooling some people for much of time: 5000 years of gem deception'. In his 'Cameo performance' in June, jewellery dealer Richard Digby spoke about the materials commonly used for cameos and intaglios, and factors likely to affect value. Maggie Campbell Pedersen was the July specialist, giving information on amber and how to identify fakes. In September jewellery valuer

Rosamond Clayton gave a presentation on jade, describing the various treatments and simulants, and assessing the quality for the purpose of valuation. Club members were able to examine a collection of rare gemstones in October, brought along by Michael O'Donoghue.

Midlands Branch

Branch meetings held at the Earth Sciences Building, University of Birmingham, Edgbaston, included a talk on 31 March by John Harris entitled 'Chasing rainbows by observing spectra', 'Arts and Crafts jewellery' by Antiques Roadshow expert Keith Baker on 29 September, and on 27 October a talk on tourmaline by Dr Michael Krzemnicki, director of education at SSEF, Switzerland. The annual summer supper party was held at Barnt Green on 17 June.

North East Branch

On 20 April David Callaghan spoke on cameos and intaglios and on 13 July Brian Dunn gave a talk entitled 'The Naughty Nineties'. Both meetings were held at the Ramada Jarvis Hotel, Wetherby.

North West Branch

Regular Branch meetings have been held at the YHA Liverpool International, Livepool 1. On 19 April Melanie Francis spoke on trends at the 2006 Tucson Gem and Mineral Fair, on 21 June Brian Jackson reviewed the garnet family, on 19 July Tracey Jukes took members for a trip around the world of coloured gemstones with a talk entitled 'Thoughts from 'a broad'', and on 20 September Gem-A Chairman Professor Alan Collins spoke on colour enhancement in diamond and how it may be detected.

Scottish Branch

The Annual Scottish Branch Conference was held at the Lovat Hotel, Perth, from 28 April to 1 May. Speakers included Dr Karl Schmetzer (keynote), Richard Digby, Alan Hodgkinson, Helen Molesworth, Dr Mark Newton and Thom Underwood. A variety of workshops and demonstrations were held on the Sunday afternoon and the

Conference concluded with a field trip on the Monday to Lochan na Lairige. (A report on the Conference was published in *Gems & Jewellery*, May 2006.)

Scottish Branch meetings moved to the new venue of Napier University, Craiglockhart Campus, Edinburgh, in June. On 13 June Brian Jackson gave a talk entitled 'Gemmological wanderings in Russia'. This was followed on 22 August by 'Gem pegmatites of Southern California' by Jesse Fisher, on 12 September with 'A history of gemmology via the literature' by Nigel Israel' and on 24 October with 'All colours of diamond' by Martin Vainer.

South East Branch

A 'Jem Jumble', a bring-and-buy sale, was held at the Gem-A headquarters on 29 October.

South West Branch

Meetings held at the Bath Royal Literary Scientific Institution, Bath, included a presentation on 23 April by Stephen Kennedy on recent developments in the UK coloured stone trade and on 8 October 'The colours of gemstones and how we see them' by Doug Garrod.

Annual General Meeting

The 2006 Annual General Meeting was held at Sotheby's, New Bond Street, London W1, on 27 June. Professor Alan Collins chaired the meeting and welcomed members. The Annual Report and Accounts were approved. E. Alan Jobbins was re-elected as President of the Association for the term 2006-2008. Alan Collins, E Alan Jobbins and Michael O'Donoghue retired from the Council in rotation and, being eligible, Alan Collins and Michael O'Donoghue were re-elected. Alan Jobbins did not seek re-election to the Council. Tony Allnutt and Peter Dwyer Hickey retired in rotation from the Members' Audit Committee and being eligible were re-elected to the Committee. Hazlems Fenton were re-appointed as auditors for the year.

Following the business part of the evening, attendees were generously entertained with wine at a private view of the 'Jewels: Antiques, Period and Contemporary'. The Association is very grateful to Sotheby's for hosting the evening, and particularly to the Directors and staff in the jewellery department for their hospitality and for the fascinating talks about some highlights of the jewellery on show.

Membership

Between 1 April and 31 October 2006, the Council approved the election to membership of the following:

Fellowship and Diamond Membership (FGA DGA)

Brohi, Nosheen, London, 2005
Callaway, Heather, Stone, Staffordshire, 2006
Suraway, Laura Katherine, London, 2006
Tsui, Tommy, Kowloon, Hong Kong, 1997

Fellowship (FGA)

Al-Hadad, Raed, Abu Dhabi, United Arab Emirates, 2006
Anderson, Nicola M., Edinburgh, Scotland, 2000
Bell, Lucy Kate, Stirchley, West Midlands, 2006
Butt, Andrew, Toronto, Ontario, Canada, 2006
Carrel, Leigh, Preston, Lancashire, 2006
Challani, Mohit, Chennai, India, 2006
Chan, Mei Fong, Kowloon, Hong Kong, 2006
Chandhok, Simran, New Delhi, India, 2006
Chaudry, Mohamed Ashraf, Rochdale, Lancashire, 2006
Costin, Charlotte, Horsham, West Sussex, 2006
Deeley, Philippa, Etchingham, East Sussex, 2006
Dunn, William A., Los Angeles, California, U.S.A., 2006
Eastwood-Barzado, Elizabeth, Dully, Switzerland, 2006
Emond, Jacinthe, Laval, Quebec, Canada, 2006
Guasrella, Rita, Vetulonia, Italy, 1996
Jones, Gary, Dudley, West Midlands, 2006
Jones, Jason Matthew, Beverley, East Yorkshire, 2006
Lam, Hazel, Kowloon, Hong Kong, 2006

Lam Mei Hei, Cally, Shatin, Hong Kong, 2006
Leung Shiu Lok, Sam, Taipo, Hong Kong, 2006
Leung, Shun Lok, Kowloon, Hong Kong, 2006
Lin, Lang-Dong, Taipei, Taiwan, R.O. China, 2006
Liu, Hongmei, Toronto, Canada, 2006
Low, H. San, Chatham, Kent, 2006
Morsink, Cornelius E., Stirling, Ontario, Canada, 2006
Murray, Helen Claire, Sutton Coldfield, West Midlands, 2006
Ong Chin Sing, Singapore, 2006
Philogene, Stephanie, Cachan, France, 2005
Rakotoarison, Dominique, Antananarivo, Madagascar, 2005
Rana, Aska, Ahmedabad, India, 2006
Tsang Kwai Ying, Kowloon, Hong Kong, 2006
Wessels, Jurie Hendrik Wyand, London, 2004
Zhu, Healy, Yiwu City, P.R. China, 2005

Diamond Membership (DGA)

Loaker, Alistair, Stevenage, Hertfordshire, 2002
Marlow, Joseph Stephen, Sutton Coldfield, West Midlands, 2006
Garcia Grandal, Victoria, London, 2006
Ng Ka Kit, New Territories, Hong Kong, 2006
Papapavlou, Despina-Maria, Christoforos, Greece, 2006
Parsonson, Chloe, London, 1996
Rice, Danielle, Halsham, East Yorkshire, 2006
Williams, Michael, London, 2006
Wong Yu Lap, Angel, Shatin, Hong Kong, 2006
Yeung Ka Yee, Anthea, Pok Fu Lam, Hong Kong, 2004

Associate Membership

Amos, William Bradshaw, Cambridge
Ayabina, Hazel, London
Ba-Bttat, Mahfood Ali Obeid, Safat, Kuwait
Bendikssen, Bjorn, Sto, Norway
Berry, John, Tenbury Wells, Worcestershire
Bilodeau, Wendy, San Jose, California, U.S.A.
Bland, Claire, London
Bouckaert, Magali, London
Branting, Andreas, London
Brooks, Candy Elizabeth, Catcott, Somerset
Buckley, Victoria, Galway, Republic of Ireland
Cabral, João R.N., Stanmore, Middlesex

Chan, Fung, Kowloon, Hong Kong
Clark, Denise, London
Elles, Sarah, Leven, Fife
Elliott, Roger, Epsom, Surrey
Evesden, Colin, South Benfleet, Essex
Gerrard, Belinda Louise, Randwick, New South Wales, Australia
Gilmore, Anne Marie, Galway, Eire
Gregoire, Roland, Bradford
Halabi-Lenvenyte, Urte, London
Hall, Gregory, Brighton, East Sussex
Harris, Kay, Penang, Malayasia
Henderson, Rheanan, Edinburgh, Scotland
Hug, Samuel, Gosport, Hampshire
Hussain, Sabina, Gainsborough, Lincolnshire
Hutson, Charles, London
Jamieson, Pauline, Edinburgh
Jones, Cressida, London
Kalman, Jonathan Paul, London
Kaneyasu, Yoshimasa, London
Kanu, Ahmed Zahra, London
Kazemi, Hamed, Bangkok, Thailand
Khan, Ehtesham, London
Khisan, Annisaa, London
Laet-Bibigc, Maria, Sao Paulo, Brazil
Larsson, Carl Niclas, Öregrund, Sweden
Learmonth, Bryony, Great Haywood, Staffordshire
Li, Zhen, London
Litter, Robert, Stanmore, Middlesex
Macfarlane, Jean, London
Melbourne, Sulayman, Notting Hill, London
Micatkovam, Lubica, London
Mirhabibi, Alireza, Tehran, Iran
Mitchell, Theresa, Swanmore, Hampshire
Morgan, Arabelle, London
Oh, Sun-Ju, Seoul, R.O. Korea
Or-Isoon, Apisara, Bangkok, Thailand
Quaife, John, Bexhill-on-Sea, Sussex
Rafferty, Frank, Ambrieres-Les-Vallees, France
Rajbanshi, Niren, London
Rao, Harvinder, Southall, Middlesex
Robichaud, Emilie Gould, Ealing, London
Robinson, Thomas Herbert, Newcastle-Upon-Tyne, Tyne and Wear
Ruthven Lloyd, Gabrielle Elizabeth, London
Saini, Amarjit, Los Angeles, California, U.S.A.
Sherin, Saira, London

Gifts

The Association is most grateful to the following for their gifts for research and teaching purposes:

Subhash C.H. Agrawal, Jaipur, India, for a rough piece of blue corundum from Orissa

Alexander Armati DGA, Henley-on-Thames, Oxfordshire, for a donation to the appeal for funds (Pearl Donation)

Eisuke Ashida FGA, Kyoto City, Japan, for a donation to the appeal for funds (Sapphire Donation)

Maggie Campbell Pedersen FGA, London, for *The Amber Book: the Catherine Palace,* text by Victoria Plaude, translated from the Russian by Valery Fateyev. Ivan Fiodorov Art Publishers, St Petersburg, 2004

Guy Clutterbuck, London, for two samples of Zambian amethyst

John Ho, Myanmar, for a collection of gemstones including: a small natural colour hot pink spinel; a flat, clear, colourless hambergite; small trapiche rubies; a chrome tourmaline; faceted clear colourless pollucite; a gem-quality serendibite from Myanmar; an almost translucent blue sodalite/hackmanite (orange under swuv); clear, colourless columnar phenacite crystals; four pollucite crystals

Jaikishan Joshi, Chennai, India, for three specimens of gastropod shell, replaced and in-filled by chalcedony and drusy quartz

A large collection of books from the estate of the late **R. Keith Mitchell**

Lauretta M. Sanders, Knotty Green, Buckinghamshire, for a green grossular garnet from Mali

Jason F. Williams FGA DGA, of G.F. Williams & Co. Ltd., Hatton Garden, London, for a selection of cut gemstones

---

Shih, Meng-Hsin, Taiping, Taiwan, R.O. China
Smith, Mona, Portland, Oregon, U.S.A.
St Vire, Caroline, Hastings, East Sussex
Stacy, Nancy, Walnut Creek, California, U.S.A.
Su, Chen-Hui, Taipei, Taiwan, R.O. China
Taylor, Barbara, Lindfield, West Sussex
Thimke, William, Oshkosh, Wisconsin, U.S.A.
Thompson, Leone, London
Trolle, Natascha, Copenhagen, Denmark
Van Den Bosch, Merle, London
Von Schantz, Casimir, Helsinki, Finland
Voytiatzi, Niki, London
Webster, Penny A., Creston, California, U.S.A.
Westlake, Ingrid, Chamonix, France
Wongdelert, Somvilai, Bangkok, Thailand
Zahoor, Iqbal, Rahimabad, Pakistan

Laboratory Membership

Eternity Jewellery, London

Transfers

From Associate Membership to Fellowship and Diamond Membership (FGA DGA)

Lam Kwok Man, May, London
Lam Kwok Yee, Monica, London
Michaels, Sarah A., Virginia Beach, Virginia, U.S.A.

From Associate Membership to Diamond Membership (DGA)

Huck, Perry, Harare, Zimbabwe
Ng Ka Kit, Ma On Shan, New Territories, Hong Kong

From Fellowship to Fellowship and Diamond Membership (FGA DGA)

Braham, Adrian David, Reigate, Surrey
Chan Wai Fong, Wah Fu Estate, Hong Kong

Chown, Philip, Sevenoaks, Kent
Fellows, Andrew Simon, Walsall,
    West Midlands
Gregory, Kerry, St Mellons, Cardiff, Wales
Haythornthwaite-Shock, Lucy, Mangotsfield,
    Bristol, Avon
Kehan, Li, Enfield, London
Ma Yaw Lan Hsiung, Ruth, Hong Kong
Pang Shing Kwan, Ma On Shan,
    New Territories, Hong Kong

From Diamond Membership to Fellowship and Diamond Membership (FGA DGA)

Appleyard, Catherine, Lewes, East Sussex
Gouros, Arte, Coulsdon, Surrey
Heywood, Natalie Louise, Enfield, Middlesex
Leung Kam Ping, Sai Kung, Hong Kong
Parkes, Gabriella, London
Tulo, Karen, Ludwigshafen, Germany
Webb, Stephen Charles, Nelson,
    New Zealand
Yiu Ka Wah, Kowloon, Hong Kong

From Associate Membership to Fellowship (FGA)

Akiyama, Claire Nozomi, Saitama-Ken,
    Japan
Badrov, Irena, London
Borg, David, Paola, Malta
Danjo, Keiji, Kofu City, Yamanashi Pref.,
    Japan
Dunn, Andrew, Reading, Berkshire
Edwards, Catherine, Salisbury, Wiltshire
Flower, Caro, Melton Constable, Norfolk
Furuya, Satoshi, Bunkyo-Ku, Tokyo, Japan
Gogna, Sanjeev, Una, Himachal Pradesh,
    India
Hayashi, Kinya, Tokushima City, Tokushima
    Pref., Japan
Huen Lai-Kei, Sheree, Richmond,
    British Columbia, Canada
Kidachi, Masanobu, Sagamihara City,
    Kanagawa Pref., Japan
Larsson, Carl Niclas, Öregrund, Sweden
Larsson, Jacqueline, Amsterdam,
    The Netherlands
Latham, Elizabeth, Wallingford,
    Oxfordshire

Matoba, Akiko, Nara City, Nara Pref., Japan
Nagao, Saeko, Kooriyama City, Fukushima
    Pref., Japan
Ogata, Etsuko, Suita City, Osaka, Japan
Okano, Makoto, Iwatsuki City, Japan
Okuyama, Muneyuki, Kohoku-ku,
    Yokohama, Japan
Robichaud, Emilie, Ealing, London
Scott, Craig John, Petersfield, Hampshire
Sherriff, Nicki, Verdun, Quebec, Canada
Soderholm, Kathryn A., Dulles, Virginia,
    U.S.A.
Tanaka, Yumi, Toyonaka City, Osaka, Japan
Thiebaut, Ivane, London
Tonkin, Claire Louise, London
Westlake, Ingrid, Chamonix, France

From Associate Membership to Diamond Membership (DGA)

Branting, Andreas, London
Chen Chih-Wei, Taichung, Taiwan, R.O.
    China
Freeman, Derek, Hove, East Sussex
Gits, Hugo, Knokke, Belgium
Kuchard, Monika, London
Rahn, Adelle, Chippenham, Wiltshire
Webster, Eric T., West Chiltington,
    West Sussex

Obituary

Rodney F. Collyer FGA (D.1953), Rubery,
Birmingham, West Midlands, died in March
2005.

Margaret Irwin FGA (D. 1971), Mickle
Trafford, Cheshire, died on 5 April 2006.

Errata

On p. 91, author address number 2, for
'Saranovy' read 'Saranovsky'

On p. 93, Figure 2, key, for 'pykrite' read
'picrite'; for 'metaarcoses' red 'meta-arkoses'; for
'Facial' read 'Facies'

On p. 94, Figure 3, top left, for 'chromic' read
'chromite'

On p. 100, Figure 13, the formula for uvarovite
should read $Ca_3Cr_2(Si_3O_{12})$

On p. 109, the first U.H. Kyi abstract, for
'pegmatic' read 'pegmatitic'

On p. 127, first column, line 18, for 'He quiet
belief …' read 'His quiet belief …'

Subscriptions 2007

It has been agreed that the membership subscription rates will remain unchanged for 2007, as set out below. Existing Fellows, Diamond Members and Associate Members will be entitled to a £5.00 discount for subscriptions paid before 31 January 2007.

	Fellows, Diamond Members and Associate Members	Laboratory Members
UK	£72.50	£250.00 + VAT
Europe	£80.00	£250.00
Rest of the World	£85.00	£250.00

Forthcoming Events

Tuesday 5 December	**London:** Private viewing of sale to include the works of Andrew Grima at Bonhams Auctioneers, New Bond Street, London W1
Saturday 9 December	**Midlands Branch:** 54th Anniversary Dinner
Tuesday 12 December	**London:** Gem Discovery Club Specialist Evening – Diaspore. CIGDEM LULE-WHIPP
Tuesday 23 January 2007	**Scottish Branch:** Stone setting workshop. DAVID WEBSTER
Friday 26 January	**Midlands Branch:** AGM followed by Annual Bring and Buy Sale and Team Quiz
Tuesday 6 February	**London:** Gem Discovery Club Specialist Evening – Freeform carved gemstones. MEMORY STATHER
Friday 23 February	**Midlands Branch:** From paste to diamonds: shedding light on colourless gems. GWYN GREEN
Tuesday 27 February	**Scottish Branch:** Notes from the Gem Testing Laboratory. STEPHEN KENNEDY
Sunday 18 March	**Midlands Branch:** Loupe and lamp training day
Tuesday 20 March	**Scottish Branch:** CIBJO and the jewellery trade. RICHARD PEPLOW
Friday 30 March	**Midlands Branch:** The cravat pin, an almost forgotten item of jewellery. JAMES GOSLING
Friday 27 April	**Midlands Branch:** Could you be a jewellery valuer? HEATHER McPHERSON
Friday 4 to Monday 7 May	**Scottish Branch Annual Conference:** Keynote speaker: PROFESSOR EMMANUEL FRITSCH

When using e-mail, please give Gem-A as the subject:

Contact details

London:	Mary Burland on 020 7404 3334; e-mail mary.burland@gem-a.info
Midlands Branch:	Paul Phillips on 02476 758940; e-mail pp.bscfgadga@ntlworld.com
North East Branch:	Mark Houghton on 01904 639761; email sara_e_north@hotmail.com
North West Branch:	Deanna Brady 0151 648 4266
Scottish Branch:	Catriona McInnes on 0131 667 2199; e-mail scotgem@blueyonder.co.uk
South East Branch:	Peter Wates, email peter_at_GASEB@yahoo.co.uk
South West Branch:	Richard Slater on 01635 553572; e-mail rslater@dnfa.com

Gem-A Website

For up-to-the-minute information on Gem-A events visit our website on www.gem-a.info

Guide to the preparation of typescripts for publication in *The Journal of Gemmology*

The Editor is glad to consider original articles shedding new light on subjects of gemmological interest for publication in *The Journal.* Articles are not normally accepted which have already been published elsewhere in English, and an article is accepted only on the understanding that (1) full information as to any previous publication (whether in English or another language) has been given, (2) it is not under consideration for publication elsewhere and (3) it will not be published elsewhere without the consent of the Editor.

Typescripts Two copies of all papers should be submitted on A4 paper (or USA equivalent) to the Editor. Typescripts should be doubled spaced with margins of at least 25mm. They should be set out in the manner of recent issues of *The Journal* and in conformity with the information set out below. Papers may be of any length, but long papers of more than 10 000 words (unless capable of division into parts or of exceptional importance) are unlikely to be acceptable, whereas a short paper of 400-500 words may achieve early publication.

The abstract, references, notes, captions and tables should be typed double spaced on separate sheets.

Title page The title should be as brief as is consistent with clear indication of the content of the paper. It should be followed by the names (with initials) of the authors and by their addresses.

Abstract A short abstract of 50-100 words is required.

Key Words Up to six key words indicating the subject matter of the article should be supplied.

Headings In all headings only the first letter and proper names are capitalized.

A This is a first level heading

B This is a second level heading

First and second level headings are ranged left on a separate line.

Third level headings are in italics and are indented within the first line of the text.

Illustrations High resolution digital files, for both colour and black-and-white images, at 300 dpi TIFF or JPEG, and at an optimum size, can be submitted on CD or via email. Vector files (EPS) should, if possible, include fonts. Match proofs are essential when submitting digital files as they represent the colour balance approved by the author(s).

Transparencies, photographs and high quality printouts can also be submitted. It is recommended that authors retain copies of all illustrations because of the risk of loss or damage either during the printing process or in transit.

Diagrams must be of a professional quality and prepared in dense black ink on a good quality surface. Original illustrations will not be returned unless specifically requested.

All illustrations (maps, diagrams and pictures) are numbered consecutively with Arabic numerals and labelled Figure 1, Figure 2, etc. All illustrations are referred to as 'Figures'.

Tables Must be typed double spaced, using few horizontal rules and no vertical rules. They are numbered consecutively with Roman numerals (Table IV, etc.). Titles should be concise, but as independently informative as possible. The approximate position of the Table in the text should be marked in the margin of the typescript.

Notes and References Authors may choose one of two systems:

(1) The Harvard system in which the authors' names (no initials) and dates (and specific pages, only in the case of quotations) are given in the main body of the text, (e.g. Collins, 2001,341). References are listed alphabetically at the end of the paper under the heading References.

(2) The system in which superscript numbers are inserted in the text (e.g. ... to which Collins refers.[3]) and referred to in numerical order at the end of the paper under the heading Notes. Informational notes must be restricted to the minimum; usually the material can be incorporated in the text. If absolutely necessary both systems may be used.

References in both systems should be set out as follows, with *double spacing* for all lines.

Papers Collins, A.T., 2001. The colour of diamond and how it may be changed. *J.Gemm.*, **27**(6), 341-59

Books Balfour, I., 2000. *Famous diamonds.* 4th edn. Christie's, London. p.200

Abbreviations for titles of periodicals are those sanctioned by the *World List of scientific periodicals* 4th edn. The place of publication should always be given when books are referred to.

Contents

Cover Picture: The head reliquary of St Eustace.
(See Crowning glory: the identification of gems on the head reliquary of St Eustace from the Basle Cathedral Treasury, p.169)